WOODHEAD PUBLISHING SERIES IN METALS AND SURFACE ENGINEERING

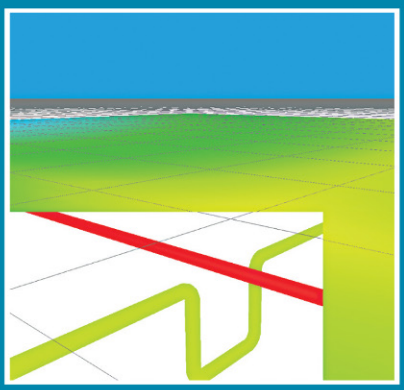

Underground pipeline corrosion

Detection, analysis and prevention

Edited by Mark E. Orazem

ROSEN
empowered by technology

WP
WOODHEAD PUBLISHING

Underground pipeline corrosion

Related titles:

Rehabilitation of pipelines using FRP composites
(ISBN 978-0-85709-684-5)

Handbook of smart coatings for materials protection
(ISBN 978-0-85709-680-7)

Sensor technologies for civil infrastructures Volume 1: Sensing hardware and data collection methods for performance assessment
(ISBN 978-0-85709-432-2)

Sensor technologies for civil infrastructures Volume 2: Applications in structural health monitoring
(ISBN 978-1-78242-242-6)

Woodhead Publishing Series in Metals and Surface Engineering: Number 63

Underground pipeline corrosion

Detection, analysis and prevention

Edited by
Mark E. Orazem

ELSEVIER

AMSTERDAM • BOSTON • CAMBRIDGE • HEIDELBERG • LONDON
NEW YORK • OXFORD • PARIS • SAN DIEGO
SAN FRANCISCO • SINGAPORE • SYDNEY • TOKYO
Woodhead Publishing is an imprint of Elsevier

WP
WOODHEAD PUBLISHING

Woodhead Publishing is an imprint of Elsevier
80 High Street, Sawston, Cambridge, CB22 3HJ, UK
225 Wyman Street, Waltham, MA 02451, USA
Langford Lane, Kidlington, OX5 1GB, UK

British Library Cataloguing-in-Publication Data
A catalogue record for this book is available from the British Library

Library of Congress Control Number: 2013955405

ISBN 978-0-85709-509-1 (print)
ISBN 978-0-85709-926-6 (online)

For information on all Woodhead Publishing publications visit our website at http://store.elsevier.com/

Typeset by Newgen Knowledge Works Pvt Ltd, India

Printed and bound in the United Kingdom

Contents

This page intentionally left blank

Contributor contact details

(* = main contact)

Editor

M. E. Orazem
University of Florida
Gainesville, FL 32611, USA

E-mail: meo@che.ufl.edu

Chapter 1

R. Norsworthy
Polyguard Products Inc.
Ennis, Texas 75120, USA

E-mail: richnors@flash.net

Chapter 2

B. Tribollet*
LISE-UPR 15 du CNRS
University Pierre et Marie Curie
4 Place Jussieu
75252 Paris cedex 05, France

E-mail: bernard.tribollet@upmc.fr

M. Meyer
GDF-Suez
361 avenue du Président Wilson
BP 33 93211 Saint-Denis La Plaine
Cedex, France

Chapter 3

P. Hopkins
Penspen Limited
Units 7-8
Terrace Level
St. Peter's Wharf
Newcastle Upon Tyne, UK

E-mail: p.hopkins@penspen.com

Chapter 4

C. Liu, A. Shankar and
M. E. Orazem*
University of Florida
Gainesville, FL 32611, USA

E-mail: meo@che.ufl.edu

D. P. Riemer
Hutchinson Technology, Inc.
Hutchinson
Minnesota, USA

Chapters 5 and 6

V. S. Sastri
Sai Ram Consultant
1839 Greenacre Crescent Ottawa
Ontario K1J 6S7, Canada

E-mail: sastrivs@rogers.com

Chapter 7

T. Bubenik
Det Norske Veritas (U.S.A.) Inc.
5777 Frantz Rd.
Dublin, Ohio 43017, USA

E-mail: thomas.bubenik@dnv.com

Chapter 8

A. Kowalski
Det Norske Veritas (U.S.A.) Inc.
5777 Frantz Rd.
Dublin, Ohio 43017, USA

E-mail: Angel.Ricardo.Kowalski@dnv.com

Chapter 9

D. Eyre
Penspen Limited
3 Water Lane
Richmond upon Thames
Surrey TW9 1TJ, UK

E-mail: d.eyre@penspen.com

Chapter 10

S. Brockhaus*, M. Ginten, S. Klein, M. Teckert, O. Stawicki, D. Oevermann and S. Meyer
ROSEN Technology and Research Center GmbH
Am Seitenkanal 8
49811 Lingen (Ems), Germany

E-mail: SBrockhaus@RosenInspection.net

D. Storey
ROSEN Technology AG
Obere Spichermatt 14
6370 Stans, Switzerland

Chapter 11

S. Brossia
DYCEUSA Inc.
8059A Corporate Blvd
43064 Plain City, Ohio, USA

E-mail: sbrossia@dyce-usa.com

Woodhead Publishing Series in Metals and Surface Engineering

1 **Nickel and chromium plating**
J. K. Dennis and T. E. Such
2 **Microbiologically influenced corrosion handbook**
S. Borenstein
3 **Surface engineering casebook**
Edited by J. S. Burnell-Gray and P. K. Datta
4 **Duplex stainless steels**
Edited by R. Gunn
5 **Engineering coatings**
S. Grainger and J. Blunt
6 **Developments in marine corrosion**
Edited by J. P. Blitz and C. B. Little
7 **Fundamental and applied aspects of chemically modified surfaces**
J. P. Blitz and C. B. Little
8 **Paint and surface coatings**
Edited by R. Lambourne and T. A. Strivens
9 **Surfacing: Core research from TWI**
TWI
10 **Recommended values of thermophysical properties for selected commercial alloys**
K. C. Mills
11 **Corrosion of austenitic stainless steels**
Edited by H. S. Katal and B. Raj
12 **Fundamentals of metallurgy**
Edited by S. Seetharaman
13 **Energy absorption of structures and materials**
G. Lu and T. X. Yu
14 **The Hatfield memorial lectures: Developments in iron and steel processing**
Edited by P. R. Beely
15 **Laser shock peening**
K. Ding and L. Ye
16 **Structural shear joints**
G. T. Hahn, C. A. Rubin and K. A. Iyer

17 **Direct strip casting of metals and alloys**
M. Ferry
18 **Surface coatings for protection against wear**
Edited by B. G. Mellor
19 **Handbook of gold exploration and evaluation**
E. MacDonald
20 **The cold spray materials deposition process**
Edited by V. K. Champagne
21 **The SGTE casebook: Thermodynamics at work: Second Edition**
Edited by K. Hack
22 **Belt conveying of minerals**
E. D. Yardley and L. R. Stace
23 **Techniques for corrosion monitoring**
Edited by L. Yang
24 **Creep-resistant steels**
Edited by F. Abe
25 **Developments in high temperature corrosion and protection of materials**
Edited by W. Gao
26 **Mineral wool: Production and properties**
B. Sirok and B. Blagojevic
27 **High-performance organic coatings**
Edited by A. S. Khana
28 **Hydrometallurgy: Principles and applications**
T. Havlik
29 **Corrosion control in the aerospace industry**
Edited by S. Benavides
30 **Multiaxial notch fatigue**
L. Susmel
31 **Titanium alloys**
W. Sha and S. Malinox
32 **Advances in marine antifouling coatings and technologies**
Edited by C. Hellio and D. M. Yebra
33 **Maraging steels**
W. Sha and W. Gao
34 **Surface engineering of light alloys**
Edited by H. Dong
35 **Sintering of advanced materials**
Edited by Z. Z. Fang
36 **Managing wastes from aluminium smelter plants**
B. Mazumber and B. K. Mishra
37 **Fundamentals of aluminium metallurgy**
Edited by R. Lumley

38 **Electroless copper and nickel-phosphorus plating**
W. Sha and X. Wu
39 **Thermal barrier coatings**
Edited by H. Xu and H. Guo
40 **Nanostructured metals and alloys**
Edited by S. H. Wang
41 **Corrosion of magnesium alloys**
Edited by G. L. Song
42 **Shape memory and superelastic alloys**
Edited by Y. Yamauchi and I. Ohkata
43 **Superplasticity and grain boundaries in ultrafine-grained materials**
A. L. Zhilyaev and A. I Pshenichnyuk
44 **Superplastic forming of advanced metallic materials**
Edited by G. Guiliano
45 **Nanocoatings and ultra-thin films**
Edited by A. S. H. Makhlouf and I. Tiginyanu
46 **Stress corrosion cracking**
Edited by V. S. Raja and T. Shoji
47 **Tribocorrosion of passive metals and coatings**
Edited by D. Landolt and S. Mischler
48 **Metalworking fluids (MWFs) for cutting and grinding**
Edited by V. P Astakhov and S. Joksch
49 **Corrosion protection and control using nanomaterials**
Edited by V. S. Saji and R. Cook
50 **Laser surface modification of alloys for corrosion and erosion resistance**
Edited by C. T. Kowk
51 **Gaseous hydrogen embrittlement of materials in energy technologies Volume 1: The problem, its characterisation and effects on particular alloy classes**
Edited by R. P. Gangloff and B. P. Somerday
52 **Gaseous hydrogen embrittlement of materials in energy technologies Volume 2: Mechanisms, modelling and future developments**
Edited by R. P. Gangloff and B. P. Somerday
53 **Advances in wrought magnesium alloys**
Edited by C. Bettles
54 **Handbook of metal injection molding**
Edited by D. Heaney
55 **Microstructure evolution in metal forming processes**
Edited by J. Lin and D. Balint
56 **Phase transformations in steels Volume 1: Fundamentals and diffusion-controlled transformations**
Edited by E. Pereloma and D. V. Edmonds

57 **Phase transformations in steels Volume 2: Diffusionless transformations, high strength steels, modelling and advanced analytical techniques**
Edited by E. Pereloma and D. V. Edmonds
58 **Corrosion prevention of magnesium alloys**
Edited by G. L. Song
59 **Fundamentals of magnesium alloy metallurgy**
Edited by M. Pekguleryuz, K. Kainer and A. Kaya
60 **Advances in powder metallurgy**
Edited by I. Chang
61 **Rare earth-based corrosion inhibitors**
Edited by M. Forsyth and B. Hinton
62 **Thermochemical surface engineering of steels**
Edited by M. Somers and E. Mittemeijer
63 **Underground pipeline corrosion: Detection, analysis and prevention**
Edited by M. E. Orazem
64 **Handbook of smart coatings for materials protection**
Edited by A. S. H. Makhlouf

Introduction

M. E. ORAZEM, University of Florida, USA

Since the beginning of the twentieth century, liquid petroleum products and natural gas have been transported by extensive underground networks of steel and iron pipes.[1,2] The American Gas Association reports that, in 2013, over 2.4 million miles of buried steel mainline pipe was used for the transport of natural gas within the United States.[3] Trunk lines for natural gas products add to this total. There are, in addition, 170 000 miles of pipeline for transport of crude oil and refined products.[4] The soil environment contains oxygen and is sufficiently conductive to allow passage of electrical current; therefore, buried steel structures are subject to corrosion. By the late 1920s, the number of leaks had begun to increase alarmingly and, by the early 1930s, all major pipeline owners were providing some measure of corrosion mitigation to their pipelines, including application of coatings and cathodic protection.[1]

Severe corrosion can lead to perforation of the pipe. As described in this book, other phenomena, such as hydrogen embrittlement, stress corrosion cracking, and microbiological influences, may lead to loss of pipeline integrity. The potential consequences include loss of product, service interruption, property damage including fire, contamination of water supplies, and loss of life. The consequences of pipe failures are increasing, due in part to encroachment of housing developments onto pipe right-of-ways. While prevention of the social and economic costs of pipeline failure is a sufficient goal in itself, corrosion mitigation is also driven by the recognition that the pipeline represents a valuable asset that should be protected.[2] Optimal allocation of resources requires proper design of pipeline systems, effective identification of locations where corrosion mitigation strategies are insufficient, and design of remediation strategies that can return an underprotected pipe to the protected condition.

This volume contains contributions from experts in the fields of corrosion and corrosion mitigation as applied to pipelines. The object of this work is to provide a basic understanding of the problems and to explore the state of the art in corrosion prevention. The contributions range from descriptions

of field applications to discussion of mathematical and physical fundamentals. The book contains two parts, the first dedicated to understanding and managing corrosion processes, and the second to methods for detecting corrosion.

In Chapter 1, Richard Norsworthy (Polyguard Products Inc., USA) provides a basic explanation of electrochemistry as it applies to the corrosion process. He discusses factors that influence corrosion both inside pipes and on the exterior surfaces, including concentration and temperature cells, environmental cracking, and microbiological influences.

In Chapter 2, Bernard Tribollet (LISE, France) and Michel Meyer (GDF-Suez, France) discuss corrosion of underground pipes induced by high-voltage electric power lines or by AC-powered railways systems. They provide a fundamental perspective on the manner in which the induced alternating potential causes corrosion, the role of cathodic protection, and the changes in local environment associated with the induced electrochemical reactions.

In Chapter 3, Phil Hopkins (Penspen Group, UK) covers the assessment of corrosion in onshore (underground) pipelines, providing a state-of-the-art review, with both recommendations and insights into the various assessment methods available today.

In Chapter 4, Chao Liu, Alok Shankar, Mark E. Orazem (University of Florida, USA), and Douglas P. Riemer (Hutchinson Technology, Inc., USA) provide a historical perspective and a mathematical framework for the development of models for cathodic protection, including calculation of both on- and off-potentials at arbitrarily located surfaces. Application of the model is presented for interpretation of ECDA results in terms of the condition of the buried pipe, simulating the detrimental influences of competing rectifier settings for crossing pipes protected by independent CP systems, and simulating the influence of coatings and coating holidays (or defects) on the CP of above-ground tank bottoms.

Vedula S. Sastri (Sai Ram Consultant, Canada) provided two chapters to this volume. In Chapter 5, he reviews sources of corrosion in underground pipelines carrying oil and gases such as hydrogen sulfide and carbon dioxide. He discusses and compares corrosion monitoring techniques such as linear polarization resistance (LPR), electrochemical impedance spectroscopy (EIS), electrochemical noise (EN) techniques and the use of sensor probes. In Chapter 6, he reviews the use of corrosion inhibitors in the oil and gas industry, including production factors affecting corrosion inhibition, criteria for selecting corrosion inhibitors, mechanisms of corrosion inhibition, and types of corrosion inhibitor.

In Chapter 7, Tom Bubenik (Det Norske Veritas (U.S.A.), Inc.) discusses electromagnetic in-line inspection tools as they relate to pipeline integrity. He emphasizes magnetic flux leakage (MFL), the most commonly

used inspection technology for pipelines, which has been successfully employed for nearly 50 years, to detect, identify, and size metal loss due to corrosion.

In Chapter 8, Angel R. Kowalski (Det NorskeVeritas (U.S.A.) Inc., USA) provides a description of pipe-to-soil potential close interval surveys (CIS or CIPS), used to evaluate the effectiveness of the cathodic protection system of a buried or submerged pipeline. CIS principles are presented together with data collection quality assurance. Examples of CIS results are provided to illustrate the advantages of the tool.

In Chapter 9, David Eyre (Penspen Limited, UK) presents the Pearson survey, the oldest above-ground survey technique for finding coating holidays on buried pipelines. This chapter describes the technique, the equipment, and recent developments. It discusses the advantages and disadvantages of the Pearson survey over similar above-ground survey techniques.

In Chapter 10, Stephan Brockhaus, Markus Ginten, Stefan Klein, Michael Teckert, Olaf Stawicki, Dorothee Oevermann, Sabrina Meyer (ROSEN Technology and Research Center GmbH, Germany) and Derek Storey (ROSEN Technology AG, Switzerland) describe in-line inspection (ILI) for detecting and qualifying flaws which would survive hydrostatic testing as well as flaws close to pipeline's failure. Successive ILI measurements conducted over a period of years can reveal the growth rate of active flaws. Because an ILI tool is driven by the propellant of the pipeline, there is no need to stop pipeline operations to inspect the line. This chapter describes a variety of techniques which comprise nondestructive evaluation (NDE).

In Chapter 11, C. Sean Brossia (Det Norske Veritas (U.S.A.) Inc.) provides his perspective on methods used for external corrosion monitoring of pipelines. He concludes that a combination of methods should be considered that provide complimentary information on the present state of the pipeline as well as trending information.

I would like to express my gratitude for the contributors to this volume. Each chapter, written independently, provides a unique and important perspective on corrosion, sensing, and corrosion mitigation associated with pipelines. I express our appreciation as well for the editorial staff of Woodhead Publishing, who had the vision, tenacity, and editorial talent to shepherd this work to completion.

References

1. John Morgan (1993), Cathodic Protection, 2nd edition, NACE, International, Houston, TX.
2. M. E. Orazem, D. P. Riemer, C. Qiu, and K. Allahar, 'Computer simulations for cathodic protection of pipelines', in *Corrosion Modeling for Assessing*

the Condition of Oil and Gas Pipelines, F. King and J. Beavers, eds, NACE International, Houston, Texas, 2004, 25–52.
3. Facts about Natural Gas, American Gas Association (2013), Washington, DC, http://www.aga.org/Newsroom/factsheets/Documents/FactsAboutNaturalGas2013.pdf, accessed 7/1/2013.
4. Enhance Pipeline Safety (2013), National Transportation Safety Board, Washington DC, https://www.ntsb.gov/safety/mwl7_2012.html, accessed 7/1/2013.

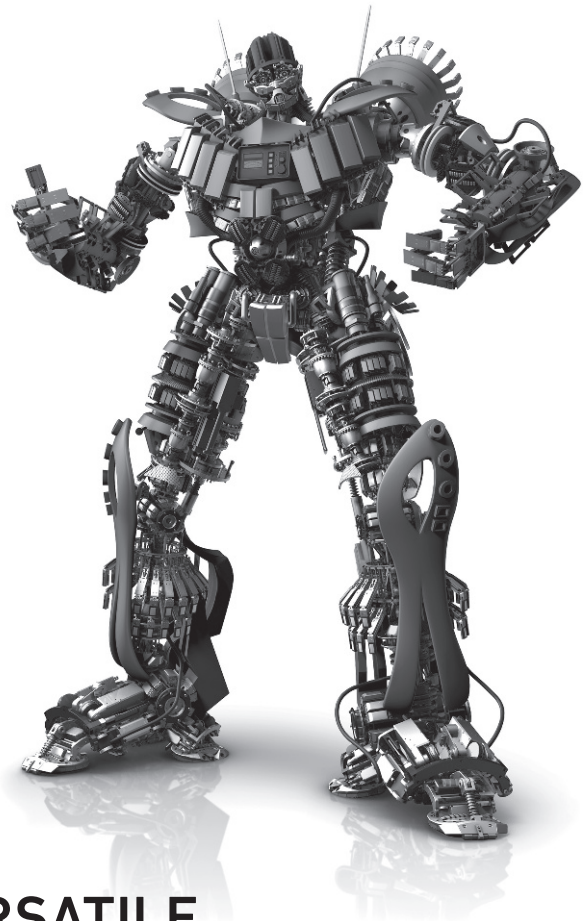

VERSATILE.

Always a leading innovator, ROSEN not only supplies pipeline customers with the latest diagnostic and system integrity technologies but also offers flexible solutions and all-round support for plants & terminals.

www.rosen-group.com

ROSEN

empowered by technology

This page intentionally left blank

Part I

Understanding and managing corrosion processes

This page intentionally left blank

1

Understanding corrosion in underground pipelines: basic principles

R. NORSWORTHY, Polyguard Products Inc., USA

DOI: 10.1533/9780857099266.1.3

Abstract: Corrosion is the deterioration of material or its properties because of a reaction with its environment. Corrosion of pipelines (external, internal, or atmospheric) will depend on the environment and the changes that occur during the life of that pipeline. Basic corrosion principles for metals will be discussed, along with a brief discussion of the typical corrosion mitigation methods. Some of the corrosion mitigation methods are coatings, cathodic protection, and inhibitors.

Key words: anode, cathode, electrolyte, coatings and cathodic protection.

1.1 Introduction

The definition of corrosion according to NACE International is 'The deterioration of a substance or its properties because of a reaction with its environment.'[1] All materials can, and do, corrode if we place them in an environment that causes that particular material to deteriorate. Since this book is about metal (usually steel) underground pipelines, the discussion will be about metals. These pipelines are exposed to many different corrosive environments, both internally and externally.

Iron-based metals are the most widely used of all the metals for pipelines. The iron is alloyed with various other metals to produce a variety of steel products that can be formed into pipe of all diameters, wall thicknesses, and lengths. This pipe is connected (usually through welding) and placed in the ground to transport various products a few meters or cross-country to locations of use. These products may be water, oil, natural gas, refined products, or a variety of other liquids, gases, and slurries. The length of the pipeline may be from a few meters to over a thousand kilometers. The diameter of the pipe will vary according to the product type and volume, but can be from a few centimeters to over a meter. Large water pipes can be several meters in diameter. The wall thickness will also vary according to the type of products and pressure requirements. In discussing corrosion processes

affecting different types of pipe, this chapter uses the following basic terms and definitions.

1.1.1 Matter

Matter is anything that occupies space. Matter can be a solid, liquid, or gas formed from elements, molecules, chemical compounds, or mixtures.

1.1.2 Elements

An element is a substance that cannot be broken down through chemical reactions; elements are the building blocks of all matter.

1.1.3 Compound

A compound is a combination of two or more elements and is a pure substance having a fixed composition.

1.1.4 Mixture

A combination of elements, compounds, or both held, together by physical rather than chemical forces is a mixture. Unlike a compound, a mixture does not have a fixed composition.

1.1.5 Molecule

A molecule is the smallest particle of an element of compound that retains all the chemical properties of that compound or element.

1.1.6 Atoms

An atom is the smallest chemical unit of an element. An atom consists of a nucleus, which contains positively charged protons, and neutrons, which are neutral in charge. Orbiting around the nucleus of an atom are electrons, which are negatively charged. Each atom is distinguished by the number of protons and electrons. The number of electrons must be equal to the number of protons for an atom to exist.

Figure 1.1 shows the two-dimensional version of a nitrogen atom. Notice the electrons are at different energy levels or orbits around the nucleus. Hydrogen is the smallest of all the atoms and is composed of only one proton and one electron. Helium is the next atom and has two

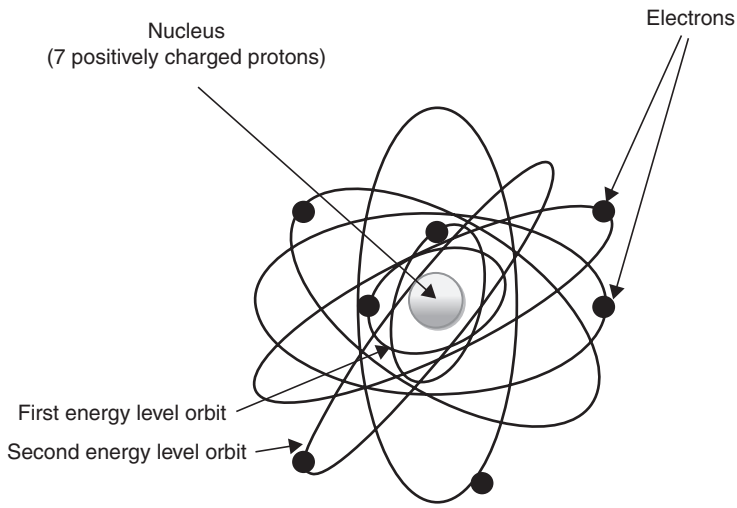

1.1 Bohr model of an atom. Notice that there are two electrons in the first energy level and five in the second energy level.

of each. The outer orbit plays a significant role in the corrosion of metals. The simple explanation is that all atoms want to have a full outer shell of electrons. Hydrogen, for example, is on the metal side of the periodic chart in the first column and is a very active atom because it easily gives up electrons to ionize and then seeks electrons to fill the void (acids). Helium on the other hand is called a noble gas and is on the far right hand column of the periodic chart. The noble gases are very stable elements and do not give up or gain electrons because their outer shells are full and they are happy right where they are. The other atoms do not have full outer shell electrons and are therefore seeking to gain or lose electrons to allow them to have a full outer shell. Most elements are found in nature in the ionized state.

1.1.7 Ions

Ions are atoms or molecules that have gained or lost electrons. A gain of electrons will create a negatively charged ion called an anion since there are more electrons (negative charges) than protons (positive charges). If there is a loss of electrons the ion is called a cation since there are fewer electrons than protons. Molecules can also become ionized with the gain or loss of electrons. This gain or loss of electrons normally occurs in the outer shell areas of the atom or molecule, but the placement of the electrons take place according to the conditions and elements involved in the process.

1.2 Electrochemical corrosion: conventional current theory

The type of corrosion that occurs on metal pipelines is called 'electrochemical'. This word provides us with a clue as to what happens in the corrosion process. There is an electrical component (transfer of electrons) and chemical component (oxidation and reduction reactions) that must be present at the same time with equivalent reactions. Each of these topics will be discussed separately. Figure 1.2 shows the basic corrosion cell used to describe the process. Four components must exist at the same time for electrochemical corrosion to occur. These are:

Anode: That part of the structure where conventional current (CC) leaves the metal and enters the electrolyte. Corrosion occurs at the sites where the CC leaves the metal.

Cathode: That part of the structure where CC re-enters the metal from the electrolyte. Protection occurs at the cathode/electrolyte interface where the CC re-enters the metal.

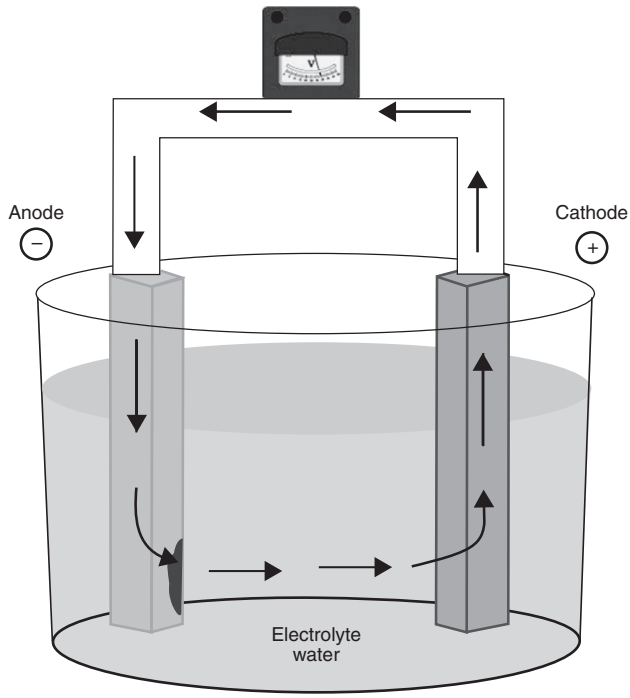

1.2 Basic corrosion cell (CC). CC leaves the anode (causing corrosion), going into the electrolyte and re-enters the metal at the cathode (providing protection) and completes the circuit through the external path back to the anode.

Electrolyte: A solution capable of conducting current by ionic flow.
External Path: An electrical connection (metal or carbon) between the anode and cathode.

When the external path connection is made between the anode and the cathode and they are placed in the electrolyte, the corrosion process begins (Fig. 1.2). As the CC leaves the metal of the anode, corrosion occurs (metal is removed). The current then moves through the electrolyte to the surface of the cathode where it re-enters the metal and protects the cathode surface. The current then completes the circuit back to its source, the anode, through the external path. This is called direct current (DC) because it must return to its source and travels in only one direction.

The CC theory was developed by Benjamin Franklin and other scientists of the 1700s. They knew there was movement, but did not know this movement was electrons in the metal and ions in the electrolyte. They arbitrarily established a convention for labeling electrical potentials and electrical (current) flow by assigning the direction of current from more positive to more negative areas in the circuit. Physicists in the late 1800s discovered the electron and found that it was the movement of these negatively charged particles that was responsible for the flow of electricity. Most people in the cathodic protection (CP) industry still use the CC theory to explain and work with the DC of corrosion cells and CP.

Corrosion cells are batteries, and batteries are corrosion cells (Fig. 1.3). A battery has two unattached, electrically different materials placed in an electrolyte. One component (the cathode) is electrically more positive than the other component (the anode). Various battery types use an electrolyte suitable for the particular service and life requirement. The fourth component of the corrosion cell in this case is the external path connection. This is represented by the switch on a flash light or the car ignition. Once the connection is made between the anode and cathode, the current flows allowing energy to perform the job intended. Once the anode becomes too depleted to provide adequate current to do the job, we must replace the battery or recharge it according to the type being used.

When using the CC theory to discuss the corrosion cell, the direction of current is defined as from the more positive to the more negative structure in the external path. When measuring DC, meters and leads are used to make the connection between the positive and negative points of the circuit by connecting to metal structures; therefore the measured current stays in the metal (external) path. This is a critical statement. When working in the field, corrosion technicians and others must remember the direction of CC through the circuit. If the direction of DC is not correctly interpreted, serious problems can develop. These will be discussed in a later chapter.

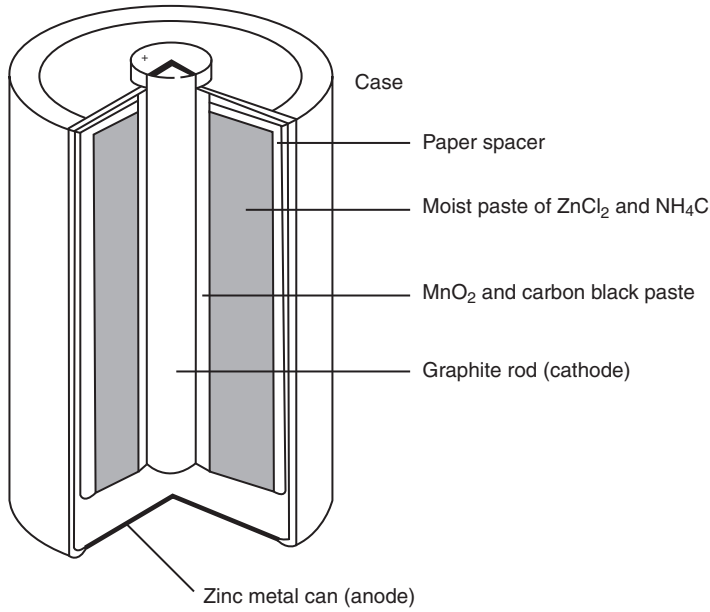

1.3 Typical battery – all batteries are corrosion cells. All corrosion cells are batteries.

If the positive lead of a volt meter is connected to the more positive metal (cathode) and the negative is connected to the more negative metal (anode) in the corrosion cell, the voltage reading will be positive. When using the conventional theory, the DC moves from the more positive cathode through the positive lead of the meter (the external path) entering the positive side of the meter and exiting through the negative terminal; therefore the reading will be positive. If the connection is made with the positive to the anode and the negative to the cathode the reading will be negative since the DC now enters the meter through the negative terminal and exits through the positive terminal. An understanding of these principles is very important for those who work with corrosion control on pipelines when taking potentials and determining current directions in related circuits. The conventional DC electrical theory is still used by most people today in the CP world. So it is critical to properly train those responsible to make sure they have a clear understanding of the direction of the current and the proper ways of monitoring and determining current flow direction.

1.3 Electrochemical corrosion: advanced theories

The reactions that take place in the corrosion cell are electrochemical in nature and are more complex than those of the conventional theory

mentioned above. Though the same four elements must exist at the same time for electrochemical corrosion to occur, the process must be understood to control the corrosion process to acceptable levels (Fig. 1.4):

Anode: That part of the structure where corrosion occurs. Corrosion occurs at the interface of the anode and the electrolyte where the (outer shell) electrons leave the metal atoms and 'migrate' toward the cathode through the external path. This leaves metal ions at the interface that enter the electrolyte to combine with ions that may be present. This half reaction is called 'oxidation' and results in the loss of electrons. Negatively charged ions in the electrolyte are attracted to the anode.

Cathode: That part of the structure where electrons in the external path reach the cathode/electrolyte surface to be consumed by ions present in the electrolyte. Positively charged ions in the electrolyte will tend to drift toward the cathode/electrolyte

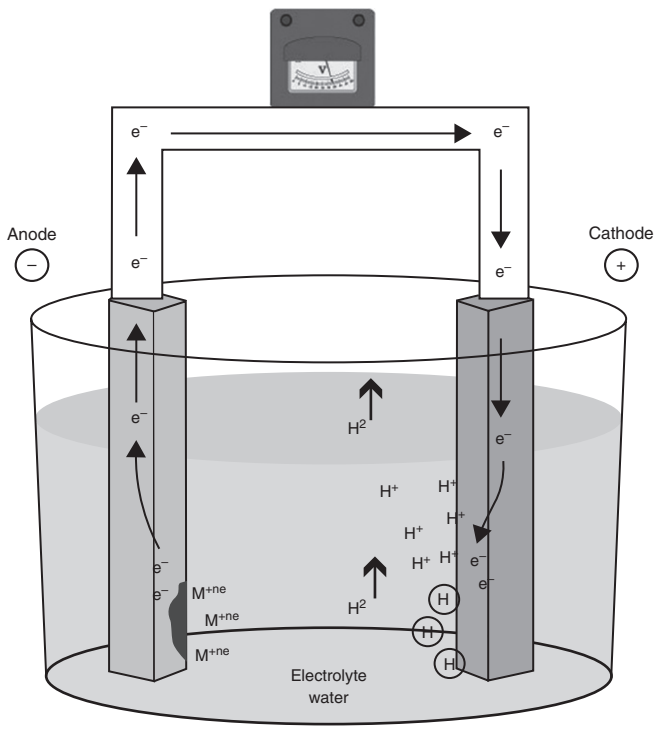

1.4 Electrochemical cell – electron flow – free electrons move from the anode at the site of corrosion (oxidation), through the external (metallic) path to the cathode where electrons are consumed by various reduction reactions at the interface of the cathode and electrolyte where protection occurs.

interface to consume these 'free' electrons. This half reaction is called 'reduction' and results in a gain of electrons. Positively charged ions in the electrolyte are attracted to the cathode.

Electrolyte: A solution capable of conducting current by ionic flow. Positively charged ions are mostly attracted to the cathode and negatively charged ions are mostly attracted to the anode.

External Path: An electrical connection (metal or carbon) between the anode and cathode that conducts electrons produced at the anode to be consumed at the cathode surface.

The electrochemical process of metal corrosion has many variables that must be considered to properly understand the process. These will be discussed in more detail later. The following explanation will be very basic, but will hopefully allow a better understanding of the basic principles of the electrochemical corrosion process. This basic process is the same for the external corrosion as it is for internal corrosion of pipelines.

For electrochemical corrosion to occur, there has to be an electrical difference between the anode and the cathode. The further apart these are electrically, the more active is the corrosion cell. The electrolyte type and the external connection resistance will play a significant role in the rate at which the corrosion will occur on the anode. Other factors will be discussed later.

1.3.1 Anode reactions (oxidation)

Oxidation is the term applied to the loss of one or more electrons from an atom or molecule, which then forms a positively charged ion that is deposited in the electrolyte. The atom or molecule decreases in negative charge. The term 'oxidation' is not necessarily associated with oxygen. The electrons being lost at the anode during the oxidation reaction are from the outer shell electrons of the metal atoms that make up the anode or anodic site where corrosion occurs. Each metal type requires a different process to make the metal ore into a 'usable' metal. Most metals are found in an ore form that consists of the metal ions known as 'cations'. Cations are positively charged because the metal ion has more positively charged protons than electrons in this form. The 'natural' state of most metals is to be in the positively ionized form without the outer shell electrons.

For most metals the process of changing from the ore form to the metal form is to use heat to drive off the oxygen and other components that have combined with the metal ore. Processing of the metal ore forces the electrons from other ions (oxygen, etc.) that are being removed by the process to

attach to the outer shell of the metal ion to form the completed metal atom. This now places the metal in an 'unnatural' state. This is one of the reasons why a metal will corrode when placed in an accommodating electrolyte. The metal wants to go back to its original state and will give up those same outer shell (negative) electrons to go back to an ion (natural state) with a positive valence. Once the metal atom is formed we typically alloy it with other metals to give the metal certain characteristics to allow it to perform in a particular environment. Iron alloys are the most widely used of all the metals for pipelines.

The corrosion process for iron happens at the anode/electrolyte surface. The iron atom gives up electrons (usually two) and forms an iron ion that breaks away and goes into the electrolyte solution where it may combine with other ions or compounds. These ions, if combined with oxygen, can form iron oxide which is the basic same compound as iron ore or rust, thereby allowing the iron to return to its natural state.

1.3.2 Cathode reactions (reduction)

At the cathode/electrolyte interface the reduction reaction occurs. At this interface, there is an exchange of electrons between the cathode metal and the ions, atoms or compounds in the electrolyte. The electrons being consumed are provided by the oxidation reaction (though not the same electrons) and so there is no corrosion at the cathode.

Reduction is the term applied to the gain of one or more electrons by an atom or molecule, which then forms a negatively charged ion or neutral element. The atom or molecule increases in negative charge. The term 'reduction' in this case refers to the change from the more positive to the more negative, thereby reducing the positive value of the atom or molecule. This reduction is not about losing weight or size.

Several reactions can take place at the cathode. Of course, the environment will play a large role in the reduction reaction and the compounds that will actually form. Here are some common reactions that occur at the cathode:

Hydrogen evolution $2H^+ + 2e^- \rightarrow 2H \rightarrow H_2 \uparrow$ or,

Oxygen reduction
(neutral or alkaline solutions) $2H_2O + 2O_2 + 4e^- \rightarrow 4OH^-$ or,

Oxygen reduction (acid solutions) $O_2 + 4H^+ + 4e^- = 2H_2O$ or,

Metal ion reduction (acid solutions) $Fe^{+3} + e^{-} \rightarrow Fe^{+2}$ or,

Metal deposition $Cu^{+2} + 2e^{-} \rightarrow Cu$

The reduction reactions at the cathode results are critical to understanding the basics of corrosion cells. If the electrolyte is acidic, hydrogen and hydrogen gas evolution will be the predominant reactions.

1.3.3 Electrolyte

The electrolyte can be any liquid material in which ions are being transported from one point to another. As defined above, these cations (positively charged) and anions (negatively charged) are the principal charge carriers in the electrolyte. All the electrochemical reactions for a corrosion cell happen in the electrolyte. The availability of these ions at the electrolyte/metal interface is one of the determining factors in the corrosion rates of a particular metal.

The acidity and alkalinity of the electrolyte is another factor that will be discussed later. Resistance and soil resistivity are affected by the amount of moisture in an electrolyte. As a soil (electrolyte) becomes wetter from rain or other moisture, salts in the soil dissolve forming ions and thereby becoming more conductive (less resistant) to current. When the soil dries during drought, the ions combine into salts, lowering the conductivity and increasing the resistance of the soil.

1.3.4 External path (electronic)

There must be an electronic path (metal or carbon) between the anode and cathode. This path allows the electrons freed from the metal atoms during the oxidation process to move from the anode to the cathode during the corrosion process. There are several theories about this movement of electrons and the method by which they move through the metal. One theory is that as one outer shell electron is produced (or lost) it bumps an outer shell electron on a nearby atom, replacing it and bumping it to the next atom where that electron replaces an outer shell electron, etc. Once this process arrives at the interface of the cathode and electrolyte, the last electron in this action is consumed (or gained) in the reduction process. This process is similar to placing tennis balls in a 3 meter length of 10 cm diameter pipe. Once the pipe is completely full of balls and one more is forced in, one must fall out at the other end at the same instant.

As one electron is lost (produced) at the anode, one must be gained (consumed) at the cathode in the very same instant. Therefore oxidation and

reduction are same time and equivalent reactions. The same number of electrons produced at the anode must be consumed at the cathode at that instant for electrochemical corrosion to occur. Note that these freed electrons move only in this external path, not in the electrolyte. The electrons in the electrolyte are all attached to atoms, ions or molecules.

If something disrupts this process, the corrosion rate changes. If this path becomes a restriction to electron flow, the corrosion process slows down. Resistance in the structure can be caused by several things. Even though all metals and carbon conduct electrons, some do it more efficiently than others. The diameter (cross sectional area) and length of this conductive path must also be considered. Contact resistances will affect the rate of electron movement. Using simple Ohms law formulas help explain many issues in basic corrosion.

1.3.5 The complete electrochemical corrosion cell

The complete electrochemical corrosion cell consists of the four items mentioned above. As shown in the cell in Fig. 1.4, all four must be present for electrochemical corrosion to occur. The 'free' electrons flow in the metal or carbon paths, not in the electrolyte. In the real world of pipelines, the electrolyte would typically be the soils and waters that surround the pipe. There are similar barriers to ionic movement because of wet/dry areas, different soil types and concentration cells. So the anode and cathode can be in different electrolyte types, but must be in the same total electrolyte environment. Remember the importance of the environment in the definition of corrosion.

The various ionic compounds in these electrolyte environments will be one of the determining factors in the rate of corrosion and the amount of current between the anode and cathode. Generally, the positively charged ions will be attracted toward the cathodic surfaces and the negatively charged ions toward the anodic surfaces. This movement of ions will be mostly in the electrolyte immediately surrounding the anode and cathode.

1.4 Other factors in corrosion

The basic corrosion cell explains many principles of the corrosion process, but many other factors influence the rate and type of corrosion that can be encountered. Many a time there is more than one type of corrosion process occurring at the same time, thereby accelerating the process.

1.4.1 Thermodynamics

Thermodynamics is the science of the flow of energy. 'Thermo' is related to heat as in the reaction that occurs when burning oil or other fuels.

'Dynamic' refers to movement. In the corrosion cell the chemical reactions create some heat (though usually not enough to detect) and there is a movement of electrons in the metal. So the corrosion cell is a thermodynamic reaction. These reactions are natural processes that tend to reduce the total energy content of a system. The energy content of metals is higher than the energy of the related corrosion products resulting from the corrosion process. In nature, metals are typically found in ore form and so they have to be refined to a usable metal. The refining process requires energy (heat or electricity) to make this change. The more reactive metals require more energy input to refine them into a usable form. These are considered 'active' metals. Metals requiring less energy to produce pure metals from their ores are known as 'noble' metals. These metals are typically more corrosion resistant and are not as active as those metals considered reactive (requiring more energy to process). This will be discussed further in the galvanic series. When metals are placed in a corrosive environment, they will naturally start the process of returning from the higher energy form into a lower energy form by combining with other elements to form chemical compounds similar to the original ore. Iron ore is primarily ferric oxide (Fe_2O_3), which is a common form of rust and iron ore.

1.4.2 Polarization

Polarization is the change in the open circuit potential of a metal as a result of current across the electrode/electrolyte interface. As (conventional) current leaves the anode and enters the electrolyte, chemical reactions take place. These reactions can retard the current flow from the anode and therefore reduce corrosion. The same is true at the cathode. As the current re-enters the metal at the electrolyte/cathode surfaces, these electrochemical reactions can retard the movement of current (ions) in the electrolyte. The effect is that the surface of the cathode will become more negative as the anode becomes more positive in potential. Polarization at the pipeline (cathode) will be critical for achieving adequate CP. Polarization and its relationship to taking potentials to determine adequate protection will be discussed in detail in later chapters.

1.4.3 Acidity and alkalinity (pH)

Whether an environment is acidic, alkaline or neutral in pH is critical to understanding the corrosion and protection process of metals, in particular CP. The definition of pH is the negative logarithm of the base 10 of the hydrogen ion concentration. This is denoted by $pH = -\log[H^+]$. The pH scale

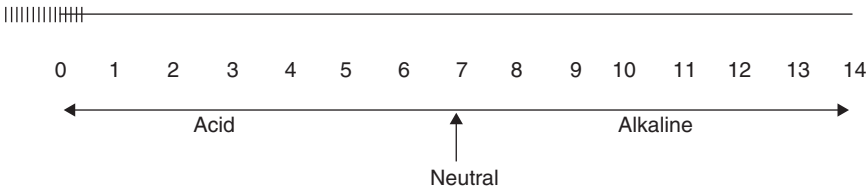

1.5 pH chart [pH = –log(H^+)] – Low pH (less than 7) is acidic [more H^+ ions], 7 is neutral and high pH (above 7) is alkaline [more OH^-].

(Fig. 1.5) is a representation of whether there is an excess of hydrogen ions (H^+) or hydroxyl ions (OH^-) present in the electrolyte. The more hydrogen ions are present in an electrolyte, the more acidic is the solution. Hydrogen ions are hydrogen atoms that have lost its one electron, so it now has a positive charge of one. The H^+ now becomes a great electron acceptor because is seeking to replace the lost electron. As shown, the ions (H^+) are attracted to the cathode where the freed electrons from the oxidation process at the anode are forced to the surface of the cathode to be consumed by these ions (H^+). The more acidic the solution the more corrosive the environment becomes (typically).

Amphoteric metals (zinc, aluminum and lead) can corrode in high or low pH levels. A high pH breaks down the protective oxide barriers that form on these metals. Since CP will create a high pH environment at the cathode, these protective CP potentials for metals must be kept to a minimum so as not to build an excess hydroxyl environment around these metals. If the CP is interrupted these metals can corrode quickly. This will be discussed in the chapter on CP.

1.5 Reference cells

Potential values between metals can be determined by comparing metal potentials to reference cells. A reference cell is a combination of a metal electrode in a solution containing a specific concentration of its ions. This will give a reproducible measurement that can be used as the stable half of the cell in a measurement when connected through a volt meter to an immersed metal. Table 1.1 gives the values of some of the standard reference cells used in the pipeline industry. There are others, but these are the most popular.

1.5.1 Copper sulfate

The copper sulfate electrodes ($Cu/CuSO_4$) are the favorite reference for pipeline corrosion control since they are very stable and rugged for field

Table 1.1 Common reference cells used in the pipeline industry as referenced to copper/copper sulfate

Reference Cell Type	Voltage Comparison
Copper/copper sulfate (CSE)	0 V
Silver/silver chloride (SSC)	−50 mV (−0.050 V)
Saturated calomel (SCE)	−70 mV (−0.070 V)
Zinc (ZN)	−1100 mV (−1.100 V)

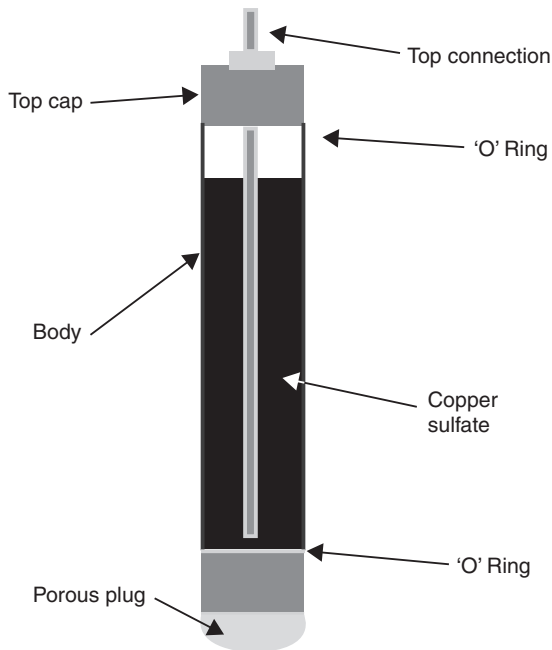

1.6 Copper/copper sulfate reference cell – the copper/copper sulfate electrode is the most popular reference cell for land laid pipelines and those in fresh waters.

use (Fig. 1.6). Most standard CP criteria to help determine adequate CP are related directly to the $Cu/CuSO_2$. $Cu/CuSO_2$ is traditionally used on soils and in fresh waters. Use in chloride environments and other contaminates can cause the potential of the $Cu/CuSO_2$ to not be stable and provide the expected results.

The $Cu/CuSO_2$ needs to be verified for accuracy at some set time frame, according to the extent of use or when contamination is suspected. This

can be performed by simply placing the used reference in a non-metal container holding tap water and comparing the voltage difference between it and a newly charged and working $Cu/CuSO_2$. The potential difference if more than 10 mV would indicate that the used cell needs to be cleaned and recharged as per company instructions.

1.5.2 Silver-silver chloride

The silver-silver chloride (Ag/AgCl) is typically used in salt water or other chloride environments. This cell can be either saturated or dry. The saturated Ag/AgCl refers to a saturated potassium chloride (KCl) electrolyte. The dry cell refers to a dry electrode immersed in seawater and the potential will vary as to the chloride content of the seawater. This will cause variations in potential reading when using dry electrodes in an electrolyte in which the composition changes, such as Ag/AgCl/seawater references in tidal estuary[2].

1.5.3 Zinc

Zinc has been used for stationary reference cells on pipelines and related structures. Zinc potentials can vary according to environment and time. Natural zinc oxides that form during the burial will change the potentials to one that is nobler than when the zinc were first buried.

1.5.4 Other references

Calomel is a mercury based reference used in laboratories. These are mercury electrodes in a specific concentration of mercury ions in varying concentrations of KCl. The hydrogen reference is very delicate and can be used only in laboratories. A variety of other metals have been used for reference electrodes, but these are not common for pipeline use. The use of reference electrodes will be discussed in later chapters.

1.6 Corrosion processes affecting pipelines

Corrosion on pipelines can take many forms. The forms of corrosion listed below are the more common types found in the pipeline industry. Most of these can be and are controlled by coatings, CP and other methods that will be discussed in detail later. Even when using these corrosion protection methods, corrosion can still be a problem if any of these fail to provide the protection intended. Many of the types of corrosion will lead to pitting and other localized corrosion.

1.6.1 Uniform corrosion

This type of general corrosion is characterized by an even, regular loss of metal from the corroding surface[3]. This is the type of corrosion you may see on older uncoated pipelines that did not have CP applied, or had CP applied after many years of service. There may be small areas where corrosion is more apparent with small areas of pitting, but the surface has an overall general loss of metal (Fig. 1.7).

1.6.2 Galvanic corrosion

The electrical potential difference in metals will cause a current (CC) to flow from the more negative (anodic) metal into the electrolyte to the more positive (cathodic) metal and return through the external path. A galvanic cell or dissimilar metal cell is the very basic corrosion cell and is seen in many applications where different metals are connected together in the presence of an electrolyte. The electromotive force (EMF) series (Table 1.2) is determined by measuring the potential of a metal in specified concentration of ions of that metal. The reason for this is that when a metal is in contact with a solution of its ions, equilibrium becomes established between a tendency for the metal to go into solution to increase the concentration of its ions and an opposing tendency for the ions to plate out on the metal and thereby reduce the concentration in solution[4]. These potentials are used to

1.7 Uniform or general corrosion on pipe surface.

Table 1.2 Partial standard EMF series of metals

Half cell	Metal	Standard electrode potential E^0 (V) *vs* SHE
Pt/Pt^{++}	Platinum	+1.200
Au/Au^{+++}	Gold	+1.498
Cu/Cu^{++}	Copper	+0.345
$H_2/2H^+$	Hydrogen	0.000
Pb/Pb^{++}	Lead	–0.126
Ni/Ni^{++}	Nickel	–0.250
Fe/Fe^{++}	Iron	–0.440
Zn/Zn^{++}	Zinc	–0.763
Al/Al^{+++}	Aluminum	–1.662
Mg/Mg^{++}	Magnesium	–2.363

Table 1.3 Galvanic series of metals in seawater

Most energy required (active, anodic, negative)	Potassium
	Magnesium
	Beryllium
	Aluminum
	Zinc
	Chromium
	Iron
	Nickel
	Copper
	Silver
Least energy required (noble, cathodic, positive)	Platinum
	Gold

establish the position of the metal in the series from more noble (positive) to more active (negative) metals. This information can be used to determine which metal would be the anode in that particular environment. One must remember that a change in the environment can change the position of a metal on the series.

The larger the potential difference, the more rapid the corrosion rate on the anodic metal. A galvanic series of metals can be determined for a variety of environments. Potential value of the metal in each electrolyte can be influenced by temperature, aeration, depolarizers and velocity of the electrolyte. Table 1.3 shows an abbreviated galvanic series of metals in seawater. The more active metal will be an anode and the more noble metal will be the cathode if these metals are connected together in this environment. Figure 1.8 shows a typical galvanic corrosion problem. A steel reducer is directly connected to a brass valve. This was a salt water disposal line and

1.8 Galvanic corrosion – internal corrosion caused from using a brass valve and steel reducer in a salt water disposal system in east Texas. This reducer had to be changed every 2–3 weeks!

so internal corrosion was caused from the galvanic difference between the brass (cathode) and steel (anode). This reducer had to be replaced every few weeks.

Welding processes can cause galvanic cells. The welding process and types of welding rods, etc. can cause electrical differences that can allow corrosion to develop either in the weld metal or the immediate surrounding area of the heat affected zone. This corrosion problem can occur internally or externally on pipelines.

1.6.3 Concentration cells

A cell may also be formed when two electrodes of the same metal are connected while lying in electrolytes that contain different substances or the same substance in different amounts.[5] Differences in salt concentration along a pipeline can cause one area to become anodic to another area. Typically, anodic sites will be formed in the higher salt concentration, unless it is a salt of the metal (not typical in pipelines). Oxygen and concentration cells formed from salts are responsible for up to 90% of corrosion in soils and natural waters.

Oxygen concentration cells cause many corrosion problems on pipelines. The areas of high oxygen concentration become cathodes and areas of low oxygen concentration become anodic areas. These concentration cells can occur at many locations along a pipeline such as:

- Ditch lines where the pipe lays on the bottom of a ditch with loose soil around the pipe will allow more oxygen on the top and sides of the pipe. In this case the bottom of the pipe will have low oxygen concentration and become the anode.
- Where pipelines pass under a road, slab, etc., there will be an oxygen concentration difference. The area just under the road will have a lower concentration of oxygen (becoming an anode) than the adjacent area just outside the edge of the road where oxygen is more available. The natural process is for the excess of oxygen to be reduced to balance the amount to the same concentration on each side, but oxygen can continue to easily penetrate the soil just outside the road edge, accelerating the corrosion just under the edge of the road. This was a major corrosion problem for pipelines before good coatings and CP were used, and it is one reason why road casings have become popular.
- Oxygen concentration can be a major problem where the pipe goes into the ground or water. Since there is a major difference in the concentration level at the soil surface than just under the soil, the anodic area will be just below the soil surface. The same principle will work where the pipe enters or leaves water environments where wave action brings a higher concentration of oxygen just above the water line than just below.
- Oxygen concentration cells can occur inside the pipeline also. In natural gas pipelines, five parts per billion of oxygen is enough to cause corrosion if water is present. This is why natural gas pipelines must control the amount of water and oxygen received from the producer. Bacteria and other microbiologically influenced corrosion (MIC) can accelerate the corrosion process when they cause nodules or other build-ups that can cause oxygen concentration differences.
- Oxygen concentration cells can develop in cervices that hold electrolyte, contaminants, bacteria and other debris that prevents oxygen from penetrating to certain areas, but just outside these areas oxygen is freely available. Cervices created by bolting (Fig. 1.9), flanges and poor welding techniques are potential areas for crevice corrosion. CP shielding caused by disbonded coatings (Fig. 1.10) will create crevices that become unprotected areas on coated buried or immersed cathodically protected pipelines.

1.6.4 Temperature cells

Corrosion cells can develop when one area of a pipe is at a different temperature than another area. The higher temperature will be anodic to the lower temperature areas. Gas transmission lines emerging from compressor stations will be higher in temperature than downstream where the gas will

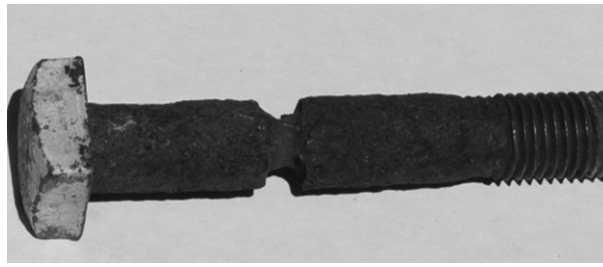

1.9 Crevice corrosion on flange bolt – Debris had settled in the horizontal flange causing crevice and oxygen concentration corrosion on all the bolts in the flange assembly.

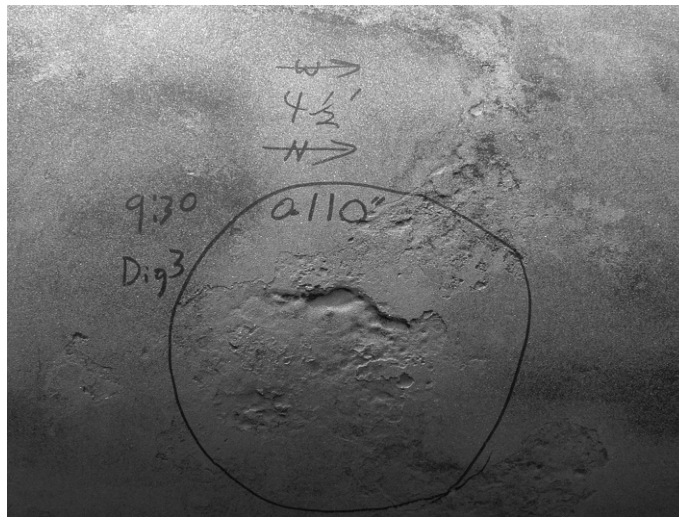

1.10 Corrosion pitting on pipeline – corrosion pitting on a pipeline caused by disbonded and CP shielding pipeline coating.

cool. There are also many areas around the world where high temperature production is required or the product must be heated to move the product in the pipeline.

Another important issue is that the higher temperature can cause coating damage. If proper coatings are not used in these areas several corrosion issues can develop such as:

- Certain coatings will cold flow toward the bottom of the pipe leaving metal exposed on top of the pipe. If adequate CP is available these areas will be protected, otherwise corrosion will develop. There have been

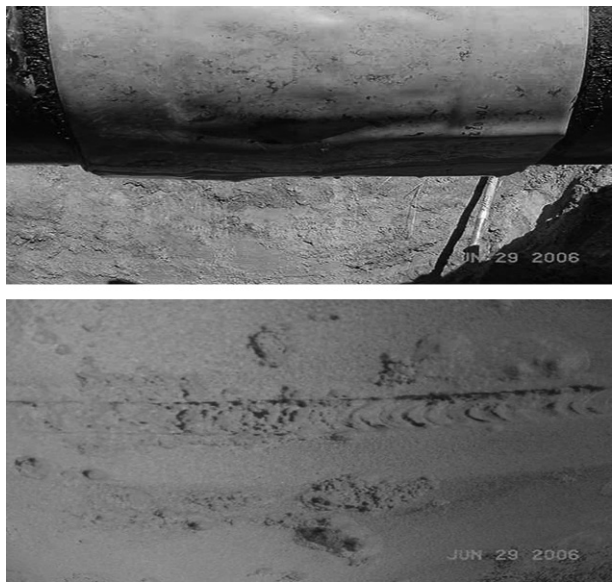

1.11 Failed shrink sleeve adhesion allowing electrolyte to enter and corrosion to proceed under the sleeve. Sleeve was applied in 1997 and failure located in 2006. The above ground potentials exceeded all NACE and ISO criteria.

cases where the pipe is in a casing and is shielded from the CP by the casing, allowing atmospheric corrosion to develop. This corrosion can go undetected until failure or is located by internal line inspection (ILI) tools.

- Shrink sleeves (Fig. 1.11), solid film backed tapes, extruded polyolefin and other CP shielding coatings can disbond or the adhesive compounds can cold flow to the bottom of the pipe leaving the top with a high dielectric strength barrier that allows water to penetrate between the remaining coating and the pipe, while blocking CP current. Once the coating disbonds (loses adhesion) oxygen concentration, bacteria and other factors can accelerate corrosion in these shielded areas. Some coating types have been proven to allow CP to be effective even when disbondments occur. When selecting a pipeline coating, the non-shielding characteristics may be more important than the other issues normally considered[6].
- Higher temperature pipelines may require more CP current to polarize the pipeline to a protected level.
- Internally, the higher temperatures can cause cells to develop according to the product and other variables.

1.7 Environmental cracking

Environmental cracking is a spontaneous brittle fracture of a susceptible material (usually itself quite ductile) under tensile stress in a specific environment over a period of time[7]. Two types of environmental cracking that are a problem for pipelines are stress corrosion cracking (SCC) or hydrogen induced cracking (HIC). In most environments, these are not the major cause of most pipeline failures but can be very dangerous.

1.7.1 Stress corrosion cracking (SCC)

SCC is an anodic process in which there is little metal loss or general corrosion (Fig. 1.12). There is an induction period where microscopic cracking can nucleate, followed by actual propagation that can be caused from corrosion developing in the cracks. These may be self-arresting or can continue to develop until failure. Four factors determine whether either of these potent environments can develop at the pipe surface: coating, soil, CP, and temperature[8]. SCC may be associated with intergranular paths through the metal and, in some cases, with a mixture of those modes[9]. The mechanism of SCC will be discussed in more depth in other chapters.

Two types of SCC are seen on the external surfaces of pipelines, high pH and near neutral pH cracking:

1. High pH SCC development involves four stages: (i) Coating disbondment occurs, allowing electrolyte to penetrate between the coating and the pipe, providing the final piece for corrosion to begin. (ii) This corrosion may then allow cracks to initiate. (iii) Initiation of cracks can continue, grow and coalesce. (iv) Larger cracks coalesce and final failure occurs[10]. For 'high' pH SCC to occur, the electrolyte under the coating has to be in a concentrated carbonate-bicarbonate solution with a pH range of 9.5–11.5. High pH SCC occurs in a potential range of –0.60 to –0.75 V *vs* a copper sulfate reference (CSE) at room temperature.
2. The near neutral pH SCC involves groundwater containing CO_2 where SCC can occur when there is inadequate CP current under a shielding coating, high resistant soils, or inadequate CP. CO_2 and the effects of CP are also important in the formation of high pH SCC under CP shielding coatings. Four factors determine whether either of these potent environments can develop at the pipe surface: coating, soil, CP, and temperature[11]. The potential for 'near' neutral SCC will be in the range of the native steel potential in a de-aerated solution and solutions pH range is from 5.5 to 7.5. Both the potential and pH for this form of cracking imply that current from the CP system does not reach the pipe surface[12]. If

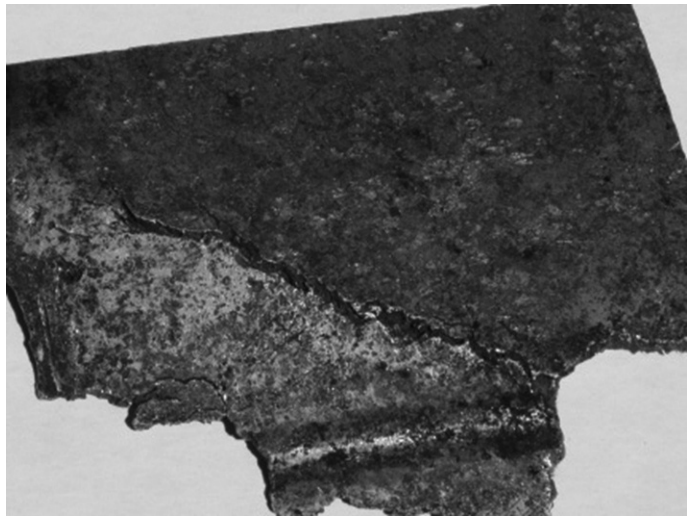

1.12 Stress corrosion cracking – SCC of stainless steel pipe. SCC occurred on the external surfaces of the pipe. Many small cracks are not visible on the b/w photo.

the disbonded coating is 'CP shielding' then the electrolyte environment under the coating will likely stay in this range.

3. As indicated above, CP shielding coatings are an important factor in external SCC on pipelines. CP current is shielded by the high dielectric strength coatings that have lost adhesion, allowed electrolyte to enter between the coating and the pipe. Since the CP is shielded by the coating, the potential cannot effectively take the coating out of the SCC potential range.

SCC is a problem that may develop for reasons other than those mentioned above, but this will be discussed in depth in a later chapter.

1.7.2 Hydrogen induced cracking (HIC)

HIC is a cathodic phenomenon. Hydrogen is generated at the cathode of a corrosion cell. The hydrogen ions are reduced to hydrogen atoms. Hydrogen atoms are the smallest atom and can diffuse into the crystal lattice of the steel. Hydrogen embrittlement will become a problem if enough atomic hydrogen penetrates, causing loss of ductility and strength which can lead to cracking:

- Normal process of corrosion or galvanic CP will not typically cause HIC, but impressed current can produce enough hydrogen to create a

problem. Care should be exercised to avoid overprotection, which can result in coating damage and may promote hydrogen damage of susceptible steels[13].

- Most agree that a polarized potential more negative than –1.05 to –1.1 V ($Cu/CuSO_4$) has the potential for generating harmful hydrogen damage to coatings or pipe metal.
- As the underground pipeline industry moves to higher strength steel and more negative CP potentials to meet industry standards, the potential for hydrogen cracking and SCC will possibly increase.
- Hydrogen damage can also occur from the reactions that occur internally in a pipeline carrying certain products that contain hydrogen producing bacteria or in areas of high H_2S production. This will be discussed in a later chapter.

1.8 Microbiologically influenced corrosion

MIC can occur on the external or internal surfaces of pipelines. Several forms of MIC can affect a pipeline, but most of the problems are caused by a variety of bacteria. These bacteria can be aerobic or anaerobic in nature.

1.8.1 External corrosion

MIC is one manifestation of the effect on corrosion by soil bacteria[14]. In unaerated soils the corrosion can be influenced by sulfate reducing bacteria (SRB). These bacteria produce hydrogen sulfide that directly attacks the iron or depolarizes the cathode. Even in aerated soils, SRBs can still be a problem because certain areas can still maintain the organisms.

More CP current may be required to provide adequate protection to the external surfaces of the pipeline. Bacteria under disbonded, CP shielding pipeline coatings will cause accelerated corrosion in an area shielded from CP. Proper evaluation of the exposed external pipeline surfaces is critical to determining the actual cause of the corrosion. Too many times, the external corrosion is blamed on inadequate CP, when more CP may not provide the needed protection because it is shielded by disbonded coating.

1.8.2 Internal corrosion

Corrosion on metals is closely associated with the formation of complex microbial biofilms on the surfaces[15]. One process inside of pipelines is that the SRBs will use the product for a food source and produce H_2S

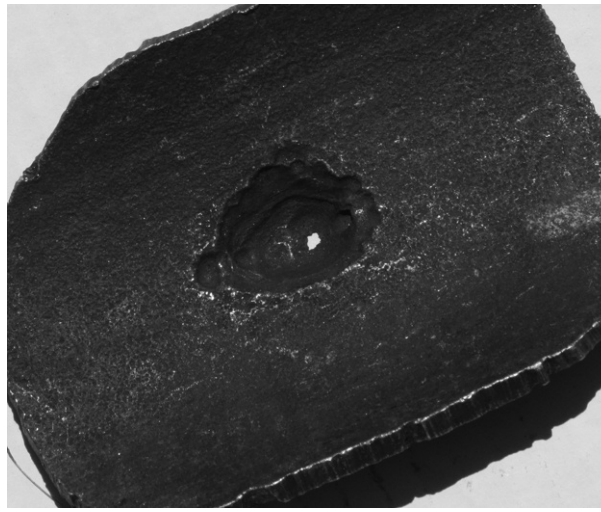

1.13 Typical corrosion from SRB – this corrosion caused from SRB's was on the internal surfaces of an oil pipeline.

that mixes with any water in a pipeline creating hydro-sulfuric acid that is corrosive to the steel (Fig. 1.13). Certain bacteria can build nodules that can cause oxygen concentration cells, while providing an area that will also be acidic. As mentioned above, excessive hydrogen can be produced, which can lead to hydrogen embrittlement or cracking in some environments.

1.9 Corrosion protection methods: coatings

Corrosion can be prevented in many cases by a variety of methods. Normally, we use several protection methods at one time to control corrosion of pipelines. Different methods are used for external and internal corrosion. This section discusses the use of coatings. It is important to remember that corrosion prevention is not a simple task and involves a combination of design, implementation of the design through well written specifications, inspection and construction practices. Once the pipeline is installed, the system must be monitored to ensure that all the corrosion prevention methods provide adequate protection.

Coatings are considered the first line of defense against corrosion in the underground pipeline industry. The amount of corrosion protection provided by a particular coating system depends on many variables[16]. There are a variety of coating types and each has advantages and disadvantages that must be considered when selecting a coating, especially

when using CP. Pipeline coatings will be discussed in more depth in a later chapter.

The selection process needs to take into account the following:

- Plant applied or field applied.
- Storage, transportation, handling and construction environment.
- Operating conditions of the pipeline (temperature, life, environment, CP, etc.).
- Failure mode of the coating (CP shielding or non-shielding if disbondments occur).

Types of plant-applied coatings include the following:

- Fusion-bonded epoxy (FBE) is the most popular plant-applied coating for North America and the UK countries. FBE is also used for the base coating of three-layer coating systems. A typical FBE formulation consists of epoxy resins, curing agents (hardeners), catalysts and accelerators, prime and reinforcing pigments, control agents (for flow and stability), and specialty ingredients[17]. Each formulation of FBE has different characteristics that must be considered when selecting a particular type. Pipeline owners or their representatives must be aware of these product differences and the way in which they impact performance[18]. One of the most important properties of FBE is that the failure mode is non-shielding to CP if disbondments occur and water penetrates (Fig. 1.14**).** Neither external corrosion nor SCC has been a problem under FBE coatings since CP can effectively protect the pipeline under any disbondments.
- Three-layer coating systems were first used in 1980 and have become popular in many countries. These systems usually consist of a FBE first layer, a modified polyolefin layer (tie layer) to chemically bond to the FBE and a thick top **layer of poly**olefin:
  - For temperatures up 80°C (175°F) polyethylene is commonly used.
  - For temperatures above 80°C (175°F) to 110°C (230°F) polypropylene is used.
- Coal tar enamel was the most popular plant-applied coating until the 1980s when FBE and three-layer coatings become more popular. Health concerns also caused some to stop using these products.
- Other plant-applied coatings are extruded (crosshead die and side extrusion) polyolefin over adhesives, asphalt, tapes and a variety of liquid coatings.

Types of field applied coatings include the following:

1.14 Fusion-bonded epoxy coating systems are known to be 'non-shielding' to CP current if disbondment or blistering occurs, therefore it is rare to find external corrosion or SCC on FBE coated pipelines with adequate CP. Photo shows poor adhesion and water under blisters, but no corrosion and a pH of 12.

- FBE can be applied in the field, but typically only on the girth weld area.
- Tape coatings have been used since 1950 as field applied coatings. These were made with a solid film backing of polyolefin or polyvinyl chloride (PVC) with a bituminous or butyl compound for the adhesive. These had and still have a problem with CP shielding when there is a loss of adhesion, and water seeps into the disbonded area between the coating and pipe, allowing CP shielding corrosion to occur.
- Geotextile (mesh) backed tapes have been in the industry for over 24 years without the same problems as the solid film backed tapes or shrink sleeves. These are now more popular (in many markets) than the solid backed tapes and shrink sleeves since they do not have the same problem with CP shielding, and the backing resists soil stresses that can cause wrinkling and disbondments[19] (Fig. 1.15**).** Because of the ease of application these are becoming more popular for girth weld on new construction (FBE or three-layer) and for rehabilitating existing pipes.
- Two-part epoxies have now become very popular for a girth weld coating on new pipe and for rehabilitation of failed coatings.
- Shrink sleeves became popular in the 1980s, but are losing favor because of CP shielding if there is a loss of adhesion. These are used for girth welds on new pipe and somewhat for rehabilitation.

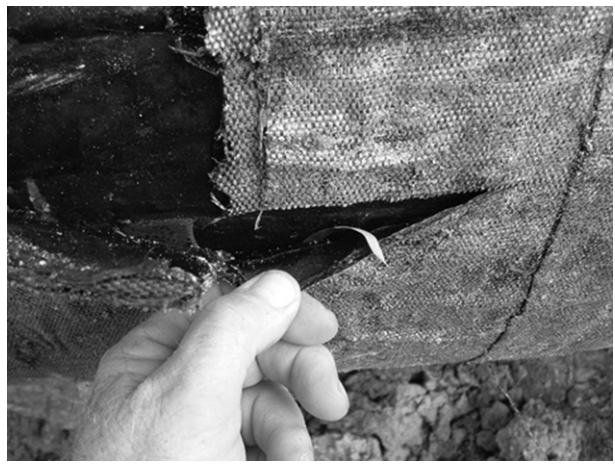

1.15 Geotextile (mesh) backed tape shows to be non-shielding to CP when a rare loss of adhesion occurs. This case shows the pipe with no corrosion after poor application technique was used allowing electrolyte to penetrate between the coating and the pipe, but the pH of the electrolyte was 10 after over 3 years of service proving CP was able to protect under this type of disbonded coating system.

- There are a variety of other coating types such as coal tar urethanes and other liquid coatings.

1.10 Corrosion protection methods: cathodic protection (CP)

CP is a technique to reduce corrosion on a metal surface by making the entire surface (to be protected) a cathode, which means it will be receiving protective current and cannot be corroding. DC is forced onto all surfaces of the pipeline[20]. There are many issues with applying and monitoring CP. These will be discussed in detail in later chapters. Bear in mind that CP can protect the pipeline only if it can actually find a path to the pipe. An electrical shield can be defined as any barrier (disbonded coatings, rocks, metal, etc.) that will prevent or divert from a pipeline, for which protection is intended, the flow of CP current from soil or water[21].

1.10.1 Galvanic CP

Galvanic CP uses the natural potential differences between the galvanic anode and the pipe to provide protection to the pipe.

1.10.2 Impressed current CP (ICCP)

Impressed current CP (ICCP) uses a power source to move the current from a very noble anode material to protect the pipe. Unlike galvanic anodes, impressed current anodes are typically nobler than the pipe. There must be a power source, such as a rectifier. Impressed current can cause interference with other metal structures in the area and lead to very rapid corrosion of the foreign structures.

1.10.3 Electrical isolation

Proper use of electrical isolation will enhance the CP system by ensuring that only those components that need to be protected are connected to return the protection current. This subject will be further discussed in later chapters.

1.10.4 Corrosion protection methods: internal line inspection (ILI) and internal control

One of the best instruments developed in the last 40 years is the ILI tools. Advancements in these tools have given the industry an opportunity to locate areas of corrosion and SCC that occur on pipelines. Though not 100% accurate, these tools are advancing in their ability to locate and identify internal and external corrosion before pipeline failures occur. The newest technology uses electro-magnetic acoustic transducer (EMAT) technology that can find SCC. One advancement in this method can also locate disbonded coating which allows the pipeline owner to be proactive instead of reactive to potential external corrosion and SCC which occur under CP shielding disbonded coatings.[10]

Control of internal corrosion is a complicated field of corrosion control that uses a combination of many methods of protection. An inhibitor is defined as 'A substance which retards corrosion when added to an environment in small concentrations'.[22] Inhibitors are used to help control corrosion on the internal surfaces of pipelines. Bactericides are used to help control the various bacteria present in many pipeline products. Pigging to clean pipelines to remove contaminants, water, wax and other detrimental materials in a pipeline are many times the most useful tool available for controlling internal corrosion. Coupons and other monitoring methods are used to help determine if these methods are successfully controlling the internal corrosion.

1.11 Conclusion

Even with all the modern pipeline construction practices, better coatings, more extensive CP and other methods of corrosion control, the pipeline industry continues to have corrosion (external and internal) on pipelines. Overall, the industry has definitely improved protection methods and reduced the extent of corrosion. Corrosion control will continue to be an ongoing process that needs to be continually monitored and improved to protect our communities, environment, and company assets. As natural resources are becoming more and more valuable, losses must be kept to the minimum as the industry strives to become perfect (which will not happen) in its corrosion control effort.

Many variables must be considered in corrosion control. The purpose of this book is to offer the industry a guide provided by experts in the various fields of corrosion control in an effort improve the daily process of protecting our infrastructure, environment and communities. Continual improvement of the process of corrosion control involves a better understanding of why we continue to have corrosion. Each environment, each material of construction, each monitoring technique, each protective method must continue to be studied and conventional thinking and methods challenged when these do not solve the problems.

1.12 Sources of further information and advice

Below are some of this author's source materials recommended for those learning the basic principles of corrosion control:

- *Cathodic Protection Survey Procedures*; NACE International Publication.
- *Coatings in Conjunction with Cathodic Protection*; NACE International Course Manual.
- *Corrosion Basics – An Introduction*; NACE International Publication.
- *Corrosion Inhibitors*; NACE International Publication.
- *Corrosion Prevention by Protective Coatings* – Second Edition; NACE International Publication.
- *Fusion-Bonded Epoxy (FBE) – A Foundation for Pipeline Corrosion Protection*; NACE International Publication.
- *Forms of Corrosion – Recognition and Prevention*; NACE International Publication.
- *Localized Corrosion*; NACE International Publication.
- NACE International Course Manuals for Cathodic Protection Tester, Technician, Senior Technician and Specialist.

- *Peabody's Control of Pipeline Corrosion* – Second Edition; NACE International Publication.
- *Uhlig's Corrosion Handbook* – Third Edition; John Wiley & Sons, Inc. Publication.

1.13 References

1. F. L. LaQue, *Corrosion Basics – An Introduction*, NACE International Publication, Chapter 1, page 5.
2. F. J. Ansuini and J. R. Dimond, 'Factors affecting accuracy of reference electrodes', *Materials Performance* Vol. **33**, No. 11, pp. 14–17 (November 1994).
3. C. P. Dillon, 'Forms of corrosion – recognition and prevention', NACE International, p. 1 (1982).
4. F. L. LaQue and N. D. Greene, *Corrosion Basics – An Introduction*, NACE International Publication, Chapter 2, p. 33.
5. A. W. Peabody and M. E. Parker, *Corrosion Basics – An Introduction*, NACE International Publication, Chapter 10, p. 205.
6. R. Norsworthy and Chic Hughes, 'Proven protection', World Pipelines (October 2007).
7. H. L. Logan, *Corrosion Basics – An Introduction*, NACE International Publication, Chapter 6, p. 111.
8. 'External stress corrosion cracking of underground pipelines', NACE International Publication 35103, Item No. 24221.
9. R. Parkins, 'Stress corrosion cracking', *Uhlig's Corrosion Handbook*, Third Edition, John Wiley & Sons, Inc., Hoboken, New Jersey, Chapter 14, p. 171 (2011).
10. R. Norsworthy, M. Jurgk, J. Grillenberger and C. Heinks, 'Importance of locating disbonded coatings with electro-magnetic acoustic transducer technology', Corrosion Paper C2012-0001673 (2012).
11. 'External stress corrosion cracking of underground pipelines', NACE International Publication 35103, Item No. 24221.
12. T. Jack, 'High consequence, low probability risk', Banff Pipeline Workshop (2011).
13. J. A. Beavers and K. C. Garrity, '*Peabody's Control of Pipeline Corrosion*', Second Edition, NACE International Publication, Houston, Texas, Chapter 4, p. 51 (2001).
14. R. L. Bianchetti, '*Peabody's Control of Pipeline Corrosion*' Second Edition, NACE International Publication, Houston, Texas, Chapter 5, p. 97 (2001).
15. J. D. Gu, T. E. Ford and R. Mitchell, 'Microbial degradation of materials: General processes', *Uhlig's Corrosion Handbook*, Third Edition, John Wiley & Sons, Inc., Hoboken, New Jersey, Chapter 26, p. 352 (2011).
16. R. Norsworthy, 'Selection and use of coatings for underground and submersion service', *Uhlig's Corrosion Handbook*, Third Edition, John Wiley & Sons, Inc., Hoboken, New Jersey, Chapter 68, p. 985 (2011).
17. T. A. Pfaff, 'FBE serves a broad market', *Hart's Pipeline Digest*, p. 20 (October 1996).
18. J. A. Kehr, '*Fusion-Bonded Epoxy (FBE), A Foundation for Pipeline Corrosion Protection*', Chapter 2, p. 39.

19. R. Norsworthy, 'Establishing compatibility', World Pipelines (February 2007).
20. J. A. Beavers, '*Peabody's Control of Pipeline Corrosion*' Second Edition, NACE International Publication, Houston, Texas, Chapter 3, p. 22 (2001).
21. J. A. Beavers, '*Peabody's Control of Pipeline Corrosion*' Second Edition, NACE International Publication, Houston, Texas, Chapter 3, p. 33 (2001).
22. N. E. Hammer, 'Scope and importance of inhibitor technology', *Corrosion Inhibitors*, NACE International Publication, p. 1.

2

AC-induced corrosion of underground pipelines

B. TRIBOLLET, LISE/CNRS, France and
M. MEYER, GDF-Suez, France

DOI: 10.1533/9780857099266.1.35

Abstract: Pipelines buried in soil are protected by a thick organic coating complemented by cathodic protection (CP). In spite of this double protection, when these pipelines are in the vicinity of a high voltage AC electrical field, such as a power line or an electrical railway for instance, corrosion may occur at the location of coating holidays (or defects). This phenomenon may be explained by a faradic rectification due to a non-linearity of interface behaviour, and by the AC field effect, as well as the impact of the AC current transfer on the chemistry of the electrolyte near the interface in the presence of CP. This chapter presents a critical review of the fundamental understanding of the AC-assisted corrosion phenomenon, and also some laboratory investigation, such as the analysis of corrosion products obtained under carefully controlled AC-corrosion tests using Raman spectroscopy. The particular role of the green rust at the interface is highlighted.

Key words: faradic current, faradic rectification, AC corrosion, cathodic protection, green rust.

2.1 Introduction

Electromagnetic fields created by high level operational alternating currents in high voltage electric power lines or in AC-powered railway systems sharing in parallel, or crossing, underground steel pipeline right-of-ways, induce electromotive forces into these pipelines. Following several occurrences of deep pitting and leaks of pipelines associated with this induction effect, it has been recognized that it may lead to specific steel corrosion where there are defects in coatings due to the alternating current flowing between these coating weaknesses and the surrounding soil.[1–4] This phenomenon has some similarities with, but also differences from, the phenomenon of corrosion of metals in electrolytes when they are subjected to alternating current transfer at the electrolyte/metal interface. This type of metal corrosion has been known for some time[5] but was traditionally not considered to be a major corrosion process for steel. The term AC corrosion described the enhanced corrosion caused by an externally applied AC current, with

a frequency typically between 15 and 60 Hz. This type of corrosion is also called AC-enhanced corrosion, or AC-induced corrosion, usually contracted to AC corrosion.

With the fast development of industry and urbanization, the demand for energy requires the construction of an increasing number of high-voltage, high-power transmission lines and the laying of large diameter, high-pressure pipelines. These pipelines are set underground to preserve environmental conditions and their laying down in the soil follows secure procedures. Since underground structures are not easy to inspect under operational conditions, there is a need for reliable above-ground monitoring techniques and assessment criteria that can confirm the preservation of their integrity with regard to any potential damage threat, including corrosion damage (Fig. 2.1).

External damage due to soil corrosiveness may threaten the integrity of underground pipelines. Protection of these assets against external corrosion is insured by a dual system comprising an anticorrosion coating, aimed at preserving the steel from contact with the soil, and a CP system to ensure electrochemical protection of the steel at coating defects. Control of external corrosion through this dual system has a very long industrial track record and, since decades, CP criteria have been elaborated by pipeline operators for ensuring an effective protection in the absence of any electromagnetic-induction effect. However, research works in the 1990s showed that, when the AC influence occurs on thick polymer coated underground steel pipelines in conjunction with CP polarization, AC-induced corrosion may occur on carbon and low alloy steels, even when the pipeline steel is polarized to a DC potential satisfying the classical CP potential criteria of

2.1 Pipelines in the vicinity of high voltage electric power lines.

–0.85 V/Cu/$CuSO_4$ electrode (copper sulfate electrode, CSE) (see for example References 5 and 6).

In this chapter, only carbon steel material will be considered even if the problem exists also for stainless steel.[7] This corrosion problem is not yet totally solved, as shown by the number of recent papers published on this topic.[8–13] Indeed, there is no consensus on the mechanism of the phenomenon, particularly as it applies to corrosion in soils, and more specifically for underground coated pipelines subjected to CP. There is no more consensus on the extent of the effect of alternating current on underground metallic structures, i.e. on the kinetics on the corrosion process.

It is well known that when AC current is transferred, or an AC voltage is applied, to a metal/electrolyte interface, under charge transfer control or mixed control, a faradic rectification occurs, due to a non-linear relationship of the current–voltage characteristics of the interface. The rectification effect leads to a shift of the free corrosion potential, as well as to an increase of the interfacial kinetics.[14,15]

This particular enhanced corrosion can be explained at least in two ways:

- By virtue of the faradic rectification at the carbon steel/electrolyte (natural soil water) interface: by shifting the free corrosion potential of the steel towards more negatives values, it is assumed that the rectification effect decreases the cathodic polarization level at a given polarized potential value.
- The alternative excursion of AC signals in anodic and cathodic domains due to the AC interference: excessive excursion of the interfacial electrochemical potential in the anodic domain may lead to steel corrosion even though the DC CP level fulfils the CP criteria recommended for CP protection of non-AC interfered pipelines.

The first phenomenon may be examined by harmonic analyses of the electrode interface. In fact, the non-linear response of the electrode interface may be fully expressed by the sum of high order harmonic responses. The second process may be apprehended by simultaneous recording of the current and the potential on an electrode subjected to an AC voltage, or else to an AC current, perturbation. From the potential signal (including the ohmic drop due to the electrolyte resistance in series with the electrode interface characteristics), the 'true', i.e. IR-free, electrode potential and its time-wise variation will be evaluated.

Using, in addition, electrochemical impedance spectroscopy (EIS), together with an equivalent electrical circuit model of the metal/electrolyte interface, this true potential allows the evaluation of the instantaneous

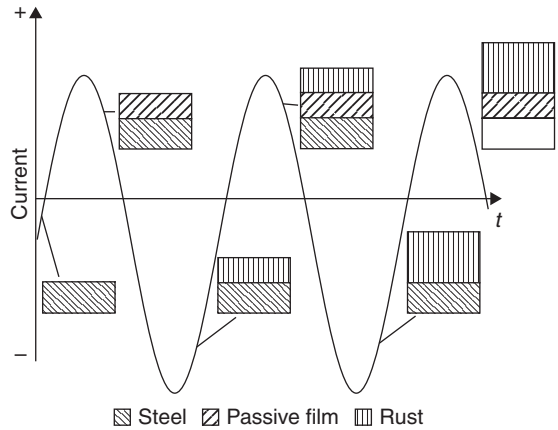

2.2 Schematic representation of the processes taking place on steel under AC interference.

current density used by the charge of the double layer capacitance. As a result, the faradic current, passing through the electrode interface under the AC perturbing signal will be evaluated.

A tentative explanation of AC corrosion was given by Büchler and Schöneich[16] according to the schematic representation given in Fig. 2.2. The authors suggested that the AC-corrosion phenomenon, on the cathodically polarized underground pipeline steels, may be attributed to destabilization of the pseudo-passive films that normally form at the external surface exposed to the ground at the coating defect, upon application of DC CP polarization of the steel. More precisely, as a consequence of the cyclic excursions of the steel electrochemical potential at the fundamental frequency of the AC perturbation, and assuming that the 'positive' excursion drives the steel surface potential in the so-called 'passivity domain', build-up of a protecting passive film occurs in the first anodic cycle while, assuming that the 'negative' excursion, in conjunction with the cathodic polarization, drives the steel surface potential below the stability domain of the passive film, it results in the reduction of the passive film. If, owing to the DC CP polarization of the steel surface, an alkaline environment is assumed at steel surface, the Fe(II) formed during the reduction of the passive film has only a limited solubility. As a consequence, it is accumulated on the metal surface, forming a porous rust layer. At each consecutive cycle a new passive film is formed underneath the rust layer, upon the 'positive' excursion of the steel surface potential, while the Fe(II) formed during the dissolution of the passive film, upon the 'negative' excursion of the steel surface potential, is added to the rust layer. Therefore, the thickness of the rust layer is increased

with every oxidation/reduction cycle. A metal loss is taking place due to such successive AC cycles, giving rise to passivation and dissolution of this passive film with every cycle.

Actually, it has been suspected, from several earlier research works on AC corrosion,[17,18] that the faradic current transferred at the steel/electrolyte interface, when subjected to an AC voltage, or else to an AC current, perturbation may be constituted of many processes. During the anodic excursion, the faradic current may be composed of the oxidation of part or all of the hydrogen adsorbed during the prior cathodic excursion at the electrode interface, the transformation of metallic iron into ferrous ions, and the oxidation of ferrous oxides into magnetite and/or ferric oxides. During this excursion, the electrode surface is likely to be covered, or partially covered, by an oxide film. Moreover, a fraction of ferrous species liberated may leave the carbon steel surface. During the cathodic excursion, the faradic current may include the reduction of the electrolyte, but also of the ferric oxides and magnetite, which should be reduced into porous ferrous oxides. Overall, the cathodic process tends to alkalinize the surrounding electrolyte whereas the anodic process rather acidifies it.

The purpose of this section is the quantitative determination of the various variables intervening in the corrosion process of carbon steel electrodes under cathodic polarization, in the presence of a high amplitude sine-wave potential modulation applied to the electrode, related to the practical AC-corrosion phenomena observed on underground coated-steel pipelines subjected to electromagnetic field interferences from perturbing systems transporting high alternating currents.

2.2 The origin of alternating voltage induced in pipelines

There is no controversy regarding the primary effect which triggers the AC-enhanced corrosion effect of underground coated-steel pipelines[19]: the alternating currents carried by the electric power circuit conductors (phase and shield wires) of any above-ground electric power line create a space- and time-varying magnetic field which couples to any extended structures such as underground steel pipelines laying in the vicinity, resulting in current and voltage induction upon the structure (see, for example, References 20 and 21).

Theoretically, the induced voltage and current levels on the pipeline are a function of the integral of the rate of change of the magnetic field with respect to depth, i.e., the limits of the integration are from the burial depth of the pipeline down to the ‘skin effect’ depth in the earth, which is on the order of several hundred metres depending upon the earth resistivity. Evaluating the integral over the area determined by the horizontal length

of the structure and the 'skin depth' is generally very difficult, since a closed form solution is not readily available.

An alternative, simpler computational method developed by Carson[22] utilizes the concept of a longitudinal electric field (LEF), which may be viewed as a distributed 'voltage source' (also called an 'electromotive force') in series with the impedance of the longitudinal electric conductor constituted by the metallic pipeline. The value E of the LEF is directly derivable from such usually known quantities as the transmission line geometry and current. The integral of the parallel component of the field at the location of the pipeline is evaluated along the length of the pipeline to obtain the voltage and current induced upon the pipeline.

The equivalence between the LEF and the time derivative magnetic field integral is established by Faraday's law. This law states that if a conducting loop is immersed in a time-varying magnetic field, B, the voltage induced in the loop is equal to the integral of the LEF along the loop, which, in turn, is equal to the integral of the time derivative of B over the area circumscribed by the loop, i.e.:

$$V = \oint E dl = -\oint \frac{\partial B}{\partial N} dA$$

For a horizontally positioned extended structure, such as a pipeline, the equivalent loop is positioned in the vertical plane with the upper horizontal side formed by the pipeline and lower horizontal side established by earth currents flowing at the skin depth, as depicted in Fig. 2.3.

Work developed by Carson allows the E value of the LEF to be determined in a straightforward manner. Integration along the length of the structure, with respect to dl, allows the voltage induced upon the structure, V, to be calculated. As a matter of fact, such a global calculation would apply only for a structure which is totally insulated from the earth and which has no leakage impedance to the earth and also has a zero series impedance along the longitudinal pipeline conductor.

Even when they are assumed to be 'perfectly' coated (i.e. without any coating defect), buried pipelines exhibit continuously distributed impedance (resistance and capacitance) to earth, together with a series impedance along their length, such that the calculation of induced voltage and current on the pipeline involves two basic steps. The first is to determine the distributed value E of the LEF existing at each location along the pipeline using Carson's computation method. The next is to model the pipeline as a distributed 'lossy' transmission line, having both a series impedance Z (per unit length of the pipeline), and a parallel admittance (per unit length of the pipeline), as well as a shunt impedance to remote earth at each of its ends.

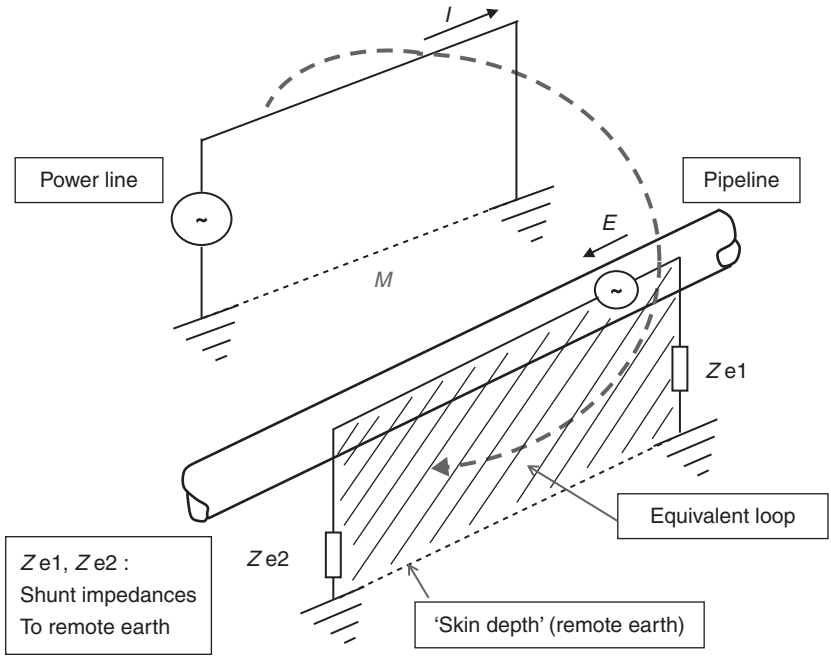

2.3 Representation of the magnetic couple between an electric power line and an underground steel pipeline, schematically represented as an equivalent loop with an earth return circuit.

The distributed voltage V along the pipeline length is then obtained by solving the well-known transmission lines differential equations relating E, V and the current I induced in the pipeline[23]:

$$\frac{dV}{dx} = E - IZ$$

$$\frac{dI}{dx} = -V.Y$$

where Z and Y are respectively the longitudinal series impedance and the transversal admittance.

As a general rule, the distributed LEF E (in V/m) induced by the current in the power line, at any location along the pipeline length, is expressed by the fundamental relationship:

$$E = I[M]\omega \qquad [2.1]$$

where

I is the current in the power line (A),
$[M]$ is the mutual inductance between the power line and the pipeline ($\Omega.m^{-1}$ s) (which has a matrix form to account for the magnetic coupling with each of the power source conductors), and
ω is the pulsation of the current (radian s^{-1}).

The mutual inductance $[M]$ is related to the geometry of the coupling, and can be considered, as a first approximation, to be inversely proportional to the square of the distance D between the line and the pipeline, and proportional to the soil resistivity.

The distributed LEF may be varying as a consequence of variation of the parameters M and D along the pipeline length.[24] On the basis of numerical simulations, commercial software is available that allows the determination of the distributed LEF $E(x)$ for each small section of the overall affected length of the pipeline, as well as solving the transmission line differential equations, and the determination of the distributed voltage $V(x)$, on account of the electrical characteristics of the coated pipeline and the geometry of the pipeline/electric power line shared right of way.[25] Theory predicts that for a straight pipeline parallel to a straight power line, voltage levels are highest at each of the pipeline ends and falls exponentially with distance from the ends, and that the two voltages at the pipeline ends are out of phase. In the case of more complex geometry, voltage peaks appear at each physical discontinuity, such as change in relative direction between pipeline and power line, change in distance to the power line, or phase change of the power line current due to an electrical discontinuity such as a power line transposition.[26]

If the coating were 'perfectly' insulating the steel pipe, the distributed voltage source would not generate any electrochemical current leakage from steel to soil. However, real buried pipelines most frequently exhibit coating defects. If, conversely, the coating presents a poor insulation property, such as in old coal tar or bituminous coated pipelines, the coating will generate uniform AC dispersion to the ground, which will cause a very low AC voltage between pipeline and remote earth and negligible AC leakage current densities, thereby not significantly creating any corrosion risk. On the other hand, when the coating exhibits discrete and small localized holidays, together with an overall high insulation resistance (in the range of $10^{10}\ \Omega m^2$ for polyethylene coatings, or even higher), the distributed voltage source, as a consequence of the electromagnetic coupling, leads at each coating holiday (or defect) to local AC current leakage from steel to earth, which may be high and may lead to the AC-enhanced corrosion phenomenon.

As the current leakage at each coating holiday is determined by the local value of the alternating voltage and by the impedance between the aperture

of the holiday and the remote earth, and as the alternating voltage variations along the pipeline length are in the end determined by the current circulating in the pipe wall section, alternating voltage and current values at coating holiday are highly coupled.

2.3 Electrical parameters affecting the AC-corrosion process

The noticeable primary phenomenon associated with the AC-corrosion process is the occurrence, at each coating holiday, of an alternating voltage difference between the pipe body and a 'remote earth' electrode. Therefore, at a given coating holiday, there are at least two 'macroscopic' electrical parameters describing the primary inductive effect (Fig. 2.4):

- the alternating voltage difference between the pipe body and a remote earth electrode U_{AC} (defined either by its root mean square (rms) or by its peak to peak value)

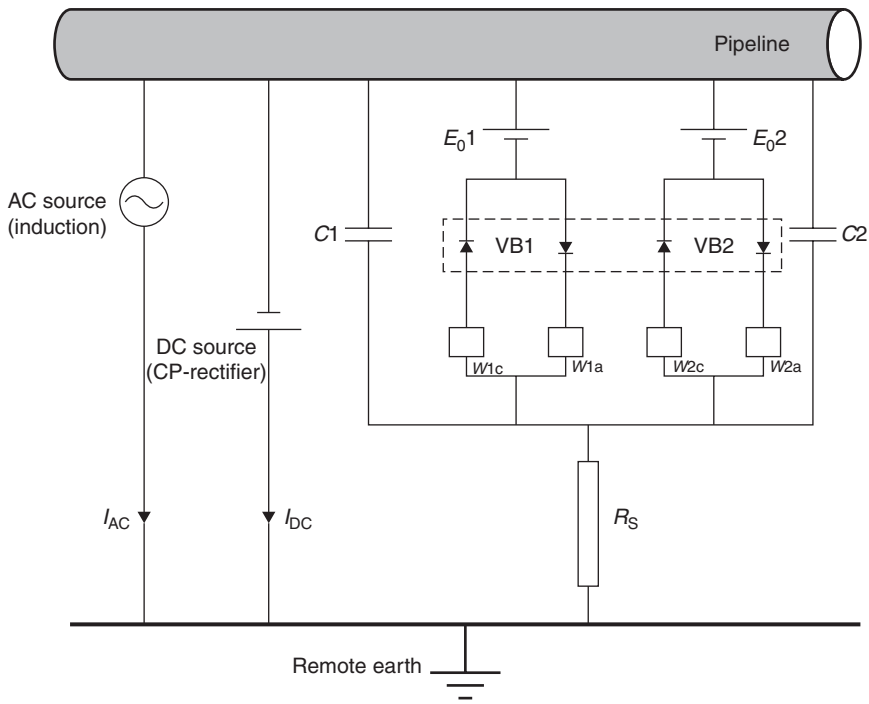

2.4 A general schematic equivalent circuit depicting the impedance between the steel to remote earth and including the AC voltage source (due to the electromagnetic interference) together with the DC source representing the cathodic protection rectifier. (*Source*: From Nielsen and Cohn.[27])

- the alternating current density I_{AC}, flowing through the holiday between its aperture and the remote earth.

Insofar as CP polarization is applied to the pipeline, two other 'macroscopic' electrical parameters may also be considered:

- the DC value of the voltage difference between the pipe body and a reference electrode located at the 'remote earth' designated as $E_{DC,ON}$
- the DC value of the current density I_{DC}, flowing through the holiday between its aperture and the remote earth.

2.3.1 Electrolyte resistance

The major effect of the electrolyte resistance R_E is to generate an ohmic drop equal to $R_E.I_{AC}$. If this resistance is the dominating term over the interfacial impedance, the effective voltage perturbation applied at the interface ('*I.R* free' voltage perturbation, designated here as U_{OFF}) is considerably reduced compared to the total voltage perturbation. At each holiday, the impedance between the steel surface and the remote earth may be represented schematically by the most general equivalent electrical circuit, shown in Fig. 2.4, as suggested by Nielsen and Cohn.[27] Assuming quasi-linear behaviour of the interface, this equivalent circuit may be simplified as shown by the circuit in Fig. 2.5, where the electrolyte resistance comprises the serial association of

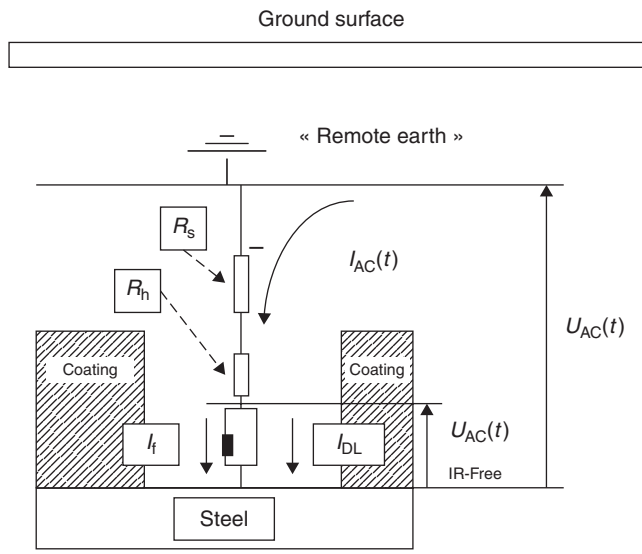

2.5 Simplified equivalent circuit model at one coating holiday, splitting the electrolyte resistance in soil and holiday components.

soil resistance R_S and the holiday resistance R_h, and the interfacial impedance is considered a charge transfer resistance R_t in parallel to a double layer capacitance C_{dl}.

By considering a coating holiday of cylindrical shape with diameter d, thickness coating e, and resistivity inside the coating holiday $\rho_{h,}$ the holiday resistance R_h is given by:

$$R_h = \frac{4\rho_h e}{\pi d^2} \qquad [2.2]$$

Assuming homogeneous resistivity of the soil, $\rho_{s,}$ this soil resistance is expressed by[28]:

$$R_s = \frac{\rho_s}{2d} \qquad [2.3]$$

2.3.2 Double layer capacitance

If the interfacial impedance is initially considered a charge transfer resistance R_t in parallel to a double layer capacitance C_{dl}, the ratio of the '*IR* free' voltage perturbation to the total voltage perturbation may be expressed:

$$\frac{U_{\mathrm{AC,IRFree}}}{U_{\mathrm{AC}}} = \frac{R_t}{R_t + R_E + j\omega R_t C_{dl} R_E} = \frac{1}{1 + R_E / R_t + j\omega R_E C_{dl}} \qquad [2.4]$$

From this expression, it appears that the '*IR* free' voltage perturbation is a fraction of the total voltage perturbation, which is highly dependent on the ratio R_E/R_t as well as on the parameter $\omega R_E C_{dl}$. A recent analysis attempted to take account of the effect of the electrolyte resistance and of the double layer capacitance on the AC-corrosion phenomenon.[29,30]

From the simultaneous recording of the instant voltage $U_{\mathrm{AC}}(t)$ and the instant total current $I_{\mathrm{AC}}(t)$, data analysis allows separation out of the faradic and the capacitive currents. This technique has been described in detail elsewhere.[14] In this work, the electrolyte resistance and the double layer capacitance could be evaluated by EIS. From evaluation of the electrolyte resistance, the instant IR-free voltage perturbation $U_{\mathrm{AC,IR\text{-}free}}(t)$ could be estimated. Also the current for the charging of the double layer I_{DL} could be evaluated, assuming a constant value of the interfacial capacitance C_{dl} by:

$$I_{\mathrm{DL}}(t) = C_{\mathrm{DL}} \left(\frac{dU_{\mathrm{AC,IRFree}}}{dt} \right) \qquad [2.5]$$

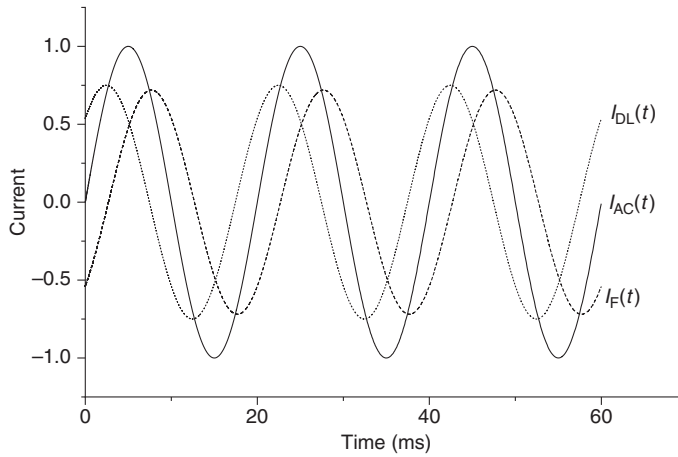

2.6 Contribution of the current for charging the double layer capacitance ($I_{DL}(t)$) and the faradic current ($I_F(t)$) on the overall current ($I_{AC}(t)$).

Hence, the faradic component of the current, $I_F(t)$, was obtained from:

$$I_F(t) = I_{AC}(t) - I_{DL}(t) \quad [2.6]$$

Figure 2.6 presents the respective contributions of the calculated currents I_{DL} and I_F to the overall current I_{AC}. It is expected, intuitively, that the contribution of the faradic current would tend to be much less than that of the charge of the double layer capacitance. However, it is observed that the I_{AC}, I_{DL} and I_F calculated amplitudes are almost of the same order of magnitude. This result can be explained by the presence of a phase shift between I_{AC} and I_{DL}, as is readily seen from Fig. 2.6. In others words, the double layer serves as the 'current reservoir' for the faradic process under AC polarization.

2.4 Harmonic analysis of AC corrosion

A simplified theoretical approach is presented in this chapter to illustrate one of the effects of the AC perturbation on the electrochemical behaviour of the interface,[31] disregarding the possible time-wise evolution of the interfacial chemistry, and hence the possible evolution of the interfacial kinetics. The electrochemical system is intrinsically non-linear, therefore the current response induced by a high AC voltage modulation is non-linear. Indeed, if we assume that the electrode process is controlled by

the activation energy only, the faradic current follows an exponential law with respect to the potential, such as would be expected for the anodic process:

$$I_a = I_{\text{corr},0} \exp(b_a(U - E_{\text{corr},0})) \quad [2.7]$$

where

b_a is the anodic kinetic coefficient (= $\alpha\, n\, F/RT$);
I_a is the faradic anodic current;
U is the interfacial potential;
α is the coefficient between 0 and 1;
n, F, R and T are respectively the number of electrons exchanged in the reaction, the Faraday number, the gas constant, and the temperature; and $I_{\text{corr},0}$ is the corrosion current in absence of AC perturbation.

In presence of an AC perturbation, if we assume in the frame of this simplified approach that: the interfacial medium remains unaffected by the AC perturbation, such that the activation controlled kinetics law depicted by Equation [2.7] above is not altered, then the potential signal at the electrode surface upon an AC voltage perturbation can be considered sinusoidal too, and may be written as:

$$U = U_0 + \Delta U \sin(\omega t) \quad [2.8]$$

ΔU represents the amplitude of the 'actual' AC signal, i.e. the interfacial IR-free voltage perturbation.

The instant faradic anodic current response can be expressed by:

$$I_a(t) = I_{\text{corr},0} \exp(b_a(U_0 + \Delta U \sin(\omega t) - E_{\text{corr},0})) \quad [2.9]$$

By the Taylor expansion of Equation [2.9]:

$$I_a(t) = I_{a,0}\left(1 + b_a \Delta U \sin(\omega t) + \frac{b_a^2 \Delta U^2 (\sin \omega t)^2}{2!} + \frac{b_a^3 \Delta U^3 (\sin \omega t)^3}{3!} + \ldots\right) \quad [2.10]$$

with $I_{a,0} = I_{\text{corr},0} \exp\left(b_a \left(U_0 - E_{\text{corr},0}\right)\right)$

The time-averaged faradic current is given by:

$$\overline{I_a} = \frac{1}{T}\int_0^T I_a(t)dt \qquad [2.11]$$

where T is the period of the AC current.

After some mathematical development as described in References 29, 32 and 33 we can obtain the following theoretical expression:

$$\overline{I_a} = I_{a,0}\left(1 + \sum \frac{b_a^{2n}\Delta U^{2n}}{2^{2n}(n!)^2}\right) \qquad [2.12]$$

The term $\sum \frac{b_a^{2n}\Delta U^{2n}}{2^{2n}(n!)^2}$ induces the so-called faradic rectification effect.

This equation shows that the mean faradic current density is related to the faradic rectification, which is itself induced by the even-number harmonics of the current response to the interfacial perturbation. The previous derivation is valid for a sinusoidal perturbation of the interfacial potential. If a sinusoidal perturbation of the overall potential is considered, the ohmic potential drop must be taken into account and the mathematical development is much more difficult.[34] From a qualitative point of view, the faradic rectification is always present.

2.4.1 Faradic rectification without oxygen

The mean faradic current is the sum of the mean anodic and cathodic currents assuming no interaction between the two processes. The two following reactions can be considered:

$$Fe \rightarrow Fe^{2+} + 2e^- \qquad [2.13]$$

$$H_2O + e^- \rightarrow \frac{1}{2}H_2 + OH^- \qquad [2.14]$$

If both the anodic and the cathodic currents follow a Tafel law, the Equation [2.12] can be applied for the two currents, so that the mean faradic current transferred to the interface can be written as:

$$\overline{I} = \overline{I_a} + \overline{I_c} = I_{a,0}\left(1 + \sum \frac{b_a^{2n}\Delta U^{2n}}{2^{2n}(n!)^2}\right) - I_{c,0}\left(1 + \sum \frac{b_a^{2n}\Delta U^{2n}}{2^{2n}(n!)^2}\right) \qquad [2.15]$$

At $U_0 = E_{\text{corr},0}$, by definition $I_{a,0} = -I_{c,0} = I_{\text{corr},0}$

If the Tafel coefficients b_a and b_c are equal, the mean value of the total faradic current transferred to the interface, given by Equation [2.15], is zero such that the corrosion potential is not modified by the AC perturbation. The mean current-mean potential curves are modified by the AC perturbation, as shown in Fig. 2.7a, and from Equation [2.12] the corrosion current can be written:

$$I_{\text{corr,AC}} = I_{\text{corr},0}\left(1 + \sum \frac{b_a^{2n}\Delta U^{2n}}{2^{2n}(n!)^2}\right) \qquad [2.16]$$

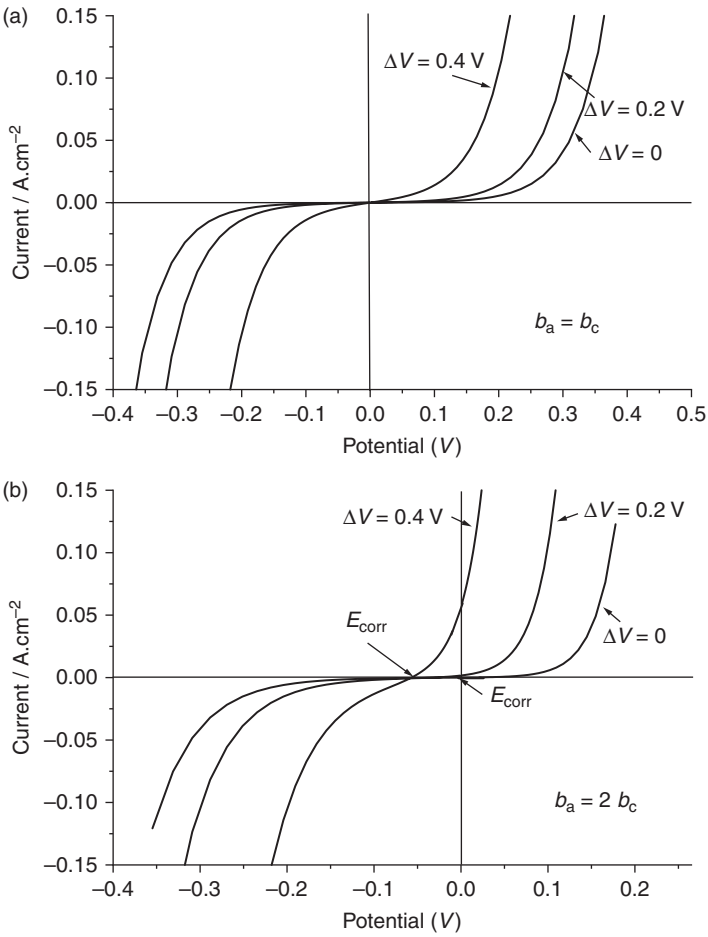

2.7 Current–potential curves derived under AC perturbation for a kinetic controlled only by Tafel kinetics (anaerobic medium). (a) $b_a = b_c$, (b) $b_a = 2\ b_c$.

If $b_a > b_c$ the faradic rectification has as a consequence less efficacy for the CP, because the corrosion potential in the presence of the AC perturbation is shifted towards more cathodic potential (Fig. 2.7b).

2.4.2 Faradic rectification with oxygen

The reduction of oxygen is:

$$O_2 + 2H_2O + 4e^- \rightarrow 4OH^- \qquad [2.17]$$

This reaction is mass-transport limited, and then the cathodic current can be written as:

$$I_{c,O_2} = \frac{1}{I_{O_2}^{-1} + I_{lim}^{-1}} \qquad [2.18]$$

where I_{O_2} is the kinetic current, which follows a Tafel law and, in the presence of AC perturbation, the corresponding faradic current–potential law is in the form of Equation [2.7]; I_{lim} is the limiting current of the oxygen; and the AC perturbation occurs at a too high frequency to affect the mass transport, so it can be assumed that I_{lim} is not modified by the AC perturbation.

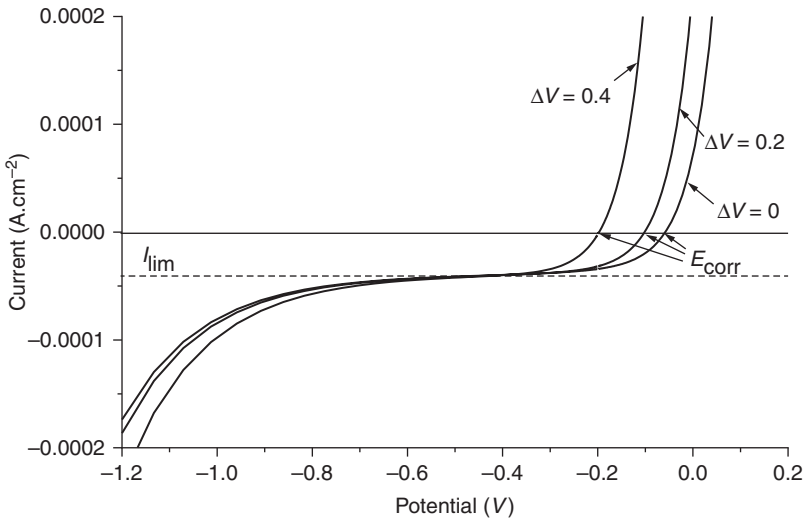

2.8 Theoretical current–potential curves derived under AC perturbation for a mass-transport limited cathodic reaction (aerobic medium).

The overall cathodic current is:

$$I_c = I_{c,O_2} + I_{c,H_2O} \quad [2.19]$$

If $b_a > b_{c,O_2}$, one can find that the shape of the current–potential curves is affected by the AC voltage perturbation as depicted in Fig. 2.8.

2.5 Cathodic protection of pipelines

It is now a well-known observation among the pipeline operators' community that the level of DC cathodic polarization applied to the steel has an effect on the AC-corrosion process as well as on the corrosion rate.[16,35–37] In particular, this phenomenon was studied in laboratory in quartz sand with artificial soil solutions. The tests results reported by the cited authors were run at variable DC on-potentials (on-potential means here potentials uncompensated for IR drops) of the CP system and at 14 and 30 V AC voltage perturbation (rms). In Fig. 2.9, the corrosion rate of all investigated coupons is plotted against the absolute value of the cathodic DC current density.

One of the most striking effects of the AC perturbation is that an increasing absolute DC current density results in increased corrosion rates, when

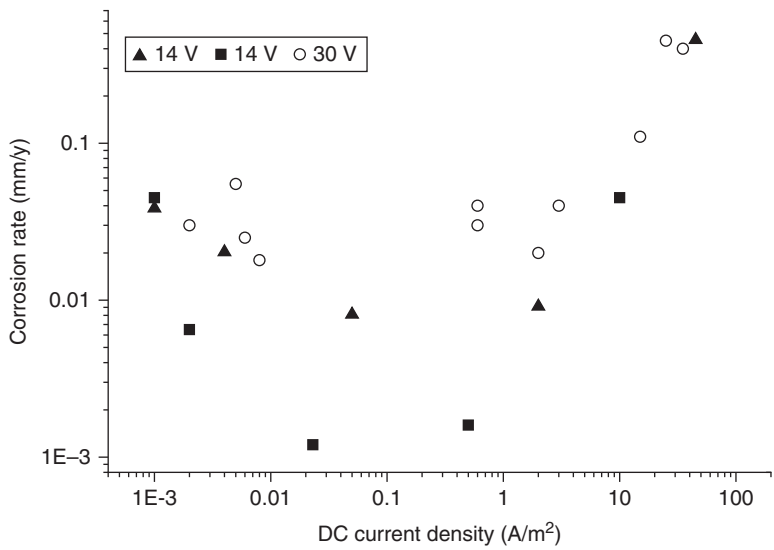

2.9 Corrosion rate of coupons at 14 and 30 V AC plotted versus the absolute value of the cathodic current density. (*Source*: From Reference 38.)

the DC current density is higher than 1 A/m^2. Conversely, at small cathodic DC current densities typically lower than 0.1 A/m^2, the corrosion rate increases when the absolute DC current density decreases, presumably due to an insufficient CP; however, the corrosion rates reached in this range of low DC current densities are far lower than the corrosion rates reached for high values of the absolute DC current density (higher than 10 A/m^2). This observation is in good agreement with the high corrosion rates observed in field applications at AC voltage below 10 V and at cathodic current densities more negative than −10 A/m^2, which shows high corrosion rates.[19] Hence, the question arises regarding the negative effect of the cathodic current on the corrosion rate.

2.5.1 Identification by Raman spectroscopy of corrosion products formed under AC corrosion[19,38]

Raman spectroscopy can be used to identify the nature of the primary corrosion products created in a short term exposure in laboratory conditions, when a cathodic protected carbon steel electrode immersed in aqueous medium is subjected to an alternative perturbation, under differently controlled conditions. In the experimental results reported in this section, a sinusoidal voltage signal was superimposed on the DC potential (at a selected cathodic potential level) and the Raman spectra were analysed. Figure 2.10 shows an example of the *in situ* Raman spectrum acquired at the steel electrode

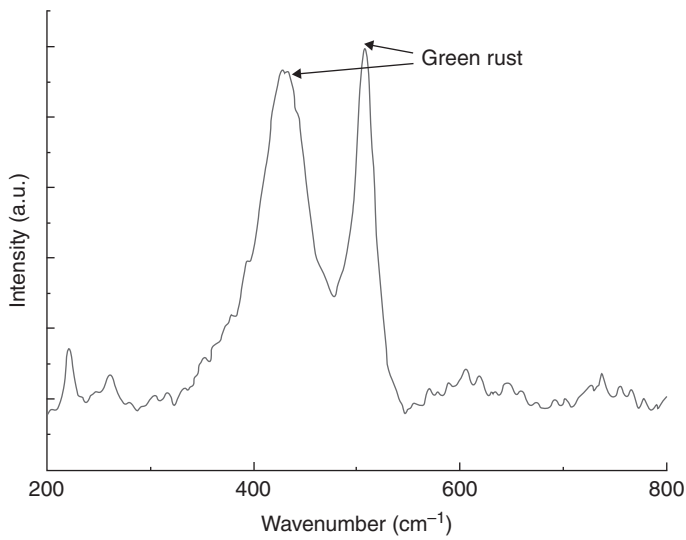

2.10 In situ Raman spectrum upon exposure of carbon steel to Evian water (U_{CP} = −1 V/SCE, ΔU = 1 V).

surface exposed to aerated mineral water with well-defined mineral composition, with U_{AC} (peak to peak) equal to 1 V, and a CP potential set at –1 V with respect to a saturated calomel electrode (SCE). A green rust compound $\left(\left[Fe^{II}_{1-x}Fe^{III}_{1}(OH)_2\right]^{x+}\left[x/n\,A^{n-}\,m/n\,H_2O\right]^{x-}\right)$ is observed after 30 min exposure to the test solution. The green rust is the first corrosion product observed, and this compound is quickly transformed into lepidocrocite (iron III oxide).

In another experiment, the *in situ* Raman spectrum was collected after 2 h of exposure to an aerated alkaline aqueous solution (0.1 M NaOH + 0.5 M NaCl) having an initial bulk pH of 13, for an applied alternative voltage perturbation equal to 6 V (peak to peak) and a cathodic potential 'ON' at –0.9 V/SCE. In this test, only the characteristic spectrum of magnetite, Fe_3O_4, is observed (Fig. 2.11). This result recalls, as was highlighted elsewhere,[39] that in a sufficiently alkaline aqueous solution, the green rust compound is no longer observable. This may be explained either by the fact that this species is not formed in significant amounts, or that it is rapidly transformed in magnetite. Whatever the mechanism, this experiment allowed the observation of corrosion under a significant rate (estimated always higher than 100 μm/year), even though the magnetite compound is developing at the steel/solution interface.

In contrast to this last test, a similar AC corrosion in a short term test (for an applied alternative voltage perturbation equal to 6 V – peak- to- peak, and for a cathodic potential 'ON' at –0.9 V/SCE), was performed in pure

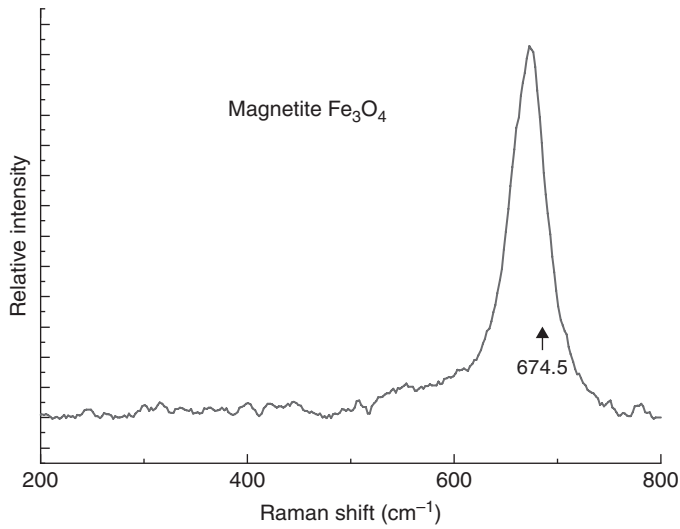

2.11 In situ Raman spectrum of steel in (0.1 M NaOH + 0.5 M NaCl) alkaline aqueous solution.

0.1 M Na OH aqueous solution without any chloride. In this case, perfectly passive behaviour was observed, with no development of any significant corrosion.

2.5.2 Interfacial pH

A constant interfacial chemistry has been hypothesized in the theoretical approach of the AC-corrosion phenomenon presented in Section 2.4. However, it is well known that, under CP with the influence of the alternating perturbation, a significant alkalization of the steel/soil interface takes place.[40–43] As this marked alkalization may increase the interfacial pH into the domain where soluble hypoferrites and soluble ferrate can form, according to the Pourbaix diagram, it may introduce a new corroding condition (see the very simplified diagram presented in Fig. 2.12).

The oxygen reduction promoted by the CP polarization induced an increase of the interfacial pH and leads simultaneously to a decrease of the solution resistivity at the immediate vicinity of the steel surface. However, notably, the diffusion of oxygen to the interface is similar to the diffusion of OH^- from the interface to the bulk, and so there is no accumulation with time of OH^- in the case where only the oxygen reduction is involved.

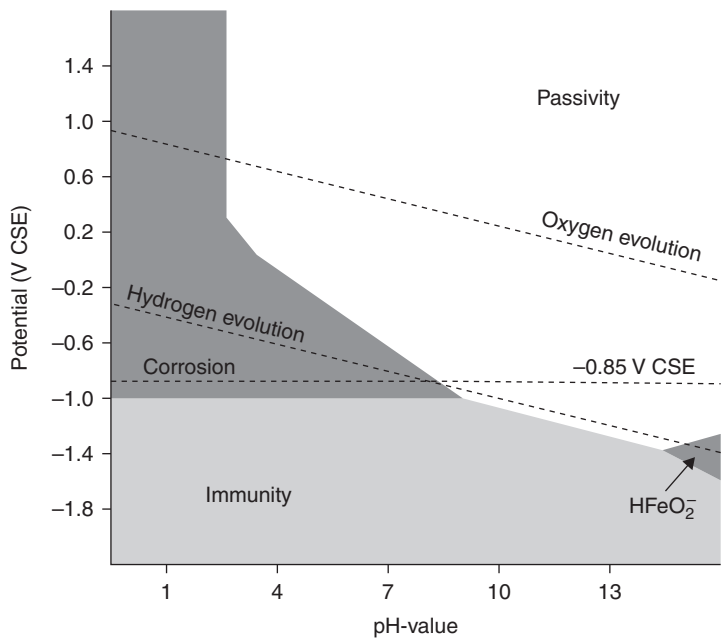

2.12 Pourbaix diagram.

It can by shown that, when CP polarization level is such that only the oxygen reduction is significantly promoted, the interfacial pH reaches a steady value which is limited according to dissolved oxygen concentration, as well as to dissolved CO_2 in the bulk electrolyte, in the range of pH = 9–10.6 when the electrolyte is aerated from the atmosphere (see Reference 44). However, an increase of the AC current density can trigger the onset of a significant promotion of water reduction, by the mere effect of the current rectification (see Fig. 2.7). As a matter of fact, as the water reduction is not mass-transport limited, in such conditions of significant promotion of water reduction, a significant interfacial pH increase is possible, sometimes far above pH = 10.6.

2.6 Analysis of AC-corrosion products

The data obtained by *in situ* Raman spectroscopy analyses showed that the corrosion products under AC corrosion are quite similar to those observed on pipeline in simulated soil conditions (soil boxes) under CP without AC signal.[45,46] Whether with or without AC voltage perturbation, under CP, in all cases the formation of green rust is observed as a transitory state. However, if the applied CP is too high, the interfacial pH becomes higher than 11 and no green rust can be thermodynamically stable.[46] At ordinary CP, the interfacial pH can also increase with the increase of the AC perturbation due to the current rectification. In the classical Pourbaix diagram, green rust is not mentioned and the corresponding models do not take into account the existence of green rust. Some recent works on green rust introduced the E-pH green rust diagrams[47] and the role of the pH at the metal surface appears obviously.

Figure 2.13 illustrates a simplified scheme describing the elementary process of corrosion products formation, under usual corrosion condition as well as under AC-perturbed conditions. In alkaline solutions without chloride ions a protective magnetite film is formed and the corrosion is very low, even for large amplitude excursions of the AC voltage. These conditions may be not relevant to the most frequent condition at steel pipeline surface under CP in 'true soils'.

According to the laboratory experimental results illustrated in Section 2.5, the existence of green rust at the interface seems to be linked to maintaining the protective layer and, according to thermodynamic consideration, this green rust can exist and be stable only for interfacial pH below ca 11. If the DC cathodic polarization level is too large, the water reduction induces a too high pH and corrosion can occur; if the AC perturbation amplitude is too large, the current rectification can induce a water reduction, which does not exist at lower perturbation, and corrosion can occur. These considerations of the interfacial pH may explain the result presented in Fig. 2.9.

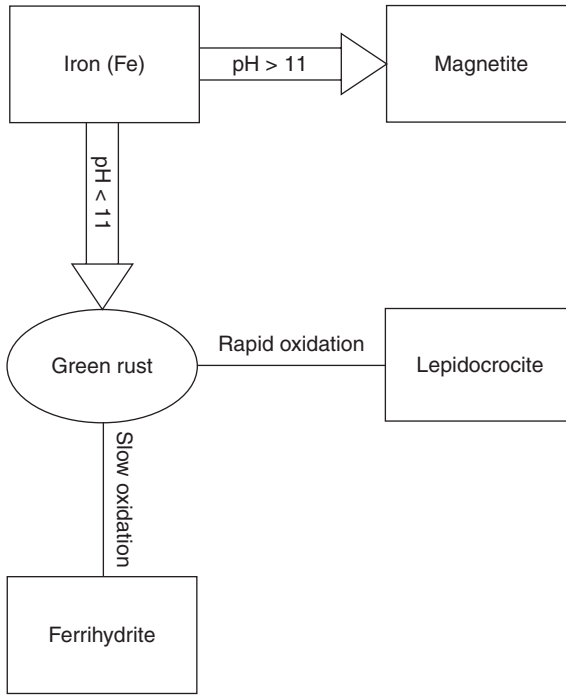

2.13 The general formation of steel corrosion products in presence of AC-induced voltage perturbation of the pipeline/soil potential from Reference 39.

A significant part of the faradic current during the AC perturbation may correspond to the reduction and oxidation of the green rust.[48]

2.7 Testing AC-corrosion processes

To confirm the conclusion of the previous discussion, some AC-corrosion experiments were performed in the laboratory of GDF-Suez with corrosion probes in solution (0.1 M Na_2SO_4, 0.05 g/L KCl). Different experimental conditions were tested with different applied cathodic polarization potentials and different amplitudes of the AC voltage perturbation. The results are presented in Fig. 2.14. These seven experiments can be classified in three groups: Group A – where the applied cathodic potential is less negative than –1V/CSE; Group B – where the DC potential is between –1.1 V/CSE and –1V/CSE; and finally Group C – where the DC potential is more negative than –1.1 V/CSE. For the experiments of Group A the attack depth does not practically increase after 1h of immersion, and the metal is well protected for all the selected AC perturbation levels. For

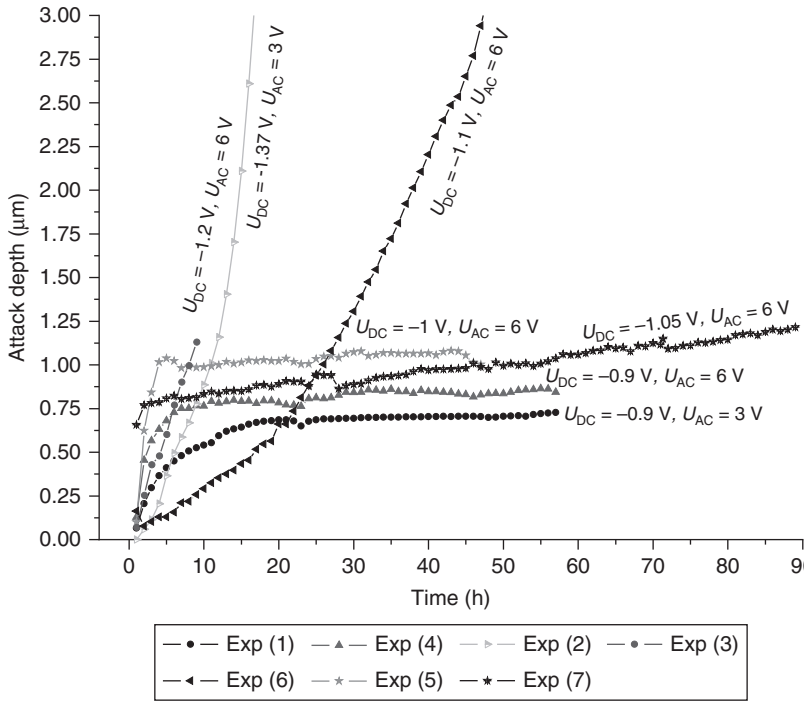

2.14 Evolution of the corrosion rate for different experimental conditions.

the experiments of Group B, the corrosion rate increases slightly in the early time period after test start, and then reaches a constant value after an initial transient phase; no stabilization of the actual depth of attack appears as for Group A, and so the corrosion risk is significant. For Group C, the corrosion rate reaches very high values, and corrosion depth is very important.

The results of Fig. 2.9 are in agreement with the data presented in Fig. 2.14; whenever the CP potential is too negative the corrosion risk increases dramatically. The previous results could be reported on the averaged (DC) current- averaged (DC) potential curves in Fig. 2.15. In this figure, the effect of current rectification appears clearly in agreement with the theoretical Fig. 2.8. The three previous groups are indicated, the limit between the different groups appears according to the DC polarization potential, and in Fig. 2.9 the limit appeared according to the DC current. The corrosion damage appears significant when the reduction of water is involved, which corresponds to an increase of the interfacial pH. The value of the interfacial pH can be related to the existence of the green rust. It

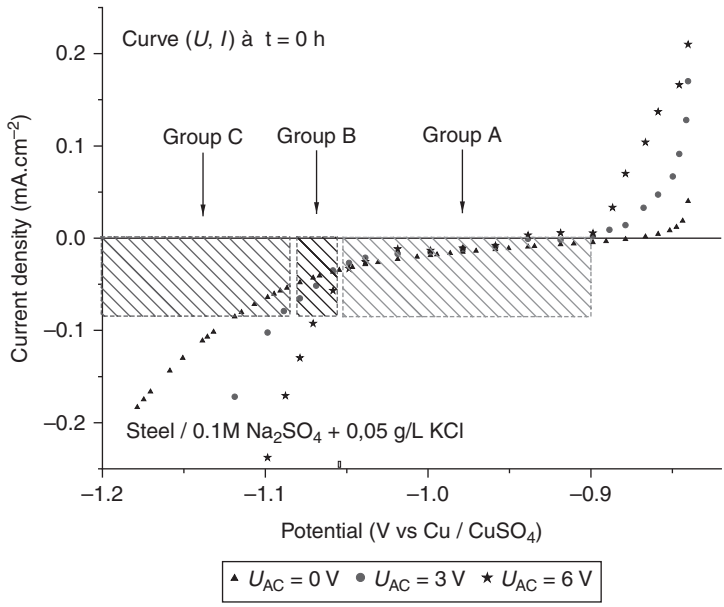

2.15 Current–potential curves corresponding to the experiments of Fig. 2.14. The potential range of the three groups is indicated.

could be concluded from this set of experiments that the metal is well protected when the conditions correspond to the presence of green rust at the interface.

2.8 Conclusion

As shown in this chapter, AC corrosion is a complex phenomenon involving multiple mechanisms and parameters. On site, the major parts of these parameters are not easy to obtain, as for example the double layer capacitance or the interfacial pH. The different parameters adopted in the currently existing CP criteria in presence of AC perturbation, such as AC current density, AC voltage perturbation, AC to DC current density ratio, are pertinent parameters but are not sufficient to assess AC corrosion. According to laboratory results, towards an improvement of the AC-corrosion threat assessment criteria, the effect of interfacial parameters should be taken into account even if these parameters are not easy to measure on site. In particular, it seems essential to find a criterion which would be able to 'control' the presence of green rust on the surface, or else would preclude water reduction at a significant level. However, it must be acknowledged that the analysis so far presented in this chapter relies only on relatively short (or

medium) term tests. Long term modification of the steel/electrolyte interface under AC perturbation still remains to be considered.

2.9 References

1. W. Prinz (1992), *AC Induced Corrosion on Cathodically Protected Pipelines*. UK Corrosion 92, vol. 1, Proceedings of NACE, Nashville, USA, 26 April-1 May.
2. F. Stalder (1997), Pipelines failures. *Materials Science Forum*, **247**, 139–146.
3. R.G. Wakelin, R.A. Gummow and S.M. Segall (1998), AC corrosion. Case histories, tests procedures and mitigation, *Corrosion 98*, NACE, paper n 565.
4. I. Ragualt (1998), 'AC corrosion induced by VHV electrical lines on polyethylene coated steel gas pipelines', *Corrosion 98*, NACE, paper n 557.
5. B. McCollum and G. Ahlborn (1916), 'Influence of frequency of alternating or infrequently reversed current on electrolytic corrosion,' *Technologic Papers of the Bureau of Standards*, No. 72, 15 August 1916.
6. W. Prinz and H.G. Shoneich (1992), 'Alternating current corrosion of cathodically protected pipelines', *Proceedings of The International Gas Conference*, 503–511.
7. L. Sjögren, G. Camitz, J. Peultier, S. Jacques, V. Baudu, F. Barrau, B. Chareyre, A. Berquist, A. Pourbaix and P. Carpentiers (2011), 'Corrosion resistance of stainless steel pipes in soil', *Materials and Corrosion*, **62**, 29.
8. A.Q. Fu and Y.F. Cheng (2012), 'Effect of alternating current on corrosion and effectiveness of cathodic protection of pipelines', *Canadian Metallurgical Quarterly*, **51** 81–90.
9. Z. Li, H. Hao and Q. Ding (2011), 'Effects of AC interference on the optimum cathodic protection potential of X70 steel in soil solution', *Anti-Corrosion Methods and Materials*, **58**, 323–327.
10. Q. Zhu, A. Cao, W. Zaifend, J. Song and C. Shengli (2011), 'Stray current corrosion in buried pipeline', *Anti-Corrosion Methods and Materials*, **58**, 234–237.
11. S. Goidanich, L. Lazzari, M and Ormellese (2010), 'AC corrosion – Part 1: Effects on overpotentials of anodic and cathodic processes', *Corrosion Science*, **52**, 491–497.
12. S. Goidanich, L. Lazzari, M and Ormellese (2010), 'AC corrosion – Part 2: Parameters influencing corrosion rate', *Corrosion Science*, **52**, 916–922.
13. A.Q. Fu and Y.F. Cheng (2010), 'Effects of alternating current on corrosion of a coated pipeline steel in chloride-containing carbonate/bicarbonate solution', *Corrosion Science*, **52**, 612–619.
14. U. Bertocci (1979), 'AC Induced Corrosion. 'The effect of an alternating voltage on electrodes under charge-transfer control', *Corrosion*, **35**, 211–215.
15. R.W. Bosh and W.F. Bogaerts (1998), 'A theoretical study of AC-induced corrosion considering diffusion phenomena', *Corrosion Science*, **40**, 323–336.
16. M. Büchler and H-G. Schöneich (2009), 'Investigation of alternating current corrosion of cathodically protected pipelines: Development of a detection method, mitigation measures, and a model for the mechanism', *Corrosion,* **65**, 578–586.
17. K. Juetner, M. Reitz, S. Schaefer and H. Schoeneich (1998), 'Rotating ring-disk studies on the impact of superimposed large signal AC currents on the cathodic protection of steel', *Electrochemical Methods in Corrosion Research VI, Materials Science Forum*, **289–292**, 107.

18. M.L. Mateo, T. Fernandez Otero and D.J. Schiffrin (1990), 'Mechanism of enhancement of the corrosion of steel by alternating currents and electrocatalytic properties of cycled steel surfaces,' *Journal of Applied Electrochemistry,* **20**, 26–31.
19. I. Ibrahim, M. Meyer, B. Tribollet, H. Takenouti, S. Joiret, S. Fontaine, P. France and H-G. Schöneich (2009), 'On the mechanism of AC assisted corrosion of buried pipelines and its CP mitigation', *IPC2008: Proceedings of the ASME International Pipeline Conference*, Vol 2 Pages: 601–625 Published: 2009.
20. E.L. Kirkpatrick (1995), 'Basic concepts of induced AC voltages on pipelines', *Materials Performances*, **34** 7, 14–18.
21. W.G. Hurley and S.J. Croall (1983), 'Electromagnetic voltage induction and mitigation on passive conductors from overhead transmission lines', *IEEE,* **PAS-102**, 7, July, 2341–2348.
22. J.R. Carson (1926), 'Wave propagation in overhead wires with ground return,' *The Bell System Technical Journal,* **5**, 539–554.
23. A. Taflove and J. Dabkowski (1979), 'Prediction method for buried pipeline voltages due to 60 Hz AC inductive coupling' part I and II, *IEEE Transaction on Power Apparatus and Systems,* **PAS-98**, 780–794.
24. M.H. Shwehdi and U.M. Johar (2003), 'Transmission line EMF interference with buried pipeline: Essential and cautions', *Proceedings of the International Conference on Non-Ionizing radiation at UNITEN (ICNIR 2003)* Electromagnetic Fields and Our Health, Selangor, Malaysia, 20–22 October 2003.
25. CIGRE Working Group 36.02 (1995), 'Guide on The Influence of High Voltage AC Power System on Metallic Pipelines', CIGRE, 1995.
26. A. Taflove and J. Dabkowski (1979), 'Mitigation of buried pipeline voltages due to 60 Hz AC inductive coupling Part I-Design of joint rights-of-way', *IEEE Transactions on Power Apparatus and Systems,* **PAS-98**, 1806–1813.
27. L. Nielsen and P. Cohn (2000), 'AC corrosion and electrical equivalent diagrams', *European Pipe Corrosion and Protection Committee CEOCOR*, International Congress, Bruxelles, Belgium.
28. J. Newman (1966), 'Resistance for low of current to a disk', *Journal, of Electrochemical Society*, **113**, 501–502.
29. H. Xiao and S. B. Lalvani (2008), 'A linear model of alternating voltage-induced corrosion', *Journal of Electrochemical Society*, **155**, C69–C74.
30. R. Zhang, P.R. Vairavanathan and S.B. Lalvani (2008), 'Perturbation method analysis of AC-induced corrosion', *Corrosion Science*, **50**, 1664–1671.
31. I. Ibrahim, H. Takenouti, B. Tribollet, X. Campaignolle, S. Fontaine and P. France (2007), 'Harmonic analysis study of the AC corrosion of buried pipelines under cathodic protection,' paper n 7042, *Corrosion NACE*.
32. K. Darowicki (1995), 'Corrosion rate measurements by non-linear electrochemical spectroscopy', *Corrosion Science*, **37**, 913–925.
33. J.-P. Diard, B. Le Gorrec and C. Montella (1998), 'Corrosion rate measurements by non-linear electrochemical impedance spectroscopy. Comments on the paper by K. Darowicki, *Corrosion Science* **37** (1995) 913', *Corrosion Science*, **40**, 495–508.
34. C. Montella (2012), 'Combined effects of Tafel kinetics and Ohmic potential drop on the nonlinear responses of electrochemical systems to low-frequency sinusoidal perturbation of electrode potential – New approach using the lambert W-function', *Journal of Electroanalytical Chemistry*, **672**, 17–27.

35. M. Büchler, H-G. Schöneich and F. Stadler (2005), 'Discussion of Criteria to Assess the Alternating Current Corrosion Current Corrosion Risk of Cathodically Protected Pipelines', in Joint Technical Meeting on Pipeline Research, paper n 26 (Arlington, VA: Pipeline Research Council International [PRCI], 2005).
36. L.V. Nielsen, B. Baumgarten and P. Cohn (2006), 'A field study of line currents and corrosion rate measurements in a pipeline critically interfered with AC and DC stray currents', *CEOCOR 2006.*
37. M. Büchler, C.V. Voüte and H-G. Schöneich (2007), 'Evaluation of the effect on cathodic protection levels on the AC corrosion on pipelines', *Eurocorr Conference Proceedings* (Frankfurt am main, Germany, Dechema, 2007).
38. I. Ibrahim (2008), 'La corrosion induite par courant alternative sur les canalisations enterrées sous protection cathodique', *Thèse de l'Université Pierre et Marie Curie*, Paris, France.
39. M.N. Boucherit (1990), 'Application de la spectroscopie Raman à l'étude de la corrosion électrochimique du fer et des aciers inoxydables', *Thèse de l'Université Paris 6*, Paris, France.
40. F. Stalder (2005), 'Influence of soil composition on the spread resistance and of AC corrosion on cathodically protected coupons', *CEOCOR, Committee on the Study of Pipe Corrosion and Protection,* 5th International Congress, Brussels, Belgium.
41. L.V. Nielsen (2005), 'Role of alkalization in AC-induced corrosion of pipelines and consequences hereof in relation to CP requirements', *Corrosion/2005*, paper n 05188 (Houston, TX: NACE 2005).
42. L.V. Nielsen, K.V. Nielsen, B. Baumgarten, H. Breuning-Madsen, P. Cohn and H. Rosenberg (2004), 'Induced corrosion in pipelines: Detection, characterization and mitigation', *Corrosion/2004*, paper n 04211, NACE 2004.
43. L.V. Nielsen, B. Baumgarten and P. Cohn (2006), 'A field study of line currents and corrosion rate measurements in a pipeline critically interfered with AC and DC stray currents' *CEOCOR 2006.*
44. C. Deslouis, I. Frateur, G. Maurin and B. Tribollet (1997), 'Interfacial pH measurement during the reduction of dissolved oxygen in a submerged impinging jet celle', *Journal of Applied Electrochemistry*, **27**, 482–492.
45. L. Lanarde, X. Campaignolle, S. Joiret, S. Karcher and M. Meyer (2004), 'Characterisation of corrosion products on pipeline steel under cathodic protection', *Eurocorr 2004*.
46. L. Lanarde, X. Campaignolle, S. Joiret and M. Meyer (2005), 'Corrosion products evolution on cathodically protected pipeline steel', *Eurocorr 2005*.
47. C. Ruby, A. Géhin, R. Aissa and J.-M.R. Génin (2006), 'Mass-balance and Eh-pH diagrams of FeII-III green rust in aqueous sulphated solution', *Corrosion Science*, **48**, 3824–3837.
48. H. Antony, L. Legrand and A. Chaussé (2008), 'Carbonate and sulphate green rusts – Mechanisms of oxidation and reduction', *Electrochimica Acta*, **53**, 7146–7156.

3

Assessing the significance of corrosion in onshore oil and gas pipelines

P. HOPKINS, Penspen Limited, UK

DOI: 10.1533/9780857099266.1.62

Abstract: Oil and gas currently provide 54% of the world's primary energy needs,[1] and these energy forms rely, mainly, on pipelines for their transportation. Accordingly, there are over 3 500 000 km of high pressure oil and gas pipelines around the world. These pipelines were built many years ago: inevitably they have corroded, and will continue to corrode. Accordingly, it is essential that this corrosion is detected, assessed and rectified. This chapter covers the assessment of corrosion in onshore (underground) pipelines. It presents a state-of-the-art review, with both recommendations and insights into the various assessment methods available today.

Key words: corrosion, pipelines, assessment.

3.1 Introduction

Oil and gas currently provide 54% of the world's primary* energy needs,[1] and there are over 50 years' supplies of proven and recoverable reserves of oil and gas.[2] These energy forms rely, mainly, on pipelines for their transportation. Accordingly, there are over 3 500 000 km of high pressure oil and gas pipelines around the world,[3] Fig. 3.1. Most of these pipelines were built many years ago: they started life in perfect condition, well protected against corrosion using external coating and cathodic protection (CP). But as the pipeline ages, its coating may also age, and then corrosion can commence. This ageing, and the problems it brings, can restrict the future use of these pipelines as they are prepared for the next 50 years of service.

Pipelines are a very safe form of transportation and have a very good safety record;[4] however, corrosion is a major cause of failure in both onshore (underground) and offshore pipelines. Figure 3.2[5] shows failure data from the USA over a 20 year period (1993–2012) on its 500 000 mile (800 000 km) network of onshore hazardous (e.g., petroleum and petroleum products)

* All energy consumed by end users, excluding electricity, but including the energy consumed at electric utilities to generate electricity.

3.1 Transmission pipeline being constructed.

Table 3.1 Consequences of pipeline failures in USA (1993–2012)[7]

	Natural gas		Liquid pipelines	
	Fatalities	Casualties	Fatalities	Casualties
Corrosion	13	4	1	18
Excavation damage	15	51	12	38
Incorrect operation	0	9	9	20
Material/weld/equipment failure	8	71	4	12
Natural force	0	2	0	1
Other outside force	0	13	3	5
All other causes	6	38	10	43

liquid pipelines and natural gas pipelines. Corrosion is not the major failure cause: 'material failures', such as weld failures, and 'excavation damage', where pipelines are impacted by earth moving equipment, piling machines, etc., are also major causes of failure. However, these corrosion failures can have deadly consequences,[6] (see Table 3.1),[7] and cause property damage of over $US20 million/annum in the USA.[8] This chapter will explain the problem of corrosion in onshore pipelines and how it is detected, and then go into the details of how corrosion is assessed to determine if it requires repair or not.

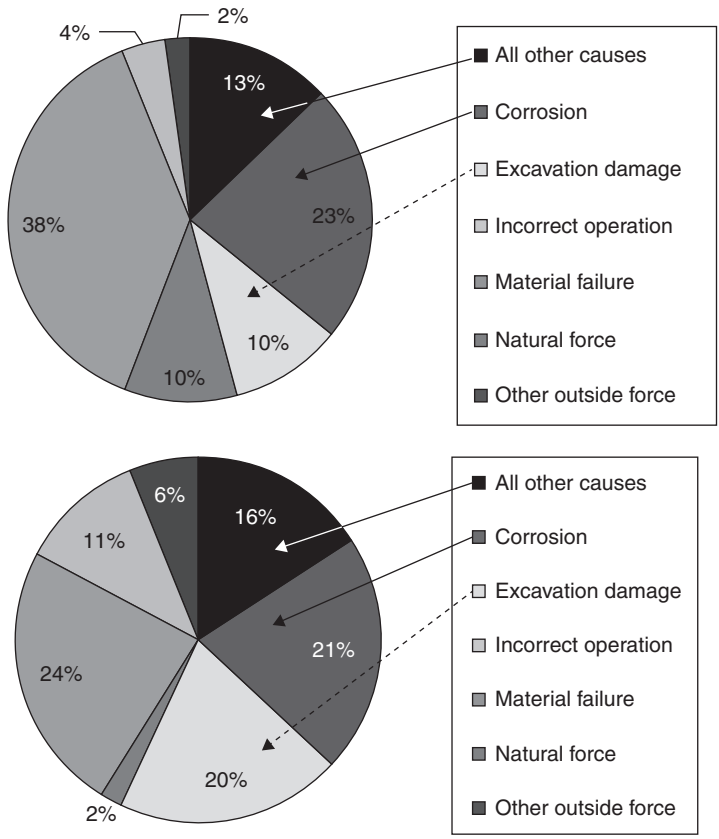

3.2 Causes of pipelines failures in onshore USA pipelines (liquid (top) and natural gas (bottom)).

3.2 Corrosion in onshore pipelines

The USA's National Association of Corrosion Engineers (NACE) defines corrosion as: '*The deterioration of a material, usually a metal, which results from a reaction with its environment*'. Therefore, corrosion is a time dependent, environmentally-assisted mechanism that causes a metal to deteriorate by reaction with its environment. Pipeline design and operation aim to minimise corrosion, but inevitably a pipeline can contain external corrosion, due to a breakdown of the coating and/or the CP system; or internal corrosion, due to the fluid in the pipeline containing corrosive elements. Figure 3.3 is an example of corrosion on an operating pipeline.

Corrosion is created within an electrochemical cell, Fig. 3.4. A pipeline's electrolyte is the surrounding soil (for onshore pipelines), and water (for subsea pipelines), Fig. 3.4. Corrosion is an oxidation process, and the

3.3 Pipelines are surrounded by earth that can lead to external corrosion.

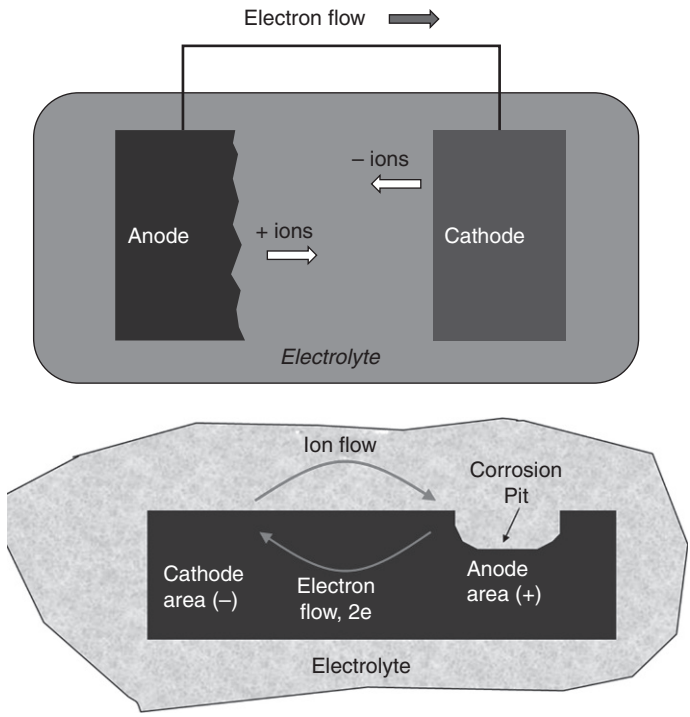

3.4 Electrochemical cell (top), and electrochemical cell in pipeline (bottom).

oxidation of a metal is corrosion. The iron (Fe) is changed, with removal of electrons (oxidation) at the anode (Fig. 3.4):

$$Fe \rightarrow Fe^{2+} + 2e^{-} \quad [3.1]$$

The electrons produced and lost during oxidation move through the metal to another location, where they are consumed in a reaction that produces hydroxyl ions at the cathode (Fig. 3.4):

$$2H_2O + O_2 + 4e^{-} \rightarrow 4OH^{-} \quad [3.2]$$

This corrosion can cause pipeline failures, Section 3.1, including deadly ruptures.[6]

3.3 Detecting corrosion

Corrosion can be detected in onshore pipelines using a variety of methods, but the most common are:

- excavation;
- above-ground surveys; and
- internal inspection using in-line tools.

Pipeline excavation is the most thorough method of detecting and measuring corrosion, but it is usually the most expensive inspection technique. It is generally used as a last resort, as it may require pressure reduction, with operational cost implications.

Above-ground surveys (Table 3.2) can be used to infer the presence of corrosion by monitoring CP and coating condition. Inspection methods include:

Table 3.2 Above-ground CP/coating surveys for onshore pipelines

Type of survey	Survey technique	Type of survey
Soil survey	Soil resistivity. Soil chemical analysis.	Soil survey
Coating survey	Pearson. Signal attenuation (Cscan). Current mapper. DCVG (can also indicate CP status).	Coating survey
CP survey	CP monitoring data e.g., off potentials. Close interval potential (can also indicate coating status).	CP survey

- CP checks.
- Direct current voltage gradient (DCVG) detects coating defects in buried pipelines by measuring the voltage gradients in the soil from the CP system.
- Pearson survey (similar to DCVG, but uses AC).
- Close interval potential surveys (CIPS) measure the pipe-to-soil potential (voltage) to determine CP coverage.

We can also internally inspect and monitor our pipelines using tools that move along with the product flow. These tools are known as in-line inspection vehicles, or pigs, Fig. 3.7. These tools can reliably detect both internal and external corrosion, and accurately size the corrosion. These tools have been used since the 1960s, and are now in common use in most liquid and gas pipelines.

3.4 Preventing corrosion

Corrosion requires four factors to be present for it to occur (Fig. 3.4):

- an anode;
- a cathode;
- a metallic path connecting the anode and cathode;
- an electrolyte.

If any of these factors is not present, or prevented (e.g., coating a pipeline to prevent contact with the electrolyte), then corrosion cannot occur. As Fig. 3.6 shows, corrosion results in:

- Metal loss (the corrosion defect can have a smooth or irregular profile, and possibly contain blunt or sharp features).
- Cracking.
- Environmental cracks, caused by a corrosive environment. Environmentally-assisted cracking includes stress corrosion cracking, sulphide stress corrosion cracking, and hydrogen induced cracking. This chapter will focus on assessing blunt corrosion, but will briefly cover the assessment of cracks; readers who want to assess cracking in pipelines should refer to the more detailed literature (e.g., see References 9–11).

3.4.1 Preventing external corrosion

External coatings are our primary protection against external corrosion: Fig. 3.5 gives examples of popular coatings used on pipelines. Pipelines are constructed using (typically) 12 m lengths of 'line pipe'. The line pipe is

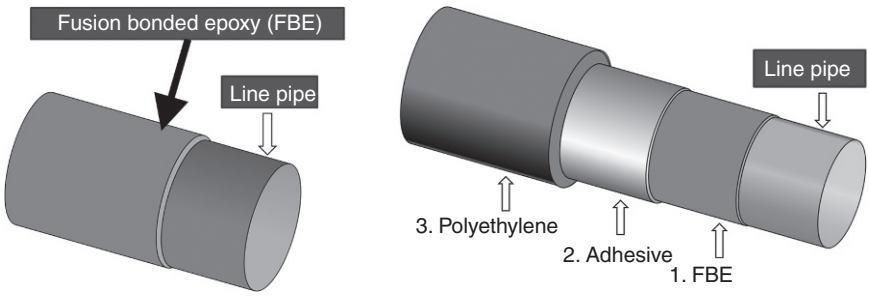

3.5 Examples of external coatings on pipelines (fusion bonded epoxy (left), '3 layer' (right)).

usually coated at a factory before delivery to the construction site. Factory coatings are excellent, but they will never be perfect. If we lose the protective coatings around the pipeline, the pipeline will be exposed to the environment. This environment (soil or seawater) will contain water and oxygen, which will cause corrosion if there is no coating protection.

Therefore, to enhance protection, operators began installing CP systems. Our CP system will protect areas of our pipeline where our coating is faulty. Hence, we need to check to see that our CP system is functioning correctly. The pipe coating condition tends to deteriorate with time; this causes an increased CP current requirement. Cathodically protected pipelines are equipped with permanent test stations, where electronic leads are attached to the pipeline to measure the pipe-to-soil potential. This potential should be sufficiently cathodic to ensure adequate corrosion protection, but not so cathodic as to produce coating damage and/or hydrogen embrittlement.

3.4.2 Preventing internal corrosion

For corrosion to occur in a pipeline, there must be liquid water present, and the water must wet the wall of the pipe: internal corrosion generally cannot occur in a pipeline unless there is an electrolyte to complete the corrosion cell. Water or other aqueous materials (such as glycols from dehydration processes) are needed to form the electrolyte. Also, other chemicals usually must be present: for example, carbon dioxide (CO_2) for the formation of dilute organic and inorganic acids; or, sulphur for the formation of acid or growth of bacteria. Once introduced, the corrosive materials may continue to damage the pipeline until they are removed, or until they are consumed in corrosion reactions.

We can prevent internal corrosion by:

- treating the product prior to entry into the line (e.g., removing water), and checking quality;

- cleaning the line to remove corrosion debris;
- mixing chemicals to 'inhibit' (slow down) any corrosion;
- lining the line pipe with a corrosion resistant alloy;
- using biocides in the pipeline to inhibit the corrosive actions of microbes that cause microbiologically influenced corrosion (MIC), and thereby reduce or eliminate MIC.

We can also include a 'corrosion allowance' (increased thickness of line pipe) to accommodate in-service, predictable, corrosion.

3.5 Assessment of corrosion

Corrosion assessment is important, as inspection methods can now easily detect its presence and size: there is therefore an increasing need to determine its severity rather than continuously to excavate and repair. This section will cover all the major methods for assessing corrosion.[12–15] Any assessment of a defect in a structure is called an engineering critical assessment (ECA): these assessments use fracture mechanics principles.[10,11] These ECAs are sometimes called 'fitness-for-purpose' assessments. Fitness-for-purpose, in a defect assessment context, means that a particular structure is considered adequate for its purpose, provided the conditions for failure are not reached.[10] It is based on a detailed technical assessment of the significance of the defect. This term, however, has different legal implications in different countries,[16] and local and national legislation/regulations may not permit certain types of defects to be assessed by fitness-for-purpose methods, or may mandate specific limits. Such issues should always be considered before an assessment. It is better to refer to the fitness-for-purpose assessment of a defect simply as an 'assessment'.

3.5.1 The development of modern assessment methodology

Fracture mechanics provides scientific understanding of the behaviour of defects in structures. The effect of defects on structures was studied as long ago as the fifteenth century by Leonardo da Vinci, but prior to 1950 failure reports of engineering structures did not usually consider the presence of cracks: cracks were considered unacceptable in terms of quality, and there seemed little purpose in emphasising this. Additionally, it was not possible to apply the early fracture mechanics work of pioneers such as Griffith to engineering materials, since it was applicable only to perfectly elastic materials, i.e. it was not directly applicable to engineering materials such as line pipe, which exhibit plasticity.

The 1950s and 1960s were periods where the safety of transmission pipelines was of interest, primarily in the USA. Early workers on pipeline defects

were faced with problems;[17–22] pipelines were thin walled, increasingly made of tough materials, and exhibited extensive plasticity before failure. The fracture mechanics methods (using stress intensity factor, K) at that time used linear elastic theories that could not reliably be applied to the failure of defective pipelines, as they would have needed:[4]

- quantitative fracture toughness data, including measures of initiation and tearing (only simple impact energy (e.g., Charpy V-notch) values were available);
- a measure of constraint (this concept was not quantifiable in the 1960s, other than by testing);
- a predictive model for both the fracture and the plastic collapse of a defect in a thin-walled pipe.

Workers[17–22] at the Battelle Memorial Institute in Columbus, Ohio, decided to develop methods based on existing fracture mechanics models, but they overcame the above deficiencies in fracture mechanics knowledge by a combination of expert engineering assumptions and calibrating their methods against the results of full-scale tests. Over a 12 year period, up to 1973,[19] over 300 full-scale tests were completed, but the main focus was on:

- 92 tests on axially orientated artificial through-wall defects; and,
- 48 tests on axially orientated artificial part-wall defects (machined V-shaped notches).

These defects are reasonable models of corrosion in pipelines (Fig. 3.6).

The workers noted that line pipe containing defects tended to fail in a ductile manner, and final failure was by collapse, although very low toughness

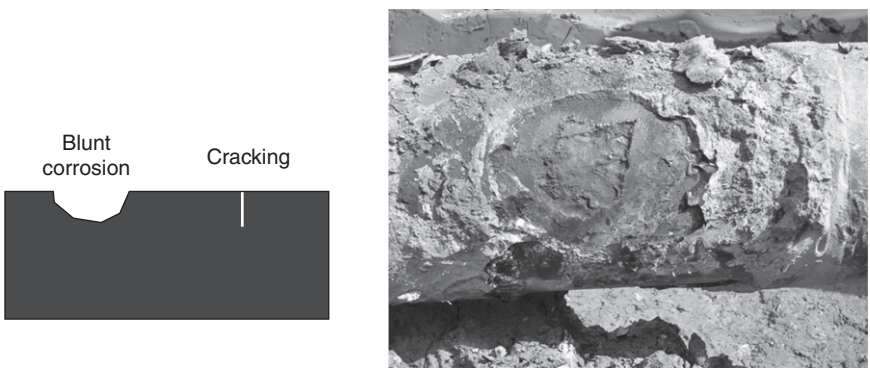

3.6 Shape of defects cause by corrosion, and 'blunt' corrosion (right) in a pipeline.

line pipe could fail in a brittle manner. The Battelle workers concluded that two basic distinctions could be made:

- 'Toughness dependent' – these tests failed at lower stresses (pressures). To predict the failure stress of these tests, a measure of the material toughness was required (e.g., the upper shelf Charpy impact energy).
- 'Strength dependent' – these tests failed at higher stresses. To predict the failure stress of these tests, only a measure of the material's tensile properties was needed.

The work at Battelle led to the development of strength (flow stress[19]) dependent, and toughness dependent, through-wall and part-wall defect equations. Flow stress was a concept introduced by Battelle to help model the complex plastic flow and work hardening associated with structural collapse. Flow strength is a notional material property, with a value between yield strength and ultimate tensile strength.[19]

The Battelle workers produced equations[19] that could predict when a through-wall defect (Fig. 3.8) would extend in length ('rupture'):

$$\frac{K_c^2\pi}{8c\bar{\sigma}^2} = \frac{C_v\dfrac{12}{A}E\pi}{8c\bar{\sigma}^2} = \ln\sec\left(\frac{\pi M\sigma_\theta}{2\bar{\sigma}}\right) \text{ toughness dependent} \qquad [3.3]$$

$$M = \sqrt{1+0.314\left(\frac{2c}{\sqrt{Rt}}\right)^2 - 0.00084\left(\frac{2c}{\sqrt{Rt}}\right)^4} \qquad [3.4]$$

$$\sigma_\theta = M^{-1}\bar{\sigma} \quad \text{strength dependent} \qquad [3.5]$$

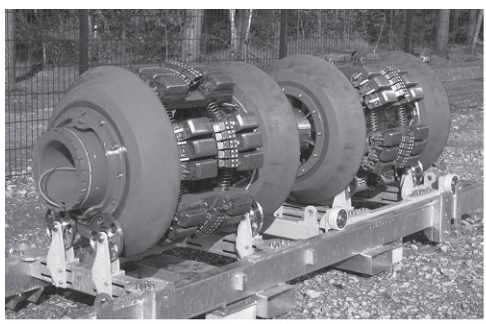

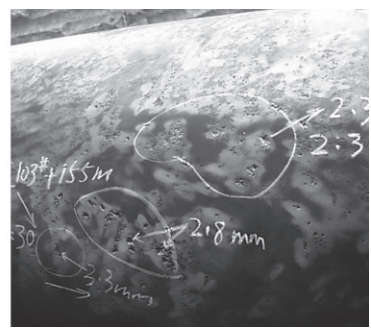

3.7 Smart pig (left), and corrosion in a pipeline (right). Smart pig image courtesy and copyright of Rosen.

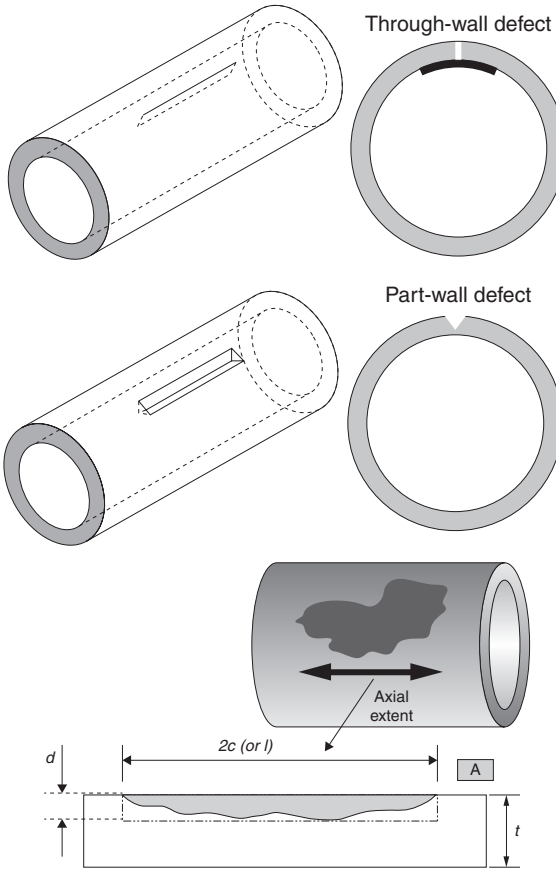

3.8 Through-wall and part-wall defects in line pipe, and equivalent corrosion defect (bottom).

In parallel, the Battelle workers produced an equation[19] that could predict the pipeline hoop stress when a part-wall defect (Fig. 3.8) failed:

$$\frac{K_c^2\pi}{8c\bar{\sigma}^2} = \frac{C_v\,12/A\,E\pi}{8c\bar{\sigma}^2} = \ln\sec\left(\frac{\pi M_P\sigma_\theta}{2\bar{\sigma}}\right) \text{ toughness dependent} \quad [3.6]$$

$$M_P = \left[\frac{1-d/t\left(1/M\right)}{1-d/t}\right] \quad [3.7]$$

$$\sigma_\theta = \bar{\sigma}\left[\frac{1-d/t}{1-d/t\left(1/M\right)}\right] \text{ strength dependent} \quad [3.8]$$

D outside diameter of pipe ($R = D/2$ = radius)
t pipe wall thickness
E elastic modulus
M Folias factor
R radius of pipe
d part-wall defect depth
σ_θ hoop (circumferential) stress at failure (or σ_f)
2_c defect axial length
C_v upper shelf Charpy V-notch impact energy
A area of Charpy specimen fracture surface
$\bar{\sigma}$ flow stress (function of σ_u (ultimate tensile strength) and σ_y (yield strength))

3.6 Particular corrosion assessment methods

The two corrosion assessment methods we are going to summarise require our line pipe to be ductile. 'Ductile' means the material:

- has passed the 'drop weight tear test' (DWTT) test criteria;
- is on the Charpy toughness 'upper shelf'; i.e., 100% shear area.

Line pipe that meets contemporary specifications[23] would satisfy these criteria, but because corrosion is blunt, the methods are applicable to lower Charpy toughness line pipe.[9] Initially we will focus on corrosion that is primarily in the axial direction, and subjected to the full hoop stress in the pipeline, Fig. 3.9. Later we will cover corrosion that is primarily in the circumferential direction. The latter corrosion will be exposed to axial stresses, as well as hoop stresses. See simple guidance in ASME B31G-2012[12] and Reference 14 for corrosion orientated in the spiral direction, or a random direction.

3.6.1 ASME B31G-2012

The popular methods used for assessing corrosion orientated in the axial direction are based on research at Battelle Memorial Institute (USA) in the 1960s and 1970s.[17–22] The first recognised method was published in the 1980s:

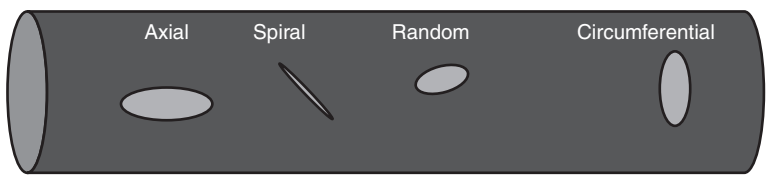

3.9 Orientation of corrosion.

Table 3.3 Various assessment levels in ASME B31G-2012

ASME B31G-2012	Method
Level 0	Acceptance levels given in tables and based on the methods in the 1984 version of the standard.
Level 1	Acceptance levels are calculated using the methods in the 1984 version of the standard. Acceptance levels are calculated using the methods in Reference 13 Acceptance levels are calculated using the methods in Reference 11
Level 2	Acceptance levels are calculated using the methods in Reference 14 Acceptance levels are calculated using the methods in Reference 11
Level 3	'Detailed' (e.g., finite element stress) analysis.

the pipeline industry then identified a need for standardised guidelines for the assessment of corrosion in pipelines. In 1984 ASME produced ASME B31G (now [12]) for assessing corrosion defects, using the early Battelle work. ASME B31G considers corrosion in pipelines under internal pressure loading only: it does not cover external loads.

ASME B31G-2012 is applicable to pipelines and bends containing:

- metal loss due to corrosion or grinding;
- metal loss that affects longitudinal or helical electric seam welds or circumferential electric welds.

Note that the welds must be of sound quality.[12] ASME B31G-2012 now gives the user a choice of four assessment levels, each with decreasing conservatism, Table 3.3. There are also choices of methods within Levels 1–3. It is not intended to cover these levels in detail, as they have been summarised before (e.g., see References 4, 9), but it is sufficient to say that the ASME B31G-2012 standard is the benchmark standard for the assessment of corrosion in line pipe. This standard allows large areas of corrosion to safely remain in an operational pipeline.

3.6.2 DNV-RP-F101

The Norwegian organisation DNV has published guidance on assessing corrosion in line pipe.[15] DNV-RP-F101 is based on full-scale tests and numerical analyses of corrosion defects,[24,25] and gives guidance on the assessment of:

- single defects and interacting defects;
- complex-shaped defects (i.e., assessing the actual profile of the defect); and,
- combined loading.

It is not applicable to line pipe grades above X80, or to cracks, and corrosion defect depth must be ≤85% wall thickness. The hoop stress to cause failure is given by:

$$\sigma_\theta = \sigma_u \left(\frac{1 - d/t}{1 - d/t\,1/Q} \right) \quad [3.9]$$

$$Q = \sqrt{1 + 0.31 \left(\frac{2c}{\sqrt{Dt}} \right)^2} \quad [3.10]$$

These equations are similar to the original Battelle equations (Equation [3.8]). DNV-RP-F101 incorporates safety factors by calculating a safe working pressure:

$$P_{sw} = FxP_f \quad [3.11]$$

where P_f is the failure pressure obtained from Equation [3.9], and F = total usage factor = F_1F_2. F_1 = modelling factor = 0.9, F_2 = operational usage factor (normally taken as equal to the 'design factor' taken from the pipeline's design standard).

DNV has said:[25] 'For old pipelines, or pipelines where the material might not have sufficient ductility, the… DNV… criteria should not be used. Modern pipeline steel materials normally have sufficient toughness to expect plastic collapse failure.' 'Plastic collapse' means the remaining ligament below the corrosion defect can tolerate ultimate tensile strength, see Equation [3.9]. Line pipe will collapse if the toughness is very high, but… what is 'high', and will older line pipe collapse? Modern line pipe is of very high toughness (Table 3.4), and should fail by plastic collapse, but older steels do not have high toughness.[26]

Table 3.4 Typical Charpy (CVN) toughness in line pipe over 7 decades[27]

Decade	1950s	1960s	1970s	1980s	1990s
Grade	X42/52	X52/60	X60/65	X65/70	X75
Typical CVN, J (ft lb)	27 (20)	41 (30)	54 (40)	88 (65)	109 (80)

Table 3.5 Comparison of corrosion assessment methods[9]

Assessment method	P_a/P_f		P_a/P_f (all data except early Grade B tests)	
	Mean	Standard deviation	Mean	Standard deviation
ASME B31G (Level 1)	1.330	0.468	1.347	0.479
Modified B31G[13]	1.184	0.285	1.194	0.289
'RSTRENG'[14]	1.170	0.177	1.188	0.168
DNV-RP F101[15]	1.178	0.318	1.205	0.309
PCORR[35,36]	1.191	0.310	1.220	0.301
API 579[11]	1.436	0.407	1.465	0.403

The standard itself states that its methods should not be applied to line pipe steel materials with Charpy values less than 27 J (20 ft lb f), see Table 3.4. For the weld, a minimum full size Charpy value of 30 J is recommended. Reference 27 supports this 27 J (20 ft lb) limit for plastic collapse: line pipe toughness less than this value may not be able to support plastic collapse. Therefore, a lower bound toughness to support plastic collapse of corrosion defects in line pipe material is ≥27 J (≥20 ft lb). There are higher estimates in the literature: plastic collapse can be expected with a minimum toughness of 82–102 J (60–75 ft lb),[28] which is similar to another estimate of 90 J (68 ft lb).[26]

3.6.3 Comparison of corrosion assessment methods

Reference 9 compares the assessment methods detailed above. The methods were assessed against a large body of full-scale test data. The predicted to actual failure pressures (P_a/P_f) are presented in Table 3.5. RSTRENG gives the most accurate predictions, P_a/P_f.

3.7 Particular issues in corrosion assessment

This chapter has so far focussed on single corrosion defects, blunt (not sharp, Fig. 3.6) orientated in the axial direction in line pipe material. This section discusses other types of corrosion.

3.7.1 Corrosion on welds

It is now generally considered that longitudinal corrosion across seam welds (other than 'autogenous' – a welding procedure that does not use filler metal such as electric resistance welded line pipe) can be treated as corrosion in 'parent plate' (i.e. as though the corrosion is in the line pipe), and this is

supported by test data (e.g., see Reference 29). Accordingly, standards (e.g., see References 10, 12, 15) allow the assessment of corrosion on welds, provided the weld mechanical properties are similar or superior to the line pipe, and the weld must be free from other defects.

3.7.2 Assessing corrosion in the circumferential direction

We have covered methods for assessing corrosion primarily in the axial direction (Fig. 3.8). We can now consider the assessment of corrosion in the circumferential direction, Fig. 3.9. Internal pressure induces a hoop stress and an axial stress: the axial stress is between 30% and 50% of the hoop stress, depending on the pipeline end restraints. Thermal loads, ground or pipe movement, loss of support (e.g., spanning), bends, supports, etc., can induce additional axial and/or bending stresses. Hence, axial stress, not hoop stress, may be the major stress acting on the corrosion defect. Therefore, we need an assessment method to assess corrosion in a pipeline subjected to high axial loads – if the corrosion is primarily in the circumferential direction, or if the corrosion has extensive width.

Kastner *et al*.[30] published a failure criterion for a circumferential part-wall defect subject to internal pressure, axial and/or bending loads. This is now the most popular method for assessing circumferential corrosion. The axial stress at failure (σ_f) is given by:

$$\frac{\sigma_f}{\bar{\sigma}} = \frac{\eta(\pi - \beta[1-\eta])}{\eta\pi + 2[1-\eta]\sin(\beta)} \qquad [3.12]$$

and flow stress is the average of σ_u and σ_y

$$\beta = \frac{c}{R}$$
$$\eta = 1 - \frac{d}{t}$$

Note that safety factors must be applied to this predicted axial stress at failure, and metal loss having a significant circumferential extent and acted on by high longitudinal stresses in compression could be susceptible to wrinkling or buckling.

Corrosion with both axial extent and circumferential extent can fail due to hoop stress and axial stress. Under pressure loading only, the axial dimension is the critical dimension, and unless the circumferential length > axial length, you do not need to consider the circumferential failure.[14] However,

if you have very high* external loads (e.g., mining subsidence or spanning) you must conduct the two calculations – failure under pressure loading (e.g., ASME B31G-2012), and failure due to the axial loads (Equation [3.12]).

3.7.3 Assessing group of corrosion defects

Corrosion often occurs in groups (colonies), Figs. 3.3 and 3.10. The failure stress of a corrosion defect can be reduced by the presence of another corrosion defect. When the failure stress of an individual defect is reduced by the presence of a neighbouring defect, we say that the defects 'interact'. ASME B31G-2012 explains interaction: 'Corrosion may occur such that multiple areas of metal loss are closely spaced longitudinally or transversely. If spaced sufficiently closely, the metal loss areas may interact so as to result in failure at a lower pressure than would be expected based on an analysis of the separate flaws'.

If the defects interact, we have to assess the defects as a single defect of length and width equal to the total dimensions, and a depth equal to the maximum depth of the group. The new total length, width and maximum depth has to be input into our failure equations. Various standards (e.g., see References 12, 15) give interaction rules. ASME B31G-2012 states:

> Flaws are considered interacting if they are spaced longitudinally or circumferentially from each other within a distance of three times the wall thickness (3t). Interacting flaws should be evaluated as a single flaw combined from all interacting flaws. Flaws are considered non-interacting if spaced outside of the above dimensions. Non-interacting flaws should be evaluated as separate flaws.

3.7.4 Assessing cracks

A crack is a very sharp defect, and it is a planar (two-dimensional) defect. ASME B31.8S-2012[31] states that a crack is a… '*very narrow, elongated defect*

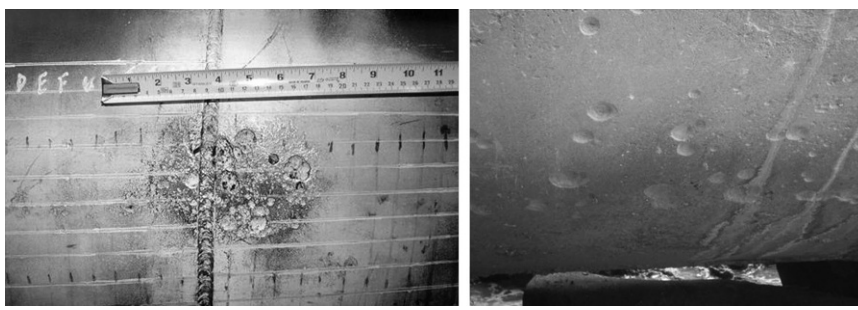

3.10 Corrosion colonies on a weld (left) and in line pipe (right).

caused by mechanical splitting into two parts'. The occurrence of cracking is generally an indication of:

- a difference between the conditions expected at the design stage and the actual operating conditions (e.g., fatigue);
- poor fabrication, manufacturing, or construction control procedures; or,
- some other poor practice, or an unexpected event.

If you detect cracking in your pipeline, it is usually:

- in or around welds (e.g., cracks caused by poor welding); or,
- in the welds or line pipe, and environmentally created (e.g., stress corrosion cracking); or,
- in fittings.

In this section we focus on cracks created by a corrosive environment in the line pipe and its weld. We have assessment methods for cracks in pipelines (e.g. see References 9–11, 32–36), but cracks are difficult both to detect and to size, leading to uncertainties in their assessment. Cracks also grow quickly if the environmental conditions are favourable (e.g., if corrosion is present, or the structure is fatigued). This growth can be difficult to predict and calculate, again adding to uncertainties in crack assessment. Therefore, we treat cracks with extreme caution, and do not generally assess them: we try to either prevent them, or detect and repair.

We cannot use the models we have used to assess corrosion (Section 3.6), as these methods are applicable to blunt defects, where the blunt defects fail by 'net section collapse': net section collapse can be considered failure when the average stress in the remaining ligament below the defect reaches the flow stress of the material (Equation [3.8]) Net section collapse is the same as plastic collapse if the flow stress equals the ultimate tensile stress.

Generally, in net section collapse, failure is not preceded by the development of a slowly tearing crack at the base of the blunt defect. Even if some tearing does occur, the strain hardening of the material and/or the redistribution of stress during the yielding will ensure that the ligament does not fail until the flow stress level is reached.[9] Blunt defects, such as corrosion, do not easily tear through the remaining ligament (as they are blunt). This allows the average stress in the ligament to reach the flow stress.

A crack can cause tearing at its tip, and this tearing can continue through the ligament. This tearing crack can prevent the stress in the ligament reaching the flow stress, and this can lead to a failure stress lower than

predicted by blunt defect models. The toughness of the line pipe now plays a key role:[9]

- This net section will not collapse if the toughness is low, as low toughness material will allow the crack to tear quickly and easily. Low toughness can lower the failure stress of a defect in a pipeline, but predicting the failure pressure of a longitudinally-orientated crack in a pipeline is relatively easy for very brittle (low toughness) material: we can use linear elastic fracture mechanics (see References 10 and 11).
- Predicting the failure pressure of a defect in very tough material is relatively easy: we can use equations such as those we use for assessing blunt defects such as corrosion (Equation [3.8]).
- The task of predicting failure pressures for cracks in materials with toughness between these two extreme values (e.g., some line pipe materials made before 1980 and some made after that time) is more difficult.

The crack assessment methods (detailed in Table 3.6) are all based on Equation [3.6]. They have been compared; for example:

- A 2009[37] publication compared the predicted failure stresses using the 'ln sec' formula, PAFFC, CorLAS, and BSI 7910 (see Table 3.6) with the failure stresses of real cracks. The methods generally gave conservative results, but difficulties in modelling the irregular crack shapes found in the field, and the differing toughness correlations/assumptions in the methods, ensured scatter in the predictions. CorLAS showed superior agreement between its predictions and the observed failure stresses.
- A 2010[38] publication concluded that cracks failing by ductile tearing in line pipe can be assessed using a variety of methods. API 579 showed very good agreement with experimental results; BSI 7910 was the most conservative method; and the ln sec formula provided conservative collapse pressure predictions.

Table 3.6 Assessment methods for cracks in pipelines

Method for assessing cracks	
API 579[11]	General fracture mechanics method.
BSI 7910[10]	General fracture mechanics method.
Battelle's 'ln sec' formula[9]	Pipeline-specific, developed at Battelle.
'PAFFC'[33,34]	Pipeline-specific (software) developed at Battelle in the USA.
'CorLAS'[35,36]	Pipeline-specific (software) developed at DNV in the USA.

It should be noted that the toughness needed to use documents such as BSI 7910 and API 579 is measured in terms of stress intensity factor, or J integral, or crack tip opening displacement (CTOD). This is a problem, as we do not usually have these fracture toughness measures for our pipeline. We usually have only a Charpy value of toughness. Hence, BSI 7910 and API 579 use simple correlations between Charpy and J, CTOD, etc. These correlations introduce inaccuracies in the calculations.[32]

Finally, note that if a crack in a pipeline is subjected to cyclic stresses, or continued exposure to the corrosive environment, it can grow rapidly. API 579 and BSI 7910 give further guidance on this time-dependent growth. Also, we must be careful when assessing a crack as the following:

- the strength and toughness of the weld is rarely known;
- the shape of the weld will introduce stress concentrations;
- residual stresses could lower the failure stress;
- the shape of the crack will be irregular; and, the crack will be difficult to size and detect.

3.8 Conclusion

Corrosion can cause metal loss defects, but pipelines can tolerate large areas of corrosion, as:

- the corrosion is blunt; and,
- the line pipe usually has sufficient ductility and toughness to tolerate the corrosion.

We have many methods for assessing blunt corrosion in pipelines. They have their origins in the work at Battelle in the 1960s and 1970s. ASME B31G-2012 presents various methods for assessing corrosion. Cracking caused by corrosion should be treated with caution, as the occurrence of cracking is generally an indication of a difference between the conditions expected at the design stage and the actual operating conditions. The cracking is difficult to assess, and any subsequent growth in a corrosive environment is very difficult to predict.

3.9 References

1. Anon. (2012), '*Key World Energy Statistics*', International Energy Agency (IEA). Paris, France.
2. Anon. (2012), '*BP Statistical Review of World Energy June 2012*', BP, London, UK. bp.com/statisticalreview.
3. M. Mohitpour, M. McManus and W. Trefanenko (2002), 'Trends in Pipeline Integrity Inspection and Rehabilitation Techniques', Proceedings of 4th International Pipeline Conference 29 September –3 October 2002, Calgary, Alberta, Canada, Paper IPC2002-27035.

4. P. Hopkins (2003), 'The structural integrity of oil and gas transmission pipelines'. In '*Comprehensive Structural Integrity*', I. Milne, R. O. Ritchie and B. Karihaloo (Eds). Elsevier Publishers, Amsterdam, Volume 1.
5. Anon., USA's Department of Transportation. Pipelines and Hazardous Materials Safety Administration website: http://primis.phmsa.dot.gov/comm/reports/safety/psi.html?nocache=631.
6. Anon. (2003), 'Pipeline Accident Report. Natural Gas Pipeline Rupture and Fire Near Carlsbad, New Mexico 19 August, 2000'. USA National Transportation Board. Report NTSB/PAR-03/01, 11 February 2003.
7. Anon., USA's Department of Transportation. Pipelines and Hazardous Materials Safety Administration website: http://primis.phmsa.dot.gov/comm/reports/safety/AllPSIDet_1993_2012_US.html?nocache=5185#_all.
8. R Fessler (2008), 'Pipeline Corrosion; Final Report', Michael Baker Jr. Report for U.S. Department of Transportation Pipeline and Hazardous Materials Safety Administration Office of Pipeline Safety, November 2008.
9. J Kiefner and K Leewis (2011), 'Pipeline Defect Assessment: A Review and Comparison of Commonly-used Methods', PRCI. May 2011. Report No. L52314.
10. Anon. (2007), '*Guide on Methods for Assessing the Acceptability of Flaws in Fusion Welded Structures*', BS 7910: 2007, British Standards Institution, London, UK.
11. Anon. (2007), '*Fitness-For-Service*', API 579-1/ASME FFS-1, Second Edition, American Petroleum Institute.
12. Anon. (1991), 'Manual for Determining the Remaining Strength of Corroded Pipelines, A Supplement to ASME B31 Code for Pressure Piping, ASME B31G-2012, The American Society of Mechanical Engineers, New York, USA.
13. J F Kiefner and P H Vieth (1989), 'A Modified Criterion for Evaluating the Strength of Corroded Pipe', Final Report for Project PR 3-805 to the Pipeline Supervisory Committee of the American Gas Association, Battelle, Ohio.
14. J F Kiefner. P H Vieth and I Roytman (1996), 'Continued Validation of RSTRENG', Pipeline Research Council International, Report Number L51749e. USA, December 1996.
15. Anon. (2010), '*Corroded Pipelines*', DNV-RP-F101. Det Norske Veritas, Norway, October, 2010.
16. A Cosham and P Hopkins (2002), 'The Pipeline Defect Assessment Manual', Proceedings of IPC 2002: International Pipeline Conference. 29 September–3 October 2002, Calgary, Alberta, Canada, Paper IPC02-27067.
17. Anon. (1965), Pipeline Research Committee of the American Gas Association. Proceedings of the Symposia on Line Pipe Research, USA, 1965, 1969, 1974, 1979, 1986, 1993. www.prci.com.
18. W A Maxey, J F Kiefner, R J Eiber and A R Duffy (1972), '*Ductile Fracture Initiation, Propagation and Arrest in Cylindrical Vessels*', ASTM STP 514, American Society for Testing and Materials, Philadelphia, pp. 70–81.
19. J F Kiefner, W A Maxey, R J Eiber and A R Duffy (1973), '*Failure Stress Levels of Flaws in Pressurised Cylinders*', American Society for Testing and Materials, Philadelphia, ASTM STP 536, pp. 461–481.

20. J F Kiefner and A R Duffy (1973), 'Criteria for Determining the Strength of Corroded Areas of Gas Transmission Lines', American Gas Association (AGA) Operating Section on Transmission Conference, AGA.
21. M E Mayfield, W A Maxey and G M Wilkowski (1979), 'Fracture Initiation Tolerance of Line Pipe', Paper F, 6th Symposium on Line Pipe Research, American Gas Association, Houston, Texas.
22. R J Eiber, W A Maxey, C W Bert and G M McClure (1981), 'The Effects of Dents on the Failure Characteristics of Line Pipe', Battelle Columbus Laboratories, Pipeline Research Committee NG18, Report No. 125, May, 1981.
23. Anon. (2007), 'Specification for Line Pipe', Forty-fourth Edition, American Petroleum Institute, October 2007.
24. O H Bjornoy and M Marley (2001), 'Assessment of Corroded Pipelines: Past, Present and Future', Proceedings of the Eleventh International Offshore and Polar Engineering Conference, Stavanger, Norway, 17–22 June 2001.
25. O H Bjørnøy, G Sigurdsson and M J Marley (2001), 'Background and Development of DNV-RP-F101 Corroded Pipelines'. ISOPE 2001, Paper no. 2001-HM-10.
26. B N Leis and T A Bubenik (2001), 'Draft Topical Report Periodic Re-Verification Intervals for High-Consequence Areas', Gas Research Institute Report GRI-00/0230, January 2001.
27. B Leis and X Zhu (2005), 'Corrosion Assessment Criteria: Rationalising their use for Vintage vs Modern Pipelines', Final Report. US Department of Transportation. Research and Special Projects Agency, USA. September 2005.
28. B N Leis and T A Thomas (2001), 'Line pipe Property Issues in Pipeline Design and Re-establishing MAOP', Paper ARC-17, PEMEX International Congress on Pipelines, Merida, Mexico, November 2001.
29. B Fu and A D Batte (1999), 'Advanced Methods for the Assessment of Corrosion Defects in Line Pipe', Health & Safety Executive Summary Report, OTO 1999-051, HSE Books.
30. E Kastner, E Roehrich, W Schmitt and E Steinbuch (1981), 'Critical crack sizes in ductile piping, *International Journal of Pressure Vessels and Piping*, Vol. **9**, pp. 197–219.
31. Anon. (2012), 'Managing System Integrity of Gas Pipelines', American Society of Mechanical Engineers. ASME B31.8-2012, New York, USA.
32. A Cosham. P Hopkins and B Leis (2012), 'Crack-like Defects In Pipelines: The Relevance Of Pipeline-specific Methods And Standards', Proceedings of the 9th International Pipeline Conference. IPC 2012. 24–28 September 2012, Calgary, Alberta, Canada, IPC2012-90459.
33. B N Leis, F W Brust and P M Scott (1991), 'Development and Validation of a Ductile Flaw Growth Analysis for Gas Transmission Line Pipe', Final Report to American Gas Association, NG-18, Catalog No, L51543.
34. B N Leis and N D Ghadiali (1994), 'Pipe Axial Flaw Failure Criteria – PAFFC', Version 1.0 Users Manual and Software, Topical Report to American Gas Association, NG-18, Catalog No. L51720.
35. C E Jaske and J A Beavers (2002), 'Development and Evaluation of Improved Model for Engineering Critical Assessment of Pipelines', Proceedings of IPC 2002, 4th International Pipeline Conference, 29 September –3 October 2002, Calgary, Alberta, Canada.

36. C E Jaske and J A Beavers (2001), 'Integrity and Remaining Life of Pipe With Stress Corrosion Cracking', Final Report on PR 186-9709, PRCI.
37. B Rothwell and R Coote (2009), 'A Critical Review of Assessment Methods for Axial Planar Flaws', Ostende Pipeline Conference, Ostende, Belgium.
38. A Hosseini, D Cronin, A Plumtree and R Kania (2010), 'Experimental Testing And Evaluation Of Crack Defects In Line Pipe', 8th International Pipeline Conference, IPC2010. IPC2010. 27 September–1 October 2010, Calgary, Alberta, Canada, Paper IPC2010-31158.

4

Numerical simulations for cathodic protection of pipelines

C. LIU, A. SHANKAR and M. E. ORAZEM,
University of Florida, USA and D. P. RIEMER,
Hutchinson Technology, Inc., USA

DOI: 10.1533/9780857099266.1.85

Abstract: Mathematical models may be used for design or evaluation of cathodic protection (CP) systems. This chapter provides a historical perspective and a mathematical framework for the development of such models. The mathematical description accounts for calculation of both on- and off-potentials at arbitrarily located surfaces, thus making this approach attractive for simulation of external corrosion direct assessment (ECDA) methods. The approach also allows simulation of independent CP systems. Application of the model is presented for three cases: (a) enhancing interpretation of ECDA results in terms of the condition of the buried pipe; (b) simulating the detrimental influences of competing rectifier settings for crossing pipes protected by independent CP systems (e.g., rectifier wars); and (c) simulating the influence of coatings and coating holidays on the CP of above-ground tank bottoms.

Key words: cathodic protection, boundary element method (BEM), modeling, tank bottoms, external corrosion direct assessment (ECDA), close interval survey.

4.1 Introduction

While simple design equations may be used to predict the performance of corrosion mitigation strategies for simple geometries, more sophisticated numerical models are needed to account for the complexity of industrial structures. For example, the limited availability of right-of-way corridors requires that new pipelines be located next to existing pipelines. Placement of pipelines in close proximity introduces the potential for interference between systems providing CP to the respective pipelines. In addition, the modern use of coatings, introduced to lower the current requirement for CP of pipelines, introduces as well the potential for localized failure of pipes at discrete coating defects. The prediction of the performance of CP systems under these conditions requires a mathematical model that can account for

current and potential distributions in both angular and axial directions. The objective of this chapter is to provide a mathematical description of a model that accounts for CP of structures and to illustrate its application to some complex structures.

4.2 Historical perspective

The design of CP systems for pipelines is typically based on the use of anode resistance formulas (e.g., Dwight's and Sunde's equations), which were developed for bare copper grounding rods.[1,2] Under these conditions, the current density at the anode is much larger than that on the pipe, and resistance formulas, which ignore the current and potential distribution around the pipe, can be used. Newman presented semi-analytic design calculations that account for the potential distribution around the pipe under the assumption that damage to the coating could be considered as having reduced the uniform coating efficiency.[3]

Such analytic and semi-analytic approaches are not sufficiently general to allow all the possible configurations of pipes within a domain, the detailed treatment of potential variation within the pipes, and the polarization behavior of the metal surfaces.[4] Thus, numerical techniques are required. Of the available techniques, the boundary element method (BEM) is particularly attractive because it can provide accurate calculations for arbitrary geometries. The method solves only the governing equation on the boundaries, which is ideal for corrosion problems where all the activity takes place at the boundaries. Brebbia first applied the BEM for potential problems governed by Laplace's equation.[5] Aoki *et al*.[6] and Telles *et al*.[7] reported the first practical utilization of the BEM with simple nonlinear boundary conditions. Zamani and Chuang demonstrated optimization of cathodic current through adjustment of anode location.[8]

Brichau *et al*. first demonstrated the technique of coupling a finite element solution for pipe steel to a boundary element solution for the soil.[9] They also demonstrated stray current effects from electric railroad interference utilizing the same solution formulation.[10] However, their method was limited, in that it assumed that the potential and current distributions on the pipes and anodes were axisymmetric, allowing only axial variations. Aoki presented a similar technique that included optimization of anode locations and several soil conductivity changes for the case of a single pipe without angular variations in potential and current distributions.[11,12]

Kennelley *et al*.[13,14] used a 2-dimensional finite element model to address the influence of discrete coating holidays that exposed bare steel on otherwise well-coated pipes. This work allowed calculations for the angular potential and current distributions. A subsequent analysis employed boundary

elements to assess CP of a single pipe with discrete coating defects.[15,16] This work provided axial and angular potential and current distributions, but was limited to a short length of pipe.

Riemer and Orazem developed a solution for longer pipelines that accounted for the current and potential distributions both around the circumference and along the length of the pipe.[17] Their approach was used to evaluate the effectiveness of coupons used for assessing the level of CP applied to buried pipelines.[18] They also used the program to assess CP of tank bottoms.[19] Their development provides a foundation for modeling CP of long stretches of multiple pipelines, including interaction among CP networks, while retaining the flexibility to account for the role of discrete coating holidays. Adaptive integration techniques were used to generate values of sufficient accuracy for the terms appearing in the coefficient matrices. An efficient non-uniform meshing algorithm was used to avoid numerical errors associated with abrupt changes in mesh size while minimizing the computational cost of the program.

4.3 Model development

The model described below was originally designed to predict the performance of one or more CP systems for an arbitrary number of long pipelines with coating holidays (defects).[17] It has been applied as well for modeling the bottoms of storage tanks.[19] The external domain, e.g., soil or water, was assumed to have a uniform resistivity. Thus, concentrations of ionic species were assumed uniform. Heterogeneous reactions were assumed to occur only at boundaries to the domain of interest, and mass-transport or diffusion effects were included in the expressions for heterogeneous reactions.

4.3.1 Governing equations

The electrolyte conductivity was assumed to be uniform except perhaps at the boundaries. Thus, Laplace's equation governs potential in the electrolyte up to a thin boundary region surrounding the electrodes, i.e.,

$$\nabla^2 \Phi_{sol} = 0 \qquad [4.1]$$

where Φ_{sol} is the potential in the electrolyte referenced to some arbitrary reference electrode. In laminar flow, the boundary (Nernst diffusion layer) may be from 50 to 100 μm and the domain would be large compared to this dimension. For very long electrodes such as pipelines, or for high current densities such as plating, the resistance of the electrode materials and cur-

rent path cannot be neglected, and the potential distribution Φ_{met} within the electrode material can be found from

$$\nabla \cdot (\kappa_{met} \nabla \Phi_{met}) = 0 \quad [4.2]$$

where κ_{met} is the electrical conductivity of the electrode material and its connecting circuitry. Then the thermodynamic driving force for electrochemical reactions at the metal–soil interface can be written as

$$V = \Phi_{met} - \Phi_{sol} \quad [4.3]$$

The two domains, electrode materials and electrolytes, are linked through the electrode kinetics by the conversation of charge, which is expressed as

$$\kappa_{met} n \cdot \nabla \Phi_{met} = \kappa_{sol} n \cdot \nabla \Phi_{sol} \quad [4.4]$$

where κ_{sol} is the conductivity of the electrolyte,

$$\kappa_{sol} = F^2 \sum_i z_i^2 u_i c_i \quad [4.5]$$

F is the Faraday's constant, 96,485 C/eq, z_i is the charge of species i, u_i is the mobility of species i, and c_i is the concentration of species i.

4.3.2 Boundary conditions

To solve Equations [4.1] and [4.2], boundary conditions of the essential kind, ($\Phi = C_1$), or natural ($\vec{n} \cdot \nabla \Phi = C_2$) are needed for all the boundaries in the system (C_1 and C_2 may be constants or functions). For electrodes, the model accounts for polarization kinetics at bare metal and coated surfaces, and at anodes. Insulators may be treated as having a zero normal gradient, i.e., $\vec{n} \cdot \nabla \Phi = 0$, and the insulating nature of the electrolyte–air interface are accounted for through a method of reflections, which is shown later to be exact under the assumption that the interface is planar.

Bare electrode

Following Yan *et al.*,[20] the flux condition on bare metal was represented by a polarization curve that included electrode oxidation, oxygen reduction, and hydrogen evolution reactions, i.e.,

$$i = 10^{\frac{\Phi_{met}-\Phi_{sol}-E_{Fe}}{\beta_{Fe}}} - \left(\frac{1}{i_{lim,O_2}} + 10^{\frac{\Phi_{met}-\Phi_{sol}-E_{O_2}}{\beta_{O_2}}} \right)^{-1} - 10^{\frac{-(\Phi_{met}-\Phi_{sol}-E_{H_2})}{\beta_{H_2}}} \quad [4.6]$$

where Φ_{sol} is the potential in the electrolyte just above the metal,Φ_{met} is the potential of the metal at its surface, i_{lim,O_2} is the mass-transfer-limited current density for oxygen reduction. The parameters β_k and E_k represent the Tafel slope and effective equilibrium potential, respectively, for reaction k. The term E_k accounts for the concentration polarization, the equilibrium potential for the reversible reaction V_k, and the exchange-current-density $i_{o,k}$. If there is supporting electrolyte, then the error due to changes in concentration polarization will be small over a broad range of current densities. When compared to a Butler-Volmer equation, the functionality of E_k takes the form

$$E_k = -\beta_a \log i_o + V_o \quad [4.7]$$

where $V_o = \Phi_{met} - \Phi_{sol}$ is the potential difference such that the anodic and cathodic terms of the full Butler-Volmer equation for reaction k are equal and β_a is the anodic Tafel slope which takes the form

$$\beta_a = \frac{2.303RT}{\alpha_a nF} \quad [4.8]$$

Expressions similar to Equations [4.7] and [4.8] can be written for the cathodic terms in Equation [4.6]. Depending on the chemistry of the electrolyte, additional anodic and cathodic terms may be added to Equation [4.6].

Coated electrode

In order to model the current demands of coated materials, such as may be seen for a long coated pipeline, a model for the polarization of a coated electrode was used. The coating was assumed to act both as a highly resistive electronic conductor and as a barrier to mass-transport. Corrosion, oxygen reduction, and hydrogen evolution reactions were assumed to take place under the coating. The potential drop through the film or coating was expressed as[15]

$$i = \frac{\Phi_{sol} - \Phi_{in}}{\rho\delta} \quad [4.9]$$

where Φ_{sol} is the potential in the electrolyte next to the coating, Φ_{in} is the potential at the underside of the coating just above the steel, ρ is the resistivity of the coating and δ is the thickness of the coating. Thus,

$$i = \frac{A_{pore}}{A}\left[10^{\frac{\Phi_{met}-\Phi_{in}-\Phi_{Fe}}{\beta_{Fe}}} - \left(\frac{1}{(1-\alpha_{Block})i_{lim,O_2}} + 10^{\frac{\Phi_{met}-\Phi_{in}-\Phi_{O_2}}{\beta_{O_2}}}\right)^{-1} - 10^{\frac{-(\Phi_{met}-\Phi_{in}-\Phi_{H_2})}{\beta_{H_2}}}\right] \quad [4.10]$$

where A_{pore}/A is the effective surface area available for reactions, and α_{Block} accounts for reduced transport of oxygen through the barrier. The coating was assumed to have absorbed sufficient water to ensure that the hydrogen reaction was not mass-transfer limited within the effective surface area. Equation (4.9) and (4.10) were solved simultaneously to eliminate Φ_{in} and relate Φ_{sol} to i.

Anodes

To account for potential draw-down at the anode, the flux condition at the anode employed a simple polarization model accounting for corrosion and oxygen reduction as

$$i = i_{O_2}\left(10^{\frac{\Phi_{met}-\Phi_{sol}-E_{corr}}{\beta_{anode}}} - 1\right) \quad [4.11]$$

where i_{O_2} is the mass-transfer-limited current density for oxygen reduction, E_{Corr} is the free corrosion potential of the anode and β is the Tafel slope for the anode corrosion reaction. Typical parameter values are given in the literature.[19,21] In order to have the necessary essential boundary conditions, Equation [4.11] was solved for Φ_{sol}, whereas Equations [4.6]–[4.10] were used as natural boundary conditions on the cathodes.

4.3.3 Numerical solution

Equation [4.1] was solved using the boundary integral method (BIM),[22] which takes the form

$$\Phi_i + \int_\Gamma \Phi\left(\frac{\partial G(\xi,x)}{\partial \vec{n}}\right)d\Gamma(x) = \int_\Gamma G(\xi,x)(\vec{n}\cdot\nabla\Phi)d\Gamma(x) \quad [4.12]$$

valid for any point i within a domain Ω, where Γ represents surfaces of electrodes and insulators and $G(\xi,x)$ is the Green's function for Laplace's equation. G relates to a source point $\xi = (x_o, y_o, z_o)$ and field point $x = (x, y, z)$ by

$$G(\xi, x) = \frac{1}{4\pi r(\xi, x)} \quad [4.13]$$

where r is defined as

$$r(\xi, x) = \sqrt{(x - x_o)^2 + (y - y_o)^2 + (z - z_o)^2} \quad [4.14]$$

Equation [4.12] is exact for any domain Ω with surface $\partial G = \Gamma$. Error will come from discretizing Equation [4.12] into a boundary element method (BEM).

When the source point i is moved to a boundary, both integrals will have a singularity at i and the quantity Φ_i appears in two places

$$c_i \Phi_i + \int_\Gamma \Phi \left(\frac{\partial G(\xi, x)}{\partial \vec{n}} \right) d\Gamma(x) = \int_\Gamma G(\xi, x)(\vec{n} \cdot \nabla \Phi) d\Gamma(x) \quad [4.15]$$

where c_i now represents the solid angle of the surface Γ at the source point, and a second order singularity appears in the first integral. It has a finite value that can be quickly shown by transforming the integral to spherical coordinates with origin i.

Half-space

In the present work, it is assumed that the domain of the electrolyte can be accounted for as a half-space with a planar boundary described by the equation $z_o = 0$. A specialization of the Green's function is used to account exactly for there being only a half-space. It is derived using the method of images[23] and takes the form

$$G_{\xi,x} = -\frac{1}{r(x_i, x_j)} - \frac{1}{r(x_i, x_j')} \quad [4.16]$$

where, as is shown in Fig. 4.1, x_j' is the reflected field point about the plane that defines the half-space, $z_o = 0$. The derivative of G with respect to the unit normal vector at the field point is

$$4\pi \frac{\partial G_{i,j}}{\partial \vec{n}} = -\vec{n}_{\mathbf{x}_j} \cdot \nabla \frac{1}{r} - \vec{n}_{\mathbf{x}_j'} \cdot \nabla \frac{1}{r'} \quad [4.17]$$

which becomes the kernel of the first integral in Equation [4.15]. At a source point on the plane of reflection, the flux in the z-direction is equal to zero. It can be verified by taking the z-component of the gradient of Equations [4.16] and [4.17] at a source point given by $\mathbf{x}_o = [x_o, y_o, z_o = 0]$

$$4\pi \frac{\partial G}{\partial z_0}\bigg|_{z_o=0} = \frac{z}{r^3} - \frac{z}{r'^3} = 0 \qquad [4.18]$$

and for the normal derivative

$$4\pi \frac{\partial}{\partial z_o}\left(\frac{\partial G}{\partial \vec{n}}\right)\bigg|_{z_o=0} = \frac{-3z^2\vec{n}_z}{r^5} + \frac{3z^2\vec{n}_z}{r'^5} - \frac{\vec{n}_z}{r'^3} + \frac{\vec{n}_z}{r^3} = 0 \qquad [4.19]$$

because at $z = 0, r = r'$.

An equation of the form of Equation [4.15] was written for each node in the mesh describing the surfaces of the components of an electrolytic system, i.e. anodes, cathodes, and insulators not accounted for through the Green's function.

The final surface to account for is the hemisphere at an infinite distance that encloses the system. The surface is assumed to have a single unknown potential, Φ_∞, and no current passes through it. One more term is added to the left hand side of Equation [4.15], which is the integral of $\Phi_\infty\left(\vec{n}\cdot\nabla G_{i,j}\right)$ over the surface of the enclosing hemisphere of the half-space. The outward normal vector to the enclosing surface centered at $x_j = (x_0, y_0, z_0)$ at the integration point $x_i = (x, y, z)$ is in the same direction as the line-segment r and of unit length and given by

$$\vec{n} = \frac{1}{r}[(x - x_o), (y - y_o), (z - z_o)] \qquad [4.20]$$

The integral can be calculated by a transformation to spherical coordinates:

$$\lim_{\rho\to\infty}\int_0^{2\pi}\int_0^{\pi/2}\Phi_\infty\left(\vec{n}\cdot\nabla G_{i,j}\right)\rho^2\sin\phi\,\mathrm{d}\phi\,\mathrm{d}\theta \qquad [4.21]$$

For any point on the plane $z = 0$, Equation [4.21] is calculated to be identically equal to 1 for the Green's function given in Equation [4.16]. The term on the left hand side of Equation [4.15] is equal to 0 since no current crosses

the surface. Because of the additional unknown, one more equation must be added that explicitly states the conservation of charge on the remaining surfaces, i.e.,

$$0 = \int_{\Gamma} \vec{n} \cdot \nabla \Phi_{\text{sol}} d\Gamma \qquad [4.22]$$

Equation [4.2], which governs the current flow within the materials of the cathode, anode, and connecting circuitry, was solved using a finite element method (FEM) in three dimensions. The same mesh used for the BEM solution in the electrolyte domain was used for the FEM solution in the electrode material domain under the assumption that the electrode was a thin annulus with negligible potential variation within the thickness of the material. The two methods were coupled by Equation [4.4], which provides a charge balance at the interface. The equation is also equal to the kinetic expressions in Equations [4.6] and [4.9]–[4.11] scaled by the conductivity, i.e.,

$$\vec{n} \cdot \nabla \Phi_{\text{sol}} = -\frac{i_{\text{kinetics}}}{\kappa_{\text{sol}}} \qquad [4.23]$$

or

$$\vec{n} \cdot \nabla \Phi_{\text{met}} = -\frac{i_{\text{kinetics}}}{\kappa_{\text{met}}} \qquad [4.24]$$

for the non-electrolyte portion of the circuit. Pipelines and anodes were joined in the non-electrolyte circuit through use of 1-D finite elements of appropriate resistance.

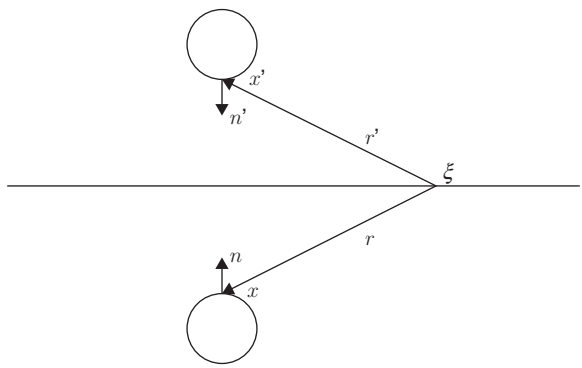

4.1 Diagram of source field and image of field.

Solving the nonlinear system

A variable transformation, $\Psi = \Phi_{met} - \Phi_{sol}$ was needed to provide stable convergence behavior for the combined BEM and FEM system of equations. Here, Ψ represents the driving force for the electrochemical kinetics. The variable Φ_{met} was eliminated from the system of equations and, upon adding the necessary terms for the potential at infinity and charge conversation, the system of equations could be written as

$$\begin{bmatrix} 0 & -G_{a,c} & H_{c,c} & H_{a,c} & -4\pi \\ 0 & -G_{a,a} & H_{c,a} & H_{a,a} & -4\pi \\ K_c & 0 & K_c & 0 & 0 \\ 0 & -\widehat{F}_a & 0 & K_a & 0 \\ 0 & -A_a & 0 & 0 & 0 \end{bmatrix} \begin{bmatrix} \Psi_c \\ \vec{n}\cdot\nabla\Phi_a \\ \Phi_c \\ \Phi_a \\ \Phi_\infty \end{bmatrix} = \begin{bmatrix} G_{c,c} & 0 \\ G_{c,a} & 0 \\ \widehat{F}_c & 0 \\ 0 & -K_a \\ A_c & 0 \end{bmatrix} \begin{bmatrix} \vec{n}\cdot\nabla\Phi_c \\ \Psi_a \end{bmatrix} \qquad [4.25]$$

where all of the unknowns have been moved to the left hand side and all the Φ terms refer to the potential in the electrolyte next to an electrode. The terms H and G are sub-matrices resulting from evaluation of the integrals in Equation [4.15]. Following the matrix notation of Brebbia *et al.*,[22] the first subscript to appear is the field point and the second is the source point. The sub-matrix K is the stiffness matrix from the FEM solution for the electrode materials and $\widehat{F}$ is the charge balance between the electrode and electrolyte domains. The sub-matrix A, given by

$$A = \int_{-1}^{1} \xi(\Gamma)\eta(\Gamma)J \, \mathrm{d}\Gamma \qquad [4.26]$$

is the surface area as represented by the shape functions for the elements used. The term J is the Jacobian of the coordinate transformations from Cartesian to curvilinear. It provides the correct weighting of the nodal values of the current density such that electroneutrality is enforced.

4.3.4 Calculation of potentials within the electrolyte

The model allows calculation of both on- and off-potentials at arbitrarily chosen locations within the electrolyte or on the electrolyte surface defined by the Green's function through the method of the images. The on-potential is defined as the potential that would be measured between a reference electrode at some point in the electrolyte and a cathode if the anodes were connected to the cathodes and current were flowing between them. The off-potential is defined as the potential difference measured between a

reference electrode at some point within the electrolyte and the cathode at a moment just after the anodes have been disconnected but the cathodes are still polarized. The method employed is summarized below.

On-potentials

The on-potential was obtained under the conditions where anodes are connected to the cathodes and, in the case of impressed current systems, are energized. The condition is straightforward to model. Using the solution for the entire electrolytic systems, points in the domains were calculated using equations described by Brebbia *et al*:[22]

$$\Phi_{\mathrm{i}} = \int_{\Gamma} G_{\mathrm{i,j}}(\vec{n}\cdot\nabla\Phi)\,\mathrm{d}\Gamma - \int_{\Gamma}\Phi(\vec{n}\cdot\nabla G_{\mathrm{i,j}})\,\mathrm{d}\Gamma \qquad [4.27]$$

where Φ_i is the unknown potential at a point not on the boundary Γ, and Φ and $\vec{n}\cdot\nabla\Phi$ are the solutions on Γ found by solving Equation [4.17].

Current density vectors can be found by differentiating Equation [4.27] at the source points.

$$\frac{\partial\Phi_{\mathrm{i}}}{\partial x_{\ell}} = \int_{\Gamma}\frac{\partial G_{\mathrm{i,j}}}{\partial x_{\ell}}(\vec{n}\cdot\nabla\Phi)\mathrm{d}\Gamma - \int_{\Gamma}\Phi\frac{\partial(\vec{n}\cdot\nabla G_{\mathrm{i,j}})}{\partial x_{\ell}}\,\mathrm{d}\Gamma \qquad [4.28]$$

where three equations of the form of Equation [4.28] are written for the three components of the current vector, $\ell = 1, 2, 3$. The resulting gradient of Φ_i is combined with the electrolyte conductivity to get the current.

Off-potentials

Off-potentials were calculated after a solution was obtained using the model described above. The anodes were removed from the problem, and the calculated potentials on the cathode were used as boundary conditions for a new calculation. As the metal under the coating is polarized and, therefore, the source of the potential, the potential used for coated electrodes was the value underneath the coating, Φ_{in} (see Equations [4.9] and [4.10]).

Equation [4.25] was rewritten dropping the anodes and using the previous solution for the potential on the cathodes as the known boundary condition, i.e.,

$$\begin{bmatrix} H_{\mathrm{p,p}} & -4\pi \\ 0 & 0 \end{bmatrix}\begin{bmatrix} \Phi_{\mathrm{in,p}} \\ \Phi_{\infty} \end{bmatrix} = \begin{bmatrix} G_{\mathrm{p,p}} \\ A_{\mathrm{p}} \end{bmatrix}\begin{bmatrix} \vec{n}\cdot\nabla\Phi_{\mathrm{in,p}} \end{bmatrix} \qquad [4.29]$$

where a new potential at infinity, Φ_∞, is found. All the values on the left hand side of Equation [4.29] are known, and the current densities, driven by the potential distribution along the cathodes, can be easily found. The new solution is then used to find the potentials within the electrolyte through Equation [4.12] using only the previous cathodes as sources.

4.4 Model validation

A computer code was written that implements the above model. The model can be compared to analytical solutions to Laplace's equation to validate the code.

4.4.1 Comparison to analytic solutions

The first comparison was made to the variation of potential around a disk electrode placed at the surface of a semi-infinite electrolyte with a hemispherical counter electrode infinitely far away. An analytic solution by Newman is available.[24] A limitation of the numerical model as implemented was that all anodes/cathodes had to be either disks or cylinders. A simple remedy would be to make the potential at infinity (Φ_∞) a known, and move it to the other side of Equation [4.17]. Then the new unknown is the total current entering or leaving the system through the hemisphere at infinity that encloses the system. In the case presented here, a counter electrode that was a factor of 4.0×10^{11} times larger than the disk was used to approximate the counter electrode in Newman's example. It was moved as far from the disk as numerically practicable.

A number of points were selected on the electrolyte surface for calculation of the potential. To illustrate the procedure, a grid of points extending away from the disk is presented in Fig. 4.2 where a calculation would be performed at each line intersection. The center section of points oriented in the r direction is used for comparison.

A comparison between the numerical and analytical results is presented in Fig. 4.3. The values of potential are in good agreement, and the error

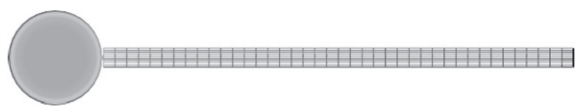

4.2 Completed mesh with points for soil surface potential calculation added. The points are represented as a grid where the intersections of the lines are the calculation points.

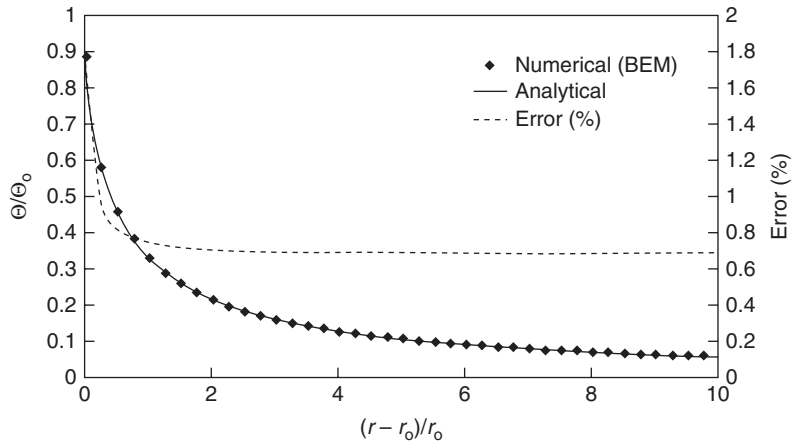

4.3 Comparison of the analytical and numerical solutions for the potential at the electrolyte surface. The term represents the distance from the edge of the disk.

between the analytical and numerical solutions is less than 1.8%. The increase in error close to the disk is the due to the fact that the numerical method cannot adequately represent the infinite current density at the edge of the disk. The constant error of 0.7% far from the disk is due to the finite size of the counter electrode and decreases as the counter-electrode area is increased.

A second validation was done against Kasper's solution for parallel cylinders of unequal size.[25] In this case, two cylinders were placed far from the electrolyte surface. One was 0.5 m diameter, the second was 0.1 m diameter, and they were placed such that their centers were 1 m apart as presented in Fig. 4.4. The boundary conditions for both surfaces were equipotential with the first set to 0 V and the second set to 1 V.

The potential in the electrolyte was calculated for a line running from the large cylinder to the small. The result is compared to the analytic solution in Fig. 4.5. The error in the numerical method does not exceed 0.1%. Therefore, given any arbitrary current and potential distribution on a set of electrodes that satisfies Laplace's equation, the resulting potential distribution within the electrolyte can be calculated with reasonable accuracy.

If the potential calculated at some point in the electrolyte is subtracted from another point at an electrode surface, one would have a reasonable approximation of a physical measurement made with a reference electrode. Therefore, the numerical method may be used to evaluate ways of using reference electrodes to determine the condition of an electrolytic system, such as a CP system or solid phase electrolytes.

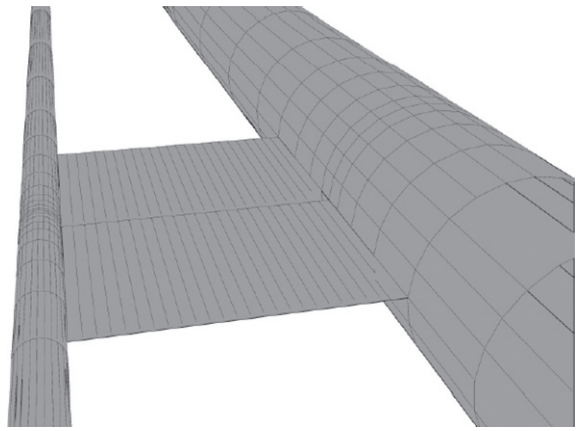

4.4 Model used to compare numerical method to Kasper's solution for two parallel cylinders. The surface between the cylinders represents the points in the electrolyte to calculate the potential.

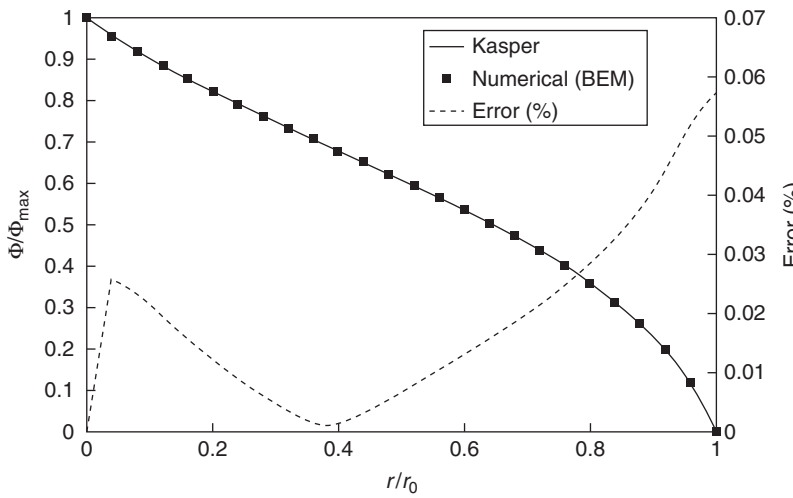

4.5 Comparison of the potential within the electrolyte to Kasper's solution for two parallel cylinders. The variable r/r_0 represents the distance from the edge of the first cylinder normalized to the distance between the cylinders.

4.4.2 Example calculation

To illustrate the manner in which on- and off-potentials are calculated, a simulation was performed for a 1.6 km (1-mile) stretch of pipe. The pipe was connected to a high-performance magnesium anode located at the 0.305 km (1000 ft) position along the length of the pipe. A 0.9×0.3 m^2 (3×1 ft^2)

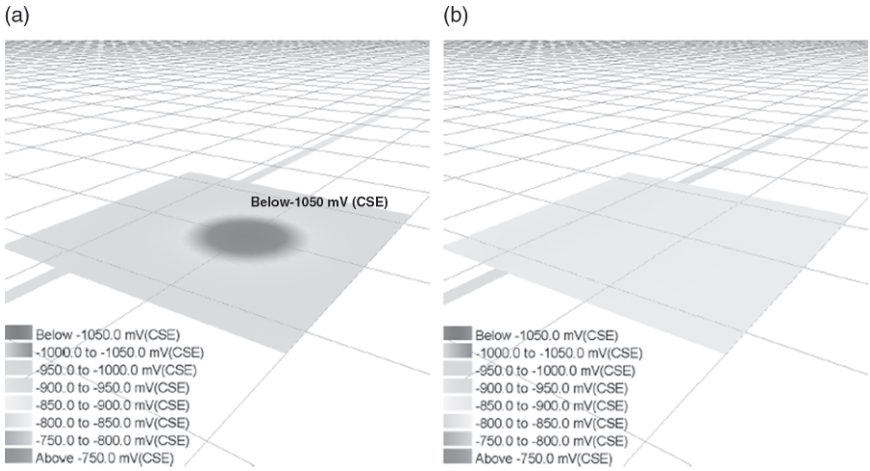

4.6 Calculated potential distribution on the soil surface above the anode (see Fig. 4.7): (a) on-potentials; (b) off-potentials.

coating defect, exposing bare steel, was assumed to be located at the 0.762 km (2500 ft) position. The pipeline was located 0.61 m (2 ft) below grade. Surface on-potentials, shown in Fig. 4.6a, reveal the location of the anode. The grid spacing used in these calculations was 6.1 m $\times$ 6.1 m (20 ft $\times$ 20 ft). For reference, the corresponding configuration of pipe and anode is presented in Fig. 4.7. As shown in Fig. 4.6b, surface off-potentials, calculated by removing the influence of the anode, obscure the anode location.

The location of a massive ($0.9 \times 0.3\,m^2$) coating defect is seen in the surface on-potentials, shown in Fig. 4.8a, in which the color scale has been changed to facilitate viewing of the potential variation. The significant change in potential at the soil surface level is seen for these calculations because the defect is large, is located at the top of the pipe, is severely under-protected, and is located very close to the soil surface. The values of the off-potential readings shown in Fig. 4.8b suggest that the pipe is under-protected. The size of the coating defect can be seen in Fig. 4.9, where a false-color image of the cathodic current is presented. The majority of CP current is delivered to the exposed steel at the coating defect.

The on- and off-potential distributions shown in Figs 4.8a and 4.8b may be measured in the field, whereas the information presented in Fig. 4.9 could be inferred only after excavation. The BEM model could be used to calculate other measurable quantities, such as the local values for current passed through the pipe. Thus, the BEM model can be used to provide information that can be correlated to the results of ECDA simulations. Such an approach has been suggested for inverse models for interpretation of field ECDA data.[26,27]

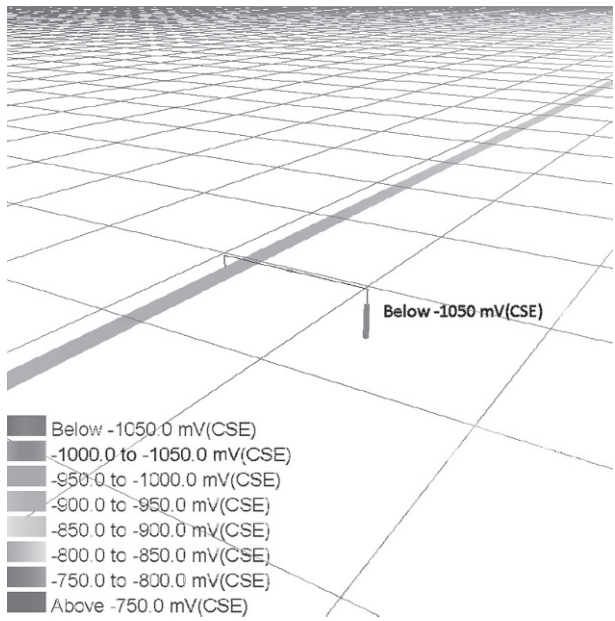

4.7 Image revealing the location of the anode and pipeline corresponding to Fig. 4.6.

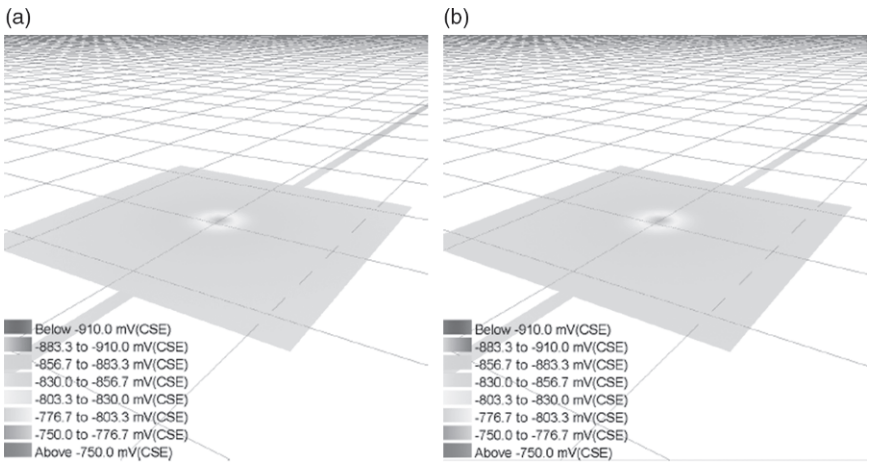

4.8 Calculated potential distribution on the soil surface above a $0.9 \times 0.3\,m^2$ ($3 \times 1\,ft^2$) coating defect exposing bare steel: (a) on-potentials and (b) off-potentials.

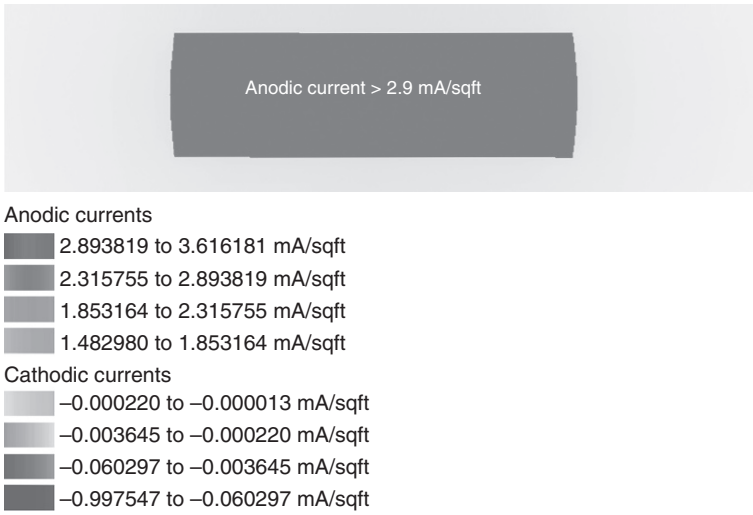

4.9 False-color image of the calculated current distribution on the surface of a coating defect.

4.5 Applications

Three applications of CP models are presented in this section. The model is used to provide guidance for assessing the condition of the buried pipes through indirect techniques based on currents and potentials measured at the soil surface. In a second example, the model is used to demonstrate the coupling between individual CP systems associated with rectifier wars. In a third example, the model is used to explore the role of coatings on protection of tank bottoms.

4.5.1 Simulations for external corrosion direct assessment (ECDA)

Indirect techniques based on currents and potentials measured at the soil surface can be used to evaluate the condition of buried pipelines. These techniques are the foundation of ECDA protocols.[28] The CP model was used to generate simulations to explore the sensitivity of close interval survey (CIS), direct current voltage gradient (DCVG), alternating current voltage gradient (ACVG), and current attenuation techniques to pipe condition.

Calculations were performed for a 16.1 km (10 mile) stretch of pipe with model parameters as listed in Table 4.1. The pipe was protected for all simulations by an impressed current CP system. The anode was located at

Table 4.1 The matrix of model runs showing the ranges of different parameters that were varied

Flaw size in^2 (cm^2)	Soil resistivity kΩ cm	Depth of cover ft (m)	Pipe outside diameter in (cm)	CP level mV(Cu/$CuSO_4$)
1 (6.5)	0.5	4 (1.22)	6 (15.2)	–799 to –700 (low CP)
16 (103)	3	8 (2.44)	12 (30.5)	–999 to –900 (med CP)
36 (232)	10	16 (4.88)	48 (122)	–1199 to –1100 (high CP)
64 (413)	50			
100 (645)	100			
	1000			

3.5 km (11 500 ft) along the length of the pipe and was placed at a depth of 1.6 km (5250 ft). The coating defect was located at 7.92 km (26 000 ft) along the length of the pipe and was placed on the top surface of the pipeline. The pipeline was located 1.21 m (4 ft) below grade. The surface potentials presented are those in close proximity of the coating defect and represent over-the-line potentials.

Soil surface potentials, calculated for a line directly above the pipe and in close proximity to a large coating flaw, are presented in Fig. 4.10. These results were generated from the mathematical model described in Section 4.3 and were intended to mimic CIS results. The nodes of the soil surface that lie directly above the pipeline were spaced 0.61 m (2 ft) apart. The smaller measurement intervals were used to improve resolution of the profiles generated. Normally, the CIS measurements are taken at intervals between 0.75 m (2.5 ft) to 1.5 m (5 ft). A dip is present for both the on-potential profile and the off-potential profile. The dips in potential are caused by the local large values of cathodic current densities associated with the coating flaw. The locally large value of current density creates a corresponding potential distribution at the soil surface. The on-potentials are more negative and at more protected potentials than the off-potentials, due to the CP system being connected for on-potential measurements and disconnected for off-potential measurements. Figure 4.10 provides a typical soil surface potential profile expected for a single coating defect. The influence of coating flaw size on the surface potential readings is presented in Fig. 4.11. The magnitude of the size of the dips increases with increasing coating defect size.

The influence of soil resistivity on the surface potential readings is presented in Fig. 4.12. As soil resistivity increased, the on-potential became more positive, indicating that the CP system's protection of the pipeline has decreased. This is due to a reduced amount of current that can reach the pipeline at higher soil resistivities. No trend was found relating the size of the dips with changes in soil resistivity. The off-potential profiles were

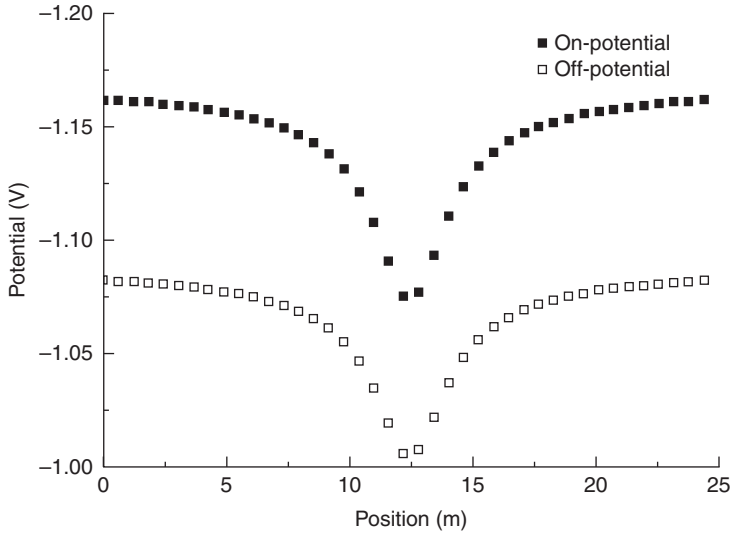

4.10 CIS data generated by the mathematical model in the proximity of a coating defect. The coating defect size was 645 cm² (100 in²) and was placed at a position 12.5 m along the length of the soil surface.

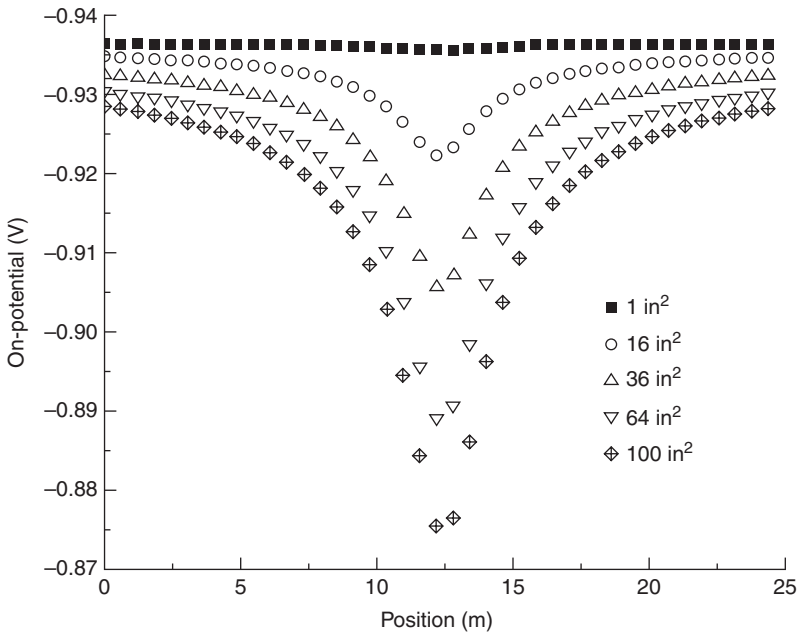

4.11 The over-the-line soil surface on-potentials as a function of position along the soil surface with coating defect size as a parameter.

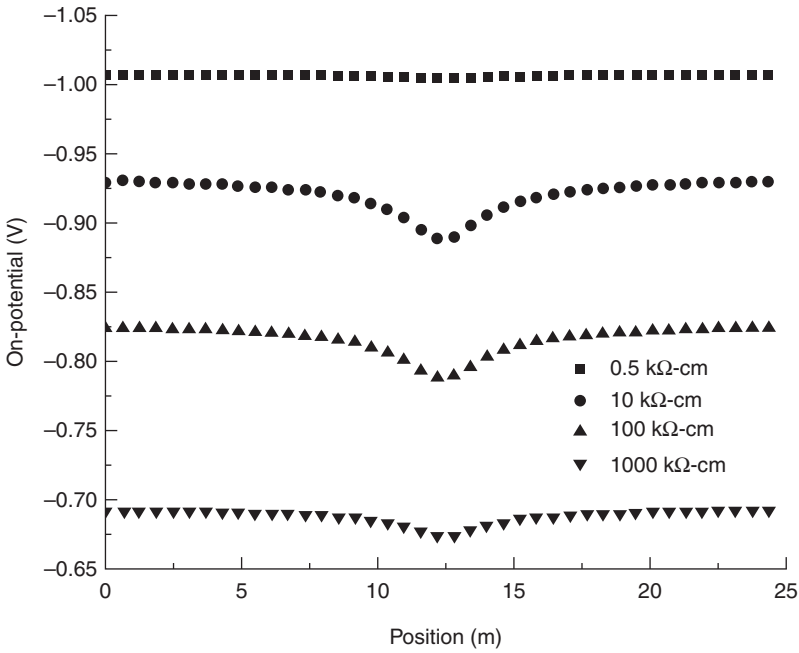

4.12 The over-the-line soil surface on-potentials as a function of position along the soil surface with soil resistivity as a parameter.

then subtracted from the on-potential profiles and are presented in Fig. 4.13. Figure 4.13 demonstrates that the difference in the on- and off-potentials also yields a dip centered at the location of the coating defect. The simulation results show that dips become smaller as soil resistivity increases. For soil resistivity values of 100 kΩ and above, no dips in potential were present, suggesting that high soil resistivities may hide the presence of a coating flaw.

The effect of soil resistivity and coating flaw (holiday) size on the value of calculated indications was first explored using software utilizing Section 4.3. Figure 4.14 was developed to show the correlation between DCVG indications in mV versus flaw size based on changing soil resistivities. Two main trends are found in Fig. 4.14. One trend is that DCVG indications in mV will increase with increasing flaw size, which is consistent with conventional knowledge. The other trend is that as soil resistivity increases the DCVG indication decreases. This trend is a result that was not initially expected. Since these are competing trends, it is of interest to determine which trend has a dominating effect on indications. By taking a closer look at Fig. 4.14, it appears that soil resistivity plays a larger role than flaw size in determining DCVG indication in mV. This is supported by the behavior

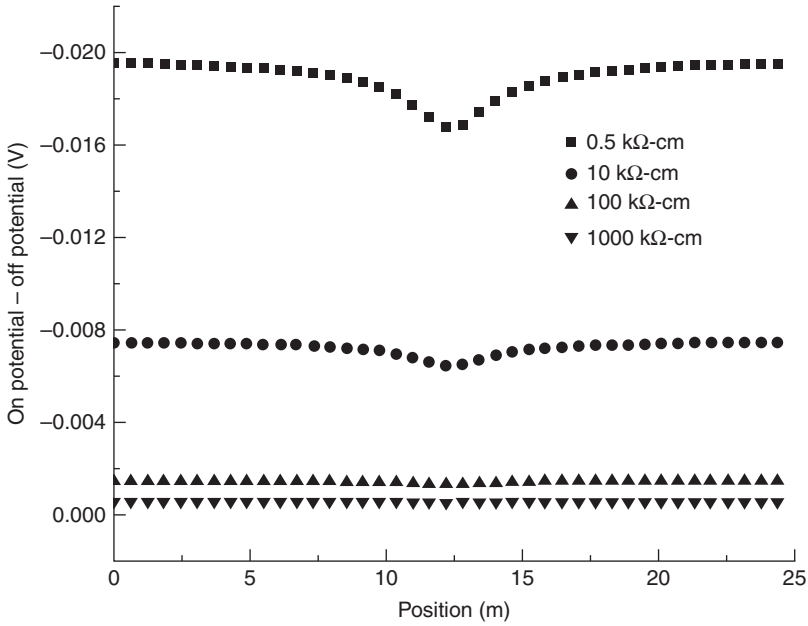

4.13 The difference in on- and off-potentials as a function of position along the soil surface with soil resistivity as a parameter.

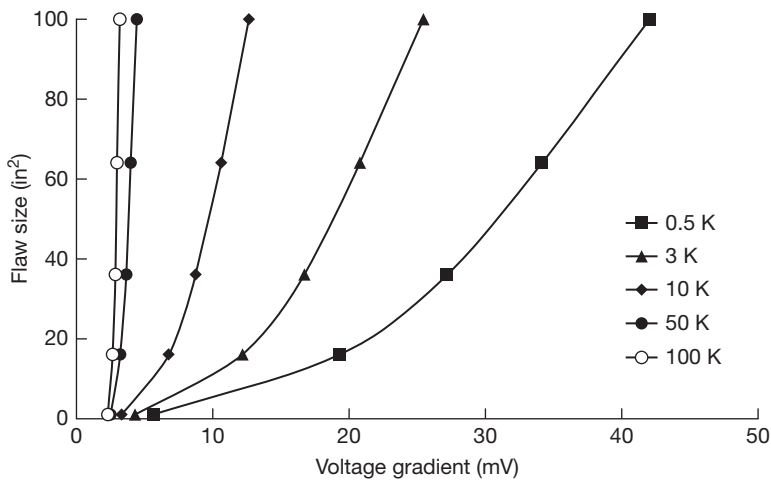

4.14 Coating flaw size as a function of the DCVG indication in mV with soil resistivity as a parameter. The pipe diameter was 12 in, the depth of cover was 4 ft, and the anode potential was 5 V.

at high soil resistivities, where the DCVG indications show almost no dependence on flaw size. Conversely, there is a wide distribution of DCVG indications at low soil resistivities. This result shows that prioritization of DCVG indications in mV can be much improved by taking soil resistivity into account.

DCVG indications were converted to percent-IR, as shown in Fig. 4.15. This plot also shows the effect of soil resistivity and flaw size on indications, except that here the DCVG indications are in percent-IR. In this case, the percent-IR calculations were made by scaling by the IR drop over the coating flaw. The results show that percent-IR indication increases both with increasing coating flaw size and increasing soil resistivity. This plot also shows that soil resistivity can have a greater effect on percent-IR values than flaw size. For example, for each soil resistivity, the relative change of indications stays the same. This means that as flaw size changes, the percent-IR indication changes by the exact same incremental value regardless of what soil resistivity that the system is at. This result shows that percent-IR indications can also be better prioritized by taking soil resistivity into account. In other words, the percent-IR indications obtained could be misinterpreted, causing an inaccurate prediction of the coating flaw severity if the soil resistivity is not known or included in evaluations. For example, in Fig. 4.15, a large percent-IR value could be due to a high soil resistivity and not necessarily a large coating flaw size.

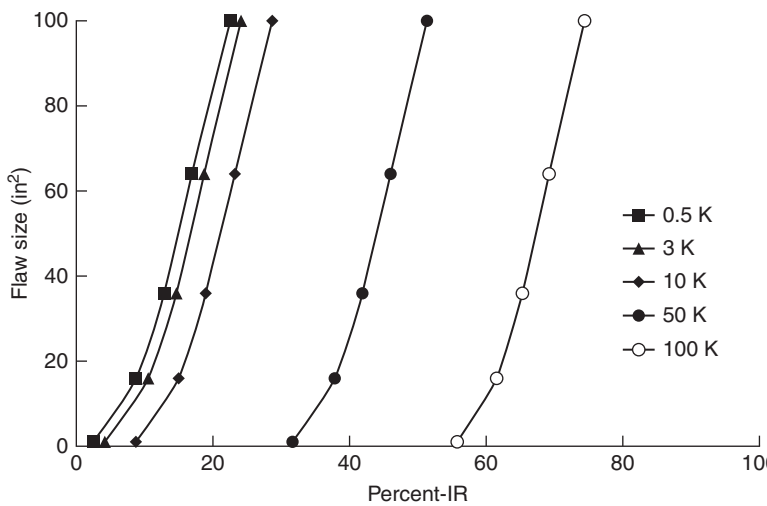

4.15 Coating flaw size as a function of the DCVG indication in percent-IR with soil resistivity as a parameter. The pipe diameter was 12 in, the depth of cover was 4 ft, and the anode potential was 5 V.

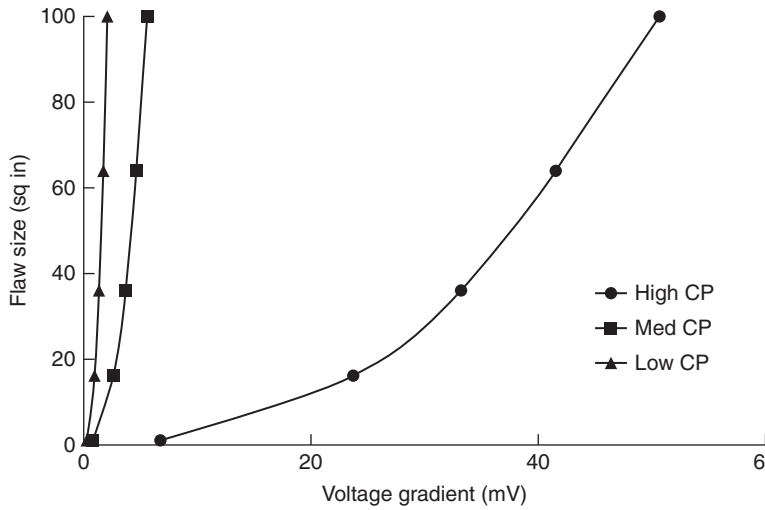

4.16 Coating flaw size as a function of the DCVG indication in mV with CP level as a parameter. The pipe diameter was 12 in, the depth of cover was 4 ft, and the soil resistivity was 500 Ω cm.

In Fig. 4.16, the effect of changing CP levels is explored on DCVG indications in mV. The CP level was adjusted by increasing the anode voltage, and CP levels were categorized by ensuring that off-potentials on the soil surface far away from the coating flaw were within certain ranges. The CP levels and their corresponding potential ranges are shown in Table 4.1. Figure 4.16 also shows that DCVG indications increase with increasing coating flaw size as previously found. However, this graph is primarily included to show that increased CP has a large effect on DCVG signal in mV. Notice that the distribution in voltage gradients in Fig. 4.16 is more apparent at larger CP levels. These larger voltage gradients at higher CP levels can be explained by a larger amount of current entering the pipeline at the flaw location. This shows that at lower CP levels, the presence of a flaw size could be undetected. Therefore, the severity of a flaw could be misinterpreted if CP levels were not taken into account. A sufficient amount of CP current is needed in order to yield a measurable voltage gradient. DCVG in percent-IR was also plotted exactly as in Fig. 4.16. This is shown in Fig. 4.17. The obvious result shown here is that the percent-IR values do not change with increased CP level. This result could be helpful in predicting flaw size based on DCVG indications in percent-IR.

Sensitivity of indications of DCVG in mV is also evaluated based on changing depth of cover as shown in Fig. 4.18. The results show that DCVG indications are more sensitive to a pipeline buried at 4 ft than at 8 ft. Although not shown here, previous simulations have further supported

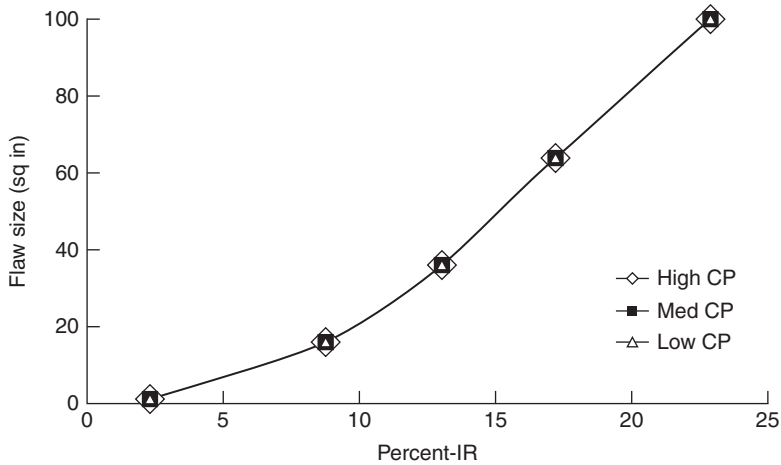

4.17 Coating flaw size as a function of the DCVG indication in percent-IR with CP level as a parameter. The pipe diameter was 12 in, the depth of cover was 4 ft, and the anode potential was 5 V. The pipe diameter was 12 in, the depth of cover was 4 ft, and the soil resistivity was 500 Ω cm.

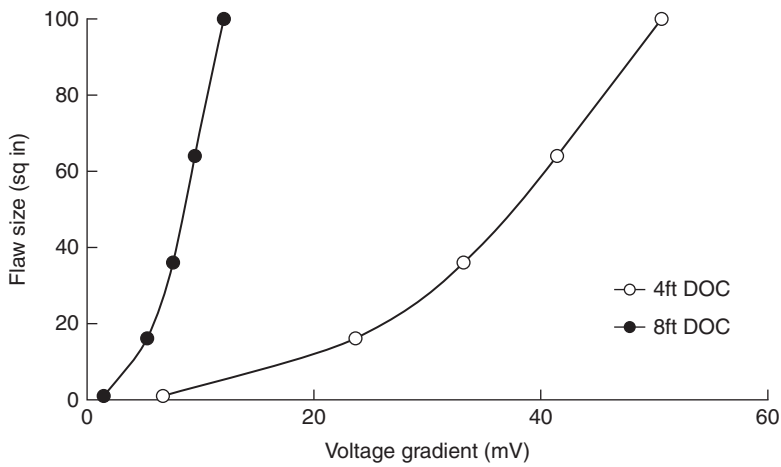

4.18 Coating flaw size as a function of the DCVG indication in mV with depth of cover (DOC) as a parameter. The pipe diameter was 12 in, the soil resistivity was 500 Ω cm, and the CP level was high.

this trend where indications at larger depths of cover are practically negligible. This trend indicates that depth of cover should be used in prioritizing indications. For similar conditions in Fig. 4.18, a plot of DCVG indication in mV is given versus changing pipe diameter. There is no clear trend found

from this result, as shown in Fig. 4.19. However, this result is not considered as proof that pipe diameter does not have an effect on DCVG indication in mV.

CIS on-potential dip (on-dip) indications are plotted against flaw size based on changing soil resistivity in Fig. 4.20. One basic trend shows that

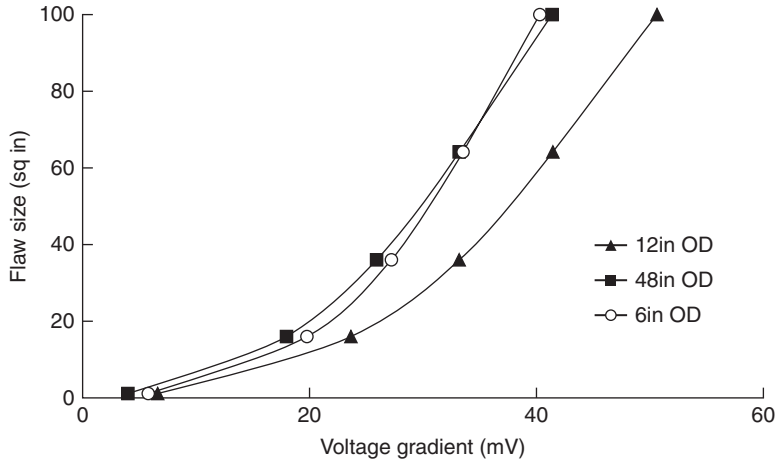

4.19 Coating flaw size as a function of the DCVG indication in mV with pipe diameter (OD) as a parameter. The soil resistivity was 500 Ω cm, the DOC was 4 ft, and the CP level was high.

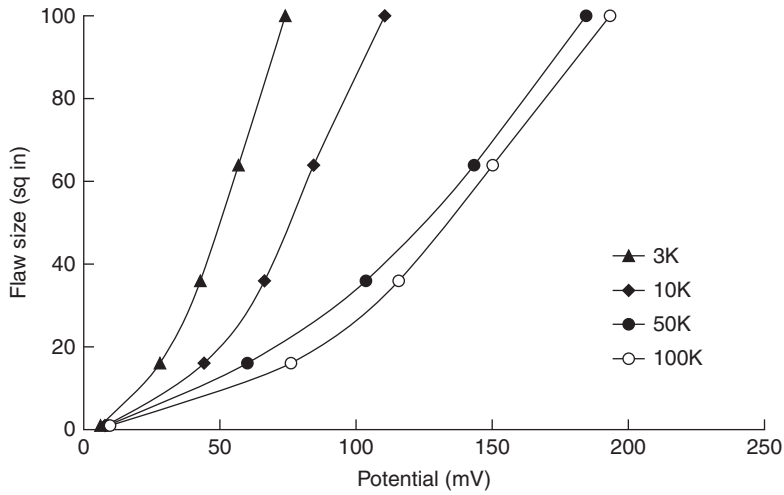

4.20 Coating flaw size as a function of the CIS on-potential dip indication in mV with soil resistivity in Ω cm as a parameter. The pipe diameter was 12 in, the DOC was 4 ft, and the CP level was high.

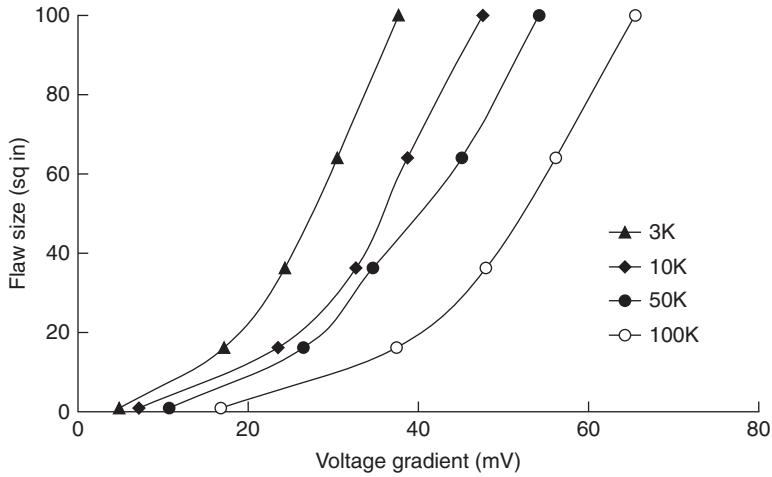

4.21 Coating flaw size as a function of the DCVG indication in mV with soil resistivity in Ω cm as a parameter. The pipe diameter was 12 in, the DOC was 4 ft, and the CP level was high.

CIS on-dip indication increases with increasing flaw (holiday) size. Another trend is that the CIS on-dips increase as soil resistivity increases. However, this result is due to increasing the anode voltage for higher soil resistivities. The anode voltage was adjusted for each simulation to maintain a high CP level (refer to Table 4.1). If the anode voltage had been held constant throughout all runs, the indications would have decreased with increasing soil resistivity. DCVG indications were also calculated for high CP levels, as shown in Fig. 4.21. Note that the DCVG trend in mV for Fig. 4.21 is opposite with respect to soil resistivity than it was in Fig. 4.14. This is because in Fig. 4.14, the anode voltage was held constant for all runs. This indicates that raising the anode voltage increases the DCVG indication found, even if soil resistivity is simultaneously increased.

Figure 4.22 is based on data from the same simulations run in Fig. 4.20. However, it shows a different result for some soil resistivities. The negative CIS off-dips initially represented an area of concern. The on- and off-potential profiles are given for a simulation that gives a negative CIS off-dip in Fig. 4.23. A general potential profile represents current direction by moving from positive to negative potentials. In Fig. 4.23, the on-potential profile shows that current enters the pipeline at the coating flaw and then travels away from the flaw based on the profile of on-potential moving from positive to negative. This behavior is normally expected for the off-potential profile as well. However, the negative CIS off-dip indicates that when the CP current is turned off, the potential flows back toward the flaw. This can

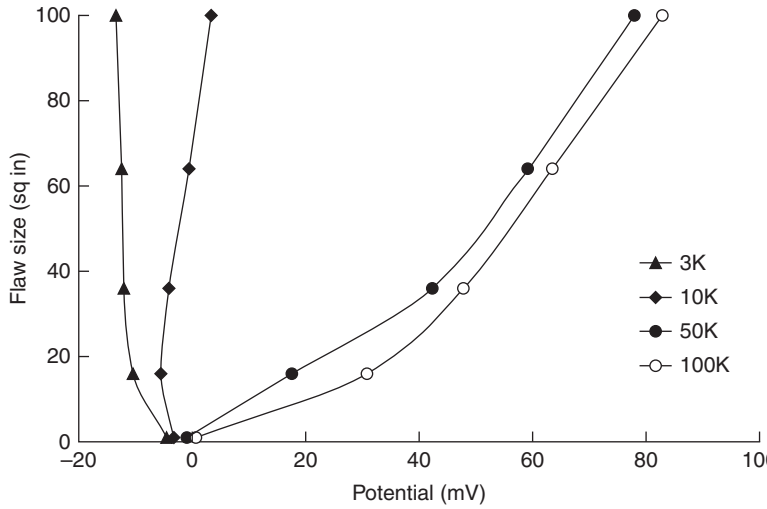

4.22 Coating flaw size as a function of the CIS off-potential dip indication in mV with soil resistivity in Ω cm as a parameter. The pipe diameter was 12 in, the DOC was 4 ft, and the CP level was high.

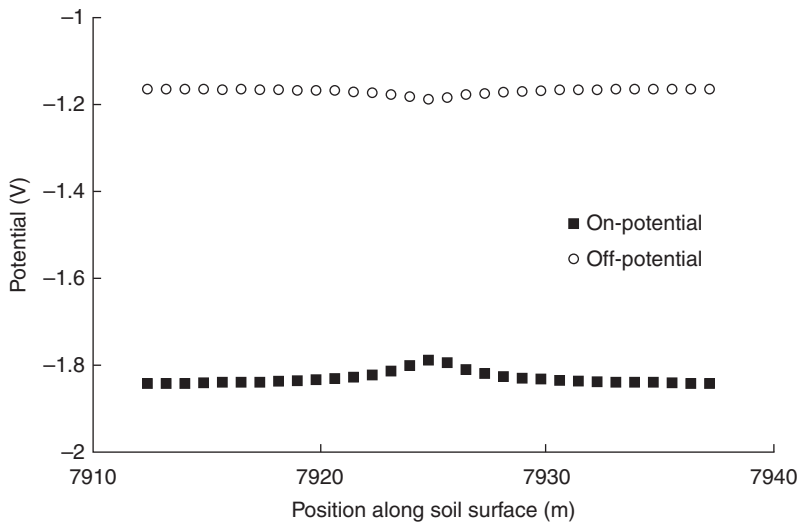

4.23 A profile of soil surface on- and off-potentials from a simulated CIS survey. The flaw size was 36 in^2, the soil resistivity was 500 Ω cm, the pipe diameter was 12 in, the DOC was 4 ft, and the CP level was high.

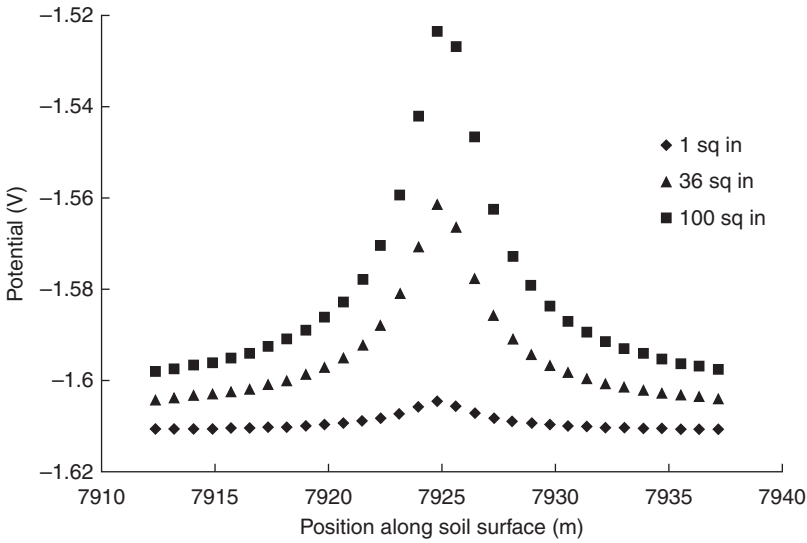

4.24 Soil surface on-potential as a function of position along the length of the pipeline with flaw size as a parameter. The anode voltage was the same for each simulation.

be attributed to the pipeline being substantially over-protected underneath the coating than it is at the flaw. This is explained to occur at low soil resistivities because the coating resistance is so much higher than the resistance of the soil when the soil resistivities are low.

Another way to prioritize CIS indication is to calculate the dips in potential to determine the relative size of the coating. From simulation data it can be shown that the size of the dip has a direct correlation with the size of the flaw. This result is shown in Fig. 4.24. This trend shows that the magnitude of the dip increases with increasing size of the coating flaw.

Coating flaw size predictors

All simulation data results were used to predict flaw size based on CIS indications. The simulation data used involve variation in CP level, pipe diameter, depth of cover, and soil resistivity. A design equation was developed which predicts coating flaw size through use of the CIS dip indications. Figure 4.25 shows all simulation data of CIS indication versus coating flaw size. The CIS indication shown represents the difference in the on-potential dip and the off-potential dip. The on-potential dip is illustrated as Dip_{on} in Fig. 4.26 and the off-potential dip is illustrated as Dip_{off}. Each of the parameters was incorporated into an expression to predict flaw size using a least squares regression method.

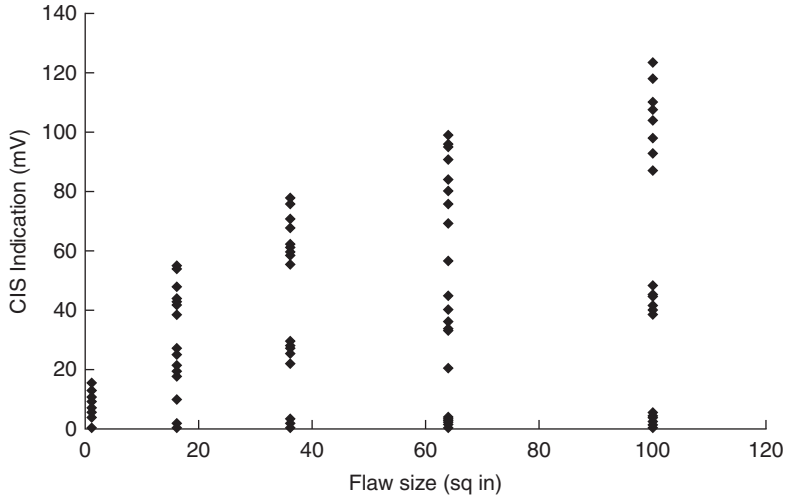

4.25 CIS indications as a function of flaw size obtained from a large set of simulations. The CIS indication is the difference between the on-potential dip and the off-potential dip, as is shown in Fig. 4.26.

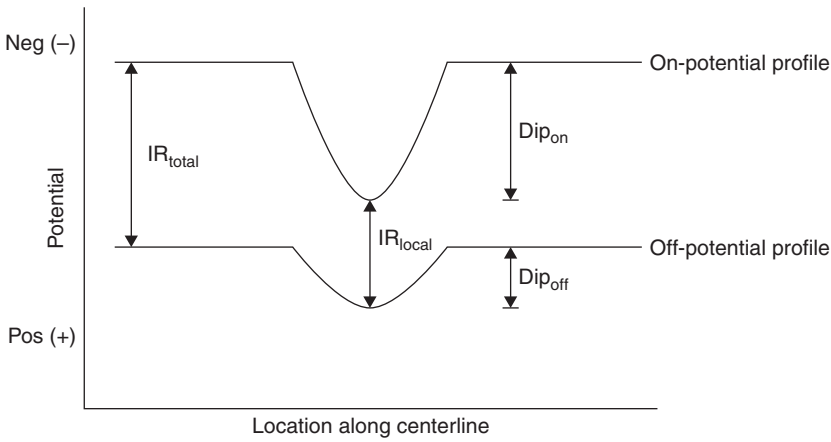

4.26 A profile of on- and off-potentials along the centerline at the soil surface.

Once the expressions for the different parameters are lumped together, a value for flaw size can be predicted within a calculated confidence interval for a given simulation. This is used to show that the CIS predictor is not predicting an exact coating flaw size, but instead a range within which the true coating flaw size should be. For each simulation run, the corresponding flaw size was predicted. A plot of actual flaw size versus predicted flaw size

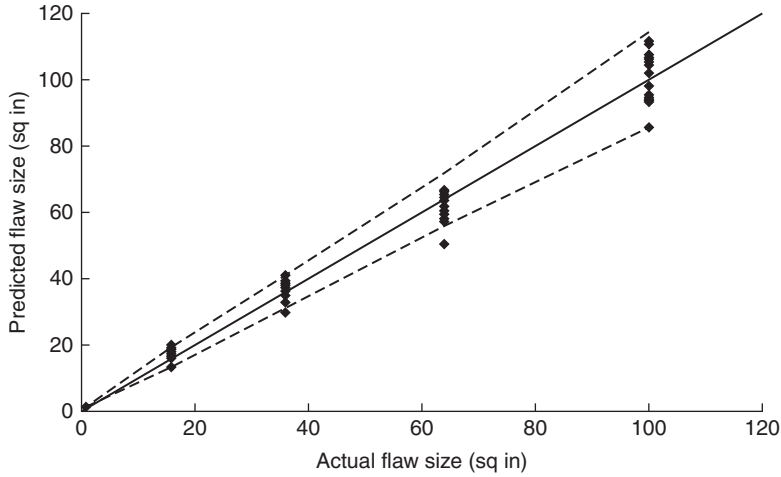

4.27 Input flaw size as a function of predicted flaw size for each simulation using CIS indications.

is shown in Fig. 4.27. Good agreement is shown in the graph, evidenced by a high R^2 value of 0.986. The calculated confidence interval is represented by the dashed lines. In order for the coating flaw size to be predicted, the soil resistivity and depth of cover must be known. Then by using CIS on- and off-dip indications, as well as the IR total value illustrated in Fig. 4.26, the flaw size can be predicted. Changes in CP levels or in the size of the pipe diameter showed no effects on the prediction of flaw size using CIS indications.

Similar development was used to predict flaw size based on DCVG indications. A separate design equation was created from this development. While the CIS predictor was based on IR drops far away from the coating flaw but along the pipeline, the DCVG predictor used IR drops far away from the coating flaw but in the direction perpendicular to the pipeline. The IR drops used in calculating percent-IR include the DCVG indication survey data needed for the predictor. For the predicted flaw size to be calculated, the soil resistivity, depth of cover, and pipe diameter must also be known. In Fig. 4.28, the agreement between predicted flaw size and actual flaw size is shown. The confidence interval for the predicted flaw size is also given by the dashed lines.

Assessment of poor coatings

Additional simulations were run to improve assessments of coatings that are in bad condition. Coatings with lower resistivities (i.e. 10^6 Ω-cm) are considered to be in poor condition. All results of this work in previous sections

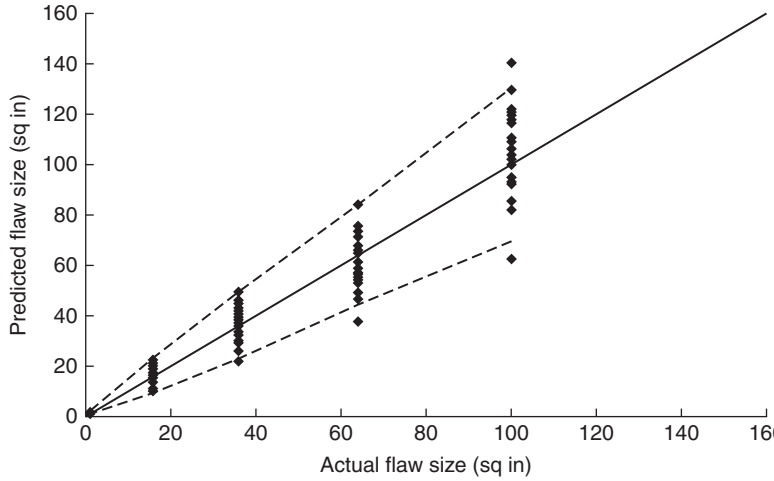

4.28 Input flaw size as a function of predicted flaw size for each simulation using DCVG indications.

have been based on detecting a coating flaw. However, this section focuses on determining if the overall coating is in bad condition. This primarily aims at helping field engineers differentiate between the conditions favorable for pipeline failure by either large continuous sections of bad coating or by a local coating flaw.

The first set of simulations involved a pipeline without a coating versus a pipeline with a good coating (i.e. 10^9 Ω-cm). The pipeline without a coating was specified as aged bare steel. The simulations with a coating had properties corresponding to that of 20 mil fusion bonded epoxy (FBE). Variations in soil resistivity, pipe diameter, depth of cover, and CP level were done by performing numerous simulations.

From these simulation results, the soil surface potentials along the centerline for each simulation run were uniform. This is because the condition of the pipeline was uniform and there was no localized current entering the pipeline due to the absence of an isolated coating flaw. The soil surface potentials were further explored in the direction perpendicular to the pipeline. The soil surface potentials were not uniform moving away from the pipeline for the aged bare steel, but they were relatively uniform for the coated pipeline. For the aged bare steel, it was found that the potential drop was not a function of position in respect to the length of the pipeline. This means that a lateral voltage gradient would be the same at any position along the pipeline, assuming it was located at the same distance away from the pipeline. In all simulations, CIS and DCVG indications in mV gave no results, due to the lack of localized current flow to a coating defect.

However, due to the potential drop moving away from the pipeline in the bare steel simulations, percent-IR calculations could be done. The lengthwise position of the percent-IR calculation was done near the center of the pipeline to be consistent with calculations of percent-IR in previous sections. However, this location is arbitrary, since potential drops were found to not change with position along the length of the pipeline. The percent-IR results showed no substantial changes with respect to variations in soil resistivity, depth of cover, pipe diameter, and oxygen blocking. It was found that ranges in percent-IR for the aged bare steel were between 65% and 85%, while the percent-IR values were all near zero for that of the 20 mil FBE coating. These results can be attributed to a large amount of current entering the pipeline for the aged bare steel due to a larger current demand to maintain the pipeline's integrity. Since a minimal amount of current was needed to protect the coated pipeline, the overall soil surface potential distribution was uniform.

Another set of simulations was performed for a pipeline with a poor coating. The coating resistivity was lowered to be equal to that of the soil resistivity. Other properties of the coating were studied, such as oxygen blocking and pore size. Percent-IR calculations found that variations in both of these parameters had no influence, since the percent-IR values were the same for each simulation run. Variations in soil resistivity and CP level all yielded the same percent-IR values. This result showed that percent-IR is insensitive to the amount of oxygen penetrating the coating.

For the final set of simulations, the oxygen blocking level and the pore size were held constant. Coating resistivity was the main parameter being varied from 10^6 Ω-cm to 10^9 Ω-cm. Soil resistivity and CP level were also varied. The percent-IR was calculated for each simulation. A relationship was found by plotting the logarithm of the ratio of coating resistivity to soil resistivity versus percent-IR. This result is shown in Fig. 4.29. The shape of data in Fig. 4.29 resembles the curve of a rotated sigmoid function. The sigmoid function with some slight modification is given as

$$P = \frac{1}{A + \exp(Bx + C)} \qquad [4.30]$$

where P represents percent-IR and x represents the logarithm of the ratio of the coating resistivity to the soil resistivity. Parameters A, B and C were adjusted to fit the function to the simulation data. The equation is rearranged for a rotated sigmoid function as

$$x = -\frac{\ln(P + 0.0124) - 12}{2.325} \qquad [4.31]$$

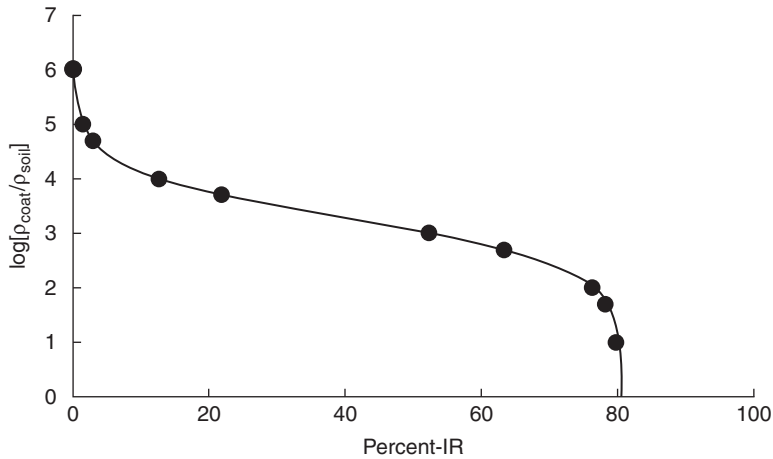

4.29 The logarithm of the ratio of coating and soil resistivity as a function of the percent-IR resulting from simulations in which parameters such as coating resistivity, soil resistivity, and CP level were varied. The line represents the model presented as Equation [4.30].

Figure 4.29 shows the simulation data fitted with the sigmoidal function. The agreement is excellent. These results are expected to be able to improve future assessments of a pipeline's coating condition.

Before using the empirical formula given, surveyors should first determine if a coating flaw is present. This can be done by CIS and DCVG surveys. If no evidence of a coating flaw is found, percent-IR measurements can still be made to help make a determination about the overall coating condition of the pipeline. Then the guideline may be followed to make an assessment. This method is recommended if coating conditions are expected to be poor. Also, they should be used after CIS and DCVG surveys have been carried out and no defects have been found. Then the percent-IR calculation can be completed to help make an assessment about the overall coating condition of the pipeline.

4.5.2 Rectifier war

The term 'rectifier war' describes the influence the rectifier for one CP system may have on an adjacent CP system. Increases in the rectifier output for one system may cause corrosion of an adjacent system. The subsequent increase in the rectifier output of that system will cause corrosion of the first system.

Two 1 km long coated pipes in a soil of 10 kΩ cm resistivity were assumed to cross, as shown in Fig. 4.30. The coating on the two pipes had the same

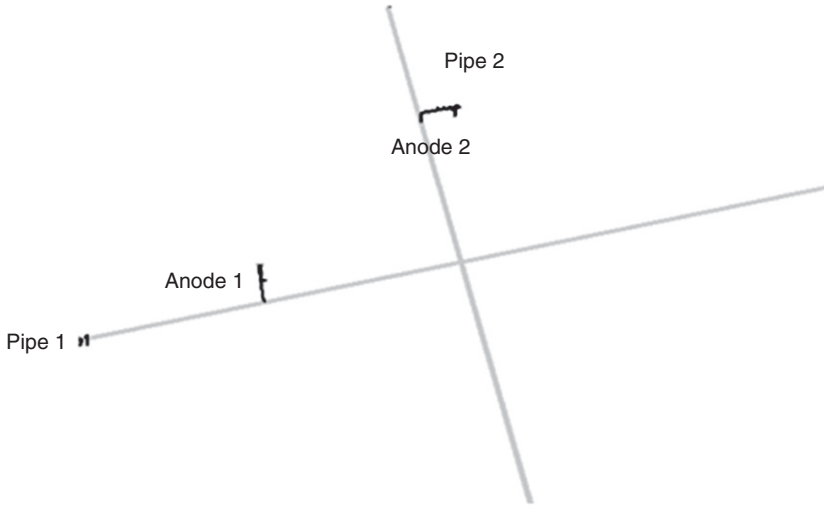

4.30 Configuration of pipes and anodes for the simulation of rectifier wars.

properties, and the pipes experienced the same level of CP at an applied rectifier voltage of 1.35 V. A comparison of the potential and current density distributions on Pipe 1 before and after introducing Pipe 2 is shown in Figs. 4.31 and 4.32 respectively. The valleys that appear in both figures were associated to the site of pipe where anodes were connected. The peaks indicate the interference between two pipes, but the interference was not very strong because the potential difference of the peak is small in Fig. 4.31.

Potential and current density distributions are shown in Figs 4.33 and 4.34, respectively for the case when the rectifier voltage for Pipe 1 was increased to 5.8 V. These two figures indicate that Pipe 1 experienced more CP than did Pipe 2, since the potential and current density distributions along Pipe 1 were more negative than that along Pipe 2. Corrosion begins to occur on the site of Pipe 2 that is associated with the cross-over section. This point can be clearly illustrated by Fig. 4.35, which provides a comparison of potential distributions of Pipe 2 in two conditions. The peak, which was above the –850 mV CSE criterion, referenced to the $Cu/CuSO_4$ electrode (CSE), indicates that the CP difference between the two pipes may result in the localized corrosion at the cross-over section on the pipe, which has less CP.

4.5.3 Tank bottoms

Riemer and Orazem had reported that, for oxygen-saturated soil, a 30.5 m diameter uncoated tank bottom cannot be protected by a deep well remote

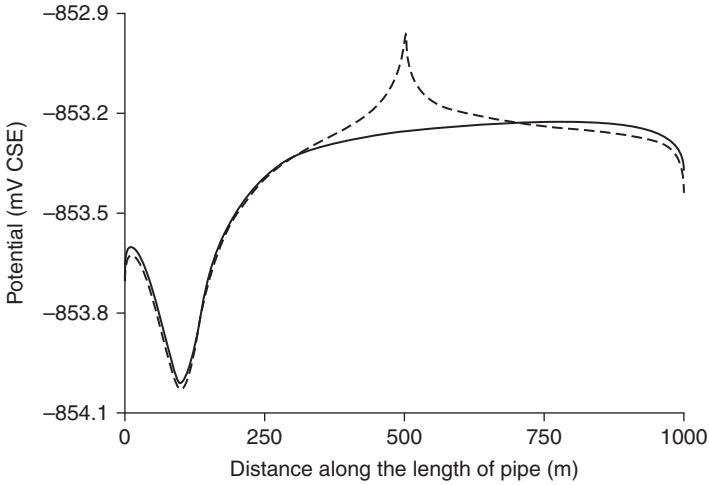

4.31 Comparison of potential distributions along Pipe 1 before and after introducing Pipe 2. Solid line: before introducing Pipe 2; dash line: after introducing Pipe 2.

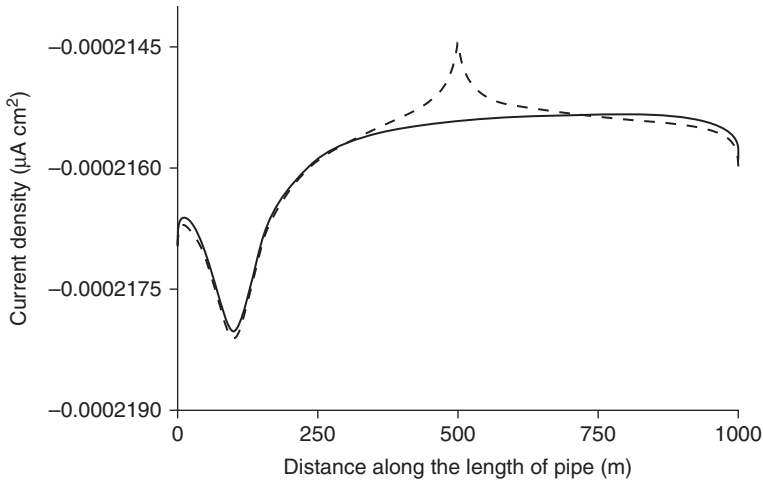

4.32 Comparison of current density distributions along Pipe 1 before and after introducing Pipe 2. Solid line: before introducing Pipe 2; dash line: after introducing Pipe 2.

ground bed located 2000 ft below the tank when the output of the anode is 14.2 A. To explore this observation, and to explore the role of coatings and coating holidays, a series of simulations were performed for a tank diameter of 45.7 m, and a 1m long anode directly below the tank bottom at a distance of 1000 m. The soil was assumed to have a uniform resistivity

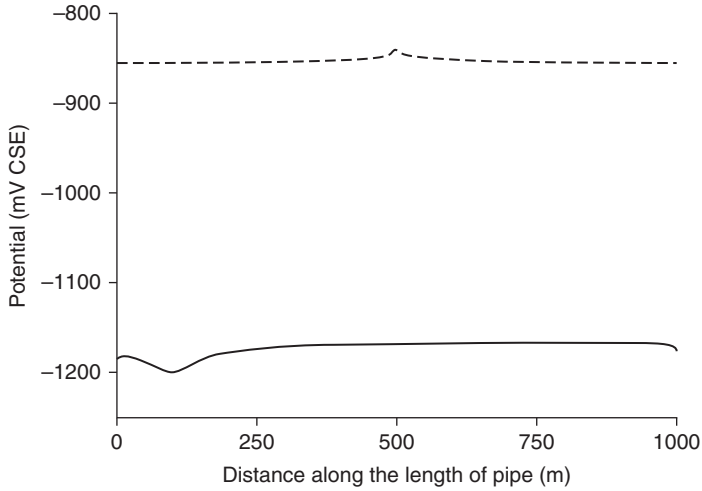

4.33 Comparison of potential distributions along Pipe 1 and Pipe 2 respectively in Condition 2. Solid line: Pipe 1; dash line: Pipe 2.

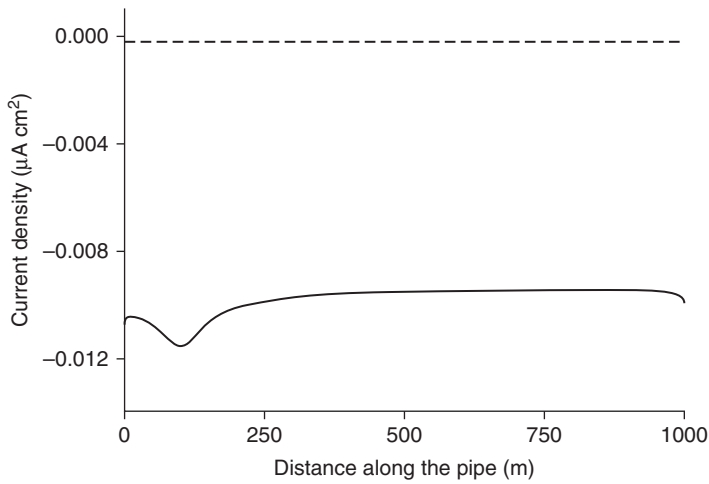

4.34 Comparison of current density distributions along Pipe 1 and Pipe 2 respectively in Condition 1. Solid line: Pipe 1; dash line: Pipe 2.

of 10 kΩ cm. The polarization parameters used are given in Table 4.2. The difference between Steels A and B is that the mass-transfer-limited current density for oxygen reduction was larger for Steel B than for Steel A, and Coating B had greater permeability to oxygen than did Coating A.

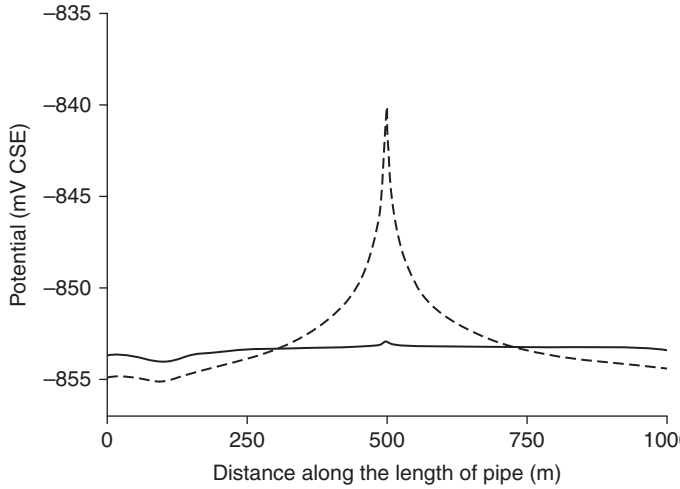

4.35 Potential distributions of Pipe 2 in Conditions 1 and 2, respectively. Solid line: Pipe 2 in Condition 1; dash line: Pipe 2 in Condition 2.

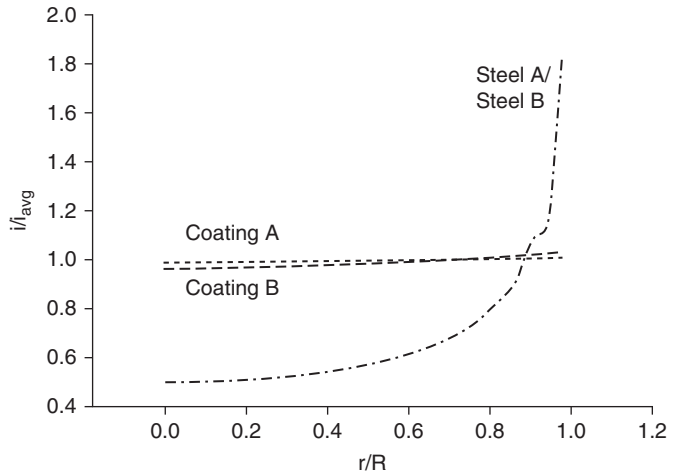

4.36 Calculated normalized current density as a function of dimensionless radius on tank bottoms with different surface properties.

The current distributions corresponding to the four cases are shown in Fig. 4.36, and the corresponding parameter values are presented in Table 4.3. In the case of Steel A and Steel B, where no coatings are present, the protection current distribution is observed to be non-uniform, with the periphery having higher current density than the middle of the tank bottom. By

Table 4.2 Parameters corresponding to tank bottom simulations (see Equations [4.6], [4.9], and [4.10])

Type of coating	Coating A	Coating B	Steel A	Steel B
Coating resistivity ρ, M Ω cm	5000	200	–	–
Coating Thickness δ, mm	0.508	0.508	–	–
Oxygen blocking α_{block}, %	99.9	99	–	–
A_{pore} / A, %	0.1	0.1	–	–
E_{Fe}, mV	–522	–522	–522	–522
β_{Fe} , mV/decade	62.6	62.6	62.6	62.6
i_{lim,O_2}, μA/cm^2	1.05	1.05	3.1	10.8
E_{O_2}, mV CSE	–172	–172	–172	–172
β_{O_2}, mV/decade	66.5	66.5	66.5	66.5
E_{H_2},mV CSE	–942	–942	–942	–942
β_{H_2}, mV/decade	132.1	132.1	132.1	132.1

Table 4.3 Tank bottom simulation results

Tank steel/coating	Steel A	Steel B	Coating A	Coating B
Type of anode	ICCP – 4750	ICCP – 15500	Standard potential magnesium	Standard potential magnesium
Potential applied, V CSE	4750	15500	–	–
Output current of anode, A	111.62	364.34	0.0092	0.0118
Cross section area of tank bottom, m^2	1641.7	1641.7	1641.7	1641.7

increasing the current output, it was possible to drive potentials to values below –850 mV CSE, as shown in Fig. 4.37. The coated tank bottoms were easily protected by the sacrificial Mg anodes. The current distributions were uniform, and the potentials were well within the protected regime.

Additional simulations were performed for coated tank bottoms with coating flaws that exposed bare steel. The coating defect was located at the center of the tank bottom and, as was done for the previous calculation, the anode was placed at a large distance from the tank. Two configurations were studied: Coating A with Steel B exposed in the center of the tank and Coating B with Steel B exposed, respectively. The coating holiday covered a relatively large 5.5 m^2 which represented 0.35% of the tank area. The soil resistivity was assumed to be uniform, with a value of 10 kΩ cm. The corresponding current and potential distributions are given in Figs 4.38 and 4.39, respectively.

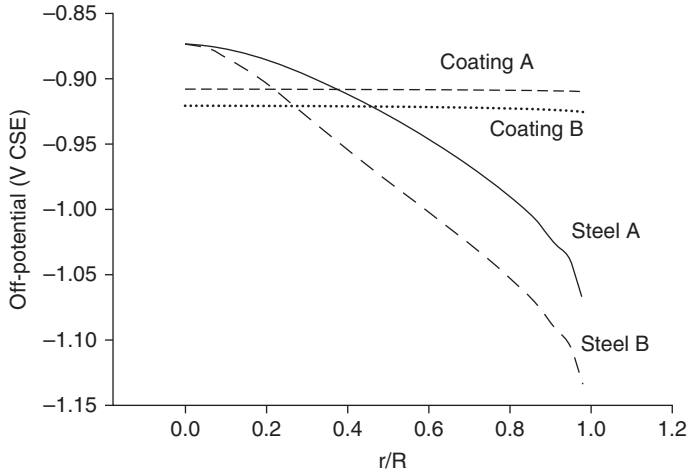

4.37 Calculated off-potential as a function of dimensionless radius corresponding to Fig. 4.36.

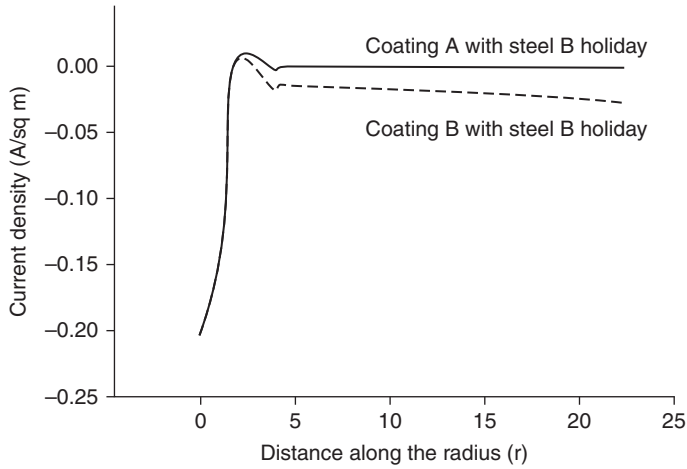

4.38 Calculated current density as a function of radial position for coated tanks with a large coating flaw at the center of the tank.

The coating flaw caused a significant change in the current distribution. The current density was highest at the center of the tank bottom at the defect. To ensure that minimum protection of the entire tank bottom in the case of Coating A was achieved, a large potential of 160 V had to be applied. This resulted in large areas of tank bottom being severely over-protected, as shown by the potential values in Fig. 4.39. In the case of Coating B, a larger potential of 1600 V was applied to ensure that minimum protection was

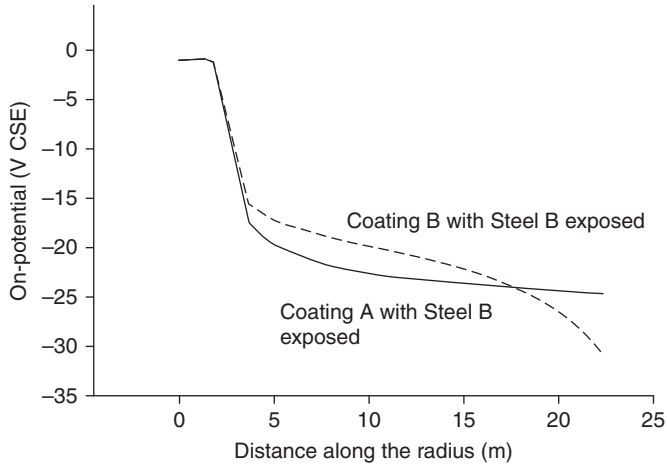

4.39 Calculated on-potentials as a function of radial position corresponding to Fig. 4.38.

achieved for the tank bottom. This also resulted in large areas of the tank bottom being over-protected, as shown by the potential values in Fig. 4.39.

4.6 Conclusion

Numerical simulations are a powerful aid to understanding the nature of CP of buried structures. The ability to calculate on- and off-potentials for surfaces facilitates interpretation of ECDA measurements to assess the condition of buried pipes. The ability to model the interactions between buried structures, and even independent CP systems, becomes important as the number of pipes placed within a right-of-way increases. The model may be applied as well to planar structures, such as the bottoms of storage tanks.

4.7 References

1. A.W. Peabody (1967), *Control of Pipeline Corrosion* (Houston, TX: NACE International).
2. L. Benedict (editor) (1986), *Classic Papers and Reviews on Anode Resistance Fundamentals and Applications* (Houston, TX: NACE International).
3. J. S. Newman (1991), Cathodic protection with parallel cylinders, *Journal of the Electrochemical Society*, **138**, 3554–3560.
4. M. E. Orazem, D. P. Riemer, C. Qiu and K. Allahar (2004), 'Computer simulations for cathodic protection of pipelines,' in *Corrosion Modeling for Assessing the Condition of Oil and Gas Pipelines*, F. King and J. Beavers (editors) (Houston, Texas: NACE International), 25–52.
5. C. A. Brebbia and J. Dominguez (1977), Boundary element methods for potential problems, *Applied Mathematical Modelling*, **1**, 371–378.

6. S. Aoki, K. Kishimoto and M. Sakata (1985), Boundary element analysis of galvanic corrosion, in *Boundary Elements VII*, C. A. Brebbia and G. Maier (editors) (Heidelberg: Springer-Verlag), 73–83.
7. J. C. F. Telles, L. C. Wrobel, W. J. Mansur and J. P. S. Azevedo (1985), Boundary elements for cathodic protection problems, in *Boundary Elements VII*, C. A. Brebbia and G. Maier (editors) (Heidelberg: Springer-Verlag), 63–71.
8. N.G. Zamani and J.M Chuang (1987), Optimal-control of current in a cathodic protection system – a numerical investigation, *Optimal Control Applications & Methods*, **8**, 339–350.
9. F. Brichau and J. Deconinck (1994), A numerical-model for cathodic protection of buried pipes, *Corrosion*, **50**, 39–49.
10. F. Brichau, J. Deconinck and T. Driesens (1996), Modeling of underground cathodic protection stray currents, *Corrosion*, **52**, 480–488.
11. S. Aoki and K. Amaya (1997), Optimization of Cathodic Protection System by BEM, *Engineering Analysis with Boundary Elements*, **19**, 147–156.
12. S. Aoki, K. Amaya and M. Miyasaka (1999), Boundary element analysis of cathodic protection for complicated structures, in Proceedings of the NACE99 Topical Research Symposium: Cathodic Protection: Modeling and Experiment, M. E. Orazem (editor),(Houston, TX: NACE International), 45–65.
13. K. J. Kennelley, L. Bone and M. E. Orazem (1993), Current and potential distribution on a coated pipeline with holidays:1. model and experimental verification, *Corrosion*, **49**, 199–210.
14. M. E. Orazem, K. J. Kennelley and L. Bone (1993), Current and potential distribution on a coated pipeline with holidays:2. a comparison of the effects of discrete and distributed holidays, *Corrosion*, **49**, 211–219.
15. M. E. Orazem, J. M. Esteban, K. J. Kennelley and R. M. Degerstedt (1997), Mathematical models for cathodic protection of an underground pipeline with coating holidays: 1. theoretical development, *Corrosion*, **53**, 264–272.
16. M. E. Orazem, J. M. Esteban, K. J. Kennelley and R. M. Degerstedt (1997), Mathematical models for cathodic protection of an underground pipeline with coating holidays: 2. case studies of parallel anode CP systems, *Corrosion*, **53**, 427–436.
17. D. P. Riemer and M. E. Orazem (2005), Modeling coating flaws with nonlinear polarization curves for long pipelines, in *Corrosion and Boundary Element Methods*, R. A. Adey (editor) (Southampton, UK: WIT Press), 225–259.
18. D. P. Riemer and M. E. Orazem (2000), Application of boundary element models to predict effectiveness of coupons for assessing cathodic protection of buried structures, *Corrosion*, **56**, 794–800.
19. D. P. Riemer and M. E. Orazem (2005), A mathematical model for the cathodic protection of tank bottoms, *Corrosion Science*, **47**, 849–868.
20. J. F. Yan, S. N. R. Pakalapati, T. V. Nguyen, R. E. White and R. B. Griffin (1992), Mathematical modeling of cathodic protection using the boundary element method with a nonlinear polarization curve, *Journal of the Electrochemical Society*, **139**, 1932–1936.
21. D. P. Riemer (2000), *Modeling Cathodic Protection for Pipeline Networks*, PhD dissertation, University of Florida, Gainesville, Florida.
22. C. A. Brebbia, J. C. F. Telles and L. C.Wrobel (1984), *Boundary Element Techniques*, (Heidelberg: Springer-Verlag).

23. I. Stakgold (1979), *Greens Functions and Boundary Value Problems* (New York: John Wiley & Sons).
24. J. Newman (1966), 'Resistance for flow of current to a disk', *Journal of the Electrochemical Society*, **113** 501.
25. C. Kasper (1940), The theory of the potential and the technical practice of electrodeposition: IV. The flow between and to circular cylinders', *Transactions of the Electrochemical Society*, **78** 147–161.
26. J. P. McKinney, M. E. Orazem, O. Moghissi and D. D'Zurko (2006), Development of ECDA criteria for prioritization of indications, Proceedings of Corrosion/2006 (Houston, Texas: NACE International), Paper 06–188.
27. J. P. McKinney, M. E. Orazem, O. Moghissi and D. D'Zurko (2009), Predicting coating holiday size using ECDA survey data, Proceedings of Corrosion/2009 (Houston, Texas: NACE International), Paper 09–146.
28. O. C. Moghissi, W. Harper, M. Celinski, V. Sottile and D. DiMeo (2004), 'External corrosion direct assessment validation through correlation between indications and control excavations', Proceedings of Corrosion /2004 (Houston, Texas: NACE International), Paper 04–187.

5

Corrosion processes and the use of corrosion inhibitors in managing corrosion in underground pipelines

V. S. SASTRI, Sai Ram Consultant, Canada

DOI: 10.1533/9780857099266.1.127

Abstract: This chapter reviews the sources of corrosion in underground pipelines carrying oil and gas, such as hydrogen sulfide and carbon dioxide. It also discusses and compares corrosion monitoring techniques, such as linear polarization resistance (LPR), electrochemical impedance spectroscopy (EIS), electrochemical noise (EN) techniques, and the use of sensor probes.

Key words: corrosion, gas pipelines, oil pipelines, corrosion monitoring, linear polarization resistance (LPR), electrochemical impedance spectroscopy (EIS), electrochemical noise (EN).

5.1 Introduction

The petroleum industry consumes a large amount of material. About 8% of the world's production of metals is used in oil production, transport, and processing. The material consumption in the petroleum industry amounts to about 32 kg of metal installed in processing equipment for every ton of processed oil. The enormous quantities of steel and other metals used in the petroleum industry are prone to corrosion to a more marked degree than in other industrial environments. The severity of the problem is such that about 1 kg of steel and other alloys per ton of oil processed is destroyed due to corrosion. Thus, it is clear that corrosion losses in the petroleum industry are considerable, and it is necessary to adopt corrosion mitigation strategies such as the use of corrosion inhibitors and selection of more resistant materials. The costs of processing one cubic meter of processed oil in 1960 are shown in Table 5.1.

Corrosion losses in the petroleum industry amounted to 11 cents per barrel of processed oil, and the losses during distillation were about 65% of the total losses. The corrosion losses of 16 cents per barrel of processed oil and a total cost of corrosion of 450 million dollars in the USA in the oil industry in 1966 have been quoted in the literature.[1] Although these data are old, they stand the test of time with respect to proportional costs.

Table 5.1 The costs of processing one cubic meter of processed oil in 1960

Total expense at the building phase	18.6%
Maintenance and repairs including inhibition costs	61.9 %
Losses connected with unmanufactured products	16.0%
Additional equipment costs	2.3%
Other miscellaneous expenses	1.2%

The data on economics of corrosion in the oil industry, although many decades old, illustrate the need for urgent attention toward efforts to mitigate corrosion in the oil industry. One of the most prudent and economic methods of combating corrosion in the oil industry is the use of corrosion inhibitors. According to the literature, the cheapest method of combating corrosion in oil pipelines is the use of corrosion inhibitors. According to Bregman, the ratio of preventable losses to inhibitor costs ranges from 4:1 to 7:1. Other methods of corrosion control, such as the use of more corrosion-resistant alloys or protective coatings, are more expensive than the use of corrosion inhibitors. Another attractive feature is that corrosion inhibitors can be applied for the protection of partially corroded equipment.

5.2 Sources of corrosion in oil and gas production

The main corrosive media and processes in the oil industry are:

- hydrochloric acid and its aqueous solutions
- hydrogen sulfide
- corrosion of steel at hydrocarbon–electrolyte interfaces
- corrosion of steel in emulsified two-phase environments
- oxygen
- naphthenic acids
- carbon dioxide.

5.2.1 The role of hydrogen sulfide in corrosion

Carbon dioxide and/or hydrogen sulfide are known to be very corrosive species in the corrosion of metals or alloys used in pipes and other tubular goods and equipment. Hydrogen sulfide is particularly harmful since it can cause sulfide stress corrosion cracking (SSCC) failure in the pipe. When high strength steel having a Rockwell hardness, R_c, in excess of 22–25 is used, sulfide cracking may occur in the form of spontaneous brittle fracture,

probably resulting from hydrogen embrittlement. Carbon steels of lower hardness are not as susceptible to sulfide cracking, but are sensitive to pitting corrosion and general corrosion in the presence of chloride. Extensive literature on the effect of hydrogen sulfide on the failure of equipment in the oil and gas industry is available.[2] Corrosion problems encountered in the oil and gas industry as related to the use of inhibitors and the mechanism of corrosion due to hydrogen sulfide are discussed in the literature.[3–15]

Hydrogen sulfide is corrosive only when it is dissolved in water. The solubility of hydrogen sulfide in water is relatively high compared to carbon dioxide and oxygen, which are the main corrosive gases present in oil and gas production systems. The acidity due to the presence of H_2S is further enhanced by carbon dioxide, which is usually present in the system. The overall process is represented by the obviously oversimplified equation:

$$Fe + H_2S \xrightarrow{H_2O} FeS + H_2S \qquad [5.1]$$

It has been shown that the corrosive effect is weak when the water content of the production fluid is low. The corrosion products are formed over the metal surface as a black powder, or as a more or less compact layer of a deposit/scale, which can reduce the rate of corrosion, with the extent of the effect dependent on the stability, crystallinity and permeability of hydrogen and the rate of formation of the corrosion product sulfide layer. The protective properties of the sulfide layers increase with increasing temperature, and the susceptibility of the underlying steel to SSCC decreases. The SSCC has been found to decrease at 65°C for high strength steel. The protective layers of troilite (Fe_7S_8), pyrrhotite ($Fe_{1-x}S$), kansite (Fe_9S_8) and mackinawite ($Fe_{1+x}S$) may be formed depending on pH, H_2S concentration, and other species such as chloride and CO_2. The nearly perfect crystal lattices of pyrite and troilite give better corrosion protection than the less perfect kansite.

It is useful to note that the sulfide layer should influence the kinetics of the corrosion processes. In the absence of oxygen, the parabolic character of iron sulfide formation was shown, i.e. a linear relation of the corrosion rate with the square root of time, indicating that the corrosion rate decreases as the iron sulfide film thickness increases.

A detailed review of the current theories of the basic steps involved in the corrosion mechanism initiated by hydrogen sulfide may be found in the literature.[16] The most probable mechanism suggested involves interaction of bisulfide (HS^-) ions on the surface of the metal with H_3O^+ ions from the electrolyte to form a catalytic complex, Fe $(H—S—H)_{ads}$. The protons of this surface complex give rise to hydrogen atoms due to cathodic polarization.

The hydrogen atoms may also recombine to form molecular hydrogen or diffuse into the metal:

$$Fe + HS^{-} \rightleftharpoons Fe\left(HS^{-}\right)_{ads} \quad [5.2]$$

$$Fe(HS^{-})_{ads} + H_3O^{+} \rightarrow Fe\left(H{-}S{-}H\right)_{ads} + H_2O \quad [5.3]$$

$$Fe\left(H{-}S{-}H\right)_{ads} + e^{-} \rightarrow + Fe(HS^{-}) + H_{ads} \quad [5.4]$$

The step involving the interaction of Fe (H–S–H) with an electron is thought to be the rate-determining factor of the cathodic reaction. The explanation has been given for the anodic reaction involving an adsorption complex:[17]

$$Fe + H_2S + H_2O = Fe(HS^{-})_{ads} + H_3O^{+} \quad [5.5]$$

$$Fe(HS^{-})_{ads} \rightarrow \left(FeHS\right)^{+} + 2e^{-} \quad [5.6]$$

$$Fe(HS)^{+} + H_3O^{+} \rightarrow Fe^{2+} + \left(H_2S\right) + H_2O \quad [5.7]$$

An intermediate complex such as Fe/H_2S ad. that generates H_2S has been proposed:[18]

$$Fe(H_2S) \rightarrow Fe\left(H_2S\right)_{ads} \quad [5.8]$$

$$Fe(H_2S)_{ads} \rightarrow Fe\left(H_2S\right) + 2e^{-} \quad [5.9]$$

$$(Fe{-}H_2S)^{2+} \rightarrow Fe^{2+} + \left(H_2S\right) \quad [5.10]$$

Another hypothesis is based on H_2S as the stable species in an acidic solution and not SH^{-} and, as a result, $Fe{-}H_2S$ will be the transient complex in the anodic reaction.[19] In the cathodic reaction, which is also accelerated in H_2S, there is a diversity of opinion, especially about the presence of HS^{-} in acid media. A suggestion has been made that the discharge of hydrogen occurs by the formation of protonated H_2S, which is more readily formed than H_3O^{+}:

$$(H_2S)_{ad} + H_3O^+ \rightarrow HH_2S^+_{ads} + H_2O \quad [5.11]$$

$$(HH_2S)^+_{ad} + e^- + M \rightarrow H - M - (H_2S)_{ad} \quad [5.12]$$

$$H_3O^+ + e^- + M \rightarrow H - M + H_2O \quad [5.13]$$

The cathodic reaction has been studied in detail by many authors.[20–22]

There is relatively little information in the literature on the localized corrosion in sour gas environments. Localized corrosion can occur by the formation of iron sulfide spots on the metal surface, which can lead to the formation of iron–iron sulfide electrochemical local cells. According to one school of thought, the composition and nature of corrosion products of the Fe_xS_y when acting as the cathode would be more important in determining a corrosion mechanism than the influence of dissolved hydrogen sulfide. The iron sulfide on the surface, primarily pyrrhotite, is an effective cathode. The anodic reaction under the sulfide layer will depend on the presence of aqueous solution at the FeS interface. Traces of polysulfide may also be formed by the reaction of H_2S with sulfur or other oxidizing agents present in the system, which can lead to the occurrence and development of localized corrosion. The nature of polysulfide species in acid media is not yet completely understood. Potentiometric studies have shown that small concentrations of H_2S react with oxidizing agents, resulting in the formation of small amounts of H_2S_2 and colloidal sulfur at temperatures up to 90°C, which leads to localized corrosion.[23]

5.2.2 The role of chloride in corrosion

The other important corrosive species is chloride, which is present in the mineralized water present at the well bottom. Corrosion due to chloride is more severe at high temperatures. Failures due to chloride can be due to intergranular corrosion and chloride stress corrosion cracking (CSCC). Both intergranular corrosion and CSCC involve anodic dissolution as a step for crack propagation. CSCC failures can occur in many materials, ranging from low alloy steels to super alloys. CSCC failures can be dangerous for parts of equipment exposed to aerated environments.

The simultaneous presence of sulfide and chloride corrosion has been observed in deep sour gas production.[24,25] The sour gas is mainly methane under high pressure without liquid hydrocarbons present. The corrosion mechanism advanced consists of the formation of ‘scabs’ of iron sulfide products involving both H_2S and chloride ions. The thin liquid film on the

metal surface in an acid gas environment will contain hydrochloric acid, which reacts with hydrogen sulfide to form iron chloride. The hydrogen sulfide in the gas reacts with iron chloride to form scab-like iron sulfide and regenerates the chloride ion, which reacts with more iron. This sequence of reactions results in high corrosion rates.

$$Fe^{o} + HCl \rightarrow FeCl_2 \quad [5.14]$$

$$FeCl_2 + H_2S \rightarrow FeS + 2HCl \quad [5.15]$$

5.2.3 The role of carbon dioxide in corrosion

Carbon dioxide is commonly produced along with gas and oil. Carbon dioxide dissolves in water to form carbonic acid, resulting in a decrease in pH. The corrosion caused by CO_2 is termed as 'sweet'. The corrosion due to CO_2 can also arise due to the injection as a method for enhanced oil recovery, which can cause downhole corrosion, and corrosion of surface equipment. A characteristic feature of CO_2-induced corrosion is pitting, which is manifested in the form of deep, sharp-edged pits. Carbon dioxide may also cause general corrosion in heat-affected zones such as welds. In deep wells, carbon dioxide forms a carbonate scale with corrosion in turbulent areas. The partial pressure of CO_2 in production fluid is cited as a controlling factor governing the corrosive attack. The following relationship has been put forward.[26]

- A partial pressure of CO_2 above 30 psi usually indicates corrosion.
- At partial pressures of 3–30 psi, corrosion may occur.
- At partial pressures below 3 psi, corrosion is generally negligible.

This rule of thumb is applicable to gas wells only. A more commonly used relationship to predict the corrosivity of acidified CO_2 brines is based on the equation due to deWaard and Williams.[27] Assuming the reduction of carbonic acid as a rate-determining step, the corrosion rate is given by the equation:

$$\text{Log. } c.r. = 0.67\left(\log P_{CO_2}\right) + c \quad [5.16]$$

where $c.r.$ is the corrosion rate, P_{CO_2} is the partial pressure of CO_2, and c is a constant.

The detailed mechanism of CO_2 corrosion in oil and gas production and advances in CO_2 have been documented in the literature.[28] The mechanism involved in CO_2-induced corrosion has been discussed in the literature. In the presence of oxygen, it is essentially the same as in oxygen alone at the same pH. In the absence of oxygen, the mechanism is as shown below in Fig. 5.1. The cathodic reaction is:

$$2CO_2 + 2H_2O \rightleftharpoons 2H_2CO_3 \xrightarrow[+2e^-]{2H^+\ 2HCO_3^- + 2e} H_2 + 2HCO_3^- \qquad [5.17]$$

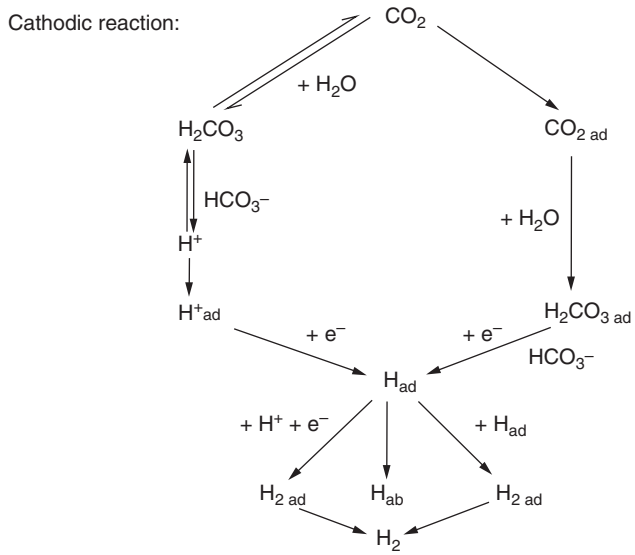

$$2CO_2 + 2H_2O \rightleftharpoons 2H_2CO_3 \xrightarrow[+2e^-]{2H^+ + 2HCO_3^- + 2e^-} H_2 + 2HCO_3^-$$

Anodic reaction:

$$Fe + H_2O \rightleftharpoons FeOH_{ad} + H^+ + e^-$$

$$FeOH_{ad} \rightarrow FeOH^+ + e^-$$

$$FeOH^+ + H^+ \rightleftharpoons Fe^2 + H_2O$$

$$Fe \rightarrow Fe^{2+} + 2e^-$$

Total reaction:

$$Fe + 2CO_2 + 2H_2O \rightarrow Fe + 2H_2CO_3 \rightarrow Fe^2 + H_2 + 2HCO_3^-$$

5.1 'Sweet corrosion' (in oxygen-free CO_2 solution).

The anodic reaction is:

$$Fe + H_2O \rightleftharpoons FeOH_{ad} + H^+ + e^- \quad [5.18]$$

$$FeOH_{ad} \rightarrow FeOH^+ + e^- \quad [5.19]$$

$$Fe(OH)^+ + H^+ \rightleftharpoons Fe^{2+} + H_2O \quad [5.20]$$

$$Fe^o \rightarrow Fe^{2+} + 2e^- \quad [5.21]$$

The total reaction is:

$$Fe + 2CO_2 + 2H_2O \rightarrow Fe + 2H_2CO_3 \rightarrow Fe^{2+} + H_2 + 2HCO_3^- \quad [5.22]$$

The ideas on which some of the conclusions and statements, based on factors such as pH, CO_2 partial pressure, temperature, water and gas production rate, have been criticized,[29] since it was considered that these represent an overall or average assessment of downhole corrosion processes and fail to account for localized corrosion, which is the cause of the failure. By measurements in 60 gas wells with large variations in production characteristics,[30] tentative correlations between general and localized corrosion rates have been made.

Two different mechanisms dependent on temperature have been identified. Below 60°C, the corrosion rate is controlled by the rate of diffusion of CO_2 to the metal surface or the rate of hydrolysis of CO_2 to form carbonic acid. Above 60°C, iron carbonate, $FeCO_3$, is formed on the metal surface, and the rates of all corrosion processes are controlled by the transfer across the iron carbonate layer. It is surmised that localized corrosion arises when the transition from the carbonic acid formation reaction to the formation of ferrous carbonate on the metal surface[31] takes place.

In the general case, the corrosion rate depends upon the permeability of the scale as well as a combination of intrinsic scale dissolution and flow rate. The rate of dissolution of iron carbonate has been found to be relatively slow, and hence the flow regime becomes the predominant factor in determining the corrosion rate in gas wells. The kinetics of corrosion reactions in the presence of an interlayer of corrosion products between the metal and corrosion media have been studied extensively.[32]

The variety of corrosion products formed in CO_2 saturated systems are: iron carbonate scale or mixed iron hydroxy-carbonate, iron-calcium carbonate, are formed, which decrease the corrosion rate.[33,34] The impact of

corrosion products on the flow dependence has been under dispute since this effect had been observed by some authors,[35,36] while this was not observed by others,[37–39] which may be due to the different corrosion mechanism in operation at low temperatures and low CO_2 partial pressures and the absence of corrosion products opposed to higher temperatures and pressures and the presence of corrosion product layers. The corrosion rates of carbon steel and some high alloy steels in the presence of iron carbonate ($FeCO_3$), as a function of temperature, partial pressure of CO_2, have been determined.[40,41]

Corrosion in oil and gas production also results in corrosion-erosion or flow-induced localized corrosion in CO_2 containing brines, related with the fact that the actual production at greater depths, at higher temperatures and pressures, and the use of smaller bore tubing results in higher velocities of the production stream. The system experiences a radical change with the introduction of a small amount of H_2S. Iron sulfide is formed as a thermodynamically stable product instead of $FeCO_3$, and magnetite may be formed at high temperatures even in the presence of high partial pressures of CO_2.[42] The low solubility of magnetite and electron conductivity compared with carbonate scale leads to pitting corrosion.[42] Magnetite may form up to 121°C, and a mixture of siderite and iron sulfide have been detected[43] at a partial pressure ratio of $CO_2/H_2S = 500$. The corrosion rate due to CO_2 may also be reduced in systems when a turbulent flow disperses the water in the hydrocarbon phase, preventing it from reaching the steel surface.[44]

5.2.4 The role of oxygen in corrosion

The role of oxygen as a corrosive agent in secondary recovery by water flooding is important. Injection water usually contains dissolved salts and a small amount of oxygen, which can cause extensive corrosion due to oxygen differential concentration cells. Corrosion due to dissolved oxygen results in pits in the drill pipe, which under stress initiate an easily propagated fatigue crack leading to failure. Oxygen causes extensive damage to water injection equipment, such as pumps, piping, water storage tanks, and injection well tubing, and the corrosion products may plug the formation. Although the role of oxygen is not well understood, the dissolved oxygen is removed mechanically by vacuum deaeration or gas stripping. Vacuum deaeration or gas stripping is not very efficient and hence an oxygen scavenger such as sodium sulfite, together with cobalt nitrate on hydrazine, is used in the removal of oxygen from the system. Hydrazine is toxic and its performance as an oxygen scavenger is not very satisfactory in comparison with sulfite or bisulfite mixed with cobalt nitrate. Oxygen-induced corrosion can be minimized by the use of inhibitors.

5.2.5 The role of bacteria in corrosion

The role of bacterial corrosion due to microorganism activity can be a significant problem, particularly in enhanced recovery processes such as water flooding. Several forms of bacteria contribute to corrosion and the most common ones are sulfate-reducing and iron bacteria. The bacteria may cause corrosion of piping, plugging of the injection or disposal wells, and souring of the fluids and reservoir. Microbiologically influenced corrosion (MIC) had been extensively studied from the industrial practice point of view, in order to arrive at cost-effective solutions in monitoring large water injection systems.[45–48] In order to avoid expensive and inefficient treatments for microbiological corrosion that are sometimes applied in industrial practice, one must direct efforts toward predicting microbiologically induced corrosion (MIC), development of efficient biocides, thorough understanding of MIC mechanisms, and better control of the eventual conversion of sweet to sour production that can be caused by sulfate-reducing bacteria. The current trends in the investigation of MIC have been discussed from the point of view of a practicing corrosion engineer facing complex corrosion control in the oilfield.[45]

When seawater is used in injection systems, the oxygen present can initiate severe damage of pumps, vessels, injection lines, and downhole injection well equipment by pitting, and can also promote growth of aerobic bacteria, leading to the formation of a biofilm on the metal surface under which sulfate-reducing anaerobic bacteria could be formed.[47] The sulfate-reducing bacteria, produced by algae or by the dense gelatinous deposits produced by iron bacteria, can be enhanced by the presence of calcium carbonate scale.[8] Biocidal treatment is equally important as that of corrosion, and can have important implications on the choice of chemical treatment of the injection water with respect to chemical compatibility.

5.3 Techniques used in monitoring corrosion inhibitors in oil and gas pipelines

Oil and gas pipeline flows are multiphase in nature, consisting of oil, aqueous (brine water), and gas phases. One of the main risks of operation of the oil pipelines is internal corrosion in the form of pitting corrosion. By ascertaining the conditions leading to corrosion, suitable strategies can be adopted to combat corrosion by, for instance, addition of suitable corrosion inhibitors, at the requisite concentrations, and/or adjusting fluid flow rate. Thus, monitoring corrosion in underground or above ground oil and gas pipelines is a crucial step in the integrity management process. In an ideal case, a monitoring technique should provide data on the effect of inhibitors on both general and pitting corrosion.

In practice, a single monitoring technique is incapable of providing data on both general and pitting corrosion. Hence, a suite of techniques are used to obtain reliable data on both general and localized corrosion. When different techniques are used, the benefits and limitations should be clearly understood, especially when the corrosion rates obtained by different methods are used to develop integrity management programs. Many factors are involved in obtaining corrosion rates from the measured parameters. The process of extraction of corrosion rates from the measured data can sometimes be complex depending on whether the data are averaged (weight loss), instantaneous (e.g. LPR and electrochemical impedance spectroscopy (EIS)), or continuous monitoring, as for example electrochemical noise (EN) monitoring.

Detailed studies on the reliability of weight loss, linear polarization resistance (LPR), EIS, EN, and externally mounted hydrogen sensor probes for monitoring performance of corrosion inhibitors in operating oil and gas pipelines have been made.[49] The loop that could take the full flow of the pipe was made of carbon steel. The loop shown in Fig. 5.2 had three pipe sections, namely inlet, replaceable, and outlet – each with a length of ~5 ft (1.5 m). The loop was attached to the operating pipeline through valve no. 1. The valve led to a 3 inch (7.62 cm) pipe, which had two ports. At the first port, a two-strip coupon ladder (preinjection) was attached, and the second port was used for injection of the inhibitor. The 3 inch pipe was attached to the inlet section that was 6 inches (15.24 cm) in diameter and

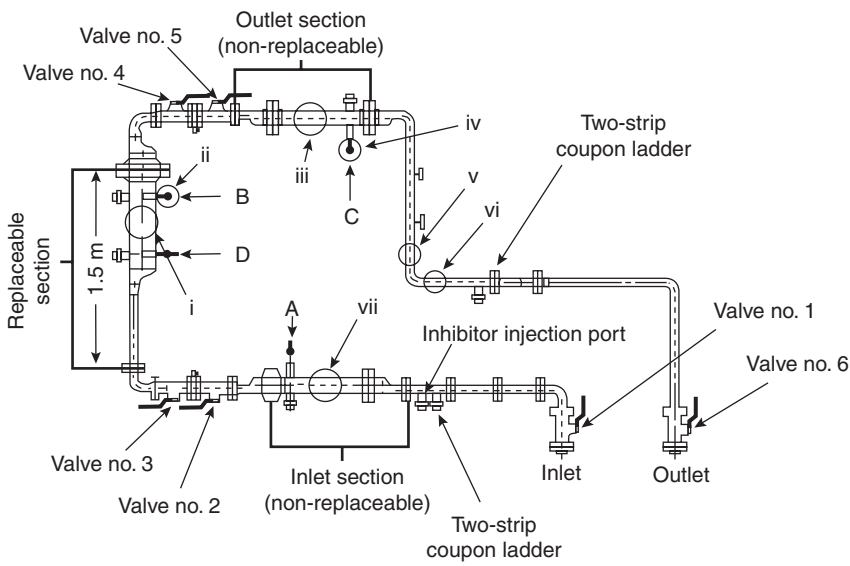

5.2 Schematic diagram of field loop.

37.2 inches (94.5 cm) long. The 6 inch section was off-centered with respect to the 3 inch pipe section in such a way that the expansion from 3 inches to 6 inches was downward. The 6 inch experimental section contained Ladder A (a three-pair, tree-coupon ladder) 32.4 inches (81 cm) from the 3 inch to the 6 inch expansion. At the other end (replaceable section end) of the inlet section, a 6 inch to 3 inch reducer was attached, which, in turn, was attached to two valves, 2 and 3, and finally to a 90° bend. The replaceable section was attached at the opposite end of the bend.

The replaceable section had a 3 inch pipe and a 6 inch or 10 inch pipe, depending on the field section. The 6 inch experimental pipe section was off-centered with respect to the 3 inch pipe section in such a way that the expansion from the 3 inch pipe to the 6 inch pipe was downward (i.e., the expansion was done such that the tops of the two pipes were level and the bottom of the 6 inch pipe was curved up to complete the weld. The 6 inch (or 10 inch) section was attached with two three-pair, tree-coupon ladders (Ladder B and Ladder D). The distance between the 3 inch to 6 inch expansion and Ladder B was the same as that between the 3 inch to 6 inch expansion and Ladder A. Ladder D was placed closer to the 3 inch to 6 inch expansion at 7.2 inches (18 cm). At the other end (outlet section end) of the replaceable section, a 6 inch to 3 inch reducer was attached, which in turn was attached to a 90° bend.

At the opposite end of the 90° bend, two valves (no. 4 and no. 5) were attached. Valve no. 5 was attached to a 3 inch to 6 inch expansion, which in turn was attached to the outlet section. The outlet section had 6 inch and 3 inch pipe sections. The 6 inch experimental section was off-centered with respect to the 3 inch valve section, such that the 3 inch to 6 inch expansion was downward. This section contained Ladder C (a three-pair, tree-coupon ladder) 32.4 inches (81 cm) from the 3 inch to 6 inch expansion, as in the inlet and replaceable sections. The 6 inch section was attached to a 3 inch pipe section. The 3 inch pipe section had a 90° bend, a 60 inch (150 cm) straight section, another 90° bend and another 32 inch (80 cm) straight section that was attached to the operating pipeline through valve no. 6. Just before valve no. 6, a two-strip coupon ladder (post-injection) was inserted in the 3 inch pipe section.

The operating conditions in the three fields are presented in Table 5.2. The field experiments were conducted in three types of fields, namely:

- gassy-oil field,
- oily-gas field,
- oil-transmission field.

For every experiment in every type of field, a new replaceable section (10 inch diameter) was used. The samples (coupons) as well as the replaceable section

Table 5.2 Operating conditions during field experiments

Conditions	Gassy-oil	Oily-gas	Oil-transmission
Gas production rate, m^3/day	17×10^3	122×10^3	This pipe section carries 99.5%
Oil production rate, m^3/day	49	28	oil with less than 0.5% water
Water production rate, m^3/day	170	31	
Gas composition	20% H_2S + 2.5% CO_2, balance hydrocarbon		Less than 0.5% H_2S + 0.5% CO_2
Temperature (°C)	60	55	55
Pressure, psi	250	250	Atmospheric
Replaceable pipe section, in.	6	10	10
Diameter of the operating pipe in the field, in.	6	10	1
Inhibitor, continuous batch	No. 1[a] and No. 3[a] No. 2[b] and No 4[c]	No. 5[d] No. 6[d]	No. 2
Concentration, ppm continuous batch	0, 50, 100, and 200 0 and 2000	0, 100, 250, 500, 1000 0 and 5000	0 and 2000

[a]Water-soluble.
[b]Oil-soluble, water-dispersible.
[c]Oil-soluble.
[d]Compositions not known.

exposed to the oil-transmission field were subjected to prepitting by drilling, punching, chemical, and electrochemical methods.[50,51] The pre-pits in each area were arranged in an arc at angles of 70, 80, 90 and 110°. On the coupon samples, the pre-pits were aligned in a row from top to bottom.

The concentrations or injection levels of inhibitors were adjusted relative to the volume of the production brine water. During batch inhibitor treatment, the pipe loop, along with coupons, was treated with a kerosene solution of the inhibitor. At each inhibitor level, the experiments were done for 15 days in gassy-oil and oily-gas fields, and for 30 days in an oil-transmission field. A new set of coupons was used for every inhibitor concentration used.

All four coupon ladders (A, B, C, and D) were used and, for a particular inhibitor concentration, there were eight – each of top, middle and bottom coupons. Of these eight coupons, four coupons were 'standard coupons' and four were made from pipe material. The chemical analysis of the pipe and standard coupons is given in Table 5.3. The 76 mm × 19 mm × 3 mm coupons

Table 5.3 Chemical composition of pipe and standard coupons

	Compositions (%)		
Element	Standard coupons	Pipe coupons	Difference
C	0.23	0.2	0.03
Si	0.24	0.18	0.06
Mn	0.72	0.63	0.09
Cr	0.08	0.072	0.08
Ni	0.06	0.049	0.01
Mo	<0.03	<0.03	0
Cu	0.17	0.18	0.01
Al	<0.006	<0.006	0
Nb	<0.01	<0.01	0
V	<0.01	<0.01	0
Ti	<0.01	<0.01	0
B	0.004	0.004	0
P	0.01	0.01	0
S	0.02	0.013	0.01
W	–	<0.02	–
Sn	–	0.0081	–
Co	–	0.0045	–
Zr	–	<0.002	–
Pb	–	<0.01	–

were positioned in such a way that the thickness of the coupons was facing the flow.

The two bottom and one of the middle six coupons on each ladder were wired for electrochemical monitoring. The wires were silver soldered onto the coupons. The junctions and electrical wires were covered with chemical-resistant epoxy. The ladder head and controlling instrument cable were connected using a military-standard six-pin receptacle. LPR and electrochemical impedance spectral (EIS) measurements were performed with a potentiostat.

EN was measured with an IL-channel instrument. Four of the twelve channels of the instrument were activated to collect data from the four ladders. The data were automatically logged. The activated channel was allowed to achieve steady state for 10 min, after which 1024 data points at a rate of 2 s per point were collected. The data collection was switched to another channel, and the process was repeated intermittently, and the potentiostat was used to make LPR and electrochemical impedance measurements.

Hydrogen flux through the pipe wall was monitored using pressure-sensitive foils, and their location is shown in Fig. 5.1. The foils were positioned at the bottom, or side, or top of the loop at 6, 9, or 12 o'clock positions respectively. Two foils were attached to the sides of traps. The stainless steel foils (15 cm × 10 cm or 15 cm × 15 cm) were glued to the external surface of the

pipe, creating a hermetic chamber. A 10 foot long capillary tubing welded onto the foil connected the chamber to a manometer. A vacuum of nearly 90 kPa was established, and the hydrogen flux was monitored by the increase in internal pressure (or vacuum loss).

The pipe sections, 6 inch replaceable section (after gassy-oilfield), 10 inch replaceable section (after oily-gas field), and 10 inch replaceable inlet and outlet sections (after oil-transmission field) were cut horizontally into two halves at 3 o'clock and 9 o'clock positions. Each piece was cut further to measure the pit distribution in 6 inch to 3 inch reducer 3 inch pipe, 3 inch to 6 inch expansion, 6 inch pipe, elbow, and trap wall. In each region, the 50 largest pits were measured and the average pit depths and standard deviations were calculated. Similarly, the pit depths in the coupon samples were measured.

5.4 Measuring pitting corrosion rates

The pit distribution in coupons exposed for 15 days without inhibitor, and the replaceable pipe section exposed for 1 year in the gassy-oil field, are shown in Fig. 5.3. In this figure, three types of pits, namely pits at 9, 12, and 3 o'clock positions (top in gas-oil phase), pits at the 6 o'clock position (bottom, in the oil-water phase), and pits at the 6 o'clock position (water phase)

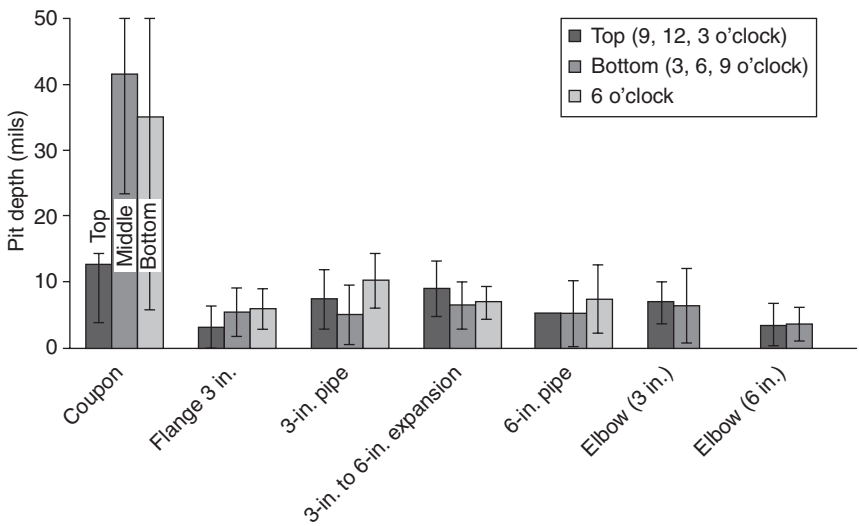

5.3 Comparison of pit depths in the coupons (no inhibitor, 15 days) and in the replaceable pipe section (1 year) exposed in gassy-oil field (refer to Fig. 5.2 for different sections of the pipe).

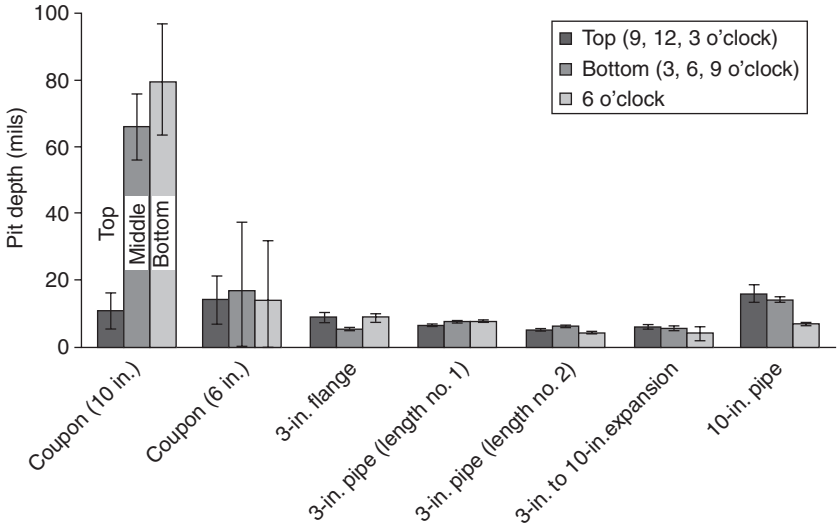

5.4 Comparison of pit depths in the coupons (no inhibitor, 15 days) and in the replaceable pipe section (8 months) exposed in oil-gas field (refer to Fig. 5.2 for different sections of the pipe).

are shown. The pits in coupons exposed for 15 days are nearly four times deeper than those in the pipe exposed for 1 year.

The comparison of pit depths in the coupons and the replaceable section of the pipe exposed to the oil-gas phase are shown in Figs 5.3 and 5.4. The pits in coupons exposed for 15 days are much deeper than the pits in the pipe exposed for 8 months. Out of the four coupon ladders, two were exposed in the 10 inch section (Ladders B and C) and two were exposed in the 6 inch section (Ladders A and D) of the pipe loop.

A comparison of the pit depths in coupons and in the replaceable section of the pipe exposed to an oil-transmission field is depicted in Fig. 5.5. Because of the lower water content of the pipeline, no appreciable growth of the pits was noted, either in coupons or in the pipe except for some pitting in the 10 inch pipe section with particular reference to the region near the expansion from 3 inch to 10 inch pipe.

Pit distribution in the inlet and outlet sections, which are exposed to all three fields and under all inhibitor concentrations, are shown in Fig. 5.6. The pit depths in the inlet and outlet sections of the pipe loop exposed for nearly 2 years are smaller than those of coupons exposed for ~15 days. Figure 5.7 represents the general corrosion rates of standard vs pipe coupons exposed for 15 days. No marked differences were noted between the two sets of coupons, although the standard coupons (Type 1018 mild steel (UNS 10180) were polished successively to 600 grit finish, while pipe sample

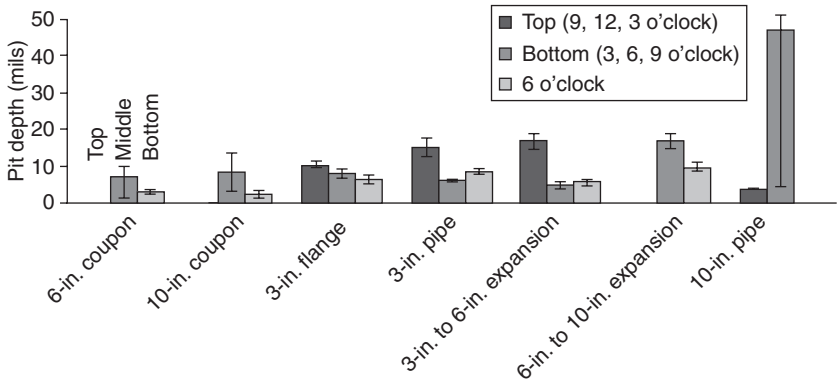

5.5 Comparison of pit depths in the coupons (treated with 5000 ppm of Batch Inhibitor No. 6, 30 days) and in the replaceable pipe section (3 months) exposed in oil-transmission field (refer to Fig. 5.2 for different sections of the pipe).

coupons (ASTM A106Gr.B) were grit blasted better than a white finish. Both the compositions (Table 5.3) and the corrosion rates are similar. It is to be noted that polishing and metallurgical differences have little effect as opposed to the location of the sample. General corrosion rates obtained by various techniques on the same coupon are illustrated in Figs 5.8– 5.10.

The corrosion rates obtained from weight loss and hydrogen foil data are shown in Fig. 5.11. The weight loss and pressure loss data were obtained from coupons exposed to pipeline and the hydrogen foil probes on the external surface of the pipe respectively. It is to be noted that no correlation between coupon weight loss and the hydrogen foil data was observed.

The trends in the variation of corrosion rates with the inhibitor concentration were used to compare the monitoring techniques.[52] For each inhibitor, the variation of corrosion rate with inhibitor concentration was determined at the top, middle, and bottom positions of the pipe. In order to compare the different corrosion monitoring techniques, a standard trend was developed. The standard trend was taken as 'the most repeated trend' (MRT) of different monitoring techniques. For example, the corrosion rates measured by one technique were: 50 at 0 ppm, 20 at 10 ppm, and 10 at 20 ppm. Then the trend in corrosion rates was 0, 10 and 20 ppm. This type of trend was deduced for each monitoring technique, and from this trend the MRT was deduced as the number of times the trend was repeated using different monitoring techniques.

Consider, for example, weight loss and linear polarization techniques. Let us assume these two techniques show a trend $0 > 50 > 100 > 200$ ppm, and the third technique (i.e.) hydrogen foils gives a trend $50 > 0 > 100 > 200$ ppm. The most repeated technique is in the order $0 > 50 > 100 > 200$. The trends

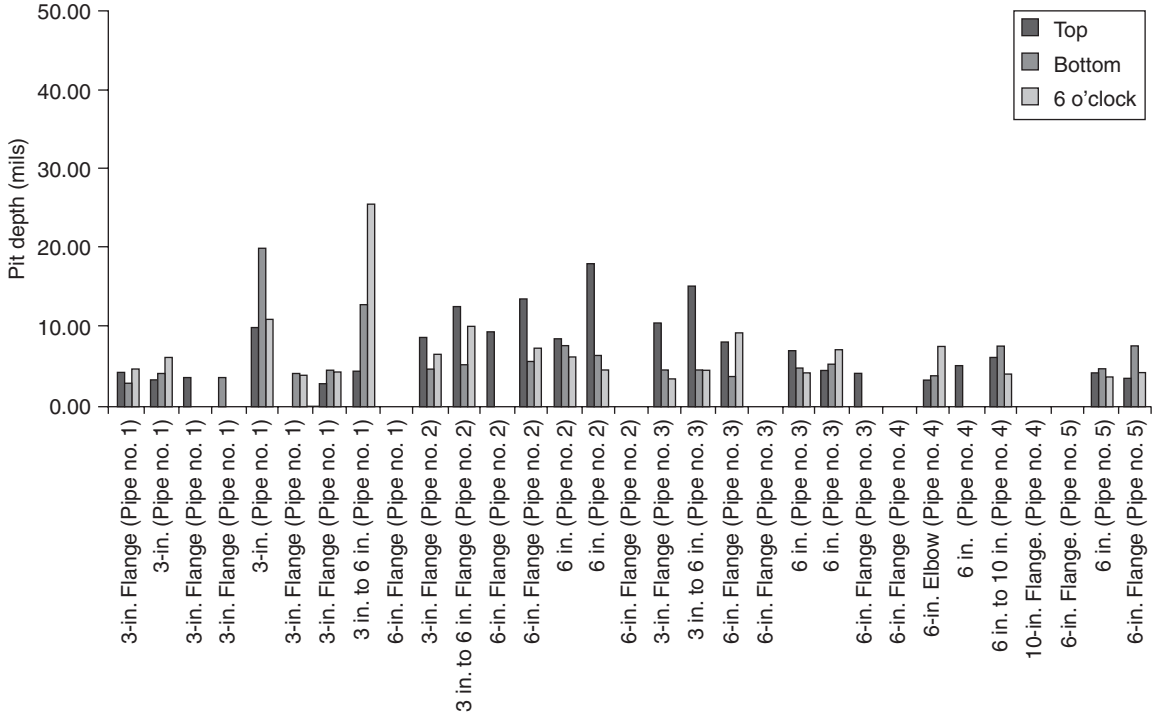

5.6 Pit depths in the inlet and outlet pipe sections (~ 2 years) exposed in all three fields (refer to Fig. 5.2 for different sections of the pipe. Pipe no. 1 = inhibitor injection port section; Pipe no. 2 = outlet section; Pipe no. 3 = inlet section; Pipe no. 4 = bend between replaceable and outlet sections; Pipe no. 5 = 90° bend between replaceable and inlet sections).

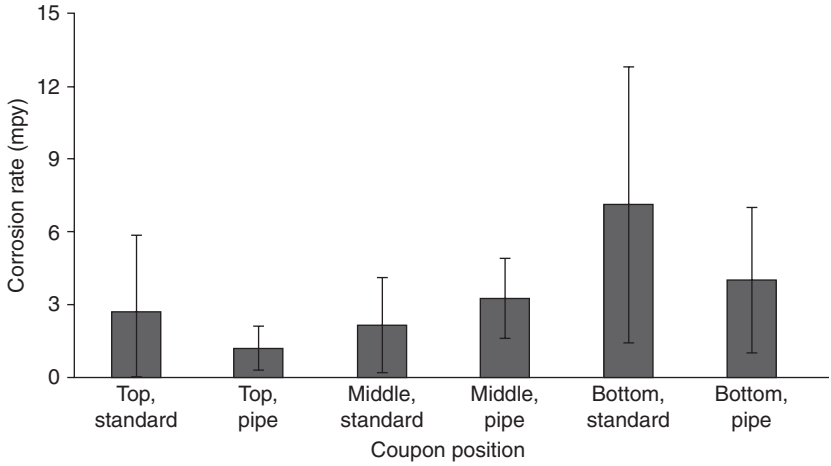

5.7 Comparison of general corrosion rate of standard and pipe coupons in gassy-oil field.

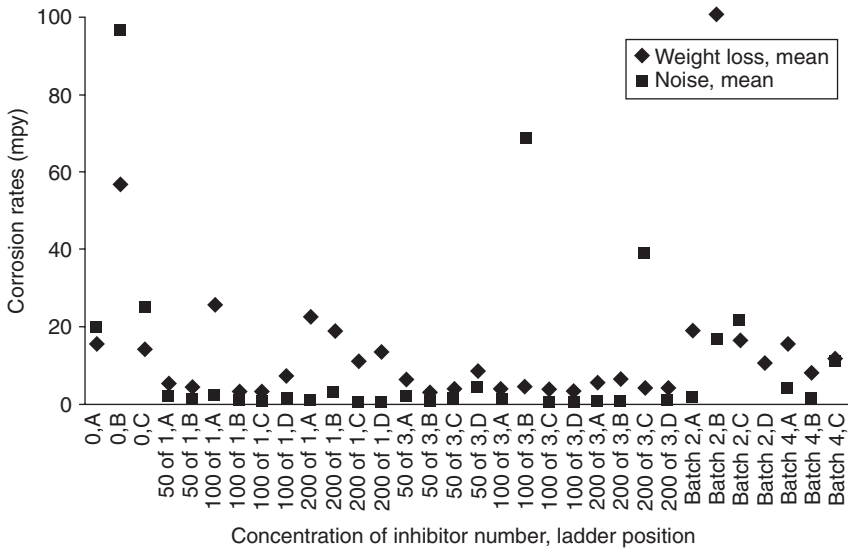

5.8 General corrosion rates of same coupon as measured by various techniques (gassy-oil field).

exhibited by the techniques were then compared with the mean repeated trend (MRT). In the above example, the weight loss data agree with MRT four times out of four comparisons (100%), while the hydrogen probe data agree two times out of four (50%). The technique with the closest agreement with MRT indicates most accurately the conditions in the pipe.

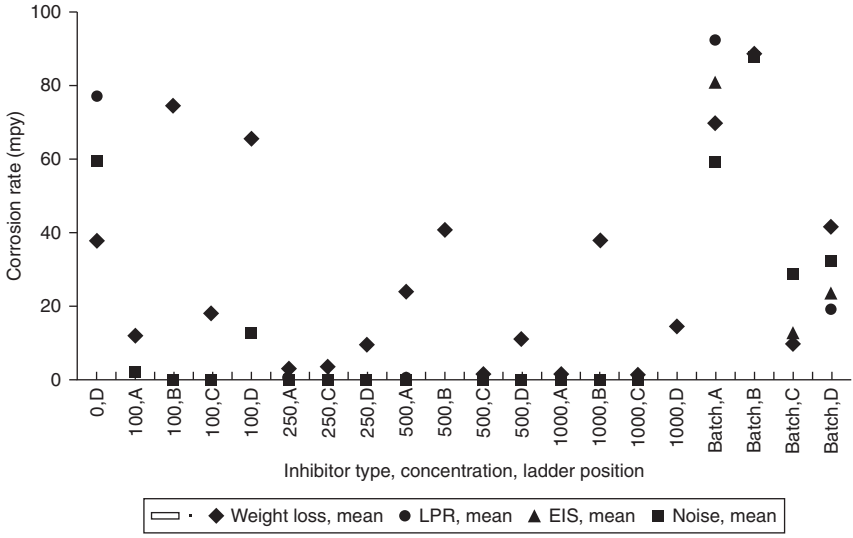

5.9 Corrosion rates of same coupon as measured by various techniques (oily-gas field).

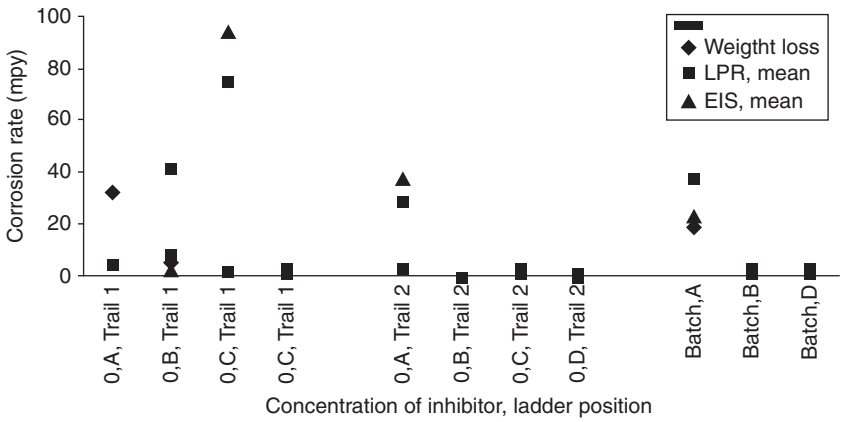

5.10 Corrosion rates of same coupon as measured by various techniques (oil-transmission field).

The MRT values obtained for general corrosion rates in gassy-oil, oily-gas and the oil-transmission field are presented in Tables 5.4–5.6 respectively. The rankings of the monitoring techniques are given in Table 5.7. For each monitoring technique, the percentage times the monitoring technique is in agreement with MRT values in each of three field conditions at the top, middle, and bottom positions were determined using the general corrosion rate

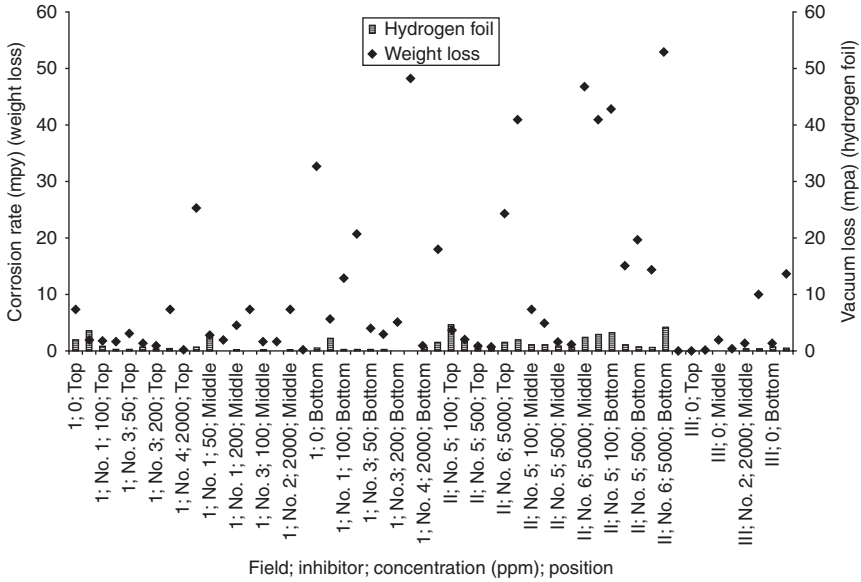

5.11 Comparison of general corrosion rates determined from weight loss and hydrogen permeation methods.

data. These calculations led to the final percentage agreement as follows: 91% EN, 89% weight loss, 70% LPR, 51% hydrogen sensors, and 33% EIS.

Pitting corrosion rates were obtained from the EN data in terms of pitting index, pitting factor, and pit indicator:

$$\text{Pitting index (PI)} = I_{\text{ms}} / I_{\text{mean}} \qquad [5.23]$$

where I_{rms} is the root mean square current noise, and I_{mean} is the mean coupling current. The PI values from 0–1 and PI value greater than 0.6 indicates localized corrosion:

$$\text{Pitting factor} = \frac{\left[\Delta i + \text{---} \Delta i\,(N)\right]}{n} \frac{\sigma_i}{I_{\text{rms}}} \qquad [5.24]$$

where Δi (1) is the current increase over a time interval, n is the number of readings taken during Δi, and σ_i is the standard deviation of current noise.

$$\text{Pit indicator} = \frac{\sigma_i}{I_{\text{mean}}} \qquad [5.25]$$

Table 5.4 Trends in the variation of general corrosion rates (gassy-oil) with inhibitor concentration

Technique	Variation of general corrosion rates (decreasing order)										
Top position											
Inhibitor	No. 1	No. 1	No. 1	No. 1	No. 3	No. 3	No. 3	No. 3	Batch	Batch	Batch
Weight loss	0	50	100	200	0	50	100	200	0	No. 2	No. 4
Pitting	0	50	100	200	0	50	100	200	No. 2	No.4	0
Hydrogen foil	50	0	100	200	0	100	200	50	0	No. 2	No. 4
MRT	0	50	100	200	0	50	100	200	0	No. 2	No. 4
Middle position											
Inhibitor	No. 1	No. 1	No. 1	No. 1	No. 3	No. 3	No. 3	No. 3	Batch	Batch	Batch
Weight loss	0	200	50	100	0	50	100	200	0	No. 2	No. 4
Pitting	0	50	100	200	0	50	100	200	No. 4	No. 2	0
Hydrogen foil	50	0	200	100	0	100	50	200	0	No. 4	No. 2
Noise	0	50	200	100	0	50	100	200	0	No. 2	No. 4
MRT	0	50	200	100	0	50	100	200	0	No. 2	No. 4
Bottom position											
Inhibitor	No. 1	No. 1	No. 1	No. 1	No. 3	No. 3	No. 3	No. 3	Batch	Batch	Batch
Weight loss	200	100	–	–	200	50	100	–	No. 2	No. 4	–
Pitting	100	200	–	–	50	100	200	–	No. 2	No. 4	–
Hydrogen foil	100	200	–	–	100	50	200	–	No. 4	No. 2	–
Noise	100	200	–	–	50	100	200	–	No. 4	No. 2	–
Noise, trap	200	100	–	–	100	50	200	–	No. 4	No. 2	–
MRT	100	200	–	–	50 and 100	50	200	–	No. 4	No. 2	–

Table 5.5 Trends in the variation of general corrosion rates (oily-gas) with inhibitor concentration

Measuring technique	Variation of general corrosion rates (decreasing order)						
Top position							
Inhibitor	No. 5	No. 5	No. 5	No. 5	No. 5	No. 6	No. 6
Weight loss	0	100	250	500	1000	5000	0
Pitting	0	100	250	500	1000	5000	0
Hydrogen foil	100	250	0	500	1000	5000	0
MRT	0	100	250	500	1000	5000	0
Middle position							
Inhibitor	No. 5	No. 5	No. 5	No. 5	No. 5	No. 6	No. 6
Weight loss	250	500	1000	–	–	–	–
Pitting	250	500	1000	–	–	–	–
Hydrogen foil	250	500	1000	–	–	–	–
Noise	250	1000	500	–	–	–	–
MRT	250	500	1000	–	–	–	–
Bottom position							
Weight loss	0	500	250	1000	–	5000	0
Pitting	0	1000	500	250	–	5000	0
Hydrogen foil	0	250	500	1000	–	5000	0
Noise	0	1000	500	250	–	5000	0
LPR	250	500	1000	0	–	5000	0
MRT	0	500 and 1000	500	250 and 1000	–	5000	0

Table 5.6 Trends in the variation of general corrosion rates (oil-transmission field) with inhibitor concentration

Measuring techniques	Variation of general corrosion rates (decreasing order)		
Top position			
Weight loss	2000	0, Trial no. 2	0, Trial no. 1
Pit rate	–	–	–
Hydrogen foil	2000	0, Trial no. 2	0, Trial no. 1
Middle position			
Weight loss	0, Trial no. 1	2000	0, Trial no. 2
Pit rate	0, Trial no. 1	2000	0, Trial no. 2
Hydrogen foil	2000	0, Trial no. 2	0, Trial no. 1
MRT	0, Trial no. 1	2000	0, Trial no. 2
Bottom position			
Weight loss	2000	0, Trial no. 1	0, Trial no. 2
Pit rate	2000	0, Trial no. 1	0, Trial no. 2
Hydrogen foil	0, Trial no. 2	0, Trial no. 1	2000
Noise	2000	0, Trial no. 1	0, Trial no. 2
LPR	2000	0, Trial no. 1	0, Trial no. 2
EIS	0, Trial no. 1	2000	0, Trial nno. 2
MRT	2000	0, Trial no. 1	0, Trial no. 2

Table 5.7 Agreement with most repeated trend

Position measuring techniques	Top			Middle			Bottom			Total			Final Rank
	No. of	No. of	% Agreement	No. of	No. of	% Agreement	No. of	No. of	% Agreement	No. of	No. of	% Agreement	%
Gassy-oil field													
Weight loss	11	11	100	11	9	82	7	1	14	29	21	72	–
Hydrogen foil	11	6	55	11	5	45	7	7	100	29	18	62	–
Noise	–	–	–	11	11	100	7	6	86	18	17	94	–
Oily-gas field													
Weight loss	7	7	–	3	3	100	6	5	83	16	15	94	–
Hydrogen foil	7	4	–	3	3	100	6	5	83	16	12	75	–
Noise	–	–	–	3	1	33	6	6	100	9	7	78	–
LPR	–	–	–	–	–	–	6	3	50	6	3	50	–
Oil-transmission field													
Weight loss	–	–	–	3	3	100	3	3	100	6	6	100	89
Hydrogen foil	–	–	–	3	0	0	3	1	33	6	1	17	51
Noise	–	–	–	–	–	–	3	3	100	3	3	100	91
LPR	–	–	–	–	–	–	3	3	100	3	3	100	91
EIS	–	–	–	–	–	–	3	1	33	3	1	33	33

The pits were measured using a micrometer on the electrochemically connected coupons and compared with the EN data such as pitting index, pitting factor, and pit indicator on the same sample coupon. While comparing pit measurements with EN pit parameters, it is necessary to note that noise measurements are instantaneous, and the pit depth measurements were done after the electrochemical experiment and pit depths on all the three electrodes, namely, working, reference and counter electrodes, are taken into account.

The pit depths measured on all three electrodes involved in the EN experiments and the noise pit parameters, namely pitting index, pitting factor, and pit indicator, were arranged in descending order. Pits were randomly initiated at various sites and different times, and for each pit formed on any one of the coupons (electrodes) there was a corresponding noise signal. The deeper the pit, the larger the noise signal. The noise signals were of high amplitude during the time the pits were growing. Each high amplitude signal was assumed to correspond to the growth of a single pit. The correlation factor, R^2, was determined from the plots of pit depths with each of the three noise pit parameters, as shown in Fig. 5.12. It is to be noted that the correlation between pit indicator and actual pits is better than the correlation with pitting index or pitting function.

The selection of corrosion inhibitors for oil and gas pipelines involves both laboratory testing and simulated field testing. The field testing involves dynamic conditions in the field and different types of monitoring methods, such as average, instantaneous, and continuous. The suitability of a monitored technique depends on the nature of the technique itself, as well as on the physical manner by which the monitoring technique can be used in the particular environment. The physical fit of the monitoring technique determines whether the data obtained are representative of the pipe or just the electrode/coupon/sensor. An experimental loop was used to evaluate both the behavior of the pipe and the coupon/electrode/sensor.

The laboratory flow loop testing done by various investigators, and the associated details, are summarized [53–65] in Table 5.8. The testing of a loop attached to an operating field pipeline was done and the pertinent details are given in Table 5.9. The field loop is a more realistic representation of the field conditions than the laboratory pipe loop.

It is useful to note that corrosion rate data obtained in the laboratory show some variability, but additional variability exists in field conditions due to the dynamic nature of the field conditions. Table 5.10 presents the fluctuations in the operating conditions of a gassy-oil field. The field experiments, in gassy-oil and oily-gas field for 15 days and for 30 days in transmission-oil fields, were done to counter the variability of the field conditions.

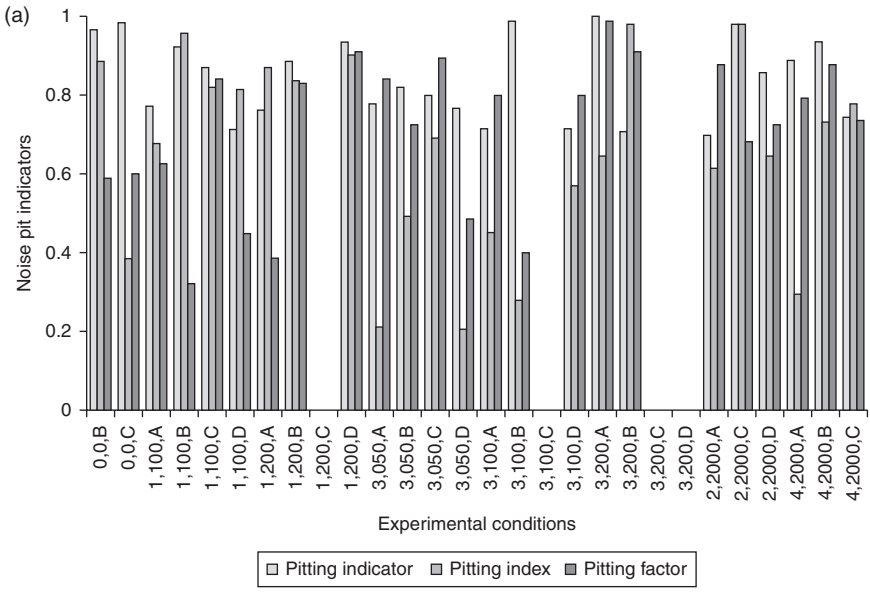

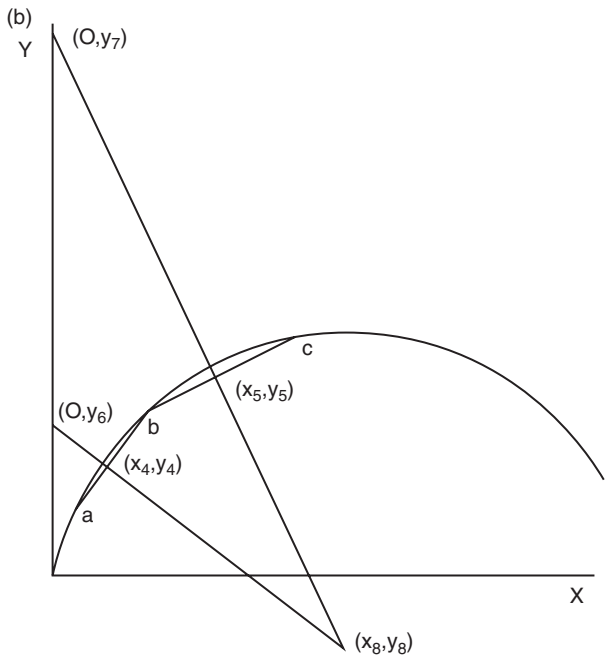

5.12 (a) *R*2 values for the correlation between measured pits vs pitting corrosion as indicated by noise measurements. (b) Three-point geometric technique representation.

Table 5.8 Characteristics of laboratory pipe loop

		Pipe dimension			Maximum[a]			
Material	Measuring techniques	Diameter of experimental section (cm)	Capacity (L)	Probes/ coupons	Flow rate (m/s)	Temperature. (°C (°F))	Pressure psi (kPa)	Reference
Nickel alloy C-276	LPR and EIS	1.5 (ID)	75	Flat and flush-mounted tubular	10	150 (270)	725 (5000)	54
Type 316 SS	EIS	10 (OD)	141	Flush-mounted	1	90 (162)	300 (2068)	55
Acrylic	EIS and electrical resistance (ER) probes	10 (ID)	141	Flush-mounted	6,9,12[b]	40 (104)	20 (138)	56
Alloy C	LPR and weight loss	1.59 (ID)	1.5	Tubular	50, 150, 990[c]	65 (150)	40 (275)	57
Type 316L SS (UNS S31600); nickel alloy C-276 (UNS N10276); and titanium (UNS R50250)	Weight loss	1.27 (OD)	–5	Annular tube	15.2	149 (300)	600 (4137)	58
SS	Weight loss	Volume/coupon ratio 161 or 2 L/cm^2		Annular tube	9	77 (170)	160 (1103)	59
Alloy C-276	LPR and weight loss	1.27	5	Tubular samples	11	93 (200)	150 (1000)	60
Type 316 SS	Weight loss and EIS	2.54 (ID)	3.78	Annular	1.8	93 (199)	595 (4100)	61

(*Continued*)

Table 5.8 Continued

		Pipe dimension			Maximum[a]			
Material	Measuring techniques	Diameter of experimental section (cm)	Capacity (L)	Probes/ coupons	Flow rate (m/s)	Temperature. (°C (°F))	Pressure psi (kPa)	Reference
Type 316 SS	Weight loss	6.5(ID)		Intrusive coupons and flush-mounted samples	5	180 (356)	870 (6000)	62
	LPR and EIS	1.27 and 2.54 (ID)		Flush-mounted ring electrodes	2–300[c]	50 (122)	Atmospheric	63
C steel (N80) or 13Cr martensitic SS (UNSS42000)	Weight loss and LPR	1.0 (ID)	0.009	Cylindrical specimen	20 (liquid) 100 (gas)	300 (572)	1450 (10 000)	64
Type 316 SS	EIS	0.9 (ID)		Flush-mounted	7	75 (135)	81 (560)	65
C-276 SS	Weight loss and electrochemical	0.6 (OD)	6	Cylindrical specimen	3	38 (100)	1000 (6895)	66

[a]Maximum values for the system or values at which the results are presented.
[b]Froude number.
[c]Wall shear stress.

Table 5.9 Comparison of laboratory and field flow loops used in the present study

Laboratory flow loop	Field flow loop (used in the present study).
Conditions controlled by the performer	Conditions set by the field operation
Usually made of corrosion-resistant materials	Made of carbon steel
Comparison between coupons/probes/electrodes in the loop and the loop itself cannot be made	A quantitative comparison between coupons and the pipe can be made, because some coupons are made out of the pipe material
Reusable (after proper cleaning)	The loop was completely destructed to determine the pit distribution on the inside wall
Fluids can be recirculated. Care should be taken to avoid saturation of solution with corrosion products	Once-through only
Electrodes/probes can be placed as a part of the loop body (with proper spacer for electrode insulation)	Safety regulation of an operating pipeline does not permit reliable placement of electrodes/probes as part of pipe body

Table 5.10 Fluctuations in the operating conditions of gassy-oil field

Experimental conditions		Production (m^3/D)			Pressure (kPa)	Temperature (°C)
Inhibitor	Concentration	Water	Oil	Gas × 10^3		
Uninhibited	0	181	66	20	2600	56
Batch no. 2	2000	160	49	18	1800	57
Batch no. 4	2000	168	51	18	1700	57
Inhibitor no. 1	50	138	37	11	2300	54
Inhibitor no. 1	100	160	42	19	2100	54
Inhibitor no. 1	200	203	43	13	1700	56
Inhibitor no. 3	50	178	42	16	1700	56
Inhibitor no. 3	100	167	49	16	1500	57
Inhibitor no.3	200	163	48	18	1600	57

There have also been studies on the effect of flow rates on corrosion. The effect of flow rate on the corrosion rate in inhibited 15% HCl showed acceleration of corrosion rate with increasing flow velocity between 65°C and 70°C. The effect of flow rate on the inhibitors tested at 125°C was negligible.[66] The methods used for the evaluation of inhibitors and changes in the metal surface induced by acid stimulation treatment consisted of reflectance Fourier transform infrared spectroscopy,[67] nuclear magnetic resonance (NMR) and size exclusion chromatography, contact angle measurement,[68] linear polarization,[69] and conventional techniques such as potentiostatic polarization,

cyclic voltammetry, and determination of concentration of iron in solutions as a function of time.

5.5 The use of coupons to measure corrosion rates

Sample coupons can be placed, removed, and replaced periodically to provide continuous data on the relative corrosivity and the inhibitor efficiency. Placement and retrieval of coupons are straightforward, and can be done under pressure without stopping production. The sample coupons are flush-mounted or placed as part of the pipe for proper pipe–coupon correlation. This type of placing sample coupons is not impossible but can be done in the operating pipe only by shutting down operations. Sample misalignment can lead to large errors in corrosion rates.[70]

The coupon and pipe behavior should be correlated to obtain meaningful results. Such correlations can be made only when the geometry and types of coupons are protruding or flush, the chemical composition of the pipe and coupons is the same, the corrosion mechanisms of coupon/electrode and the pipe are the same and the electric isolation of coupon/electrode from the pipe exists. Improper positioning of sample coupons is subject to erosion from the edges. In the cases of coupons/electrodes protruding in nature are subject to exposure to severe flow conditions unlike the pipe and represents a worst-case corrosivity of the pipe.

Protruding coupons/electrodes in general showed higher pitting rates than the pipe itself. Slight differences in the metallurgy of the sample coupons and surface finish (polishing) had very little effect on the corrosion behavior as seen in Fig. 5.7. Sample coupons placed in the top portion of the pipe exposed to gas-oil phases were subject to less corrosion. Sample coupons placed in the middle of the pipe were exposed to oil and water phases and subject to moderate to severe corrosion. The samples in the bottom of the pipe were exposed fully to corrosive brine and corroded and pitted to a greater degree. The sample coupons at the bottom of the pipe represent the worst-case corrosive scenario of the pipeline.

5.6 Comparing different monitoring techniques

Corrosion rates obtained by various techniques in oil and gas pipelines can be compared as follows. The weight loss technique proved to be the most reliable technique for monitoring corrosion inhibition of general and pitting corrosion rates. The weight loss data agreed about 90% MRT. Since the method is time-averaged, some prior knowledge or judgment is required with respect to the duration of sample coupon exposure.

The LPR general corrosion rate agreed nearly 70% of the time with MRT (Table 5.8). In many practical situations, the Tafel slopes were taken

as $\beta_a = \beta_c = 60$ V or 100 V/decade. The calculated corrosion rates from electrochemical data with assumed Tafel slope values have been found to be correct within a factor of 2.2. This is a non-destructive, straightforward, simple technique that can be used for long-term monitoring in oil and gas pipelines. This technique gives instantaneous general corrosion rates, so that the effect of inhibitors and the variation in inhibitor concentration can be determined. The technique does not give any information on localized corrosion.

General corrosion trends obtained by EIS agreed with MRT about 33% of the time. Collection of data by EIS over a wide frequency range requires a long time. Fast Fourier transform (FFT) reduces the time duration of collection of data to a considerable extent. For instance, the FFT technique can be used to obtain data at 20 frequencies between 0.001 Hz and 0.1 Hz in 1000 s, as opposed to data at one frequency in 1000 s by conventional methods. This technique requires a physical model to analyze the data. The technique also requires an equivalent circuit representing the corroding metal coated with a porous non-conducting film.

A geometric technique, in which the centers formed by three successive data points at three frequencies are determined, was used for analyzing the AC impedance diagrams (Fig. 5.12) obtained experimentally.[71] The equivalent electrical circuit that represents a simple electrochemical reaction, along with the impedance diagram, is shown in Fig. 5.13. The charge transfer resistance (polarization resistance) R_p can be evaluated from the diameter of the semicircular impedance diagrams. Corrosion rates are then related to

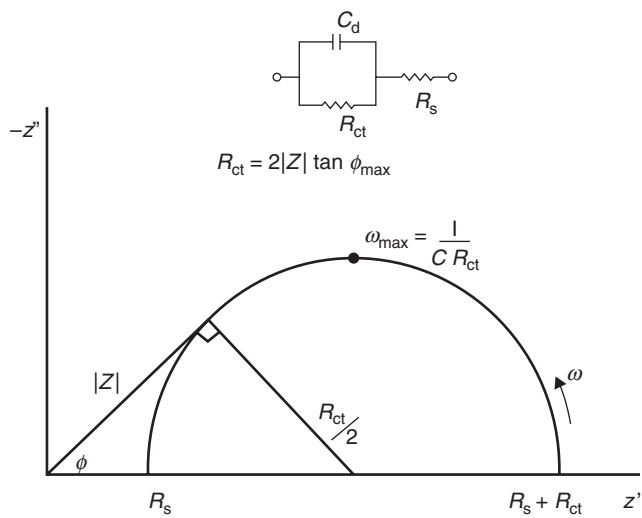

5.13 Representation of equivalent circuit.

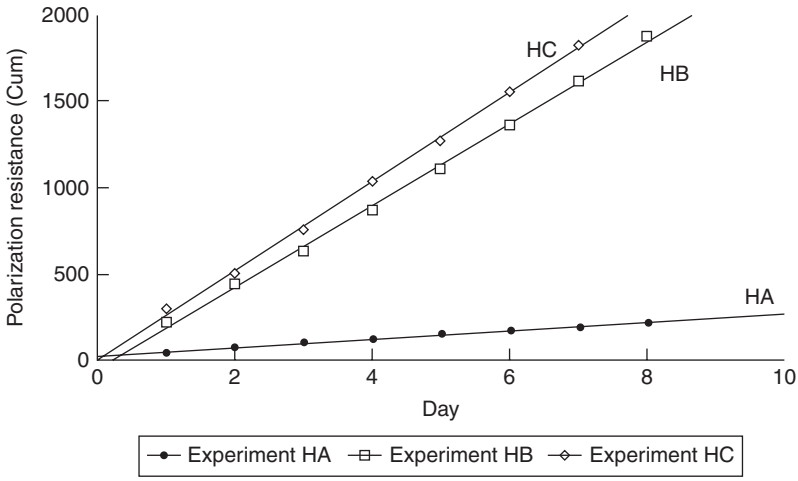

5.14 Cumulative polarization resistance vs time.

R_p, the polarization resistance ($1/R_p$) by the Stern-Geary low overvoltage approximation of the Butler-Volmer equation.

The data on polarization resistance for process water devoid of any inhibitor, and process water containing inhibitors HB and HC, are shown in Fig. 5.14. The cumulative polarization resistance for solutions with inhibitors increases rapidly, while the value stays the same for process water devoid of inhibitor. The sum of depression angles is shown in Fig. 5.15 for the two inhibitors as a function of time. The sum of depression angle shows a steep increase in process water devoid of inhibitor, and a very small increase in depression angle in solutions with inhibitors (HB and HC). The depression angle is indicative of localized corrosion. Thus AC impedance is capable of monitoring corrosion in the field as well as in the laboratory by obtaining the R_p values at three frequencies.

The general corrosion rate trend obtained by the EN technique agreed to 90% of MRT. When a sample coupon is exposed to corrosive fluids, several events such as general corrosion, erosion corrosion due to flowing fluids, passive film formation and breakdown, pit initiation, and repassivation occur. Each event generates an electrochemical current, the magnitude and sign of which depend on the nature of the event. All the EN fluctuations are measured. During pit growth, a higher magnitude current signal is observed. This signal is manifested as the standard deviation the magnitude of which is greater than the mean current value. The ratio of standard deviation to the mean current indicates pit growth, known as the pit indicator equation, σ_i/I_{mean}. The EN method has been found to be a promising method for monitoring corrosion in oil pipelines. A typical electrochemical cell, and the

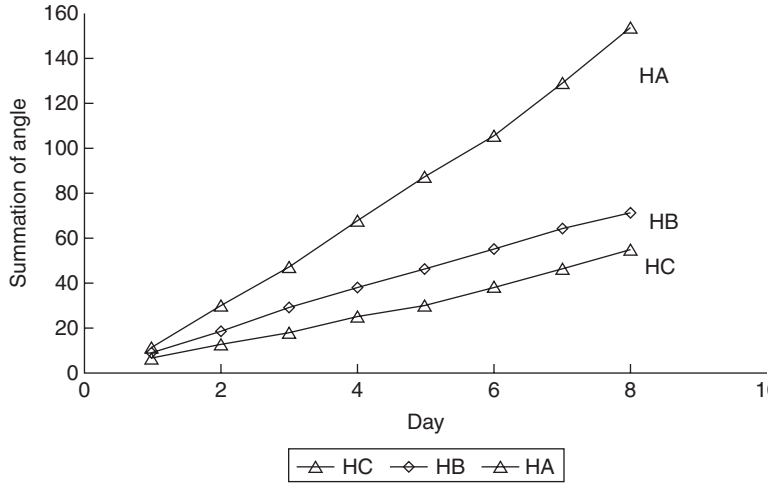

5.15 Summation of angle vs time.

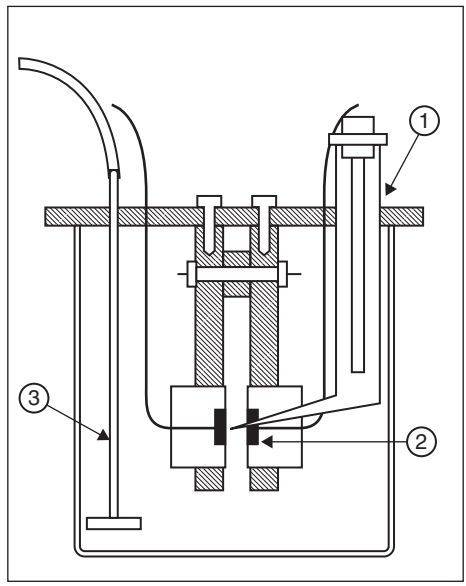

1) Calomel reference electrode
2) Steel specimen
3) Gas purge

5.16 Electrochemical cell.

experimental arrangement of the apparatus used in potential noise measurements, are shown in Figs 5.16 and 5.17 respectively. Figure 5.18a shows the electrochemical potential noise response in process water with and without added inhibitor as a function of time.

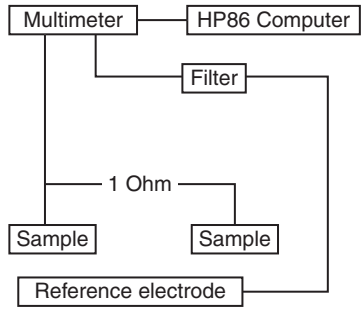

5.17 Apparatus used for potential noise measurements.

The results obtained from the hydrogen permeation technique did not correlate with the data obtained from intrusive techniques. The hydrogen permeation method of monitoring internal corrosion rates is nonintrusive. Some of the factors that influenced hydrogen permeation measurements are gluing of foil, length of the capillary tube, temperature fluctuations, pipe wall thickness, and the fraction of hydrogen atoms produced by the corrosion reaction that enter the foil. This technique may be used in pipelines where corrosion occurs in small areas in which water accumulates, but is not recommended in pipelines in which corrosion occurs over larger surface areas.

5.7 Conclusion

A survey of monitoring techniques based on categories listed in NACE 3T 199, such as direct intrusive physical techniques, direct intrusive electrochemical techniques, direct nonintrusive measurement techniques, indirect online measurement techniques, indirect offline measurement techniques, and MIC measurement technique resulted in the data illustrated in Fig. 5.18b, 5.18c, 5.18d, 5.18e, 5.18f, and 5.18g.

The techniques for monitoring internal corrosion in pipelines can be broadly classified into direct intrusive physical techniques, direct intrusive electrochemical techniques, direct nonintrusive techniques, indirect online monitoring techniques, indirect offline monitoring techniques, MIC monitoring techniques, and new techniques.

The more reliable the technique, the greater its usage, but no single technique is outstanding and unique in meeting all the requirements of corrosion monitoring. The factors that influence decisions for selecting an appropriate monitoring technique are the reliability of the technique and its tolerance to the variable operating conditions.

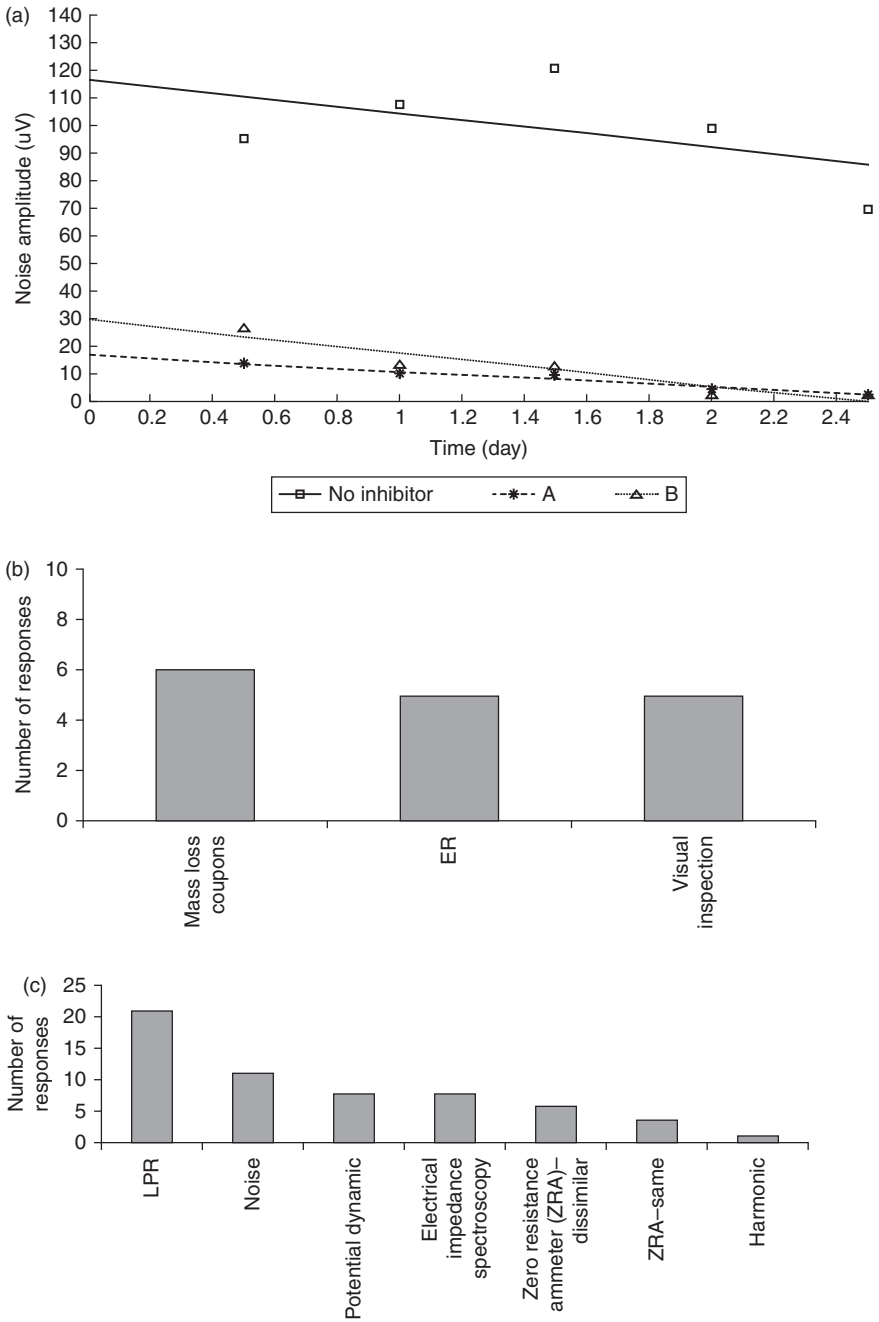

5.18 (a) Potential noise amplitude vs time. (b) Direct intrusive physical techniques. (c) Direct intrusive electrochemical techniques. (d) Direct nonintrusive measurement techniques. (e) Indirect online measurement techniques. (f) Indirect offline measurement techniques. (g) MIC measurement techniques.

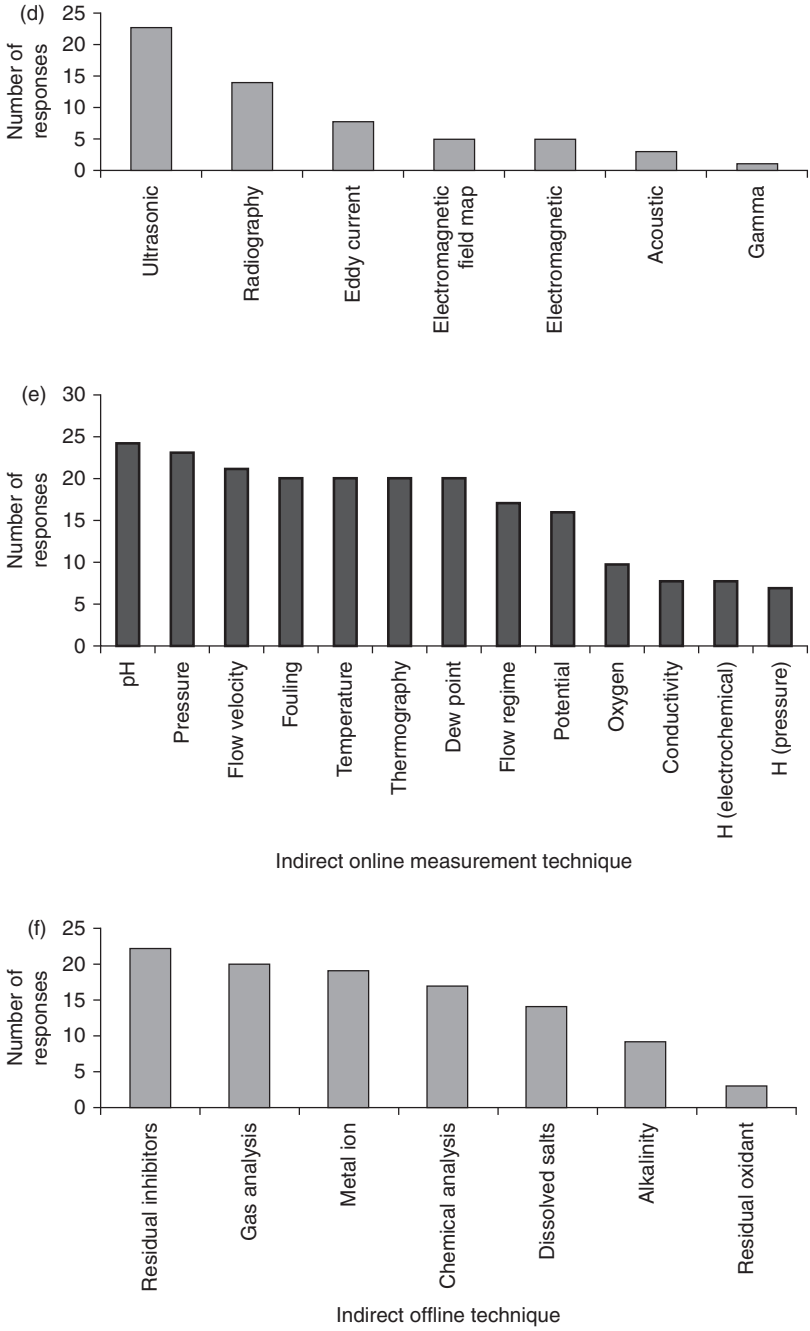

5.18 Continued

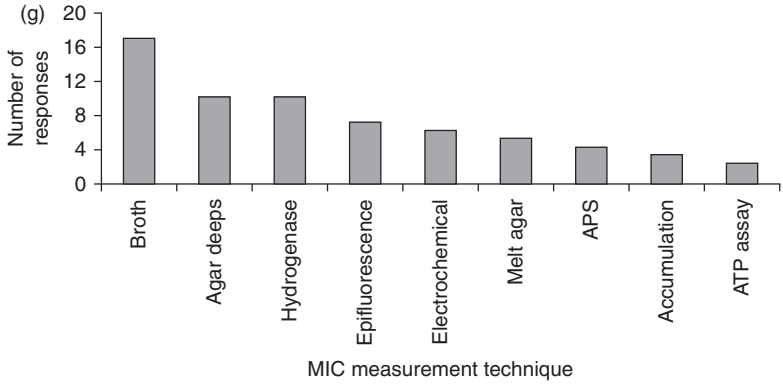

5.18 Continued

It is useful to note that the survey were not analyzed based on the technical background of the respondents, nor was the ratio of people in different categories established. Therefore, the error due to person bias of respondents was included in the results. Thus, the results of the survey of monitoring techniques should be considered more as a trend at the time the survey was commissioned.

5.8 References

1. Nestle A (1973), *Corrosion Inhibitors in Petroleum Production Primary Recovery*, Houston, NACE.
2. Tuttle R N and Kane R D (1973), *H_2S Corrosion in Oil and Gas Production: Classic Paper*, Houston, NACE.
3. Bregman J I (1966), 'Proc. 2nd SEIC', *Ann Univ Ferrara*, n.s., Sez V., suppl. no. 4, 549.
4. Bregman J I (1971), 'Proc. 3rd SEIC', *Ann Univ Ferrara*, n.s., Sez. V, suppl. no. 5, 339.
5. Foroulis Z A (1980), 'Proc. 5th SEIC', *Ann Univ Ferrera*, Sez. V, suppl. no. 7, 1029.
6. Lahodny-Sarc O (1985), 'Proc. 6th SEIC', *Ann Univ Ferrara*, Sez V, suppl. no. 8, 1313.
7. Hausler R H and Stegmann D W (1990), 'Proc. 7th SEIC', *Ann Univ Ferrara*, n.s., Sez. V, suppl. no. 5, 427.
8. Reiser K (1966), 'Proc. 2nd SEIC', *Ann Univ Ferrara*, n.s., Sez. V, suppl. no. 4, 459.
9. Balezin S A and Kemhadze T V (1971), 'Proc. 3rd SEIC', *Ann Univ Ferrara*, n.s., Sez. V, suppl. no. 5, 427.
10. Schmitt G and Bruckoff W (1980), 'Proc. 5th SEIC', *Ann Univ Ferrara*, n.s., Sez. V, suppl. no. 7, 323.

11. Hausler R H, Goeller R A and Rosenwald R H (1971), 'Proc. 3rd SEIC', *Ann Univ Ferrara*, n.s., Sez. V, suppl. no. 5, 399.
12. Horvath J, Rauscher A, Hackl L and Marta F (1971), 'Proc. 3rd SEIC, *Ann Univ Ferrara*, n.s., Sez. V, suppl. no. 5, 851.
13. Horvath J, Hackl, L and Rauscher A (1966), 'Proc. 2nd SEIC', *Ann Univ Ferrara*, n.s., Sez. V, suppl. no. 4, 447.
14. Hackl L, Horvath J, Marta F and Olar O (1976), 'Proc. 4th SEIC, *Ann Univ Ferrara*, Sez. V, suppl. no. 6, 212.
15. Dougherty J A and Alink B A (1990), 'Proc. 7th SEIC', *Ann Univ Ferrara*, n.s., Sez. V, suppl. no. 9, 1299.
16. Rozenfeld I L, *Inhibitory Korrozii*, Moscow, Himija, 307.
17. Iofa Z A (1970), *Zashch Metallov*, **6**, 491.
18. Antropov L J and Panasenko V F (1974), *Itogi nauki i tekhniki, ser. Korroziya i zashchita ot korrozii*, 4, 46.
19. Szklarska-Smialowska S and Lunarska E (1981), *Werkstoffe und Korrosion*, **32**, 478.
20. Volmer P (1965), *Corrosion*, **21**, 69.
21. Kaesche H (1970), *Werkstoffe und Korrosion*, **21**, 185.
22. Schmitt G and Rothmann B (1975), *Werkstoffe und Korrosion*, **28**, 597.
23. Rhodes P R (1976), *Electrochem. Soc. Meeting*, Las Vegas, v. 76–2, no. 107, 300.
24. Morris C (1979), 54th *Ann. Conf. Soc. Pet. Eng. of AIME*, Las Vegas, proc. paper no. 8310.
25. Hambly T W (1981), *J Petrol Technol*, 792.
26. Cron C J and March G A (1983), *J Petrol Technol*, 1033.
27. DeWaard C and Milliams D E (1975), *Corrosion*, **31**, (5), 177.
28. Newton L E, Hausler R H and Godard H P (eds) (1984), *CO_2 Corrosion in Oil and Gas Production, and Advances in CO_2 Corrosion*, Houston, NACE.
29. Burke P A and Hausler R H (1984), *Ann. Conf. and 1984 Corrosion Show*, New Orleans, *Paper* no. 288.
30. Burke P A and Hausler R H (1984), *Ann. Conf. and 1984 Corrosion Show*, New Orleans, *Paper* no. 288.
31. Hausler R H and Stegmann D W (1990), 'Proc. 6th SEIC', *Ann Univ Ferrara*, n.s., Sez. V, suppl no. 9, 1247.
32. Hausler R H (1985), 'Proc. 6th SEIC', *Ann Univ Ferrara*, n.s., Sez. V, suppl. no. 8, 41.
33. Grauer R (1981), *Werkstoffe und Korrosion*, **32**, 113.
34. Suiger P C and Schumm W I (1970), *J Am Water Works Ass*, **62** (3), 198.
35. Gatzke L K and Houster R H (1983), *Corrosion*, Anaheim, Ca, NACE.
36. Bradburn J B (1983), *CO_2 Corrosion in Oil and Gas Production: Selected Papers*, Newton L E and Hausler H R (eds.), Houston, NACE, 142.
37. DeWaard C and Milliams D E (1975), *Corrosion*, **31**, 177.
38. Schmitt G and Rothmann B (1978), *Werkstoffe und Korrosion*, **29**, 237.
39. Schwenk W (1974), *Werkstoffe und Korrosion*, **25**, 643.
40. Masamura K, Hashizume S, Nunomwia K, Sakai J and Matsushima I (1983), *Int Corrosion Forum*, Anaheim CA, NACE, paper no. 55.
41. Ikeda A, Ueda M and Mukai S (1983), *Int Corrosion Forum*, Anaheim CA, NACE, paper no. 45.
42. Dunlop A K, Hassell H L and Rhodes P R (1983), *Int Corrosion Forum*, Anaheim CA, NACE, paper no. 46.

43. Latimer W M (1938), *Oxidation Potentials*, New York, Prentice Hall.
44. Lotz, V, Van Bodegon L and Ouwehand C (1991), *Corrosion* (NACE), **47**(8), 635.
45. Farquhar G B (1993), *Mat Perform*, **32** (1), 53.
46. Galbraith J M and Lofgren R L (1987), *Mat Perform*, **26** (9), 42.
47. Donham J E (1991), *Mat Perform*, **30** (8), 53.
48. Dewar E J (1986), *Mat Perform*, **25** (7), 39.
49. Papavinasam S, Revie R W, Attard M, Demoz A and Michaelian K (2003), *Corrosion*, **59**, 1096.
50. Attard M, Papavinasam S, Revie R W, Demoz A, Donini J C and Michaelian K (2000), *Mater Perform*, **39**, 10, 58–61.
51. Demoz A, Michaelian K H, Donini J, Papavinasam S and Revie R W (2001), *Pipeline and Gas Industry*, **84**, 10, 48–53.
52. Papavinasam S, Revie R W, Demoz A and Michaelian K (2002), *Corrosion/2002*, paper no. 02495, Houston TX, NACE.
53. Kvarekval J and Gulbrandsen E (2001), *Corrosion/2001*, paper no. 01025, Houston TX, NACE.
54. Hong T and Jepson W P (2001), *Corr Sci*, **43**, 1839.
55. Wang H B, Shi H, Hong T, Kang C and Jepson W P (2001), *Corrosion/2001*, paper no. 01023, Houston TX, NACE.
56. Abayarathna D, Naraghi A and Grahmann N (2000), *Corrosion/2000*, paper no. 21, Houston TX, NACE.
57. Fu, S L and Strickland J b (1993), *Corrosion '93*, paper no. 117, Houston TX, NACE.
58. Dougherty J A and Ahn Y S (1999), *Corrosion '99*, paper no. 4, Houston TX, NACE.
59. Srinivasan S and Kane R D (1999), *Corrosion '99*, paper no. 14, Houston TX, NACE.
60. Choi H J, Cepulis R L and Lee J B (1988), *Corrosion '88*, paper no. 209, Houston TX, NACE.
61. Schmitt G, Bruckoff W B, Faessler K and Blummel G (1990), *Corrosion '90*, paper no. 23, Houston TX, NACE.
62. Efird K D, Wright E J, Boros J A and Hailey T G (1993), *Corrosion*, **49**, 992–1003.
63. Denpo K and Ogaa H (1993), *Corrosion*, **49**, 442.
64. Gerretsen J H, Damen S, Visser A and Lotz U (1993), *Corrosion '93*, paper, no. 84, Houston TX, NACE.
65. Eaton P E and Sutton G (1994), *Corrosion /94*, paper no. 30, Houston TX, NACE.
66. Frenier W W (1991) *Mat Perform*, **30** (1), 39.
67. Frenier W W and Samuelson M L, *Corrosion 91/82*, Houston TX, NACE
68. Frenier W W, Lopp V R and Growcock F W (1985) 'Proc. 6th SEIC', *Ann Univ Ferrara*, n.s., Sez V., suppl. no. 8, 183.
69. Hausler R H (1986) *Corrosion '86, International Corrosion Forum*, paper no. 275, Houston TX, NACE.
70. Postlethwaite J, Wang Y and Bergstrom D J (1997), *Corrosion*, **53**, 595.
71. Roberge P R, Halliop E, Asplund M and Sastri V S (1990), *J Appl Electrochem*, **20**, 1004–1008.

6

Types of corrosion inhibitor for managing corrosion in underground pipelines

V. S. SASTRI, Sai Ram Consultant, Canada

DOI: 10.1533/9780857099266.1.166

Abstract: This chapter reviews the use of corrosion inhibitors in the oil and gas industry. It discusses production factors affecting corrosion inhibition, criteria for selecting corrosion inhibitors, mechanisms of corrosion inhibition, and types of corrosion inhibitor.

Key words: corrosion inhibitors, corrosion media, gas pipelines, oil pipelines, Sastri equation, steel pipes, structure–activity relationships, underground pipelines.

6.1 Introduction

It is a well-recognized fact that corrosion inhibitors have contributed to the economical long-term operation of gas and oil wells. The application of inhibitors with respect to corrosion in primary and secondary recovery has been extensively discussed.[1–7] Many inhibitor formulations have been developed for use in corrosion control in drilling and completion of wells in shallow geological formations. The suitability of an inhibitor depends on good thermal and chemical stability under the pipeline transport conditions carrying oil, along with corrodents such as hydrogen sulfide and carbon dioxide. It is needless to state that a thorough examination and understanding of the mechanism of inhibition and the surface interactions of metal–corrosive agent and metal–inhibitor are necessary.

6.2 Types of inhibitors

Commercial inhibitors available under trade names provide very little information on their composition. Commercial inhibitor formulations consist of one or more inhibitor compounds, along with other additives such as surfactants, film enhancers, de-emulsifiers, and oxygen scavengers. The inhibitor solvent package can also be critical with respect to solubility or dispersibility and hence application and/or performance of the products.

Early corrosion inhibitors were formaldehyde and other organic inhibitors and inorganic compounds such as chromates, polyphosphates, and arsenic compounds.[8] Most of the inhibitors in current use in producing wells are organic nitrogenous compounds. The basic types have long chain hydrocarbons (C_{18}) as part of their structure.[2,3] Nearly 90% of the inhibitors in use at present are based on long chain aliphatic diamine, or on long carbon chain imidazolines. Various modifications of these inhibitor structures to change the physical properties, such as reaction with ethylene oxide with long chain compounds to produce polyoxy-ethylene derivatives of varying degree of brine dispersibility, have been made. Many carboxylic acids are used to make salts of amines or imidazolines.[9] The most commonly used inhibitors in the petroleum industry belong to the following classes:

- amides/imidazolines
- salts of nitrogenous molecules with carboxylic acids
- nitrogen quaternaries
- polyoxyalkylated amines, amides, imidazolines
- nitrogen heterocyclics, and compounds containing P, S, and O atoms.

The principles of production and the effectiveness as inhibitors of quaternary nitrogen compounds as surfactants, biocides, and de-emulsifiers have been documented.[9,10] In practice, inhibitors need to be water soluble, and imidazoline is made water soluble by the addition of acetic acid, a suitable solvent, and a surfactant. By replacing acetic acid with a high molecular weight acid and an aromatic base as a solvent, imidazoline can be made an oil soluble inhibitor. Imidazoline undergoes hydrolysis in water to give an amide, which leads to the question as to the actual species that functions as the inhibitor and the overall inhibition mechanism in an oil/water system. Usually, a suitable non-ionic or cationic surfactant is added to the oil soluble inhibitor to make the inhibitor dispersible in water. The addition of surfactant may also reduce the tendency for the formation of scale of solid deposits, such as iron sulfide, which can cause pitting.

Organic inhibitors offer protection by forming a hydrophobic film on the metal surface. The effectiveness of the film-forming organic inhibitors depends on the chemical structure, composition, and their affinities for the metal surface. Since film formation is an adsorption process, the temperature and pressure in the system are important factors.

There are many hypotheses and theories in explaining the inhibitive action of long chain nitrogenous inhibitors. One of the classical concepts is known as the ‘sandwich’ theory, in which the bottom part of the ‘sandwich’ is the bond between the polar end of the molecule and the metal surface. The degree of protection depends on the strength of the bond. The central

portion of the sandwich is the non-polar end of the molecule, and the extent to which it protects from corrosion depends upon the degree to which this portion of the molecule can cover or wet the surface. The top portion of the sandwich is the hydrophobic layer of oil attached to the long carbon tail of the inhibitor. This oil layer serves as the external protective film, covering the inhibitor film and creating a barrier to both outward diffusion of ferrous ion and inward diffusion of corrosive species.[3] The organic amines have been shown to affect both anodic and cathodic areas of the metal.[19] It is thought that the anodic inhibition occurs through the transfer of electrons from the metal to the positively charged inhibitor instead of migration towards the cathodic areas of the metal. The predominant cathodic inhibition is probably due to both physisorption and chemisorption. The inhibitor chemisorption involves transfer of electrons from the inhibitor to the metal. The bond between the metal and inhibitor is a coordinate bond:

$$M + I \rightarrow M - I \qquad [6.1]$$

The inhibitive effect of some oils containing straight chain or aromatic mercaptans in sour brines is attributed to the formation of lattice-like polysulfides, which gives corrosion protection in the presence of acids.[4] Fatty acids and fatty amines are used as inhibitors in media such as oxygen, carbon dioxide, and hydrogen sulfide. Mixtures of fatty acids and fatty amines are used as inhibitors in CO_2 and H_2S media. These inhibitors form a protective hydrophobic film. The presence of iron sulfide film under the inhibitor film was detected.

Experiments with presulfided samples showed that the effect of inhibitor was both enhanced and prolonged. The experiments involving presulfided samples showed filming inhibitors to be more effective when used intermittently rather than in a continuous treatment. Based on weight loss measurements and polarization measurements at high fluid velocities, it was shown that the corrosion rate of iron in the presence of H_2S is controlled by mass transfer through an iron sulfide film, or an interfacial exchange mechanism, or both. The controlling thickness of the iron sulfide film was found to be small, the adsorption of inhibitor was irreversible, and the thickness of the protective sulfide film was limited.

The rate of transport of inhibitor to the corroding metal surface has to equal the residual corrosion rate to maintain adequate protection. The measurements were done in a solution saturated with H_2S to ensure the low solubility of the sulfide film in an acid medium of pH ~4–5. The alkyl ammonium ion can displace protons in the protonated iron surface complex. Inhibitors can influence the value of the surface complex constant as well as the pH. When the reaction is considered in detail, it is assumed that the iron sulfide layer is covered by a water layer. The adsorbed proton dissociates and is consequently solvated. Both the free alkyl ammonium ion and bisulfide ion are solvated.

During adsorption, a neutral complex is formed. This complex is hydrophobic and displaces the water molecules from the iron sulfide surface. An inhibitor with a higher lipophilic character will be more permanently adsorbed. Thus the increasing efficiency of amines increases with increasing chain length in corrosion inhibition due to the decrease in solubility in water.

Pitting corrosion of stainless steel in the presence of H_2S and chloride was inhibited in the presence of carbamide and thiocarbamide.[11,12] A tentative explanation based on the formation of a surface complex Fe HS^-_{ad} stabilized by a cationic organic inhibitor has been proposed. The Fe (H-S-R) complex formed on the surface prevents anodic metal dissolution.

The mechanisms of inhibition of both general and localized corrosion in sour media with respect to hydrophobicity and molecular structure have been elucidated.[13] A classification of corrosion inhibitors in terms of the hard and soft acid and base (HSAB) principle was advanced for the first time by Sastri *et al*. The HSAB principle can be used to rationalize various interactions between the metal and the corrosion inhibitors. According to the HSAB principle, hard acids tend to form complexes with hard bases, and soft acids with soft bases. Some of the characteristics of hard and soft acids and bases are size, electronegativity, polarizability, and charge. The HSAB principle can be used to describe the formation of iron sulfide, followed by Fe–SH species and the bonding of iron to the nitrogen atom of the inhibitor molecule in sour media. Iron atoms as soft species bond to the soft base SH^-.

6.3 The effectiveness of corrosion inhibitors in particular corrosion environments

Corrosion inhibitors that minimize the corrosion by interfering with the action of bisulfide on iron metal or by formation of iron-inhibitor complex which is immune to corrosion are discussed. Corrosion inhibition in carbon dioxide medium is also discussed.

6.3.1 Corrosion inhibition in sour media

Sour gas production in oil pipelines can lead to the production of elemental sulfur, which in turn can lead to plugging of the tubing. This requires the injection of a solvent downhole. The corrosion of steel in brines in the presence of H_2S and sulfur involves locally generated HCl and the appearance of hydrogen blistering.[14] Conventional inhibitors such as imidazolines are not only inefficient but can accelerate corrosion under sulfur deposits,[15,16] by facilitating the cathodic reaction. Conventional inhibitors cannot penetrate through the solid sulfur deposits on the metal to function as inhibitors. Thus chemicals that will displace the sulfur deposits and protect the metal from corrosion must be explored.

In order to locate suitable inhibitors, the mechanism of corrosion, such as the localized corrosion of steel induced by sulfur, should be understood.[17] Factors such as Cr, Mo, and Ni content in the alloys, temperature, H_2S partial pressure, and chloride on the sulfur-induced corrosion were studied.[18] Elemental sulfur, either dissolved or undissolved as a separate solid or liquid phase, acts as an electron acceptor in the cathodic reaction. In dissolved sulfur, the cathodic reaction is diffusion-controlled and moderate corrosion rates are observed. Electron-conducting metal sulfide surfaces act as catalysts for electron transfer, resulting in a high corrosion rate. Consequently, all the steps leading to the formation of metal sulfide and hindering charge transfer from metal to sulfur atoms, such as the use of passivating agents, chromates, dichromates, and hydrogen peroxide, are useful in the case of carbon steel. In oil production, greater protection is achieved with adsorption type inhibitors such as amines up to 232°C.

Many factors influence the effectiveness of organic inhibitors. The correlation between the molecular structure of organic inhibitors such as aliphatic amines, imidazolines, and amidoamines in deaerated hydrogen sulfide media has been observed. Factors such as solubility and hydrophobicity were dominant in function as inhibitors and conjugation and polar effects were equally important.[18] Corrosion product layers play an important role in corrosion and protection. In the presence of sulfide layers, the inhibitors influence the electronic and ionic transfer across the solid phase interphase.

In the case of carbon dioxide corrosion, the inhibitors affect the solubility of carbonate scale. Corrosion control in oil wells flooded with carbon dioxide[19] showed imidazolines to be successful in corrosion protection. The inhibitor was incorporated in the carbonate corrosion product layer, but was more effective in the sulfide layer than in the carbonate corrosion product layer. Better inhibition was observed with nitrogen–phosphorus compounds, or compounds with sulfur in the organic molecules.

Laboratory electrochemical measurements of iron electrode in CO_2 saturated brine with three commercial inhibitors showed the carbonate film to be a barrier to inhibitor molecules.[20] Advanced studies on the structural effect of quaternary ammonium compounds on H_2S and CO_2 corrosion showed improved inhibition with the polar headgroup size and the number of carbon atoms in the alkyl chain. The better inhibition was attributed to the formation of close packed layers stabilized by the steric effect of polar groups and the hydrophobic nature of the layer.[21]

To mitigate corrosion damage in CO_2 media in oil and gas systems, development of corrosion inhibitors was directed towards field application. Flow-induced corrosion was done in autoclaves.[31] Imidazoline was found to be very effective, and 99% inhibition was obtained. It is necessary to carry out both laboratory and field evaluation of inhibitors.[31] Another test under known hydrodynamic conditions that stimulate turbulent flow in pipeline,

flow line, and production tubing has been done to evaluate inhibitors in brine/carbon dioxide/oil systems.[22] A critical review of laboratory test methods for inhibitors used in oil wells has shown that many types of tests should be performed for the final selection of suitable inhibitors.[23]

The importance of the interaction between the inhibitor molecular structure and the crystal structure of the corrosion products has been shown by experimental observations on the change of surface structure from uninhibited to inhibited metal sample in a methane gas well containing H_2S and CO_2. The presence of oxygen, along with H_2S and CO_2, in an aqueous/hydrocarbon phase can occur in sour gas gathering systems. The gas drawn off the casing of pumping wells may contain small amounts of oxygen introduced with air due to leakage in the vacuum lines which can cause both general and pitting corrosion. Organic sulfophosphates were shown to be effective inhibitors in this situation. The corrosion inhibition in this medium can be improved by a liquid hydrocarbon due to its emulsion-forming tendency and synergistic behavior.[24]

6.3.2 Corrosion inhibition in bacterial environments

In water-flooding the inhibitors described under primary production are used. The most effective and commonly used inhibitors are the quaternary salts of fatty acids on the imidazoline-type inhibitors. These inhibitors also serve the purpose of good bactericides and dispersive agents. Mixtures of amino-methylene phosphonate and zinc salts have been used in circulating water systems and have been found to be more effective inhibitors than mixtures of zinc salt and inorganic phosphate. Organic sulfonates have also been used. Another important problem in water-flooding is bacterial corrosion control. The most effective and commonly used agents consist of chlorine, aldehydes, long chain organic nitrogenous compounds.[3,25]

Microbiological corrosion is caused by:

- algae
- slime formers
- sulfate-reducing bacteria
- iron bacteria.

Algae and slime formers grow in the form of gelatinous masses and cause plugging problems.[5,26,27] Bacterial corrosion is caused by sulfate-reducing bacteria and anaerobic sulfate reducers, by removing hydrogen from the metal surface leading to depolarization and accelerating corrosion through the formation of pits. The bacteria utilized the hydrogen to reduce sulfate and give rise to H_2S, which is corrosive and toxic and leads to souring the reservoir. The hydrogen sulfide produced by the sulfate-reducing bacteria

causes extensive corrosion.[28,29] The application of laboratory microbiological and electrochemical methods of testing to field testing[30] has been reported.

To prevent microbiologically induced corrosion, methods for both laboratory and field application[31,32] have been developed for determining bacterial activity and for selecting suitable biocides. Several methods are available for detecting underdeposit corrosion caused by microorganisms.[33] Aerobic iron bacteria, such as sphaerotilus and gallionella types, convert soluble ferrous iron present in large amounts in water to hydrated insoluble ferric oxide. Many chemical compounds can act as inhibitors as well as agents for bacterial control such as chlorinated phenols and mercurials in water-flooding operations. If chlorine is used for bacterial control and not controlled within tight limits, it can cause corrosion of pipework handling injection water.

6.3.3 Corrosion inhibition in oxygenated environments

Oxygen is invariably present in drilling muds. The most effective control of corrosion is to keep it out of the system. The drilling fluid is exposed to the atmosphere as it circulates through the pit and so it is difficult to keep the system free of oxygen. The type of corrosion is pitting of the drilling equipment. A number of factors cause corrosion of drilling equipment in the presence of oxygen. Oxygen activity in drilling muds is also determined by a number of factors.

Compounds such as sodium hexametaphosphate, phosphate esters of organic alcohols, and organic phosphonates may function as anodic inhibitors. It is useful to note that these inhibitors also act as thinning agents of non-dispersed muds. Tannins and lignins also act as thinning agents of muds, in addition to their inhibitive influence. Sodium chromate, which is usually used in oxygenated systems, is not recommended for use in muds containing reducing agents, due to its toxicity as well as economy in comparison to film-forming inhibitors.

6.3.4 Corrosion inhibition in acidic environments

Stimulation of oil and gas wells is done by acidizing. Because of the low permeability of some formations containing hydrocarbons, these do not flow readily into the well. Formations of limestone or dolomite are treated with HCl and a mixture of HF and HCl if the rock is sandstone. The acid is pumped down the tubing into the well. The acid etches channels that provide a path for the oil and gas to enter the well.

Many inhibitors such as high molecular weight nitrogenous compounds, such as those used in primary production, or the reaction products of the nitrogenous compounds with unsaturated alcohols, have been used. Commercial inhibitors contain alkyl or alkylaryl nitrogen compounds and acetylenic alcohol such as 1-octyn-3-ol. These products are toxic, present handling problems, and their effectiveness falls off with time.

The mechanism of inhibition of API grade J55 steel commonly used for tubing in wells at 95°C and inhibited by dodecyl pyridinium bromide (n-DDPB) and 1-octyn-3-ol in 37% HCl was studied and explained by adsorption of the inhibitors on a chloride-covered surface of metal displacing water molecules. In the case of octynol, the adsorbed molecules undergo chemical reaction to form the protective film. Thus, octynol could be termed a secondary inhibitor, while DDPB is an example of a primary 'interface' layer inhibitor and is more sensitive to temperature and acid (HCl) than the former.[34]

Oxygen-bearing inhibitors useful in concentrated HCl solutions include cinnamaldehyde and alkynols such as alpha-alkenyl phenones. These compounds, in combination with surfactants, provide protection similar to acetylenic alcohols. The less toxic inhibitor cinnamaldehyde, a natural component of cinnamon oils, was found to provide excellent protection[35] to steel in 15% HCl.

6.3.5 Corrosion inhibition in carbonic acid

Carbonic acid corrosion can lead to failures at the pH 2–10 range in one-phase or two-phase media, leading to general corrosion, local corrosion in the form of pitting, corrosion-erosion, and a special type of failure – chalky failure. This type of failure is characteristic of CO_2 failure. The main factors that influence the rate and intensity of corrosion and the type of corrosion failure are the temperature, pH, and partial pressure of CO_2. Temperature is an important factor. The rate of corrosion of steel below 60°C in solutions devoid of oxygen is controlled by the kinetics of evolution of H_2, which in turn is determined by the formation of H_2CO_3. The corrosion rate in the temperature range of 60°C–100°C is controlled by the chemical dissolution of layers of siderite. The corrosion rate depends on pH, with lower pH causing an increase in corrosion rate. This pH dependence is ambiguous to the observation probability of fracture under a layer of deposits in carbonic acid media at pH greater than 7 is high.

The rate of corrosion in CO_2 medium is given by the equation: [36]

$$\text{Log } \nu_k = 6.467 - 1710/(273.2) + t) + 0.67 \text{ log } P_{CO_2} \qquad [6.2]$$

where v_k is the average loss of mass of metal (g/m^{2}h) expressed in terms of depth of corrosion (mm/y), P_{CO_2} is the partial pressure of CO_2 in Mpa, and t is the temperature in °C. This relationship is satisfied when $P_{CO_2} < 1$ MPα and $t < 140°C$.

Another empirical equation which accounts for the pH of stratal and dead water in oilfields may be written as:

$$\text{Log } v_k = 3.996 + 1730/(273.2 + t) + 0.32 \text{ pH} + 0.3651 \log P_{co_2} \quad [6.3]$$

This equation is applicable under the following conditions

$$10 < t\,(°C) < 60\ ;\ 5.4 < \text{pH} < 7.6\ ;\ 0.001 < P_{co_2}\,(\text{MPa}) < 0.1$$

$$85 < HCO_3^-\ (\text{mg/L}) < 600$$

The corrosion due to the presence of CO_2 is an electrochemical phenomenon consisting of the formation of hydrogen on the cathode, which results in the formation of carbonate-oxide film on the metal surface. The two approaches to prevention of CO_2 corrosion are: (i) inhibition of the cathodic process, and (ii) formation of protective carbonate-oxide film. The cathodic process can be inhibited by:

- inhibitors that can displace HCO_3^-, H_2CO_3, and CO_2–H_2O species from the metal surface
- inhibitors that can form films of the mixed type that were impermeable to depolarizers
- inhibitors that can bond to HCO_3^-, H_2CO_3, and CO_2–H_2O species.

To different extents, the inhibitors belonging to all three types can prevent the anodic process. The inhibition of the cathodic process will predominate.

Although one would predict that organic compounds similar to carbonate ions would be useful inhibitors, it is not the case in practice. Amines, amides, imidazoles, nitrogen-bearing heterocyclics, and quaternary ammonium bases have been found to inhibit the anodic process. These do not function as efficient inhibitors in a CO_2 medium. Inhibitors containing nitrogen, sulfur and phosphorus, nitrogen, oxygen, or sulfur and phosphorus may be used with the hope that they will form mixed films that are impermeable to depolarizers.[37]

The two approaches for forming protective carbonate-oxide films are:

- regulating the pH
- regulating the temperature.

The pH can be controlled by neutralization and being kept at 8–10, which helps in the formation of siderite. Regulation of temperature is not feasible by means of chemical additives. When films or deposits of heterocyclic atoms are present at pH > 7, organic inhibitors can be adsorbed and show general corrosion and pitting as well. The type of inhibitor suitable for this purpose depends on the nature of the surface film or deposit. The inhibitors should be able to either penetrate the pores of 'insoluble' deposits and reach the surface of the metal, or enhance the protective properties of 'soluble' deposits. Thus, the ability of the inhibitor to perform is determined by the degree to which the dimensions of the molecules correspond with the dimensions of the pores in the film. The correspondence between the three-dimensional structure of the inhibitor and the structure of the crystalline deposit is the most important factor in determining the effectiveness of the inhibitor.

In the case of unstable deposits that grow rapidly in media of pH > 7, the useful inhibitors are those that bond with cations such as (Ca^{2+}, Fe^{2+}) or help break up the crystal. The pH in carbonic acid media can be controlled by using organic bases and their salts such as dimethylamine, ethylenediamine, methoxypropylamine, morpholine, and sodium salt of mercaptobenzothiazole (NaMBT). These additives regulate and maintain the pH of 9, which helps the formation of HCO_3^- and CO_3^{2-} ions leading to the formation of protective carbonate films.[38,39] The basicity constant (K_B) defines the neutralizing ability and the coefficient of distribution of the amine in the liquid and gas phases, $K_d = C_g / C_w$, where C_g and C_w are the concentrations of the amine in the gas and aqueous phases, respectively.

Morpholine, cyclohexylamine, and sodium salt of 2-mercaptobenzothiazole are anodic inhibitors. Amines form organic cations and displace water from the metal surface. Adsorption of amine cations decreases the reactivity of the system and the current needed to passivate the surface.[40]

A method to predict corrosion when a series of organic amines are used has been proposed.[41] It was found that corrosion of carbon steel could be stimulated by adding small amounts of bases such as monoethanolamine, cyclohexamine, and diallylamine to a 0.5% solution of NaCl containing 250 mg/L acetic acid saturated with CO_2 (0.1 MPa). The protective effect was observed when the concentration of the amines was low (32–48 g/L). The protective effect due to the amines is due to an increase in carbonate ion concentration.

The use of neutralizing amines to protect the metal equipment in oil and gas fields from CO_2 corrosion is successful in the early stages, since the metal surface is covered with siderite only, which prevents further damage. It is useful to note that it is difficult to obtain protective carbonate-oxide films on oilfield equipment by means of neutralizing amines. This is particularly the case when flooding is used, due to the instability of stratal water.

Table 6.1 Characteristics of oil fields

Characteristics of the field	Field 1	Field 2
Total length, oil-collecting	5	–
Pressurized	15	55
Length of reservoirs replaced		
Oil-collecting	–	15 (21%)
Pressurized	150 (19%)	40 (18%)
Oil output 10^6 (tons/yr)	4	0.8
Water contamination (%)	92–99	70
Flow velocity (m/s)	0.3–0.5	0.5–1.0
Temperature (°C)	30–60	20–10
Mineralization (g/L)	250–260	125
Content (mg/L)		
CO_2	0–200	200
H_2S	Traces	Traces

Table 6.2 Data on inhibition of oil reservoirs

Field (system)	Inhibitor dosage	Corrosion rate, mm/y		Accidents per year
		General	Pitting	
Oil-collecting reservoirs	None	0.13/0.17–0.78	1.19–2.7	1200 (weekly)
	Koreksit 7798 100 g/ton (4h) 15–35 g/ton	<0.04/0.01	0.12–0.2	None
	None	0.5 – 1.0/ 0.5–1.0	0–0.15	75
	Koreksit 6350 100 g/ton (1 day) 25–30 g/ton	<0.01/0.5	<0.01	None
Pressurized reservoirs	Koreksit 6350 100 g/ton (1 day) 25–30 g/ton	<0.01/0.01	<0.01	None

The neutralization method is not useful in old equipment, since it is already covered with a layer of deposited corrosion products.

Inhibitors that function by a cathodic mechanism may be used in CO_2-induced corrosion. The inhibitors can be used either on a clean surface or on a surface covered by carbonate-oxide film or a layer of deposits. In some cases, corrosion inhibitors give better protection on samples covered with corrosion products than clean metal samples. This observation is in keeping with the operation of the interphase inhibition mechanism with corroded samples and the interface inhibition mechanism with clean metal samples.

Table 6.3 Data on inhibition of ruptures of oil pipelines

Inhibitor	Concentration g/m^3	Test time months	Number of ruptures	Percent protection	
No inhibitor	0	7	22	–	–
RA – 23 D	25–30	12	15	90	89
KRTs–3	100 (1 day) 25 (perm)	6	0	85	83
KRTs–3G	100 (1 day) 25 (perm)	6	0	89	87
Koreksit 7798	25	–	–	68	67
	50	–	–	80	73
	100 (permanent)	5	14	63	61
Neftekhim-3	50	–	–	53	52
	100 (permanent)	5	12	81	79
SNPKh-6302	50	–	–	67	68
	100 (permanent)	5	9	82	81

Two inhibitors, Koreksit 7798 and Koreksit 6350 manufactured by US company Naklo-Edson, were tested in two oilfields in western Siberia. These inhibitors can be regarded to be of the second type. The characteristics of the field are given in Table 6.1. The effectiveness of the two inhibitors in field conditions is given in Tables 6.2 and 6.3. The conditions in the fields are as follows: CO_2: 200 mg/L, H_2S: trace, temperature: 20–70°C, pH: 6–7. The pitting rate was 2.7 mm/y and an average of 1.19 mm/y. The cost of replacing the damaged pipelines in the two fields was 16 million dollars, while the cost of inhibitors was 4.9 million dollars.

6.4 Criteria used in the selection of inhibitors in sour media

The corrosion problem in oil pipelines containing hydrogen sulfide is very serious.[42] The corrosive attacks in oil wells consist of electrochemical, sulfide stress corrosion cracking, erosion corrosion, hydrogen embrittlement, blistering, microbiological corrosion, and galvanic and electrolytic corrosion. Hydrogen sulfide causes pronounced increase in the corrosion rate; for example, the corrosion rate of mild steel increased from 10 mpy in synthetic oil fluid to 60 mpy as the hydrogen sulfide content increased from 0% to 100%.

To understand the corrosion problems in oil pipelines, it is necessary to identify the various corrosive species present in the medium containing hydrogen sulfide as a function of pH (Table 6.4). The data given in Table 6.4 were obtained based on the two dissociation constants K_1 and K_2 being 8.9×10^{-4} and 1.3×10^{-13}. At a pH of 4, molecular hydrogen sulfide

Table 6.4 Concentration of various species of hydrogen sulfide as a function of pH

pH	4	5	6	7	7.5	8	8.5	9	10
C_{H_2S} (%)	99.9	98.9	91.8	52.9	26	10.1	3.4	1.1	0.1
C_{HS^-} (%)	0.1	1.1	8.2	47.1	74	89.9	96.6	98.9	99.9
C_s = (%)			–	–	–	–	–	0.01	0.1

is present, and at pH 6.0 bisulfide concentration reaches 8.2%, reaching 47% at pH 7.

In many gas deposits, H_2S is 5 to 10 mass percent, with the concentration in water condensate of 250–500 ppm. In addition to H_2S, sour gas contains CO_2, which is the agent responsible for low pH. Iron sulfides have been identified in the corrosion products at different concentrations of hydrogen sulfide:

$$Fe + H_2S \rightarrow FeS + 2H^+ + 2e^- \qquad [6.4]$$

This reaction scheme is a simpler presentation of the various complex steps involved in the actual mechanism.

Many mechanisms for hydrogen sulfide corrosion have been advanced in the literature.[43–47] The most usual mechanism of the accelerating effect of hydrogen sulfide involves the formation of a molecular surface complex, $Fe\left(H-S-H\right)_{ads}$, which on cathodic polarization yields hydrogen atoms. Some of the hydrogen atoms may recombine, while others diffuse into the metal:

$$Fe + HS^- \rightarrow Fe\left(HS^-\right)_{ads} \qquad [6.5]$$

$$Fe\left(HS^-\right)_{ads} + H_3O^+ \rightarrow Fe\left(H-S-H\right)_{ads} + H_{ads} \qquad [6.6]$$

$$Fe\left(H-S-H\right)_{ads} + e- \rightarrow Fe\left(HS^-\right)_{ads} + H_{ads} \qquad [6.7]$$

Corrosion inhibitors used in the past to combat corrosion in sour wells included aldehydes, cyanamides, thiourea, and urea derivatives.[48] The most commonly used inhibitors are organic amines. While organic amines are less effective inhibitors in acid media, inhibition by amines in the presence of hydrogen sulfide is greatly enhanced.[49]

The experimental data obtained[49] show a synergistic effect in the presence of hydrogen sulfide. Normally, hydrogen sulfide promotes corrosion and hydrogen embrittlement, but hydrogen sulfide has been found to increase the corrosion inhibition efficiency of organic amines. The synergistic effect observed in the presence of hydrogen sulfide has been attributed to bisulfide anions (SH^-) adsorbed on iron acting as anion bridges facilitating the adsorption of a cation-type inhibitor:

$$R{-}NH_2 + H^+ \rightarrow RNH_3^+ \qquad [6.8]$$

$$Fe{-}SH^- + RNH_3^+ \rightarrow Fe\,HS{-}H_3N^+{-}R \qquad [6.9]$$

The surface compound Fe(HS–R) is unable to supply protons for the cathodic process, and also impedes the anodic metal ionization reaction.

6.4.1 Surface analysis of sulfide films

Rozenfeld *et al*.[50] studied the nature of films formed on Armco iron in 0.5% NaCl, 250 ppm of acetic acid saturated with hydrogen sulfide by electron diffraction, Auger electron spectroscopy, X-ray photoelectron spectroscopy (XPS), and secondary ion mass spectroscopy (ion microscopy). Auger spectral data showed the presence of a protective layer 300 Å thick consisting of Fe, S, C, and O. The following observations were made in the XPS spectra. The Fe 2 $P_{3/2}$ peak shifted to lower binding energy, indicating a reduced charge on the Fe atom. The unresolved doublet peak of N_{1s} showed two types of nitrogen: (i) Fe–N and (ii) C=N. The peak due to N_{1s} shifted to a higher energy, showing the donation of the one pair of electrons on nitrogen to iron. The peak due to 2 P of sulfur showed the presence of SH^- groups. Electron diffraction data showed the presence of Fe–S (mackinawite) on the iron metal. Ion microscopy gave peaks due to 15 (NH^+), 70 (FeN^+) 43($COHN^-$), 14 (N^+), 27 (CNH^+), and 71 ($FeNH^+$).

6.4.2 Criteria for selection of inhibitors

The most obvious first step in the selection of inhibitors for a solution to a particular corrosion problem is a literature search for reports on the use of inhibitors on identical or similar systems, followed by experimentation to obtain the optimum conditions for using inhibitors in the systems on hand. The mechanism of the corrosion inhibition process is also useful in the selection of inhibitors to solve practical corrosion problems. Basic information on the mechanism of corrosion inhibition can be

obtained by corrosion potential measurement, polarization techniques, radiotracer techniques, modern surface analytical techniques such as XPS, Auger electron spectroscopy, secondary ion mass spectrometry, etc. Electrochemical techniques, along with surface analysis techniques, provide basic information on the mechanism of the corrosion inhibition process on hand.

Evaluation of the effects of inhibitors on current output, effects on anodic and cathodic polarization characteristics of metals, and suppression of polarographic maxima are useful in screening inhibitors for various applications. Some of the important criteria in the selection of inhibitors, such as hydrophobicity, electron density on the donor atom of the inhibitor molecule, and the effect of substituents in the inhibitor molecule, are discussed in the following sections.

6.4.3 Hydrophobicity of inhibitors

Three classes of inhibitors have been studied:

- imidazolines
- imidazoles
- fatty amines.

They were studied[51] in a deaerated medium containing 5 g/L of ammonium chloride saturated with hydrogen sulfide at a pH of 4.0. In the case of some imidazoline derivatives and aliphatic fatty amines, corrosion inhibition efficiency increased with increase in concentration of the inhibitor, finally reaching a plateau. In the case of some substituted imidazole derivatives, the inhibition efficiency increased very slightly at first, followed by a significant increase and then reached a plateau, with increasing concentration of the inhibitor. The concentration at which a break in slope was observed agreed well with the critical aggregation concentration of the inhibitor. Inhibition by imidazoline derivatives increased at 35°C compared with room temperature, and the temperature of 35°C corresponds to the Kraft temperature at which association of the inhibitor molecules takes place. In the case of substituted imidazolines, the inhibition efficiency increases with an increase in the number of carbon atoms present in the hydrophobic chain and decreases beyond 10–14 carbon atoms in the chain.

These observations show that there is a relationship between the formation of aggregates in solution and changes in the inhibition efficiency of the compound studied. This can be attributed to structural changes in the adsorption layer. Using polarographic techniques, the effect of micellization on the structure of the electrical double layer and the adsorption potential of micelles has been documented.

The Hansch model was used[51,52] to provide a quantitative basis for the correlation of corrosion inhibition efficiencies with the hydrophobicity parameter. This is based on the assumption that the behavior of the corrosion inhibitor is similar to the behavior of a drug molecule with respect to the receptors of the host organism. The inhibition efficiency (log l/c) of the substituted amines $[CH_3-(CH_2)_nNH_2]$ was calculated using the equation:

$$\log\ (1/c) = a.f^2 + bf + c \qquad [6.10]$$

where 'f' is the hydrophobicity factor for amines with n ranging from 7 to 17.

The data obtained show that the progressive increase in corrosion inhibition efficiency parallels the increase in hydrophobicity of the substituted amines up to an 'n' value of 14, and the corrosion inhibition efficiency does not bear any relationship to the basicity of the amine. The inhibition efficiency and the hydrophobicity factor increase progressively, paralleling the decrease in critical micelle concentration. Similar analysis for imidazoline derivatives used the equations:

$$\text{Log } i_{\text{corr}} = af^2 + bf + c \qquad [6.11]$$

$$\text{Log } i_{\text{corr}} = af^2 + bf + c \log|p| + d \qquad [6.12]$$

This analysis generated useful data. The data[51,52] show that the corrosion currents vary with varying values of the hydrophobicity factor. It is also shown that the equation involving both hydrophobicity (f) and polarity (p) parameters gives a better agreement than when hydrophobicity alone is taken into account. Corrosion inhibition efficiency increases to a maximum for a hydrophobic chain containing 10–14 carbon atoms, and then decreases when the number of carbon atoms increases beyond 14. This indicates that the transport of the active substance to the receptor plays an important role in micellization.

These relationships involve a modification in the electrical double layer for concentrations in the vicinity of critical micelle concentrations. The results for imidazoline derivatives show better correlation at concentrations close to critical micelle concentrations than at concentrations further removed from critical micelle concentrations. This approach is promising, from both the theoretical and practical points of view, since it opens up the possibility of rationally selecting an inhibitor and the importance of a knowledge of Kraft temperature and critical concentrations of the inhibitor compounds being used.

6.4.4 Effect of inhibitor structure on corrosion inhibition

Corrosion inhibition by a variety of substituted pyridine compounds was studied[52] in a medium of pH 4.5 containing 3000 ppm of hydrogen sulfide at an inhibitor concentration of 5×10^{-3} M. The data were interpreted on the basis of the Hammett equation:

$$\log\left(\frac{k_x}{k_a}\right) = \rho\sigma \qquad [6.13]$$

where k_x and k_a are equilibrium constants for the substituted chemical compound and parent molecule respectively, ρ is a constant that depends upon the nature of the reaction being studied, and σ is a constant that depends upon the electronic nature of the substituent, and this has been obtained both by calculation and empirically.

All the substituted pyridines affected the corrosion rates. The corrosion inhibition efficiency with compounds containing electron-donating substituents was found to be higher than with those containing electronic-withdrawing substituents. For pyridines substituted in the 3 and 4 positions, plots of logarithm of corrosion protection coefficient (γ) vs σ_R substituent constant and the basicity (pKa) of the amine gave pairs of straight lines intersecting at a point corresponding to unsubstituted pyridine. When the electron density at the nitrogen atom is increased ($\sigma_R < 0$), the protection increases sharply, and when electron withdrawing substituents are present ($\sigma_R > 0$), the protection increases very slightly.

The σ values are indicative of the electron-donating and withdrawing abilities of the substituents in the organic molecules and, with the advent of fast computers, these are giving way to energy of the highest occupied molecular orbital (E_{HOMO}) and energy of the lowest unoccupied molecular orbital (E_{LUMO}) calculated by quantum chemical methods.

Hansch[53] put forward a quantitative structure–activity relationship (QSAR) taking into account the solubility/dispersion term for correlating biological activity with chemical structure. Based on Hansch's ideas, Growcock *et al*.[54,55] used a chemisorption model for the corrosion inhibition of steel in HCl by cinnamaldehyde derivatives and advanced the following expression:

$$\text{Log } R = a_0 + a_1 E_{(\text{LUMO or HOMO})} + a_2 \log p \qquad [6.14]$$

where R represents the degree of inhibition, a_0, a_1 and a_2 are best-fit constants, E is the energy of the lowest unoccupied orbital or highest occupied

molecular orbital, and p is the solubility/dispersibility term that is related to the ratio of partition coefficients of the substituted and unsubstituted organic inhibitor.

It was observed that no single QSAR was adequate in rationalizing the experimental data obtained on the substituted cinnamaldehyde inhibitors, and this was attributed to the different modes of chemisorption – non-planarity of some substituted compounds, and the necessity for optimizing the geometry of the inhibitor.

The QSAR used in the literature shows that the effectiveness of corrosion inhibitors depends upon factors such as the electron density of the donor atom in the inhibitor molecules, molecular geometry and the size of the inhibitor molecule and the solubility/dispersibility of the inhibitor. With the advent of modern surface analytical techniques, such as X-ray photoelectron spectroscopy, which is capable of giving experimental data on the ionization energies of the donor atoms in organic inhibitor molecules and also other orbital energies, use of these data in making some correlations on the performance of inhibitors appears promising. More recently[56] the percent inhibition by aliphatic amines was correlated with the calculated and experimentally obtained ionization energies of the electrons on the nitrogen atom, as well as the correlation of σ values with corrosion rates of some methyl pyridines.

6.4.5 Extended Hückel theoretical (EHT) calculations

EHT calculations were performed on some aliphatic amines, and the data generated on the charge on the nitrogen atom along with E_{HOMO} and E_{LUMO} are tabulated in Table 6.5. The charge on the nitrogen atom, E_{HOMO} and E_{LUMO} are plotted against the percent inhibition in Figs 6.1–6.2 respectively. It is evident that the percent inhibition increases with an increase in the charge on the nitrogen atom, and also with decreasing values of E_{HOMO} and E_{LUMO}. It is interesting to note that an increase in charge of the nitrogen atom by 0.015 resulted in an increase in inhibition of 10%. ΔE_{HOMO} and ΔE_{LUMO} values of 0.52 and 0.42 eV respectively resulted in an increase

Table 6.5 EHT data on aliphatic amines

Inhibitor	Z_n	E_{HOMO}	E_{LUMO}
Methylamine	–0.6841	–13.2771	0.6224
Ethylamine	–0.6954	–12.9107	0.3807
Propylamine	–0.6986	–12.7735	0.1456
Isopropylamine	–0.7042	–12.8110	0.1645
Butylamine	–0.6989	–12.6510	0.0938

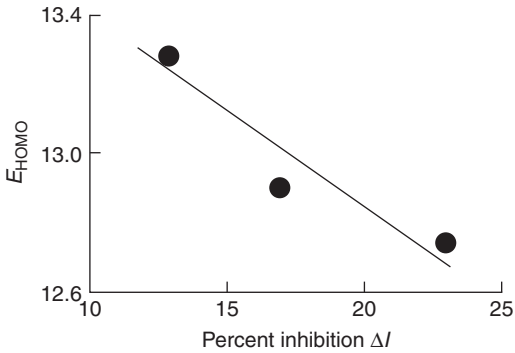

6.1 Plot of E_{HOMO} vs percent inhibition for aliphatic amines.

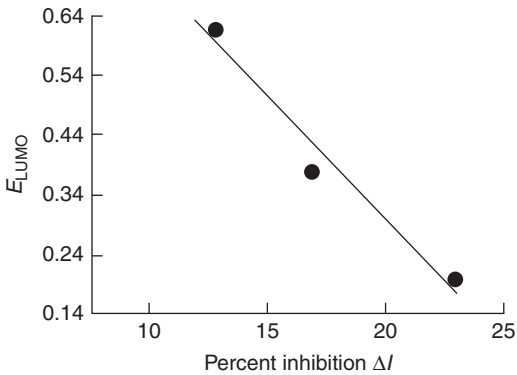

6.2 Plot of E_{LUMO} vs percent inhibition for aliphatic amines.

Table 6.6 EHT data on substituted pyridines

Inhibitor	Z_n	E_{HOMO}	E_{LUMO}	Corrosion rate	σ
Pyridine	−0.777	−9.206	−12.554	0.388	0
2-Methyl	−0.805	−9.151	−12.444	0.304	−0.17
3-Methyl	−0.777	−9.191	−12.497	0.308	−0.069
4-Methyl	−0.794	−9.084	−12.389	0.216	−0.17
3,5 Dimethyl	−0.777	−9.183	−12.441	0.278	−0.14
2,4 Dimethyl	−0.821	−9.031	−12.285	0.171	−0.34
2,5 Dimethyl	−0.806	−9.148	12.378	0.194	−0.24
2,6 Dimethyl	−0.832	−9.073	−12.364	0.250	−0.34
2,4.6Trimethyl	−0.846	−8.949	−12.203	0.210	−0.51
2- Amino	−0.826	−9.116	−12.545	0.139	−0.66
2-Hydroxy	−0.835	−9.058	−12.492	0.444	−0.37

of 10% inhibition. This shows that suitable substituents in the inhibitor molecules can produce a pronounced increase in the degree of corrosion inhibition, and this result is significant in designing inhibitor molecules for corrosion inhibition.

The data obtained from EHT calculations on substituted pyridine derivatives along with the corrosion rates are presented in Table 6.6. In Figs 6.3 and 6.4, the corrosion rates are plotted against E_{HOMO} and E_{LUMO}. Considering the simplifications made in EHT calculations, the correlations are good. A difference of 0.21 eV in E_{HOMO} and E_{LUMO} results in reduction in corrosion rate of 0.208. The corrosion rate with pyridine as inhibitor was 0.388, which dropped to 0.170 in the case of 2.4 dimethyl pyridine as the inhibitor. The

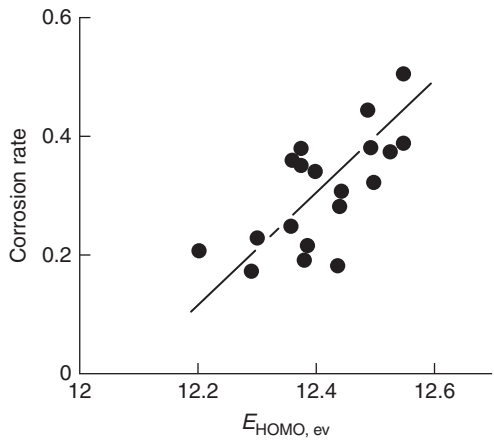

6.3 Plot of E_{HOMO} vs corrosion rates of pyridine derivatives.

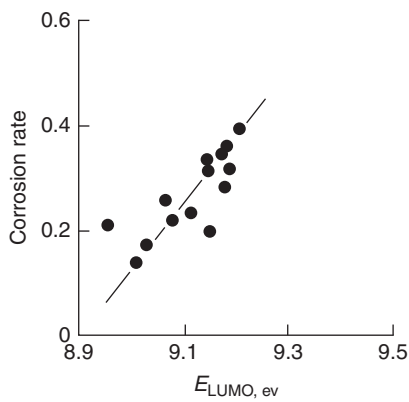

6.4 Plot of E_{LUMO} vs corrosion rates of pyridine derivatives.

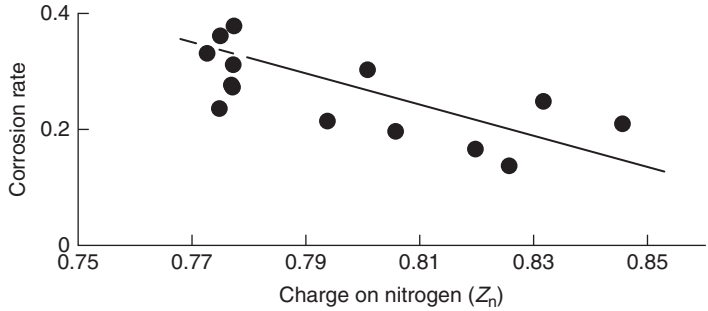

6.5 Plot of Z_n vs corrosion rates of pyridine derivatives.

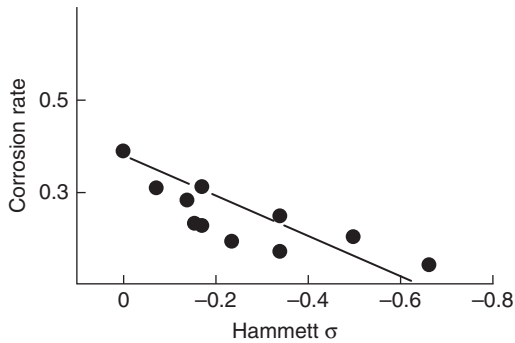

6.6 Plot of σ vs corrosion rates of pyridine derivatives.

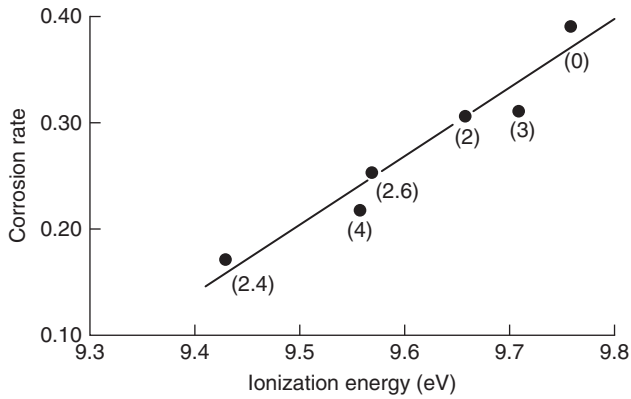

6.7 Plot of ionization energy vs corrosion rates for pyridine derivatives.

calculated charge on the nitrogen atom in the pyridine derivatives is plotted against the corrosion rate in Fig. 6.5. This correlation shows a decrease in corrosion rate with increase in the electron density of the donor nitrogen

atom. An increase in charge of 0.044 resulted in a decrease of corrosion rate of 0.388–0.171. Figure 6.6 shows a plot of corrosion rate as a function of Hammett σ values. The corrosion rate decreases as the negative value of σ increases.

The experimentally obtained ionization potential data for methyl substituted pyridines are plotted against the corrosion rates (Fig. 6.7). It is clear that suitable substituents in the inhibitor molecule can result in a pronounced decrease in corrosion rate. A decrease in ionization potential from 9.76 to 9.43 eV resulted in a decrease in corrosion rate from 0.388 to 0.170. Thus it is clear that by proper choice of substituted inhibitor molecules, corrosion inhibition of the order of 90–100% can be achieved.

6.5 Mechanisms of corrosion inhibition

Corrosion inhibition by inhibitors can be classified into three types of mechanisms, namely

- interface inhibition
- interphase inhibition
- intraphase inhibition.

Interface inhibition involves a direct bond between the metal (M) and the functional group in the inhibitor (I):

$$M + I \rightarrow M - I \qquad [6.15]$$

Interphase inhibition involves the oxides of the corroding metal and the inhibitor moiety such as the inhibition of corrosion of iron by chromate:

$$Fe^0 \rightarrow Fe_2O_3 \qquad [6.16]$$

$$CrO_4^{2-} \rightarrow Cr_2O_3 \qquad [6.17]$$

$$Fe_2O_3 + Cr_2O_3 \rightarrow Fe_2O_3 \cdot Cr_2O_3 \qquad [6.18]$$

Intraphase inhibition involves the repair of iron oxide passive film by inhibitors such as sodium molybdate in the form of a monolayer of molybdenum, as contrasted with several monolayers of chromium oxide transferred from the inhibitor to the metal in interphase inhibition. It is also thought that molybdenum takes part in the repair of defects in the iron oxide film.

6.5.1 Structure–activity relationships

The Hammett equation may be written as:

$$\text{Log } I / I_o = \rho\sigma \qquad [6.19]$$

where I is the percent inhibition with the substituted inhibitor, I_o is the percent inhibition with the parent unsubstituted inhibitor, σ is the Hammett parameter, and ρ is a constant characteristic of the system.

The data on percent corrosion inhibition obtained by using both parent inhibitor (I_o) and substituted inhibitor (I) and the fraction of charge, $\Delta\Delta$N due to the substituent (the fraction of charge of the substituent inhibitor, minus the fraction of charge of the unsubstituted parent inhibitor), have been found to obey a Sastri equation of the type:

$$\text{Log}\frac{I}{I_o} = K\,\Delta\Delta N \qquad [6.20]$$

where K is the Sastri constant similar to the Hammett constant, ρ. It is to be expected that σ and $\Delta\Delta N$ are related to each other, in that both signify the electronic effects due to the substituent in the parent inhibitor molecule.

The analysis of the data on corrosion inhibition of iron by substituted pyridines in HCl, H_2SO_4 and H_2S media resulted in the data given in Table 6.7. The data obtained by analysis through the equations show the following trends in corrosion inhibition of iron with methyl substituted pyridines. In general, the values of the Hammett constant for meta-derivatives are greater than ortho-derivatives. The Hammett constant shows a decreasing trend with increase in inhibitor concentration. The trends in the variation of the Sastri constant (K) parallel the trends in the variation of the Hammett constant, which is to be expected since both equations involve the electronic charge on the donor atom of the inhibitor molecule. The following trends in the data have been observed:

- $\rho_{H_2SO_4} > \rho_{HCl} > \rho_{H_2S}$ for both meta and ortho-substituted inhibitors
- $\rho_m > P_0$ in HCl, H_2SO_4, H_2S
- ρ (1%, 2% inhibitor > ρ (3% inhibitor) in H_2SO_4
- $K_{H_2SO_4} > K_{HCl} > K_{H_2S}$ for both meta- and ortho-substituted inhibitors
- $K_m > K_0$ in HCl, H_2SO_4 and H_2S solutions
- K (1%) > K (2%) > K (3%) inhibitor.

The trends noted above for ρ and K are similar since Hammett's parameter σ and the Sastri parameter $\Delta\Delta N$ are related and signify the electronic

Table 6.7 Corrosion inhibition and Hammett and proposed Sastri parameters

System	Hammett constant, ρ	Sastri constant, K	Value of ratio $\Delta\Delta N/\sigma$
Iron-methyl pyridines			
HCl medium			
meta-derivatives	0.622	10.01	0.0620
ortho-derivatives	0.357	8.05	0.0397
H_2SO_4 medium			
meta-derivatives			
1% v/v inhibitor	1.34	18.75	
2% v/v inhibitor	1.29	18.07	0.0714
3% v/v inhibitor	0.408	5.71	
pH4.5 3000 mg/L H_2S			
meta-derivatives	0.423	6.27	0.066
ortho-derivatives	0.179	4.74	0.038
Iron-aniline			
HCl medium			
Para derivatives	0.681	24.8 (13.6)	0.0299 (0.0385)
Iron-benzimidazole			
Ortho-derivatives			
10^{-4} M inhibitor		24.5 (34.3, 14.6)	
10^{-3} M inhibitor		10.06 (13.9, 6.4)	
10^{-2} M inhibitor		3.25 (4.06, 2.43)	

density transmitted by the substituent in the inhibitor molecule to the metal. The adsorption of chloride on an iron electrode occurs more readily than does sulfate. The potentials of adsorption at zero point charge for chloride and sulfate are –461 and –438 mV respectively. Using radioactive isotopes, a greater extent of adsorption of chloride than bisulfate has been noted.[57] Thus, in the solution, displacement of chloride adsorbed on iron by the inhibitor is more difficult to accomplish than of bisulfate, and hence inhibition in H_2SO_4 solution is greater than in HCl solution. This difference in adsorption of chloride and bisulfate on a Pt electrode has been established.[57] The inhibition in H_2S solution involves the operation of a dual mechanism, namely by pyridines assisted by bisulfide in a synergistic pathway.

The ρ and K values for meta-substituted inhibitors are greater than for ortho-substituted derivatives, due to the electronic charge transfer, the ρ and K values at lower inhibitor concentrations being greater than at higher inhibitor concentrations. This dependence on the inhibitor concentration indicates that the electronic charge effects are more significant at lower inhibitor concentrations, which correspond to lower coverage of the metal surface by the inhibitor.

The para-substituted anilines give a ρ value of 0.68 and K value of 24.8 for the methyl and bromo derivatives. The lower value of 13.6 given in brackets for K corresponds to thiocyanatoaniline. In this case, it is possible to have interaction

of thiocyanate-iron and iron-aniline interaction. The two adsorption modes are Fe–NH_2 and Fe–NCS which result in the lower *K* value of 13.6.

The *K* values of iron-substituted benzimidazoles decrease progressively when the inhibitor concentration increases from 10^{-4} to 10^{-2} M, indicating that the electronic effects due to the substituents are significant at lower concentrations of the inhibitor. The values of *K* given in parentheses in Table 6.7 refer to 2-hydroxyl and 2-amino benzimidazole derivatives. In the case of 2-aminobenzimidazoles, a second interaction, namely Fe–NH_2, in addition to primary Fe–benzimidazole nitrogen, might be responsible for the observed degree of inhibition.

Considering the iron-inhibitor system, the data show the following trends:

$$\rho_{\text{aniline}} \geq \rho_{\text{pyridine}}$$

$$K_{\text{aniline}} \approx K_{\text{benzimidazoles}} > K_{\text{Pyridine}}$$

High values of *K* indicate that the corrosion is sensitive to the substituents in the inhibitor molecule. Lower *K* values indicate:

- lower sensitivity to the substituents
- operation of an inhibition mechanism other than the direct interaction of the metal and inhibitor, such as the synergistic mechanism in the inhibition iron corrosion by pyridines in H_2S medium through Fe–SH or Fe–NS interaction in the case of the iron–aniline system.

The variation of *K* values with inhibitor concentration indicates the variation of the extent of coverage of the metal by the inhibitor, and the substituent effects are prominent at lower concentrations of the inhibitor.

The main advantage of the proposed Sastri equation is its predictive capability for the selection of inhibitors, for example in predicting that the introduction of mercapto group (SH) in aniline or pyridine or benzimidazole inhibitors could produce a considerable increase in the corrosion inhibition of iron.[58]

The effect of substituents in the parent organic inhibitor molecules has been correlated with changes in electron densities in the bonding functional groups as noted below:

- substituted pyridines[59–62]
- substituted anilines[60,63]
- substituted aliphatic amines[63]
- amino acids[65]

- benzoic acids[66]
- aliphatic sulfides[67]
- the electron density at the bonding functional groups in the inhibitor molecules was ascertained from Hammett and Taft constants,[62,66] nuclear magnetic resonance data[60] and quantum chemical calculations.[68]

Quantum chemical calculations give data on:

- E_{HOMO} and the lowest unoccupied molecular orbital (E_{LUMO})
- the fraction of electronic charge on the donor atom of the inhibitor (ΔN)
- the heat of reaction between the metal and the inhibitor (ΔH)
- the degree of softness of the inhibitor (i.e., $E_{HOMO} - E_{LUMO}$).

Pearson enunciated the HSAB principle. In accordance with the principle, hard acids form complexes with hard bases, and soft acids form complexes with soft bases. The probable mechanism of corrosion of iron in a hydrogen sulfide medium involves the formation of a surface complex $Fe(-HSH)_{ad}$ and bonding to the nitrogen atom of the inhibitor such as pyridine (Fe–HSH–pyridine)

Inhibitors can be classified according to Sastri's proposed scheme as: (i) hard inhibitors, such as fluoride phosphate and carbonate; (ii) soft inhibitors such as RSH, RS, and R_3P; and (iii) borderline inhibitors, such as aniline and pyridine (see Table 6.8).

Molecular orbital theoretical calculations of corrosion inhibitors such as ethyl pyridines used in hydrogen sulfide media enabled correlation of corrosion rates with the fraction of electronic charge transferred from the inhibitor to the metal as shown in Fig. 6.8. The corrosion inhibition by aliphatic amines is thought to involve the equilibria:

$$RNH_3^+ (sol) \rightleftharpoons RNH_2 + H^+ \rightleftharpoons RNH_2 - Fe^0 \qquad [6.21]$$

where $R–NH_2–Fe^0$ is chemisorbed amine. The degree of chemisorption depends on the strength of the metal–amine bond. The relative order of effectiveness of aliphatic amines is:

Table 6.8 Inhibitors classified according to Sastri's proposed scheme

Hard inhibitor	Soft inhibitor	Borderline inhibitor
F^-, PO_4^{3-}, CO_3^{2-}	RSH, RS, R_3P	$C_6H_5NH_2$, C_5H_5N
Hard acids	Soft acids	Borderline acids
Fe^{3+}, Cr^{3+}, Al^{3+}	Cu+, M^0 (metal atoms) Bulk metals	Fe^{2+}, Ni^{2+}, Cu^{2+}, Zn^{2+}

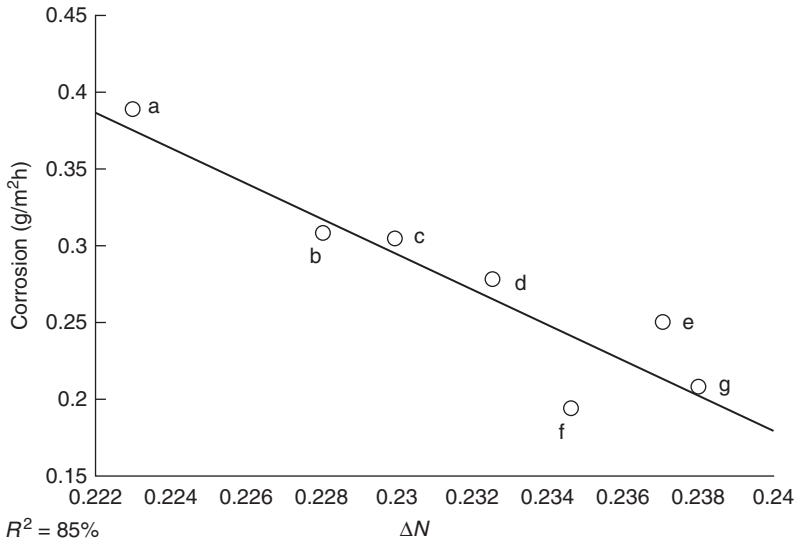

6.8 Correlation of ΔN with corrosion rates of pyridine derivatives: (a) pyridine; (b) 3-methyl pyridine; (c) 2-methyl pyridine; (d) 3,5-dimethyl pyridine; (e) 2,6-dimethyl pyridine; (f) 2,5-dimethyl pyridine; (g) 2,4,6-trimethyl pyridine.

$$R_2NH > R_3N > RNH_2$$

where R is a methyl group, and

$$R_3N > R_2NH > RNH_2$$

where R is an ethyl, propyl, butyl, or amyl group.

Aliphatic amines are better inhibitors than aromatic amines. Heterocyclic amines, such as pyridine, are better inhibitors than aromatic amines, such as aniline, but less effective than the corresponding saturated amines. The following is the order of effectiveness of inhibitors:

Cyclohexylamine > pyridine > aniline

Piperidine > pyridine

Dicyclohexylamine > diphenylamine

The introduction of a methyl group in aniline results in an increase in the degree of corrosion, due to the hyperconjugation of the methyl group. The degree of inhibition of toluidines is in the order:

o-toluidine > p-toluidine > m-toluidine > aniline

Sulfur-containing inhibitors are better than nitrogen-containing inhibitors because of the greater polarizability of the sulfur atom over the nitrogen atom. Sulfur is less electronegative than nitrogen (2.5 compared to 3.0) and has two lone pairs of electrons for bonding compared with one pair of electrons in nitrogen.

The order of effectiveness of mercaptans as inhibitors is:

amyl > butyl > propyl > ethyl > methyl

and of sulfides is:

butyl > propyl > ethyl > methyl

Aromatic sulfides are less effective than aliphatic sulfides. For example, thiophenol is less effective than ethyl mercaptans. Thiocresols are better inhibitors than thiophenol.

Alcohols and phenols are poor inhibitors since they contain more electronegative oxygen, which does not form a coordinate bond readily. Based on the same reasoning, selenium compounds are expected to be good inhibitors, and ethyl selenide is found to be a good inhibitor. The corrosion inhibition by aldehydes is in the order:

butyraldehyde < acetaldehyde < propionaldehyde < formaldehyde

The introduction of a double bond in a compound appears to increase the extent of corrosion inhibition. An example is the inhibition effect of allyl alcohol as compared to ethyl alcohol. Another example of the effect of the double bond is the inhibitive effect of allyl thiourea in comparison to thiourea. Crotonaldehyde has been found to be a better inhibitor than butyraldehyde. Thioureas are better inhibitors than urea, and thiocyanates are better than cyanates.

6.5.2 Inhibitor field theory of corrosion inhibition

The inhibitor field theory of corrosion propounded by Sastri *et al*.[69,70] may be described as follows: corrosion inhibition of metals involves the transport of the inhibitor to the metal surface, followed by the adsorption of the inhibitor on the surface of the metal. The adsorbed inhibitor on the metal surface may be viewed as a coordination complex. The metal–inhibitor complex may be hexacoordinated with one metal–inhibitor bond and five metal–water bonds of quasi-distorted octahedral geometry, the whole complex occupying a lattice site of the metal surface as shown in Fig. 6.9. Alternatively, the metals resulting from the initial stages of corrosion may interact with the inhibitor and form a monoinhibitor penta-aquo metal complex layer in the Helmholtz double layer near the metal, leading to corrosion inhibition as shown in Fig. 6.10. In the metal–inhibitor complex, the metal can be any transition metal, such as iron, copper, and titanium (known as transition metals), in which the *d*-orbitals are populated with electrons. The ions Ti^{3+}, Fe^{2+}, and Cu^{2+} have d^1, d^6, and d^9 electron configurations respectively. In other words, Ti^{3+}, Fe^{2+}, and Cu^{2+} have 1, 6, and 9 electrons in the '*d*' orbitals. The inhibitor group that is bonded to the metal is also known as a ligand.

According to the inhibitor field theory propounded by Sastri *et al*.[70] the metal–inhibitor complex can be considered as an aggregate of metal and

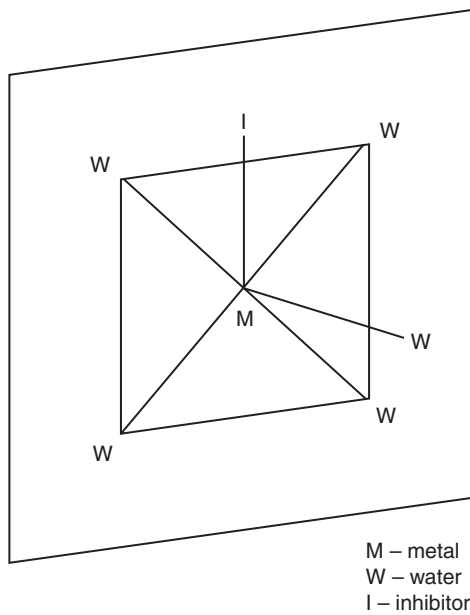

6.9 Disposition of monoinhibitor penta-aquo-distorted metal complex adsorbed on the metal surface.

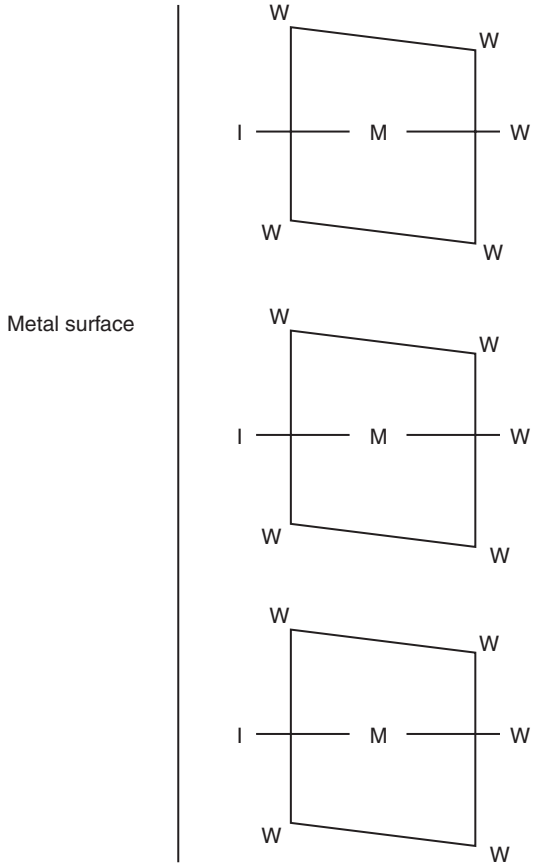

6.10 Disposition of monoinhibitor penta-aquo metal complex in Helmholtz double layer near the metal surface.

inhibitor molecules held together by electrostatic forces. In the case of the Ti^{3+} ion, it is surrounded by ligands/inhibitors containing lone pairs of electrons available for donation to the metal.

The model then assumes that the effects of metal–inhibitor complex formation on the transition metal ion in the electrostatic field of inhibitor molecules situated at the corners of a regular octahedron are as shown in Fig. 6.11. The angular dependence of the wave functions of the '*d*' electrons d_{xy}, d_{yz}, d_{zx}, $d_{x^2-y^2}$, and d_{z^2} are shown in Fig. 6.12. A glance at Fig. 6.11 shows that an inhibitor with negative charge will be repelled by the electrons in $d_{x^2-y^2}$, and d_{z^2} orbitals more than an electron in d_{xy}, d_{yz}, d_{zx}. The fivefold '*d*' orbitals will be split by a regular octahedral environment of inhibitor molecules into two groups, namely, d_{xy}, d_{yz} and d_{zx} with electron density pointing away from the inhibitor and $d_{x^2-y^2}$ and d_{z^2} with electron density pointing

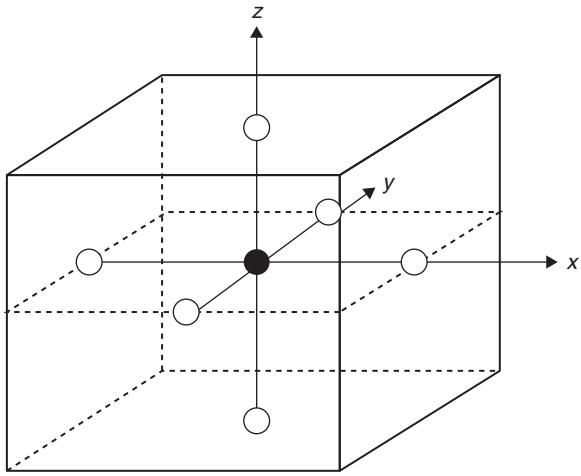

6.11 Octahedral arrangement of a metal complex.

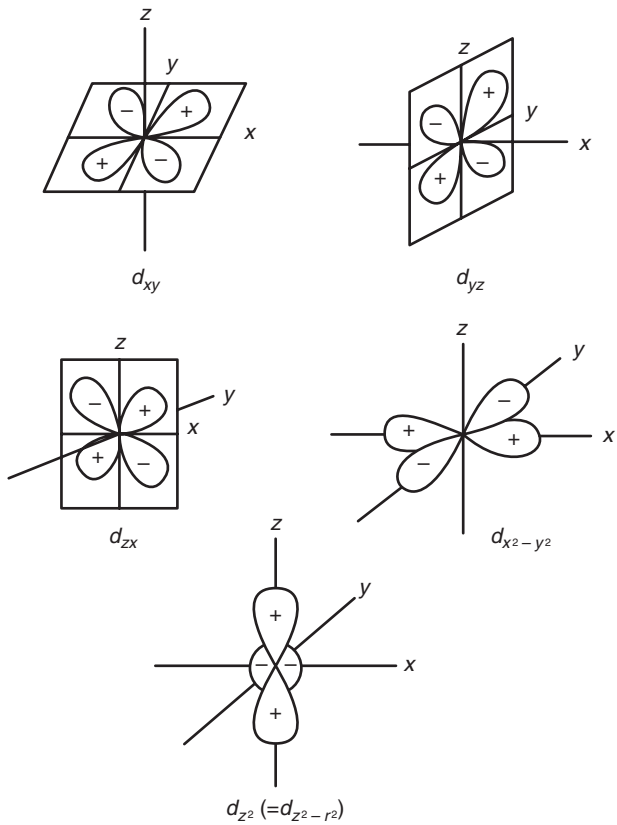

6.12 The angular dependence of the wave function of d electrons.

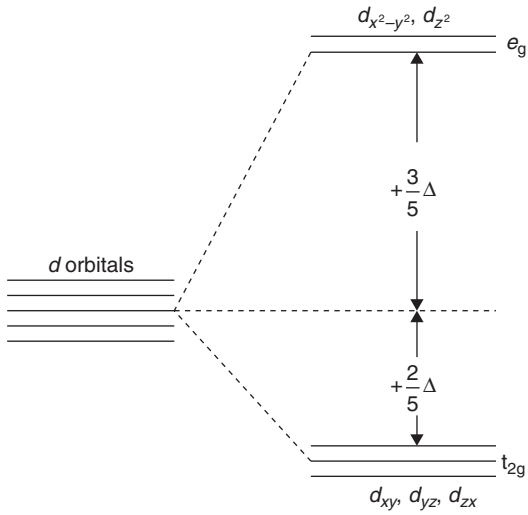

6.13 Splitting of *d*-orbitals in octahedral environment.

toward the inhibitor. Thus the '*d*' orbitals with electrons will be split into two levels t_{2g} (d_{xy}, d_{yz}, d_{zx}) and e_g ($d_{x^2-y^2}$, d_{z^2}) as shown in Fig. 6.13. The two levels correspond to –2/5Δ and 3/5Δ with weighted mean energy as zero:

$$3\,\mathrm{x}\left(\frac{-2}{5}\Delta + 2\frac{3}{5}\Delta\right) = 0$$

The 10 Dq values or Δ or $E_1 - E_2$ the energy separation of the two sets of orbitals t_{2g} (d_{xy}, d_{yz} and d_{zx}) and e_g (d_{z^2}, $d_{x^2-y^2}$) indicates the strength of the metal–inhibitor bond.

6.5.3 Application of inhibitor field theory to metal–inhibitor systems

The data on percent inhibition of corrosion of iron and copper by aniline and benzimidazole inhibitors are as follows in Tables 6.9 and 6.10. The ratio of inhibitor field parameters for Cu^2/Fe^{2+} of 1.25 is comparable to a high value of 1.88, the ratio of inhibitor stabilization energies. The corrosion inhibition of iron by hydroxy and amino substituted ethylenes gave rise to the following order of inhibition:

$$\mathrm{HO(CH_2)_2\,OH} < \mathrm{HO\,(CH_2)_2\,NH_2} < \mathrm{H_2N(CH_2)_2\,NH_2}$$

Table 6.9 Data on corrosion inhibition of iron and copper

System	Percent inhibition	Ratio of percent inhibition (Cu/Fe)
Iron-aniline	52, 43	1.57, 1.90 Average 1.74
Copper-aniline	81.82	
Iron-benzimidazole	60.00	
Copper-benzimidazole	92.11 99.00	1.54 Average 1.65 1.60

Table 6.10 Inhibitor field parameters for iron and copper

System	10 Dq (cm^{-1})	Ratio of 10 Dq	Inhibitor field stabilization energy Cu^{2+}/Fe^{2+} 6 Dq (4 Dq)
Fe^{2+} – ethylenediamine	12 800	1.25	1.88
Cu^{2+} – ethylenediamine	16 000		
Fe^{2} – ammonia	12 500	1.20	1.80
Cu^{2+} – ammonia	15 000		

Table 6.11 Data on iron-inhibitor systems

System	Percent inhibition	Ratio
Iron-benzimidazole (Fe-BI)	60.0	Fe – BISH/Fe-BI
Iron-mercaptobenzimidazole (Fe-BISH)	88.0	1.47
Iron-aminobenzothiozole (Fe-ABT)	85.0	$\frac{\text{Fe-ABT}}{\text{Fe-ABI}} = 1.42$

$$\frac{10\text{Dq(Fe-BISH)}}{10\text{Dq(Fe-BI)}} = \frac{13\,500}{10\,000} = 1.35$$

Inhibitor field strength order: BISH > BI ; (N,SH) > N
Inhibitor field strength order: O, O < O, N < N, N < NSH
Order of 10 Dq for iron: 9400 < 10 850 < 12 500 < 13 500

The inhibitor field strength order O, O < O, N < N,N is in keeping with 10 Dq values. The ratio of corrosion inhibition values of diaminoethylene to monoamino monohydroxy ethylene inhibitors, 1.71 and 1.41 are comparable with the 10 Dq ratio of 1.30.

The data on corrosion inhibition of iron by benzimidazoles, mercaptobenzimidazoles, and amino-benzothiazole, along with 10 Dq values, are given in Table 6.11. The substitution of the mercapto group (SH-) in benzimidazole results in an increase in the percent inhibition (i.e., from 60% to 88%). The ratios of percent inhibition of iron-mercaptobenzimidazole to iron-benzimidazole and iron-aminobenzothiazole to iron-benzimidazole work out to 1.47 and 1.42 respectively. These values of the ratios are comparable to 1.35 the ratio of 10 Dq values. Thus, the inhibitor field strength sequence for inhibition of iron corrosion with inhibitors containing different functional groups as BISH, ABT > BI (N,SH) > N where BISH is mercaptobenzimidazole, ABT is amino-benzothiazole BI (N,SH) is benzimidazole with a SH substitution and N for bare amino compound is in keeping with the degree of inhibition.

The overall inhibitor field strength sequence for the corrosion inhibition of iron with inhibitors containing different functional groups along with the 10 Dq values may be written as:

$$O, O < O, N < N, N \leq N, SH$$

The observation that the inhibitor effectiveness order parallels 10 Dq order is useful in the prediction of the effectiveness of the inhibitor with the available values of 10 Dq.

It is important to recognize that corrosion inhibition of metals by organic corrosion inhibitors containing electron donor atoms such as nitrogen in amines and sulfur in the mercapto group involves the formation of the metal–donor atom complex. Hence, the extent of corrosion inhibition must be related to the stability constant of the metal–inhibitor complex, which in turn is related to the inhibitor field energies as shown in Table 6.12, and Figs 6.14 and 6.15 respectively.

These correlations confirm the operation of inhibitor field theory and the mechanism in corrosion inhibition in a hydrogen sulfide medium. These

Table 6.12 Data on stability constants and inhibitor field energies

System	Log K	Inhibitor field energy (cm^{-1})	Percent inhibition
Fe–Trimethyl aniline (N)	1.335	2083	51.0
Fe-Schiff bases (N.O.)	3.65	4028	85
Fe-Triazoles (N)	5.85	4167	94.8
Fe-en (2N)	7.65	4170	56
Cu-en (2N)	10.63	5120	90
Cu-MBT (s)	6.30	3440	73

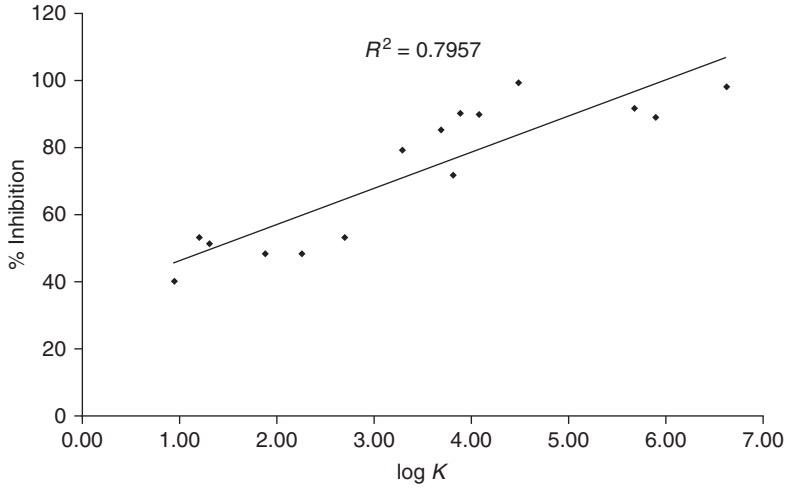

6.14 Plot of logarithm of stability constants against percent inhibition.

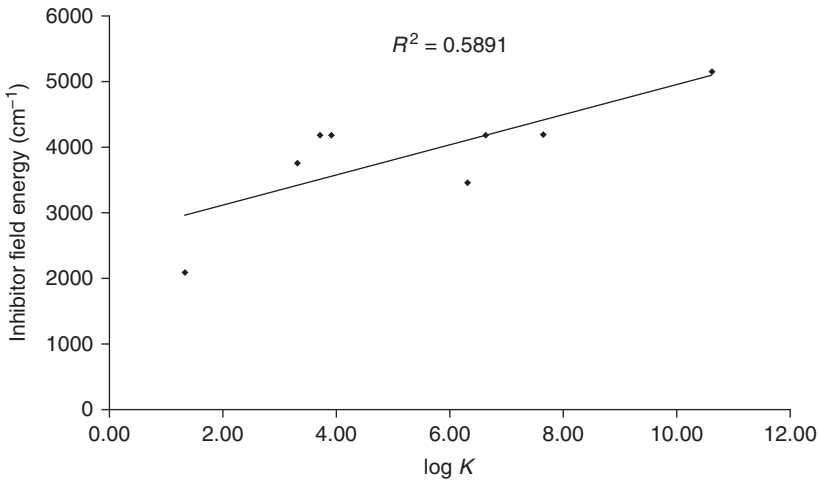

6.15 Plot of stability constant against inhibitor field energy.

correlations are useful in predicting the type of inhibitors that will prove to be good corrosion inhibitors with favorable values of stability constants and inhibitor field energies in the case of transition metals with d^n configuration.

The main corrosive media encountered in the oil industry are:

- HCl and its aqueous solutions
- hydrogen sulfide

- corrosion of steel at hydrocarbon–electrolyte interfaces
- corrosion of steel in emulsified two-phase environments
- oxygen
- naphthenic acids
- carbon dioxide.

Commercial inhibitors generally consist of one or more inhibitor compounds with other additives such as surfactants, film enhancers, de-emulsifiers, oxygen scavengers, etc. The inhibitor solvent package used can be critical with respect to solubility/dispersibility characteristics and hence application/performance of the products. The most frequently used inhibitors belong to the following classes:

- amides/imidazolines
- salts of nitrogenous molecules with carboxylic acids
- quaternary nitrogen salts
- polyoxyalkylated amines, amides and imidazolines
- nitrogen heterocyclics and compounds containing P, S, and O.

6.6 Types of inhibitors

The following is a general list of inhibitors quoted in monographs:

- long chain aliphatic diamine/imidazoline (C18)
- long chain diamine/imidazoline + ethylene oxide to give polyoxy-ethylene derivatives
- aliphatic or aromatic mercaptans
- fatty acid and fatty amine mixture
- organic sulfophosphates.

Particularly useful in CO_2 corrosion inhibition are:

- dimethylamine, ethylenediamine
- methoxypropylamine, morpholine
- sodium salt of mercaptobenzothiazole
- cyclohexylamine.

Imidazoline derivatives are salicylic or sebacic salts of 1–(2–hydroxyethyl)–2–heptadecylglyoxalidyne, rosin amine RN $(CH_2–CH_2–Ac)_2$ HCl, where R = abietyl. They are a mixture of:

- linoleic acid and hexadecylamine
- lauric acid and octadecylamine

- amides of fatty acids and aliphatic diamines
- aklyldiamines and their compounds with ortho- and pyrophosphoric acids
- alkyl polyamines
- diphenylguanidine hydrochloride
- 2-hexyl-2-hexyl-2-imidazoline
- alkylamidoacids
- ester of 2-butyn-1,4 diol, and oleic acid
- lead naphthenates
- mixture of hydroxylamine and Sb_2O_3 where $HORNH_2$, R = C_2–C_{18} N-stearyl triethylenetetramine, benzoyl peroxide, thiourea, and ammonium polysulfide.

Amines, diamines, imidazolines, and pyrimidines and salts of these amines are combined with fatty and naphthenic acids and sulfonates. Protective films formed by insoluble compounds such as carbamide, thiocarbamide, tributylamine, and tetrabutyl ammonium sulfate may inhibit corrosion.

6.6.1 Sulfur derivatives

Cycloalkane sulfonates, polysulfides, 2-mercaptoalkyl acetic acid, bis-2-thiazolinyl-alkylenes, thiourea, and thiocarbamide can be useful inhibitors in a sour gas medium. The review of some patent literature lists a number of formulations for use in a sour medium, shown in the following sections.

6.6.2 Imidazoline derivatives

- Synthesized by the condensation of mixtures of fatty acids or pure fatty acids or naphthenic acid or stearic or lauric acid with diethylenetriamine or dipropylenetriamine.
- Condensation product of two moles of naphthenic acid with a mole of dipropylenetriamine.
- Mixture of 2-heptyl-2-imidazoline, formaldehyde and diethyl phosphite to give imidazoline phosphite.
- Product from the reaction of polyamines, H_2N $(CH_2–CH_2–NH)_x$ R, x = 2–7 and oleic or linoleic or palmitic or stearic acid.
- Product of reaction of naphthenic acid and EDTA.
- Produce of reaction of fatty acids with EDTA along with urotropine.
- 2-amidoethyl or 3-amidopropyl imidazoline with sulfur.
- Tetrahydropyrimidine + sulfur.
- 70–98 parts of imidazoline derivative + one part of benzotriazole + o-toluidine, p-toluidine, morpholine and 2–30 parts of o-nitrophenol.

6.6.3 Aliphatic fatty acid derivatives

- Product from condensation of unsaturated C_{12}–C_{24} fatty acids with maleic anhydride mixed with triethanolamine.
- Mixture of 2–25 parts of unsaturated fatty acid dimers and one part by weight of alkyloxyphenols.
- 1–80 parts by weight of aliphatic amines bound with 1–20 parts of low molecular mass fatty acids and 1–20 parts by weight of C_{20}–C_{30} acid mixture of hydroxyl acids, dimers, and polymeric fatty acids.
- Mixture of 25 parts by weight of C_{18}–C_{20} fatty amines, 35 parts of fatty acids and 40 parts of oil.
- Mg salt of lauric acid, sodium nitrite, benzotriazole, and ethanolamine in water.
- Melting diamine with salicylic acid and dilution with oil.
- Mixture of polyamides of fatty acids with acetylenic derivatives.
- Mixture of polyamides of fatty acids with acetylenic derivatives along with cyclohexanol, cyclohexanone, and cyclohexamine.
- Amide of H_2N–$(R_1$–$NH)_n$ R_2 (R_1 = C_2–C_6 alkenes, R_2 is H or OH substituted hydrocarbon group) and aliphatic carboxylic acid mixed with product of neutralization of C_2–C_{12} dicarboxylic acid with hydroxyamines.
- Diamides by reduction of amines with dicarboxylic acids.
- Thiol ester of type $XC(:O)_m$ $RC(:O)_x$ where R is C_2–C_8 alkyl, m = o or C_{28}–C_{36} alkyl, m = o or 1, x = $C_{1–5}$ dithiol.

6.6.4 Amines

- Macrocyclic tetramines.
- Mixture of 2-propyl, 3-ethyl, 5-ethyl pyridine, and 5-ethyl N-butyl pyridinium halide.
- Benzidine (C_6H_5 NH C_6H_5); C_6H_5 NH–C_3H_4–C_6H_5.
- Mixture of $(Et)_2$ NH, $(i\text{-}Pr)_2NH$, Et_3N, n-$BuNH_2$ $(n\text{-}Bu)_2$ NH, $(n\text{-}Bu)_3N$.
- Product of reaction of amines with epichlorohydrin and converted to phosphate.
- Product of reaction of alkyl succinic acid with amines, $CH_3(CH_2)_n(CH_2)_3NH_2$ (n = 7–13).
- Reaction product of dicyclohexylamine, N-isopropylaniline and morpholine with spindle oil at 75°C for 160 min.
- 10–80 parts of triethanolamine, 2–10 parts of diethanolamine, 3–10 parts of polyethylene glycol (M.W. 200–800) and 20–80 parts of water.
- Methyl ethanolamine, methyldiethanolamine, ethyl ethanolamine and ethyldiethanolamine.
- 261 parts of ethylenediamine, 9 parts of piperazine, 5 parts of diethylenetriamine and 726 parts of water.

- Ethoxylated, propoxylated alkyl phenolamine and/or its salts. Alkoxylated alkyl phenolamine is reacted with acid and used. This formulation gave 96% protection at 3–7 ppm of inhibitor.

6.6.5 Miscellaneous compounds

- 5-Phenyl, 1,2,4-triazole-3-thione, 5-naphthyl, 1,2,4 triazole-3-thione and α – [1,3 chlorophenyl-3-p-bromophenyl-propan-1-one] benzoyl hydrazine gave 90% inhibition.
- Phosphoric and phosphonic esters of hydroquinone.
- Nitropyrazole.
- Mannich bases obtained from cycloalkyl phenols and salts of morpholine and piperidine.

6.7 Summary of corrosion inhibitors used in oil pipeline media

Some of the inhibitors found to be useful in oil and gas pipeline atmospheres such as carbon dioxide and hydrogen sulfide are given in Table 6.13.

Table 6.13 Corrosion inhibitors used in oil pipeline media

Metal/alloy	Medium	Inhibitor
Steam condensate return lines	Carbonic acid	Octadecylamine in dispersion or emulsion form
Ferrous metal	Synthetic seawater salt spray at 20°C for 100 h	Waxy film formers (i) Lanolin (10%) + 90% white spirit (ii) Barium salt of petroleum oxidate (10%) + 90% white spirit Oily film formers (i) Lanolin ester (7%) + 10% mineral oil + 83% solvent (ii) 2% long chain fatty amine + 15% mineral oil + 83% distillate (iii) 0.2% fatty acyl derivative of amino acid + 0.2% substituted imidazoline + 40% mineral oil + 59.6% white spirit
Ferrous metal	SO_2	Tall oil and industrial oils
Iron alloys	Humidity chamber	Hexamethylene tetramine and sodium nitrite
Cold rolled iron	90% RH, 40°C	Hexamethylene tetramine, Pb, Ca, Al sterates and aromatic or aliphatic acids

Table 6.13 Continued

Metal/alloy	Medium	Inhibitor
Iron	Atmospheric corrosion	Amine benzoates, piperidine m-nitrobenzoate
Ferrous alloys	Field tests	Mixture of sodium nitrite triethanolamine and naphthenic acid
Steel	Humid atmosphere	Acyl derivatives of lanolin or penta-erithritol, glycerol, sorbitol in oils, kerosene or organic solvents
Steel	Acid, NaCl	Aliphatic amines, RCH:NR (R = alkyl)
Carbon steel	H_2S	Alkyl products of 3,5 methyl pyrazole
Steel	H_2S, condensates of natural gas wells	Phenol, p-t-butyl phenol P-t-amylphenol, thio, dithiobisphenols
Steel	H_2S, CO_2, 3% NaCl at 80°C	100 ppm of N-tridecyl maleamic acid Tridecylamine salt (85% I)
Ferrous alloys	H_2S in highly mineralized medium	Ethylammonium pyrocatechol borate
Ferrous metals	H_2S	N (aminoethyl) ethanolamine/ ethylenediamine, propylene-diamine /N (aminoethyl piperazine Piperazine / methylamine Bis (propylamine) contg. V^{4+} or V^{5+}
Steel	H_2SO4, $(NH_4)_2SO_4$ H_2S	Quinoline, isoquinoline, methyl quinoline, pyridine bases
Iron	H_2S, CO_2, 3% NaCl	1 (aminoethyl)-2-isooctyl-2 imidazoline reacted with 5% S at 150° for 2 h; 250 ppm gave 70% Inh.
Iron	H_2S, CO_2, 3% NaCl	250 ppm of 1-(2-oleoamidoethyl)-2-imidazoline + 10% sulfur gave 83% inhibition
Steel	5% NaCl + H_2S	1-monoglyceride-3-allyl ether Increase in chain length C_5–C_{12} increase in degree of inhibition
Steel	H_2S, CO_2, 5% NaCl pH 3.6	Diethylaminoacetonitrile 0.005 g/L 7.22 mm/y; 0.05 g/L–0.2 mm/y
Steel	5% NaCl, 0.5% HAc	Dodecyl trimethylammonium chloride (98% inhibition)
Steel	5% NaCl, 0.5% HAc	30 ppm of salt from reaction of oleyl pyridine and butyl chloride (97% inhibition)
Steel	5% NaCl, 0.5% HAc	20 ppm of polyamide from reaction of lauric acid and triethylene tetramine (98% inhibition)

(*Continued*)

Table 6.13 Continued

Metal/alloy	Medium	Inhibitor
Steel	5% NaCl, 0.5% acetic acid saturated with H_2S	Substituted imidazolines with nine carbon atoms in chain and 2-aminoethylenes – best inhibition observed.
Steel	H_2S, O_2 petroleum wells	Heptyl, 2,5 ditertiary butyl-4 hydroxy phenyl phosphite 200 mg/L gave 97% inhibition
Steel	Saturated with H_2S	Amine acetylenic alcohols or esters, 1 g/L – 83 – 97% I
Steel	H_2S	Sulfoureide 100–400 mg/L – 100% I
Steel	3% NaCl + 0.4% HAc sat. with H_2S	R : CON(H) NH_2 – naphthenic acid anhydride
Steel	3% NaCl + 0.4% HAc sat. with H_2S	Hydrazides, amides, N-N'di-methylamino or N-N-diethyl-amino esters of naphthenic acid
Carbon steel	NaCl + H_2S	Diethylenetriamine-N-N dibutyro nitrile, diethylaminoacetonitrile
	0.05% NaCl pH 3.6 sat. with H_2S	Diallylamino acetonitrile, Piperidinobutyronitrile (0.005 to 1.0 g/L)
		Diethylaminoacetonitrile 0.05 – 1.0 g/L gave 99% I.
Carbon steel	H_2S	1-butyl – 3(5)-methyl-4-nitro pyrazole 0.2 wt.%
Steel	Gas condensate H_2S 2.5–3 g/L	Bis (ethanolaminomethyl) – imidazoline – 2 thione
		Bis (dibutylaminoethyl) imidazoline – 2 thione>99% I
Steel	Sour gas wells (H_2S, CO_2)	$C_2H_5NH_2$ + S good inhibition
Steel	Saturated with H_2S	Hexamethylenediamine (99% inhibition)
Steel	Gas condensate with water saturated with H_2S	Mixture of 2,3 and 2,4 dimethyl and 2,4,6 trimethyl pyridine 0.25–0.5 wt. percent, 95% inhibition
Steel	Benzene: water (1:1)	Amineethyl derivative of
	0.04% HAc saturated with H_2S	p-methoxy
		Phenol, 200–1000 mg/L – 100% protection
Mild steel	H_2S, CO_2	500 ppm of reaction product of tetradecyl bromide and alkyl pyridine + 50 ppm NH_4SCN-94% I
Steel	Gasoline, H_2S	Reaction product of naphthenic acid with diethylene triamine and oleic acid-10 mg/L, 93% inhibition

Table 6.13 Continued

Metal/alloy	Medium	Inhibitor
Steel	CO_2, H_2S	500 ppm of alkyl pyridinium bromide and 500 ppm NH_4SCN – 90% inhibition
Steel	Acetic acid + H_2S	N_7N-dialkylethyl esters of cyclo-pentanecarboxylic acid
Steel	HAc + H_2S + NaCl + benzene	Dialkylaminoalkyl esters of 3-cyclohexene carboxylic acid, 4-methyl-3 cyclohexene carboxylic acid
Steel	20% HCl, NaCl saturated with H_2S	Alkylbenzyl pyridinium chloride – 1% concentration
Steel	H_2S at 25°C, 45°C	Monoethanolamine
Steel	Petroleum, NaCl, H_2S	N-hydroxyalkylamides
Steel	Crude oil, 3% NaCl saturated with H_2S	Amides and their derivatives (alkyl sulfonates with urea; dialkyl urea and sulfoderivative of propionic acid)
Steel	HAc, HCl, NaCl, H_2S	Alkyl benzyl triethanol ammonium chloride
Carbon steel	Gasoline 3%NaCl, HCl, HAc, saturated with H_2S	MePh (O) $(CH_2)_3SCH_2NR_2$ (R=Me, Et NR_2 = morpholino) At 1 g/l – 92% inhibition
Steel	H_2S	Neutralization product of sulfo acids with H_2N-CH_2-CH_2-OH and pyridine; sulfonated residue of pinene with NH_2-CH_2-CH_2OH and $(C_{14–15})$ $NH_3^+x^-$ 80–90% inhibition
Steel	SO_2, H_2S, HCl	Triethanolamine oleate
Steel	Petroleum, NaCl + H_2S	Dialkyldimethyl ammonium chloride
Steel	Seawater, sat. with H_2S	Imidazoline phosphoramide 4–16 ppm of (EtO)2 P(O) NH(CH_2-$CH_2NH_2NH)_2$H·HCl gave 82% inhibition
Steel	Brine saturated with H_2S	Product of reaction of pyridine with alkylbenzyl chloride (90% inhibition)
Steel	3% NaCl, pH 1.0 saturated with H_2S	Diamine dioleate from stearic acid salt of monodiamine (C_{19}) and salicylic acid and salt of didiamine (C_{18}) and salicylic acid: > 90% inhibition
Steel	CO_2, H_2S	10 g/L of sulfur in ethylamine
Steel	5% NaCl, 0.5% acetic acid, saturated with H_2S	10 ppm of dodecyltrimethyl ammonium chloride

(*Continued*)

Table 6.13 Continued

Metal/alloy	Medium	Inhibitor
Steel	5% NaCl, 0.5% HAc saturated with H_2S	• Reaction product of oleylpyridine and butylchloride • 20 ppm of polyamide obtained by dehydration of lauric acid and triethylene tetramine • 20 ppm of quaternary imidazoline derivatives
Carbon steel	2% NaCl saturated with H_2S	25 ppm of reaction product from diethanoltriamine and naphthenic acid (25 ppm)
Steel	H_2S	Quinoline, isoquinoline, methyl quinoline, pyridine bases
Steel	H_2S	250 ppm of product of 10% sulfur mixed with 1-(aminoethyl)-2-isooctyl-2-imidazoline
Steel	H_2S	250 ppm of product of 10% sulfur mixed with 1-(2-oleoamidoethyl)-2-imidazoline (83% inhibition)
Steel	H_2S	(Diethylamino) acetonitrile 0.05 g/L gave corr. rate – 0.2 mm/y
Steel	H_2S	Dodecyl triethylammonium chloride (98% inhibition)
Steel	H_2S	10 ppm of salt from reaction of oleyl pyridine and butylchloride (97% I)
Steel	H_2S	20 ppm of polyamide from reaction of lauric acid and triethylene tetramine (98% I)
Steel	H_2S	Heptyl, 2,5 ditertiary butyl-4 hydroxy phenyl phosphite, 200 ppm-97% I
Steel	H_2S	Amine acetylenic alcohols or esters, 1 g/L 83–97% I
Steel	H_2S	Sulfoureide 100–400 ppm – 100% I
Steel	H_2S	Diethylaminoacetonitrile, 50–1000 ppm – 99% I
Steel	H_2S	Bis (ethanol amino methyl) imidazoline – 2 thione Bis (dibutylaminomethyl) imidazoline – 2 thione (99% I)
Steel	H_2S	Hexamethylenediamine (99% I)
Steel	H_2S	Mixture of 2,3; 2,4 dimethyl and 2,4,6 trimethyl Pyridines 0.25–0.5 wt.% (95% I)
Steel	H_2S	Aminoethyl derivative of p-methoxy phenol 200–1000 ppm (~ 100% I)

Table 6.13 Continued

Metal/alloy	Medium	Inhibitor
Steel	H_2S	500 ppm of reaction product of tetradecyl bromide and alkyl pyridine together with 500 ppm of NH_4SCN (94% I)
Steel	H_2S	500 ppm of alkyl pyridinium bromide and 500 ppm of ammonium thiocyanate (90% I)
Steel	H_2S	1000 ppm of Me Ph(O) $(CH_2)_3$ S CH_2NR_2 (R = Me, Et, morpholino)-92% I)
Steel	H_2S	Triethanolamine oleate/ dialkyldimethyl ammonium chloride or reaction product of pyridine with alkylbenzyl chloride (90% I)
Steel	H_2S	Reaction product of diethanolotriamine and naphthenic acids; 25 ppm

The following inhibitors tested in ASTM D1384 protocol gave 90% corrosion inhibition and these inhibitors might prove suitable in CO_2 and H_2S medium:

1. 100 ppm of thiourea.
2. Morpholine caprylate/sebacate/laurate/oleate.
3. Dicyclohexyl ammonium acetate.
4. Ammonium caprylate.
5. Ethanol ammonium caprylate/stearate.
6. Diethanol ammonium caprylate.
7. Triethanol ammonium caprylate.
8. 1,2 Diaminoethane caprylate.
9. 1,2 Diaminoethane with dimethyl ethanolamine.
10. Dibutylammonium caprylate.
11. N-phenylthiourea along with potassium iodide.
12. 500 ppm of 2-amino-6-chlorobenzothiazole.

6.8 References

1. Bregman J I (1966), 'Proc. 2nd SEIC', *Ann Univ Ferrara*, n.s., Sez V., suppl. no. 4, 549.
2. Bregman J I (1971), 'Proc. 3rd SEIC', *Ann Univ Ferrara*, n.s., Sez V., suppl. no. 5, 339.
3. Faroulis Z A (1980), 'Proc. 5th SEIC', *Ann Univ Ferrara*, n.s., Sez V., suppl. no. 7, 1029.
4. Rosenfeld I L (1977), *Inhibitori Korozii, Khimiza*, Moscow, 307.
5. Gonik A A (1976), *Korozija naftepremislevega obrudovanija i mjeri je preduprezdenija,* Moscow, 'Nedra', 49.
6. Nestle A, Dunlop A K and Busch H E (1973) in *Corrosion Inhibitors*, Nathan C C (ed.), Houston TX, NACE, 61, 76, 102.
7. Bregman J I (1963), *Corrosion Inhibitors*, New York, Macmillan.
8. Reiser K (1966), 'Proc. 2nd SEIC', *Ann Univ Ferrara*, n.s., Sez V., suppl. no. 4, 459.

9. Parker R C (1983), in *Chemicals in the Oil Industry*, Ogden P H (ed.), RSC special pub. 45, London, 199.
10. Kelley J A (1983), in *Chemicals in the Oil Industry*, Ogden P H (ed.), RSC special pub. 45, London, 150.
11. Horvath J, Salem T M, Abd El-Naby J, El-Sayed Khalil, Hackl L and Rauscher A (1976), 'Proc. 4th SEIC', *Ann Univ Ferrara*, n.s., Sez V., suppl. no. 6, 743.
12. Antropov L I and Pogrebova I S V (1973) in *Itogi nauki i tekhniki, Korroz i zashch metallov*, 2, 27.
13. Roberge P R and Sastri V S (1990) *Proc. 11th Int. Corrosion Congress*, Florence, Italy, 3, 355.
14. Schmitt G and Bruckoff W B (1989) *Corrosion '89*, paper no. 620, Houston TX, NACE.
15. Dougherty J A and Alink B A (1990) 'Proc. 7th SEIC', *Ann Univ Ferrara*, n.s., Sez. V, suppl. no. 9, 1299.
16. Frenier W W and Growcock F B (1990) 'Proc. 6th SEIC', *Ann Univ Ferrara*, n.s., Sez V., suppl. no. 9, 661.
17. Schmitt G (1991) *Corrosion*, NACE, **47** (4), 285.
18. Dupin P, Viloria-Vera D A, DeSavignac A, Lattes A, Sutter B and Haicour P H (1980) Proc. 5th European Symposium on Corrosion Inhibitors, Ferrara, Italy, 301.
19. Martin L R (1984) *Int Corrosion Conf and Forum* NACE, New Orleans, paper no. 285.
20. Valand T and Bugga K (1985) 'Proc. 6th European Symposium on Corrosion Inhibitors', *Ann Univ Ferrara*, Italy, 1401.
21. Bernard D, Haim M and Pou T E (1985) 'Proc. 6th European Symposium on Corrosion Inhibitors', *Ann Univ Ferrara*, Italy, 1497.
22. Dawson J L, Shih C C, Miller R C and Palmer J W (1991) *Mat Perform*, **30**, 43.
23. Martin R L, French E C and Dougherty J A (1989) *Mat Perform*, **28**, 46.
24. Martin R L, Anand R R, Wilson D and Abrahamson D E (1971) *Mater Prot Perform*, **10**, 33.
25. Bradburn J B (1983) in *CO_2 Corrosion in Oil and Gas Production: Selected Papers*, Newton L E and Hausler H R (eds) NACE, 142.
26. Wolfson L L (1960) *Corrosion*, **16**, 298t.
27. Bradburn J B (1983) in *CO_2 Corrosion in Oil and Gas Production: Selected Papers*, Newton L E and Hausler H R (eds) NACE, 142.
28. Cord-Ruwisch R, Kleinitz W and Widdel F (1987) *Mat Perf*, **1**, 97.
29. Campbell S A, Scannell R A and Walsh F C (1990) *Ind corrosion*, **8**, 7.
30. Tuoviane O H and Cragnolino G (1986) 'Review of microbiological and electrochemical techniques in the study of corrosion induced by sulphate-reducing bacteria', in *ASTM STP 908*, Moran G C and Labine P (eds), Philadelphia, ASTM, 413.
31. Bernard F, Pou T E and Haim M (1985) 'Proc. 6th SEIC', *Ann Univ Ferrara*, n.s., Sez V., suppl. no. 8, 1465.
32. Pope D H and Zintl T P (1989) *Mat Perform*, **28** (11), 46.
33. Frenier W W, Growcock F B and Lopp V R (1988) *SPE Production Eng*, November 1988, 584.
34. Growcock F B, Frenier W W and Lopp V R (1985) 'Proc. 6th SEIC', *Ann Univ Ferrara*, n.s., Sez V., suppl. no. 8, 167.
35. Frenier W W and Growcock F B (1990) 'Proc. 6th SEIC', *Ann Univ Ferrara*, n.s., Sez V., suppl. no. 9, 661.

36. DeWaard, C and Lotz U (1993) *Corrosion 93*, paper no. 69, Houston TX, NACE.
37. Lahogny-Sarc O (1985) 6th European Symposium on Corrosion Inhibitors, Ferrara, Italy, 1313.
38. Crolet J I (1993) 10th European Corrosion Congress, Barcelona, 5–8 July 1993, paper no. 270.
39. Crolet J I and Bonis M R (1991) *SPE Production Engineering*, 6, no. 4, 445.
40. Rozenfeld I L and Persiantseva V P (1986) *Inhibitors of Atmospheric Corrosion* (in Russian), Moscow, Nauka.
41. Andreev N N and Kuznetsov Yu I (1998) *Corrosion* (NACE), paper no. 2, 41.
42. Bergman J I (1963) *Corrosion Inhibitors*, New York, MacMillan.
43. Makrides A C and Hackerman N (1953) *Ind Eng Chem*, 1954, 46, 523, 47, 1773.
44. Iofa, Z A (1970) *Zaschita Metallov*, **6**, 491.
45. Panasenko V F (1972) Candidate's dissertation, Polyteckh. Inst. Kiev.
46. Bolmer P (1965) *Corrosion*, **21**, 490.
47. Kasche, H. (1970) *Werkstoffe und Korrosion*, **21**, 185.
48. Antropov L I and Panasenko V F (1975) *Itogi nauki i tekhniki, ser. Korroziya i zashchita ot korrozii*, **4**, 46.
49. Rozenfeld I L (1981) *Corrosion Inhibitors*, New York, McGraw-Hill.
50. Rozenfeld I L, Bogomolov, Gorodetskii A E, Kazanskii L P, Frolova L V and Shamova L I (1982) *Zaschita Metallov*, **18**, 163.
51. Dupin P, De Savignac A and Lattes A (1982) *Information Chemie*, no. 228/229, 169.
52. Dupin P, De Savignac A and Lattes A (1982) *Werkstoffe und Korrosion*, **33,** 203.
53. Hansch C and Fujita T (1964) *J Am Chem Soc*, **86**, 1616.
54. Growcock F B (1989) *Corrosion*, **45**, 1003.
55. Growcock F B, Freiner W W and Andreozzi P A (1989) *Corrosion*, **45**, 1009.
56. Perumareddi J R, Sastri V S and Roberge P R (1991) *Int Symposium on Materials Performance, 36th Annual Conf. of Metallurgists of CIM*, Aug. 1991, Ottawa, Pergamon, 195.
57. Horanyi G (2004) *Corr Sci*, **46**, 1741.
58. Sastri V S, Perumareddi J R and Elboujdaini M (2005) *Corros Eng Sci Technol*, **40**, 270.
59. Ayers R C and Hackerman N (1963) *J Electrochem Soc*, **110**, 507.
60. Cox P F, Every R L and Riggs O L (1964) *Corrosion*, **20**, 299t.
61. Vosta J and Eliasek J (1971) *Corros Sci*, **11**, 223.
62. Donahue F M and Nobe K (1965) *J Electrochem Soc*, **112**, 886.
63. Donahue F M and Nobe K (1967) *J Electrochem Soc*, **114**, 1012.
64. Altsybeeva A I, Levin S Z and Dorokhov (1971) A P, *3rd European Symposium on Corrosion Inhibitors*, Univ. of Ferrara, Ferrara, 501.
65. Grigoryev V P and Kuznetsov V V (1969) *Prot Met*, **5**, 356.
66. Kiyama A A and Nobe K (1970) *J Electrochem Soc*, **117**, 999.
67. Brandt H, Fischer M and Schwabe K (1970) *Corr Sci*, **10**, 631.
68. Gece G (2008) *Corr Sci*, **50**, 2981.
69. Sastri V S and Perumareddi J R, unpublished data.
70. Sastri V S, Perumareddi J R, Lashgari M and Elboujdaini M (2008) *Corrosion*, **64** (8), 283.

This page intentionally left blank

Part II

Methods for detecting corrosion

This page intentionally left blank

7

Electromagnetic methods for detecting corrosion in underground pipelines: magnetic flux leakage (MFL)

T. BUBENIK, Det Norske Veritas (U.S.A.) Inc., USA

DOI: 10.1533/9780857099266.2.215

Abstract: This chapter discusses electromagnetic in-line inspection tools as they relate to pipeline integrity. It covers magnetic flux leakage (MFL), the most commonly used inspection technology for pipelines. MFL has been successfully used for nearly 50 years to detect, identify, and size metal loss due to corrosion.

Key words: in-line inspection, magnetic flux leakage, pipeline integrity, smart pig.

7.1 Introduction

An in-line inspection tool is a self-contained device that moves through a pipeline with the product or fluid in the pipe. Pipeline operators use in-line inspections along with other activities to evaluate and monitor the integrity of hundreds of thousands of miles of lines. Combinations of these activities constitute the overall integrity management program of the pipeline operator. This chapter discusses electromagnetic in-line inspection systems as they relate to pipeline integrity. It summarizes the capabilities of various tools, and discusses how the tools are best used.

MFL is the most common electromagnetic inspection technology for metal loss and has been used for 50 years in pipeline systems around the world. It has successfully found defects that could have led to failures. Understanding its capabilities and weaknesses is critical in using the results of an inspection. Other electromagnetic technologies include those based on eddy currents and electromagnetically induced ultrasonics. Each of these technologies is newer and less widely used than MFL. These technologies are generally being developed to detect and size cracks rather than metal-loss anomalies.

7.2 Background and definitions

This chapter is based, in large part, on Bubenik *et al*. (2000). In-line inspection tools are also referred to as smart pigs. These tools inspect the full thickness of the pipe wall and are designed to look for conditions such as metal-loss corrosion, cracks, and other anomalies.

An in-line inspection involves collecting data continuously along a pipeline and interpreting the data. The data are analyzed using software and manual techniques. The inspection and data analysis are referred to as an inspection system in this chapter.

Data analysis has three primary steps: detection, identification, and sizing. Detection involves recognizing a measurable signal that is above a threshold value and differentiating it from other signals. Signals can be from any number of conditions, such as natural pipeline variations in wall thickness or metallurgy.

Determining the source of the signal is called identification. During the identification phase, the source is determined to be, for example, a pipeline component or potential metal-loss anomaly. Next, for suspected defects, the anomaly is sized. Sizing involves estimating the dimensions of an anomaly from the measured signals. For metal loss, inspection vendors usually estimate the length, depth, and width.

Sizing is used to determine the severity of an anomaly from the inspection signal. If the anomaly fails one or more acceptance criteria, it is referred to as a defect. If it does not fail, it is considered an imperfection.

7.3 Typical inspection system capabilities

Electromagnetic in-line inspection tools are typically designed to detect and size one type of anomaly, most commonly metal-loss corrosion. The reliability with which the tool finds such anomalies is a function of the depth, length, and width of the metal loss. Detection is best for large metal-loss anomalies with relatively sharp edges. Most inspection vendors claim depth detection thresholds of 5–15% of the wall thickness and threshold lengths of several times the wall thickness. Detection reliabilities (i.e., probabilities of detection) are usually quoted at the detection threshold. A common probability of detection is 90% or 95% for anomalies whose depth is greater than 10% of the wall thickness.

The probability of correct identification varies with the size and shape of the anomaly. For example, a common probability of correct identification is 95–98% for metal-loss corrosion greater than the detection thresholds. The corresponding probability for other types of metal loss, such as gouging, is less.

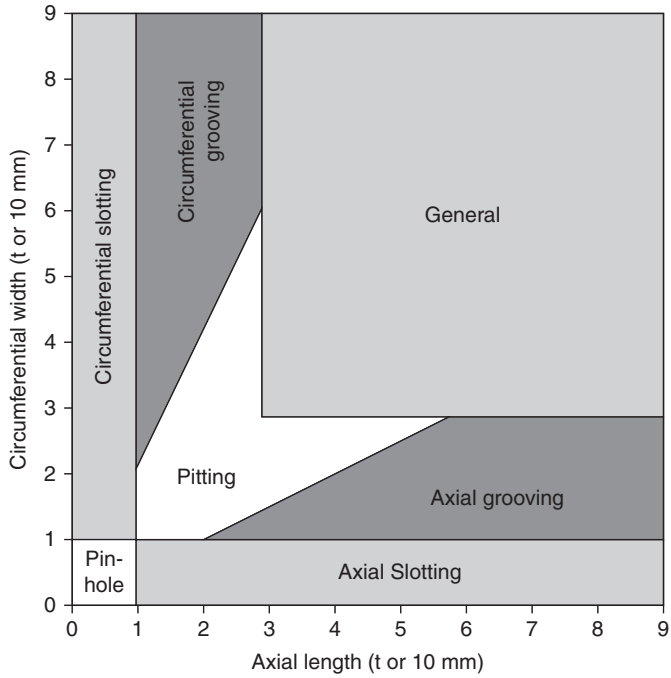

7.1 ILI sizing chart.

Like detection and identification, sizing accuracies with electromagnetic tools are a function of the size and shape of an anomaly. Figure 7.1 shows sizing categories as a function of anomaly length and width. Most inspection systems are capable of accurate sizing in some, but not all, categories shown, but few systems are capable of accurately sizing in the pin-hole category.

Inspection capabilities are not necessarily constant during a smart pig run. Many operational conditions affect and often decrease accuracy and reliability. For example, high velocities reduce detection reliability. The detection reliability and sizing accuracy can therefore vary during an inspection. Consequently, it is important to control those operational conditions to increase detection reliability and sizing accuracy during an inspection.

Regardless of the controls used during a smart pig inspection, no inspection is perfect. Smart pigging cannot detect every condition that could threaten the integrity of a pipeline, just as no medical diagnosis can detect all illness in humans. Smart pigging, like hydrotesting and all other pipeline maintenance tools, has limitations. Understanding these limitations allows

smart pigging to be used to its greatest advantage in combination with other activities.

7.4 Magnetic flux leakage (MFL) pigs

MFL pigs were first introduced in the mid 1960s. Since then, in-line inspection capabilities have evolved, and they continue to evolve today. MFL is the oldest and most commonly used inspection method for pipelines. It can reliably detect metal loss due to corrosion and, often, gouging. In addition, while not designed for this purpose, MFL systems can sometimes find metallurgical and other geometric anomalies, such as dents.

7.4.1 Principles and technologies

MFL starts with a magnet. A magnet has two ends, called north and south poles. The poles exert forces on iron and steel. This force of attraction is caused by the magnetic field. Figure 7.2 illustrates the flux lines around a magnet and its poles as calculated using finite-element analyses. The magnet is the dark gray bar near the top of the figure. Flux lines represent the strength and direction of the magnetic field, where dense lines imply a strong magnetic field. The curved sections attached to the poles are magnetic material (steel or iron), which is used to channel magnetic flux in a particular direction.

When a magnet is placed next to a pipe wall, most of the flux lines pass through the pipe wall, as shown in Fig. 7.3. The pipe wall is a preferred path for the flux because it is easier to magnetize. While most of the flux lines concentrate in the pipe wall, a few pass through the surrounding media. Figure 7.4 shows that flux leakage occurs at a metal-loss anomaly,

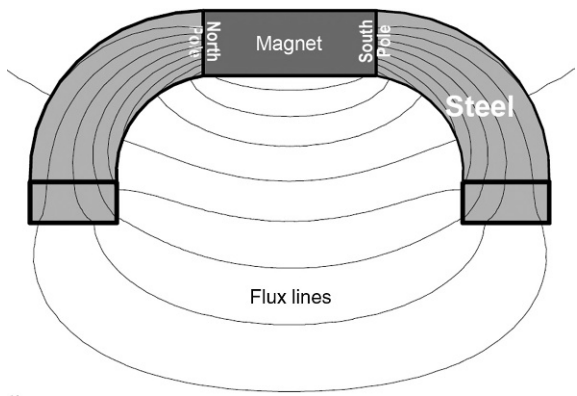

7.2 Flux lines around a magnet.

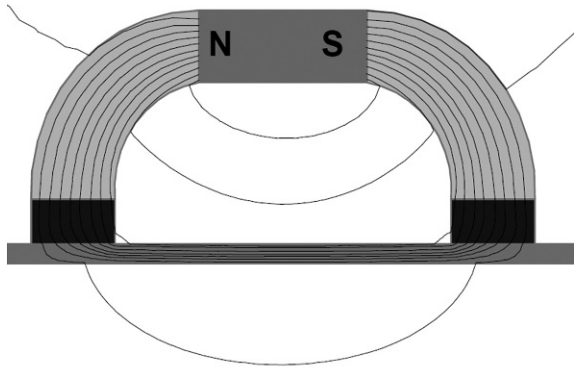

7.3 Flux lines at the pipe wall.

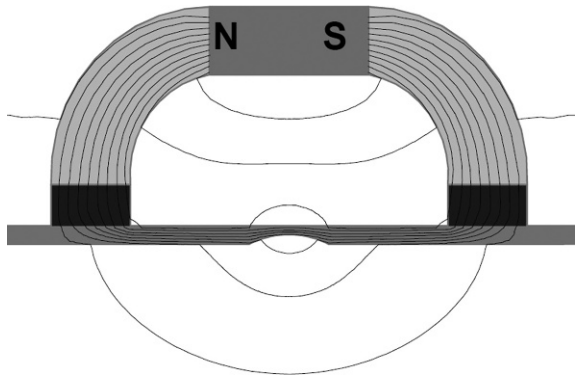

7.4 Flux lines at an anomaly.

where there is a local decrease in the thickness of the pipe. At the anomaly, the flux that had been carried by the lost metal must go somewhere. Some are carried by the thinner section, and some 'leaks' from both surfaces of the pipe.

A sensor positioned on the inside (magnet side) of the pipe is typically used to measure the magnetic field adjacent to the pipe wall. At a metal-loss anomaly, the sensor records a higher flux density or magnetic field, which indicates the presence of an anomaly. In this manner, an MFL pig detects an anomaly that causes flux to leak. The measured leakage field depends on the depth, length, width, and shape of the anomaly, as well as the magnetic properties of the nearby material. To characterize the anomaly, the measured leakage field must be analyzed.

Groups of sensors are contained in sensor heads that are mounted between the magnets. These heads are spring mounted and move along the inner pipe

wall. Maintaining close contact with the pipe wall is important because the distance between a sensor and the pipe wall affects the measured signal.

To summarize, MFL tools apply the principles of flux leakage inside the rugged environment of a pressurized and flowing pipeline. A magnetizing system applies a magnetic field as the tool moves through the line. Anomalies distort this applied field, producing flux leakage. The amount of flux leakage depends on the size and shape of the anomaly, as well as the magnetic properties of the nearby pipe steel. Sensors measure flux leakage, and a recording system stores the measurements inside the inspection tool. The measurements are analyzed after the inspection is completed to identify anomalies, determine their origin, and estimate the anomaly geometry and severity.

7.4.2 Magnetization direction

Magnetization direction plays an important role in establishing the capabilities of an MFL inspection system. Most MFL tools magnetize in the axial direction and create flux lines that run parallel to the pipe axis. All MFL systems are more sensitive to anomalies that cut across flux lines than those that are parallel to the flux. Therefore, tools that use axial magnetization are more sensitive to anomalies that are circumferentially wide because they cut across flux lines. They are less sensitive to anomalies that are circumferentially narrow.

Some MFL tools are designed to magnetize in the circumferential direction. These tools are most sensitive to axially long anomalies and, as expected, least sensitive to axially short anomalies. Other tools magnetize in a spiral pattern. These implementations are more sensitive to any anomaly that is not aligned with the corresponding flux lines.

Engineering mechanics shows that axially long anomalies are generally more severe than axially short anomalies. Circumferential width plays a lesser role. Why do all MFL tools not magnetize in the circumferential or spiral direction? The answer lies in the complexity of the resulting MFL tools and signals, and how parameters such as tool speed affect signal strength and shape.

7.4.3 Velocity and other effects

A moving magnetic field (an MFL in-line inspection tool) in a conductor (the pipe) will induce electrical currents in the conductor. These currents, in turn, affect the applied and leakage fields. As a result, MFL inspection is velocity dependent. The electrical currents induced by the movement of an MFL tool depend on the direction of motion relative to the flux direction. When the motion and flux direction are the same, there is a small effect. When the directions are perpendicular, the effect is much greater. As a

result, circumferentially applied fields (and circumferential MFL tools) are more sensitive to velocity than axially applied fields (and axial MFL tools). Spirally applied fields are somewhat sensitive to velocity.

Mechanical stress and strain affect the magnetic properties of the pipe steel. A change in magnetic properties, in turn, affects the applied field strength and uniformity. As a result, stress makes analysis of inspection data more difficult. Stress effects are most pronounced at lower magnetic field strengths. So, most inspection companies design their systems with very strong magnets.

7.4.4 Assessing MFL results

The relationships between MFL signals and anomaly geometry and severity are complex. It is important to understand three key concepts. First, there is not a one-to-one relationship between the MFL signal components and anomaly dimensions, such as depth, length, and width. For example, deep anomalies create strong signals in most MFL tools except when the anomaly is long and narrow. For long narrow anomalies, the signals become increasingly smaller as the anomaly width decreases. For axial cracks, the signal essentially disappears!

The second key concept is that the tool design and inspection conditions affect the measured signals. Designers of any piece of equipment make compromises to make the equipment easier to use or cheaper to build. Inspection vendors are no exception. Tradeoffs are frequently made to improve the capabilities in one area at the expense of those in another.

Third, inspection conditions affect the signals. Previously mentioned examples include tool velocity (which can vary significantly during the inspection of a natural gas pipeline) and separation between the sensor and the pipe wall. Other examples include remnant magnetization (magnetization left from previous inspections), changes in wall thickness and pipe grade, and the presence of nearby metallic objects. These examples are not all-inclusive.

7.5 Summary of MFL strengths and weaknesses

Table 7.1 shows some of the advantages and disadvantages of three key variables that affect MFL tool design. Magnetization direction is a dominant parameter, with tradeoffs being between sensitivity to long narrow anomalies, velocity effects, and tool complexity. Magnet pole spacing is also important. Tight spacing provides the ability to traverse tight bends, but with less accurate detection and sizing of some anomalies. Magnet strength affects detection and sizing accuracy. Stronger magnets are often used, which makes signal interpretation easier for metal-loss anomalies, but with reduced sensitivity to some anomaly types.

Table 7.1 Some advantages and disadvantages of commonly seen MFL tool configurations

Factor	Advantages	Disadvantages
Axial magnetic fields	Less sensitive to velocity than with circumferential or spiral magnetic fields	Less sensitive to long narrow anomalies than circumferential or spiral magnetic fields
Circumferential magnetic fields	More sensitive to long narrow anomalies than with axial or spiral magnetic fields	Compared to axial magnetic fields: • More sensitive to velocity • Less sizing accuracy for most anomalies • Requires second magnetizer
Spiral magnetic field	Sensitive to both long narrow anomalies and short wide anomalies	More complex signal to evaluate than with axial or circumferential magnetic fields – less accurate detection and sizing of some anomalies Less sensitive to anomalies in the direction of the spiral magnetic field Requires second magnetizer
Magnet poles that are close together	Ability to pass through tight bends	More sensitive to velocity than with poles that are widely spaced
Magnet poles that are far apart	Less sensitive to velocity than poles that are closely spaced	Cannot pass through tight bends
Stronger magnets	Easier to analyze leakage fields	Less sensitivity to mechanical damage
Weaker magnets	More sensitivity to metallurgical anomalies and mechanical damage	More difficult to analyze signals than with strong magnets

As a consequence of these and other tradeoffs, each smart pig has unique strengths and weaknesses, making one type of pig more appropriate for certain types of anomalies or conditions. Some improvements expand the range of anomaly types detected by the pig, while others address entirely different problems. Selecting the 'right' pig for each job is important.

7.5.1 Estimated MFL pig capabilities

Knowing that each pig has strengths and weaknesses is important, but quantifying pig capabilities is more important. Because every pipeline is unique, the capabilities vary and it is difficult to obtain objective measures of pig performance under all conditions. Inspection vendors general provide performance specifications, which give estimated capabilities under typical pipeline operating conditions.

Table 7.2 shows a typical set of sizing accuracies for MFL tools that magnetizes in the axial, circumferential, and spiral direction. The anomaly

Table 7.2 Typical MFL performance specifications

	General	Pitting	Axial grooving	Circumferential grooving
Axial MFL				
Depth at probability of detection (POD) = 90%	**0.10 t**	0.12 t	0.20 t	0.12 t
Depth sizing accuracy at 80% confidence	**±0.10 t**	±0.15 t	±0.20 t	±0.15 t
Length sizing accuracy at 80% confidence	**±15 mm**	±12 mm	±15 mm	±12 mm
Width sizing accuracy at 80% confidence	±20 mm	**±12 mm**	**±12 mm**	±20 mm
Circumferential MFL				
Depth at POD = 90%	0.15 t	0.15 t	**0.10 t**	0.15 t
Depth sizing accuracy at 80% confidence	±0.15 t	±0.19 t	**±0.15 t**	±0.20 t
Length sizing accuracy at 80% confidence	**±15 mm**	±12 mm	**±15 mm**	±15 mm
Width sizing accuracy at 80% confidence	**±15 mm**	±15 mm	±15 mm	**±8 mm**
Spiral MFL				
Depth at POD = 90%	**0.10 t**	**0.10 t**	0.15 t	**0.10 t**
Depth sizing accuracy at 80% confidence	**±0.10 t**	**±0.10 t**	**±0.15 t**	**±0.10 t**
Length sizing accuracy at 80% confidence	±20 mm	**±10 mm**	±20 mm	**±10 mm**
Width sizing accuracy at 80% confidence	±20 mm	±20 mm	±20 mm	±20 mm

descriptions at the top of each column refer to the categories defined earlier in Fig. 7.1. Note that the capabilities shown are typical – prospective buyers of MFL inspection services should always check the actual performance specification of a given tool.

The inspection system that performs best in each category is highlighted in Table 7.2. As expected, the axial and spiral inspection systems are less sensitive to axial grooving and more sensitive to circumferential grooving than a tool that magnetizes in the circumferential direction. The circumferential tool is also somewhat less sensitive to general and pitting metal loss.

7.6 Conclusion and future trends

In-line inspection technologies are evolving, not static. This evolution is leading to smart pigs with expanded and improved capabilities. As these capabilities enter the marketplace, additional and more powerful inspection systems will be available for monitoring pipeline integrity.

MFL inspection systems are the oldest type of smart pig used by the pipeline industry. Axial MFL tools have the longest history and are best understood. Consequently, future improvements for this type of system are expected to be modest. Circumferential and spiral tools are newer and have more room for improvement.

There are also ongoing developments on the use of multiple technologies on a single in-line inspection tool. These developments include combinations of technologies to either expand the range of anomaly types covered by the system (e. g., denting and metal loss) or to improve the detection and sizing of one or more anomaly types (e.g., metal-loss corrosion). The use of caliper and MFL inspection technologies is an example of the first, while using MFL and ultrasonic wall measurement technologies is an example of the latter.

For all tools, ongoing developments will lead to improvements in capabilities, but like all other technological developments, they will require time before they are widely available. Development time is needed for the basic analysis methodologies, tool design concepts, and testing under normal pipeline operating conditions. This latter step is crucial and time consuming; it can easily take years to accomplish. This step is essential, though, in providing inspection equipment that is rugged, reliable, and accurate.

In-line inspection is a powerful tool that can and should be part of the integrity management programs of pipeline operators. Smart pigs are not a panacea, though, and they are not the ‘right’ tool for every application. Consequently, each case should be considered separately, weighing the strengths and weaknesses of different pigs against the expected conditions on a pipeline. The analyses must then match the reported anomaly

population, and appropriate decision models must be used to ensure that the most important risks to pipeline integrity have been addressed.

7.7 Sources of further information and advice

- **American Gas Association (AGA)** – The AGA represents and advocates the interest of more than 200 local energy companies that deliver clean natural gas throughout the United States.
- **Gas Research Institute (GRI) –** This organization ceased operations in 2006 and its assets (physical and human) were transferred to the not-for-profit R&D organization Gas Technology Institute (GTI).
- **GTI** – The GTI, formed in April 2000 by the combination of the GRI and the Institute of Gas Technology (IGT), is a leading research, development and training organization serving the global natural gas industry and energy markets.
- **Interstate Natural Gas Association of America (INGAA)** – INGAA is a trade organization comprising 25 members, advocating regulatory and legislative positions of importance to the natural gas pipeline industry in North America and providing a key link between natural gas producers and consumers.
- **NYSEARCH –** NYSEARCH is a voluntary R&D sub-organization of the Northeast Gas Association currently serving 19 member companies from North America (although membership is not limited to any geographic region). NYSEARCH works collaboratively with Pipeline and Hazardous Materials Safety Administration (PHMSA) and other R&D organizations. A large part of its focus is product development and technology transfer.
- **Operations Technology Development (OTD) –** OTD is a not-for-profit corporation led by its 23 members, who serve over 26 million natural gas customers in the United States and Canada and pool their collaborative funding and resources to address current and future industry needs.
- **Pigging Products & Services Association –** Further information on the current capabilities of MFL and other in-line inspection systems can be found at the website of the Pigging Products & Services Association, http://www.ppsa-online.com/.
- **PHMSA –** PHMSA establishes national policy, sets and enforces standards, educates, and conducts research with the aim to protect people and the environment from the risks of hazardous materials transportation.
- **Pipeline Research Council International (PRCI) –** PRCI is a not-for-profit membership organization that implements R&D for the energy pipeline transmission industry, including 38 of the world's leading pipeline operating companies.

7.8 References

Bubenik, T., Nestleroth, J. B. and Leis, B. N. (2000) *Introduction to Smart Pigging in Natural Gas Pipelines*, Gas Research Institute Report Number GRI-00-0247, Chicago, IL.

Interstate Natural Gas Association of America (INGAA) and the American Gas Association (AGA) (2012) *Report to the National Transportation Safety Board on Historical and Future Development of Advanced In-Line Inspection Platforms for Use in Gas Transmission Pipelines*, Washington DC.

8

The close interval potential survey (CIS/CIPS) method for detecting corrosion in underground pipelines

A. KOWALSKI, Det NorskeVeritas (U.S.A.) Inc., USA

DOI:10.1533/9780857099266.2.227

Abstract: Pipe-to-soil close interval surveys (CIS) or close interval potential surveys (CIPS) are used to evaluate the effectiveness of the cathodic protection system of a buried or submerged pipeline. CISs are conducted as an integral part of maintaining the safe operation of the pipeline, and they provide in-depth knowledge and information required to maintain pipeline integrity. In this chapter CIS principles are presented, together with data collection quality assurance. Examples of CIS results are provided to illustrate the advantages of the tool. CIS not only provides information on locations along the pipeline where external metal loss has occurred or may be occurring, but it also provides valuable information to identify the probable cause of external corrosion and to develop mid- and long-term plans to effectively mitigate it.

Key words: structure-to-electrolyte potential, pipe-to-electrolyte potential, IR drop error, reference electrode, current interrupter, Instant Off potential, cathodic protection, external corrosion.

8.1 Introduction

A close interval potential survey is a series of structure-to-electrolyte direct current (DC) potential measurements performed at regular intervals to evaluate the level of polarization on buried or submerged structures such as steel pipelines (Fig. 8.1). The acronyms CIS (for close interval survey) and CIPS (for close interval potential survey) are used interchangeably to refer to this type of survey.

When buried or submerged structures are protected with a cathodic protection (CP) system, the CIS may be used to assess the level of CP of the structure. When buried or submerged structures are not protected with a CP system, the CIS may be used to identify areas on the structure where corrosion may be occurring. CISs are commonly performed over buried pipelines worldwide, and can be used, in conjunction with other aboveground survey tools, to identify areas on the structure where corrosion is most likely to occur.

Typically, for buried pipelines, the most common method used to mitigate external corrosion is the combination of protective coating and CP and, to achieve effective external corrosion mitigation, a balance between the coating condition and the level of CP should be established. CIS provides very useful information to corrosion engineers when trying to establish the balance between the coating condition and the CP, as it not only provides information about the CP level, but it is also capable of identifying areas where significant coating damage may exist on the buried structure.

Aligning data from CIS with the location of external metal loss sites along the pipeline may be valuable to pipeline operations; locations of external metal sites may be obtained from in-line inspections (ILI) and/or excavations; the combined analysis of these data will provide pipeline operators relevant information for implementing short-term remedial actions to reduce the probability of a leak or rupture due to external corrosion, and it will also provide information to develop mid- and long-term plans to effectively mitigate external corrosion.

The purpose of a CIS, when conducted over a structure with CP applied, is to obtain a representative series of potentials throughout a structure to evaluate criteria for adequate CP, to identify local deficiencies in a CP system, to assist in identifying the cause(s) of such deficiencies, and to aid in determining remedial actions to enhance the level of CP. The purpose of a CIS when conducted over a structure without CP is to identify areas that may be corroding, referred to as 'hot-spots,' and also to identify possible interference from other structures with CP. The CIS obtains structure-to-electrolyte potentials at relatively short intervals along the structure, such as 1 m (3-ft), 1.5 m (5-ft), and 3 m (10-ft).

Structure-to-electrolyte potential measurements are taken for many different purposes, such as testing for the following[1]:

- confirming compliance with adequate CP criteria
- electrical isolation of the structure
- electrical continuity
- shielding
- stray current
- evaluation of coating condition.

Because structure-to-electrolyte potential measurement is the main element of a CIS, it is important to understand the principles.

A structure-to-electrolyte potential is commonly referred to as a structure-to-soil or pipe-to-soil potential. According to NACE SP0207-2007,[2] the definition of a structure-to-electrolyte potential is: the potential difference between the surface of a buried or submerged structure and the electrolyte that is measured with reference to an electrode in contact with the electrolyte (see Fig. 8.1).

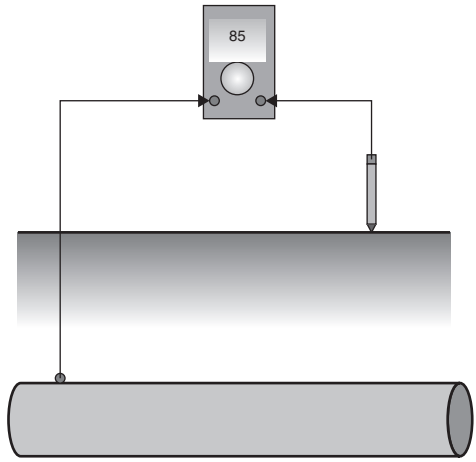

8.1 CIPS configuration.

8.2 Equipment

The basic equipment required to measure a structure-to-electrolyte potential are[3]:

- voltmeter
- reference electrode
- electrical connections.

A voltmeter is required to measure the potential difference between the structure and the electrolyte accurately, typically ±1 mV. To minimize errors caused by contact resistance, and other errors in the measurement circuit, the voltmeter should have a high input impedance; typical specifications for soil application may require 10 MΩ or greater. When the number of structure-to-electrolyte potentials to be measured and recorded is large, the use of a field data-logger[4] is recommended, as it will facilitate data post-processing and will reduce or minimize data handling errors. Examples of voltmeters and data-loggers used for CIS are presented in Fig. 8.2.

These voltmeters usually have one terminal designated 'common' (COM), and is either black or has a negative (–) symbol. The positive terminal is either red or has a positive (+) symbol. The positive and negative symbols in the meter display indicate the current direction through the instrument.

According to NACE SP0207-2007,[2] the definition of a reference electrode is: an electrode whose open-circuit potential is constant under similar conditions of measurement, which is used for measuring the relative potentials of other electrodes. The reference electrode is required to measure the potential of the structure/electrolyte half-cell versus a stable reference potential, the reference electrode. Examples of reference

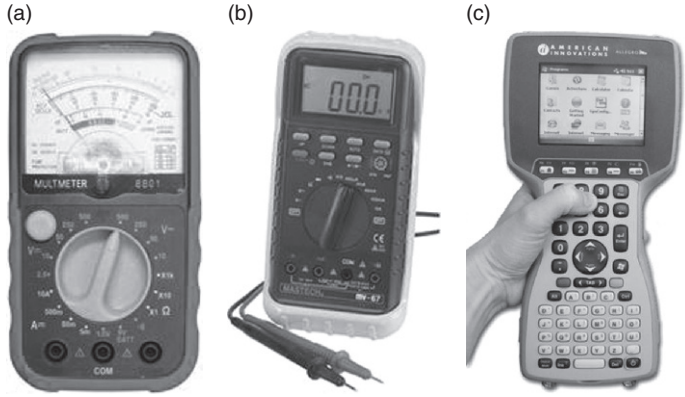

8.2 Examples of voltmeters and data-logger (a) analog (b) digital (c) data-logger.

electrodes used when conducting CIS are saturated copper/copper sulfate (CSE) and silver/silver chloride (Ag/AgCl). The components of a CSE are presented in Fig. 8.3.

Reference electrodes should be calibrated periodically with respect to a master reference electrode (MRE) to ensure desired accuracy. An MRE is typically an uncontaminated reference electrode used only for calibration purposes. The accuracy of a field reference electrode can be verified by placing it with the MRE in a common solution such as fresh water, and measuring the voltage difference between the two electrodes. A maximum voltage difference of 5 mV[3] between an MRE and another reference electrode of the same type is usually satisfactory for pipeline potential measurements.

Electrical connections are required to complete the structure-to-electrolyte potential measurement circuit. Insulated test leads are normally used to connect the reference electrode to a terminal of the voltmeter. It is common practice to connect the reference electrode to the negative (common 'black, or marked with a negative sign – terminal of the voltmeter) (see Fig. 8.4).

The other terminal of the voltmeter is connected to the structure at test stations, or aboveground features such as valves. It is a common practice to connect the structure to the positive (red) terminal of the voltmeter or data-logger.

When conducting CIS over long pipeline sections, insulated wire spools are used to keep the data-logger connected to the pipe while measuring the potentials (see Fig. 8.5).

Under normal conditions, the structure-to-electrolyte potential of steel buried in soil measured versus a CSE is a negative value when the reference electrode is connected to the negative terminal and the structure to the positive terminal of the voltmeter. The polarity of the structure-to-electrolyte

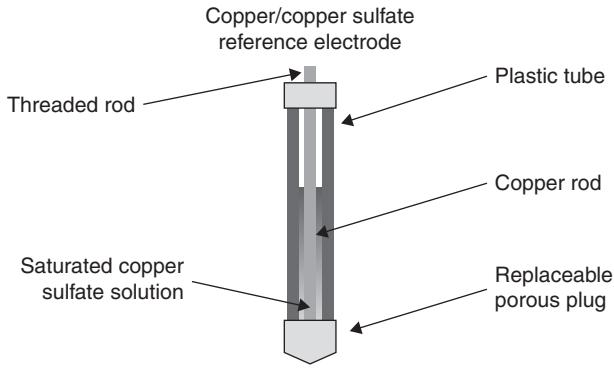

8.3 Components of a copper/copper sulfate reference electrode (CSE).

8.4 Connection of the reference electrode to the black terminal of a CIS data-logger.

(a) (b) (c)

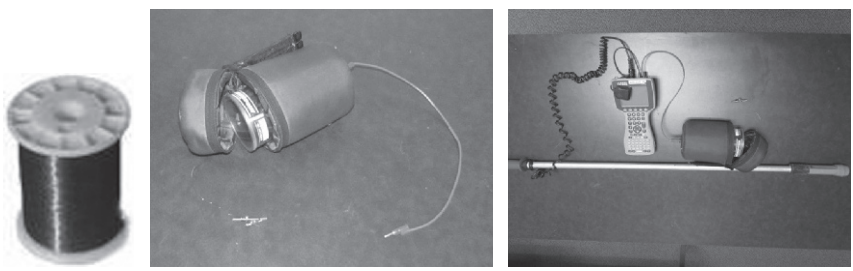

8.5 CIS electrical connections. (a) #34 insulated gauge wire spool; (b) wire dispenser with connection to test station and test lead to connect to data-logger or voltmeter; (c) data-logger connected to CSE reference electrode and wire connection.

potentials is very important when analyzing CIS results; it is important to document the connections to the voltmeter.

8.3 Data collection

All electrical connections should be made so as to establish a low-resistance electrical connection, and should not be made on test leads or wires conducting high current values, such as negative returns of rectifiers, galvanic anodes leads, or bond wires.

Accurate structure-to-electrolyte potential measurements of a buried pipe are made with the reference electrode placed close to the metal/electrolyte interface of the pipe. The common practice, however, is to place the reference electrode as close to the pipe as practicable, which is usually at grade above the centerline of the pipe (see Fig. 8.6).

The pipe-to-soil potential measurement value obtained from the configuration shown in Fig. 8.6 includes the following voltage drops across:

- voltmeter
- test leads
- reference electrode
- electrolyte
- coating, if applied
- pipe; and
- pipe surface/electrolyte interface.

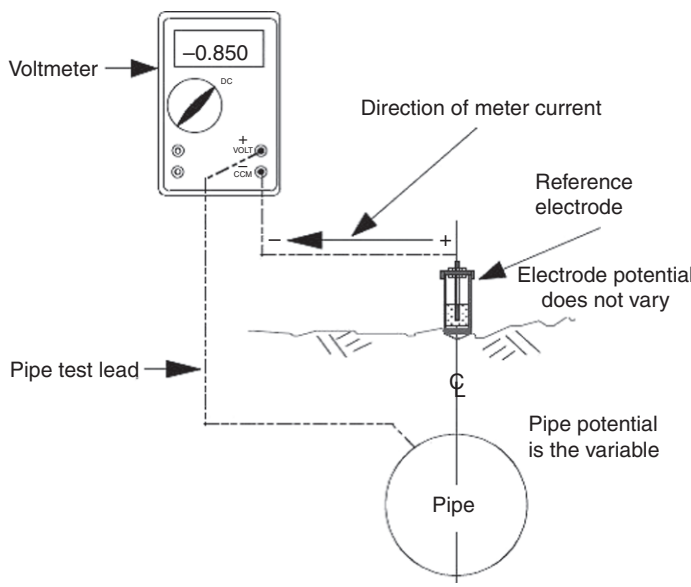

8.6 Pipe-to-soil potential measurement configuration.[5]

NACE International adequate CP criteria established in SP0169-2007[6] indicates that external corrosion control can be achieved at various levels of cathodic polarization depending on environmental conditions. External corrosion control for buried steel or cast iron piping is obtained when a negative (cathodic) potential of at least 850 mV with respect to a CSE contacting the electrolyte is obtained. Voltage drops other than those across the structure-to-electrolyte boundary, normally referenced as IR drop, must be considered for valid interpretation of this voltage measurement.

8.3.1 IR drop consideration

The most common method used to minimize IR drop during CIS is the use of synchronized current interrupters installed at influencing CP current sources. Other methods include the use of CP coupons and step-wise current reduction, but are usually not practical except at discrete locations. All components of IR drop result from current in a resistive path. The true polarization of the pipeline can be measured if all currents are instantaneously interrupted. In practice, these conditions are rarely achieved; however, the error can be minimized to obtain sufficiently accurate measurements. Often, there is current that affects the potential measurements that is not a result of the CP system. Sufficient influencing current must be interrupted to measure potentials to the desired accuracy.

Current interrupters are devices used to temporarily open the CP circuit. Typically, close to zero IR drop is achieved by temporarily interrupting the current and instantly reading the structure-to-electrolyte potential, normally referred to as the 'Instant Off' pipe-to-soil potential. This potential should be read quickly, since the structure will begin to depolarize with time. Fig. 8.7 shows an example of a current interrupter.

Current interrupters are essentially a mechanical or electronic relay connected to a very precise chronometer, normally Global Positioning System (GPS). Multiple units can be synchronized to cycle in unison, allowing multiple current sources to be interrupted, effectively removing known influencing current from the structure at the same time. With no current, the IR drops are minimized and the Instant Off potential measured could be considered the polarized potential of the pipeline, and may be compared to criteria for adequate CP.

When minimizing IR drops using current interrupters, the following should be considered:

Influencing DC Sources: Pipe-to-electrolyte potential measurements may be affected by several different types of current sources. These may be, but are not limited to, the CP systems of the pipeline company that are not in contention with the subject pipeline; CP systems of foreign pipelines causing stray current on the subject pipeline; DC light rail crossings; and high

8.7 GPS synchronized current interrupter.

voltage DC transmission lines not properly grounded, which also could affect the potentials. All of these current sources should be accounted for when performing the survey, to obtain accurate pipe-to-soil potentials. If the foreign currents cannot be properly interrupted it should be noted, as it may change the priority of any anomaly found in the area of influence of the foreign current.

Long-line, or telluric currents can cause currents along the pipeline. These currents cannot be interrupted and may be measured by indirect methods, such as measuring and comparing near ground (NG) and far ground (FG) potentials, and IR voltage drops between consecutive test stations.

Synchronization: As previously mentioned, all current sources must be interrupted simultaneously and in synchronization to obtain an IR drop free pipe-to-soil potential for a given location on a pipeline.

Interference Bonds: An 'interference bond' is defined as an intentional metallic connection between metallic structures in contact with a common electrolyte and designed to control electrical current interchange between the systems. The interference bond can either be draining current to a foreign pipeline (non-critical) or receiving current from the foreign pipeline (critical). In either case, this will affect the pipe-to-soil potential measurements. As such, all current sources affecting the location of the bonds to the pipeline should be synchronously interrupted with all other current sources that may affect the pipeline.

Valid structure-to-electrolyte potential measurements require proper reference electrode placement and contact with the electrolyte. Acceptable

reference electrode placement from the center line of the pipeline depends on the depth of burial, the diameter of the pipeline, and the desired accuracy. A typical specification may allow a deviation of no more than one pipe diameter from the center line of the pipeline. Locating and temporarily marking the position of a pipeline is required prior to conducting a CIS in order to follow the pipeline route and minimize IR drops. Personnel performing pipe location and marking should review alignment drawings so that they can identify changes in directions, pipeline crossings, and other features before locating the pipeline.

8.4 Conducting a CIS

A safe and successful CIS depends on well-performed pre-survey activities. Before conducting a CIS, the following activities may be considered:

- Type of survey, survey interval (maximum space between consecutive reads).
- Pipeline name(s)/number(s), pipeline diameter and wall thickness.
- Construction practice (welded, couplings), age of the pipeline.
- Pipeline system maps and pipeline alignment sheets.
- Existence and location of water body crossings.
- Paved areas, depth of cover.
- Location of cased crossings.
- Type of coating (pipe and joints).
- Product being transported and the direction of flow.
- Location, topography.
- Start and end engineering station numbers.
- Company procedures, equipment availability, calibration, consumables (wire, reference electrodes, flags, marking paint, first aid kits, vehicles, maps).
- Qualification requirements, equipment calibration.
- CP data: type, location, and operating conditions of DC sources (influencing).
- Location of test stations, electrical isolation devices, bonds.
- Location of underground metallic structures in close proximity of the pipeline to be surveyed.
- Location of foreign CP sources, AC mitigation systems, parallel overhead power lines.
- Landowner information, permits requirements, access point to the right-of-way.
- Prior CP data: annual test point survey data, prior aboveground survey data.

Precautions:

- Measure the voltage between the rectifier case and ground before touching the case.
- Open the case expecting to find biting insects, rodents, or snakes.
- Inspect rectifiers for abnormal sounds, temperature, or odors.
- Document and report the abnormal conditions found.
- Switch off the AC voltage supply before installing a current interrupter or each time the taps are adjusted.
- Ensure all connections are well adjusted, and secure any exposed electrical terminals in a locked container when the rectifier is not attended.
- Measure structure AC voltage-to-ground on the pipeline before taking DC structure-to-electrolyte measurements. If the AC voltage-to-ground is equal to or greater than 15 VAC (Alternating Current Volts), practice safety measures detailed in company procedures and follow guidelines detailed in NACE Standard SP0177.[7]
- Take AC structure-to-ground voltage readings at frequent intervals when working near high-voltage AC (HVAC) power lines.
- Do not work on the structure when there are lightning and/or thunderstorms in, or close to, the survey area to avoid potential shocks.

When conducting a CIS, the following activities may be considered:

- Verify that the structure has been properly located, and verify the condition of the right-of-way (see Fig. 8.8).
- Check the operating condition of the CP system before, during, and after the CIS; this may be accomplished by setting a stationary data-logger at a test station located within the survey segment. See Fig. 8.9 for an example of a stationary data-log of an interrupted CIS.
- Wire gauge, color, label, and terminal identification number should be recorded when multiple wires are found at a test station (see Fig. 8.10).
- The interruption cycle of the DC current sources should be defined to avoid depolarization of the structure, capture valid data, and allow for an acceptable survey speed. It is a good practice to use an interruption cycle where the On period (closed cycle) is three times the Off period (open cycle).
- It is a good practice to verify the synchronization of the current interrupters before recording data during the survey and after completing the CIS; this may be accomplished by capturing waveforms before, during, and after completing the survey. Figure 8.11 shows the start of a survey waveform.

8.8 Pipeline right-of-way in good condition for CIS.

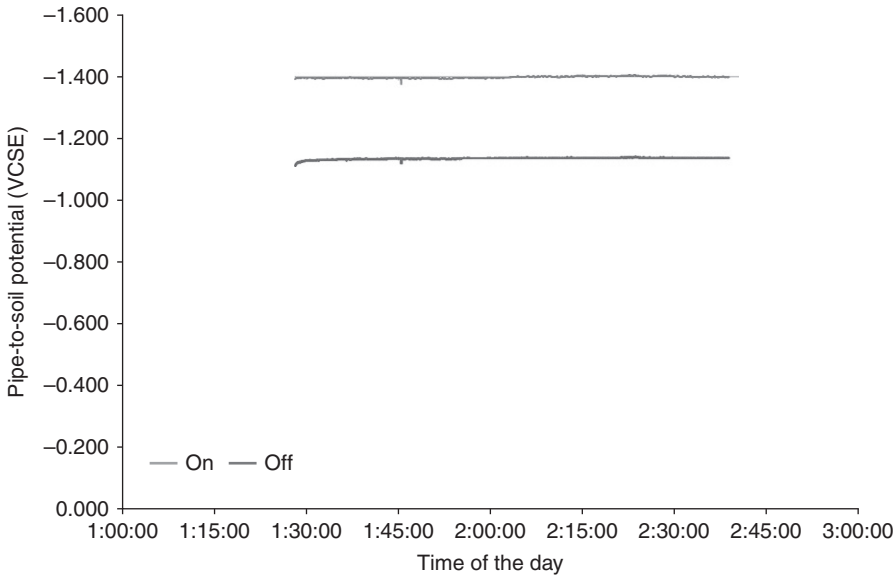

8.9 Interrupted CIS stationary data log.

- Modern CIS data-loggers have the ability to set a time delay for capturing the pipe-to-soil potentials (On and Instant Off). This allows pipe-to-soil potentials to be recorded away from the anodic or cathodic 'spikes' associated with the interruption of the CP system.

  Analysis of the waveform allows for proper determination of the time delay required for proper data collection. Figure 8.12 shows the spike phenomena and the time delay determination.

8.10 Multiple wire pipeline test station.

If the goal of a CIS is to evaluate the CP level of a pipeline section, the entire length of the sections should be surveyed. The survey direction should be documented and reported. It may be reported as either an upstream or downstream direction survey. The location of aboveground reference points, locating marks, and pipeline appurtenances should be recorded on a field book or data-logger. A sample of data that should be recorded when conducting a CIS is presented below:

- Pipeline operation and location name.
- Line identification and size.
- Start point, connection point, and type (test station, valve, riser) of connection point to the pipeline.
- Weather conditions (temperature, rain/sunny day, terrain condition).
- Technician identification; equipment used, including serial number and calibration records.
- Reference electrode daily calibration; identification of MRE.
- NG, FG, and IR drop at test stations; the comparison of the NG, FG, and IR drop between tests stations will help determine possible current on the pipe when the CP system is switched off; some companies define threshold values for maximum IR drop between test stations before stopping the survey.
- Current and polarity at bonds.
- AC potentials at test station and other pipeline appurtenances.

In terms of CIS data processing, the following activities may be considered after completing a survey day:

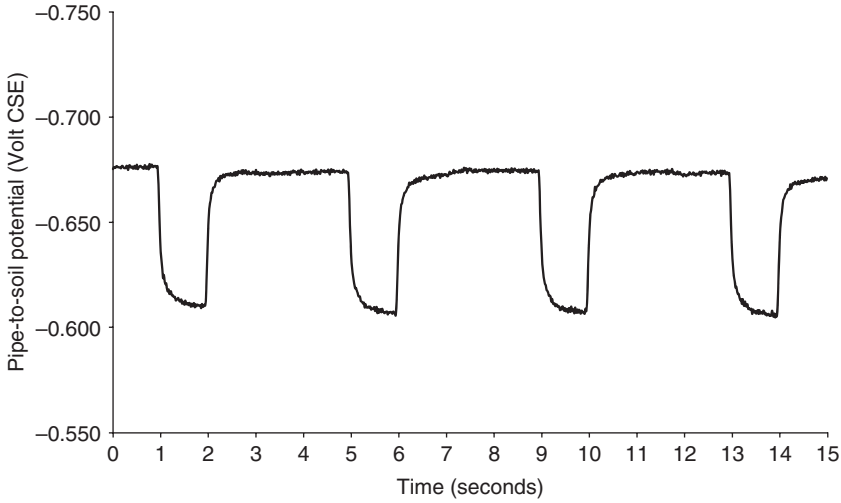

8.11 Waveform captured at the start of the day.

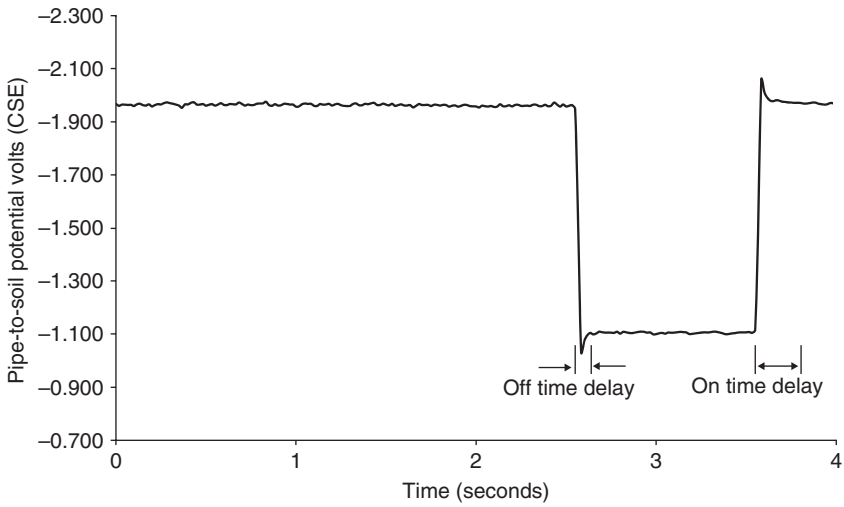

8.12 Anodic and cathodic spike phenomena associated with CP current interruption.

- Review CIS data after completion of the survey to ensure that their validity is not compromised by any of the factors that may invalidate the data (presented in the section CIS data validation) or any other that may invalidate the survey data.
- Any survey section with invalid data may require re-survey.
- Before re-surveying a section, the origin of the data invalidation should be identified and corrected to avoid additional re-survey.

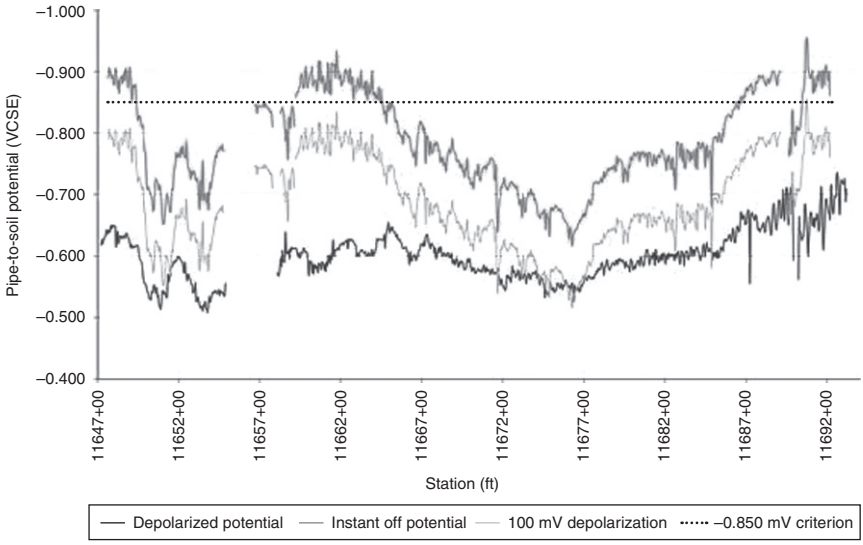

8.13 Interrupted and depolarized CIS plot.

- The data from the CIS and stationary loggers should be uploaded to ensure that data associated with the survey day are complete.
- Waveforms should also be uploaded to document proper current interrupter synchronization.
- Compare the survey station number of key features with the station numbers on the alignment sheet.
- The survey data should be plotted for post-job analysis. An interrupted and depolarized CIS plot is presented in Fig. 8.13.

8.5 CIS data validation

The following factors may generate invalid CIS data:

- missing data
- improper stationing or distance measurement
- no connection to the structure (an open circuit in the measurement circuit, such as a broken test lead, voltmeter lead, unknown isolating devices, or lack of electrical continuity along the pipeline)
- connection to the wrong structure
- improper line location or reference electrode placement
- excessive scatter or high-contact resistance
- inaccurate or improperly calibrated reference electrodes or voltmeter
- broken wires/high-resistance electrical connections
- inadequate wire insulation or electrical short circuits

- improper/inadequate IR drop correction and high-induced AC potentials
- structure depolarization
- changing operating conditions of CP current sources.

Other causes of measurement error are listed in Section 8.6 of NACE Standard TM0497.[8]

8.6 Assessing results

As defined in the Introduction, a CIPS is a series of structure-to-electrolyte DC potential measurements performed at regular intervals to evaluate the level of polarization on buried or submerged structures such as steel pipelines. From the results of the CIS plotted in Fig. 8.13, areas that do not meet NACE criterion of a negative (cathodic) potential of at least 850 mV with respect to a CSE may be identified (Instant Off Potential less negative (below the –0.85 V line) than –0.85 V CSE. Other criteria, such as the 100 mV of polarization, may be verified visually when the data are plotted and compared (in Fig. 8.13 areas where the 100 mV depolarization line is less negative than depolarized potential do not meet the 100 mV polarization criteria).

Areas of damaged coating may also be identified when CIS data is plotted. Typically, coating damage may be identified when the On and Instant Off potentials converge and the IR drop between them is reduced. Figure 8.14 shows examples of possible coating damage identified by CIS.

Another assessment performed using CIS data is identification of areas with CP overprotection. Typically cathodic overprotection is defined when polarized pipe-to-soil potentials are more negative than –1.2 V. At this CP level there are at least two possible detrimental effects. The first is known as cathodic disbondment; high CP levels are associated with generation of an environment with high pH (10–11), which accelerates the degradation of the coating. As the coating degrades, more CP current is required for achieving adequate CP. Adding additional CP also may increase areas with overprotection, which in turn will even further accelerate the coating degradation. Without proper mitigation this phenomenon may significantly reduce the protective life of the coating.

The second detrimental effect is the possibility of hydrogen induced cracking. The electrochemical reaction normally occurring at these areas of overprotection is hydrogen evolution; atomic hydrogen may migrate into the steel structure of the pipe at these locations and then form hydrogen molecules at defects on the pipe (vacancies, pores, etc.). This phenomenon generates stresses on the pipe that may induce formation of cracks, which under certain conditions may propagate and conduce to a pipe rupture or failure. Figure 8.15 shows overprotection areas identified by CIS.

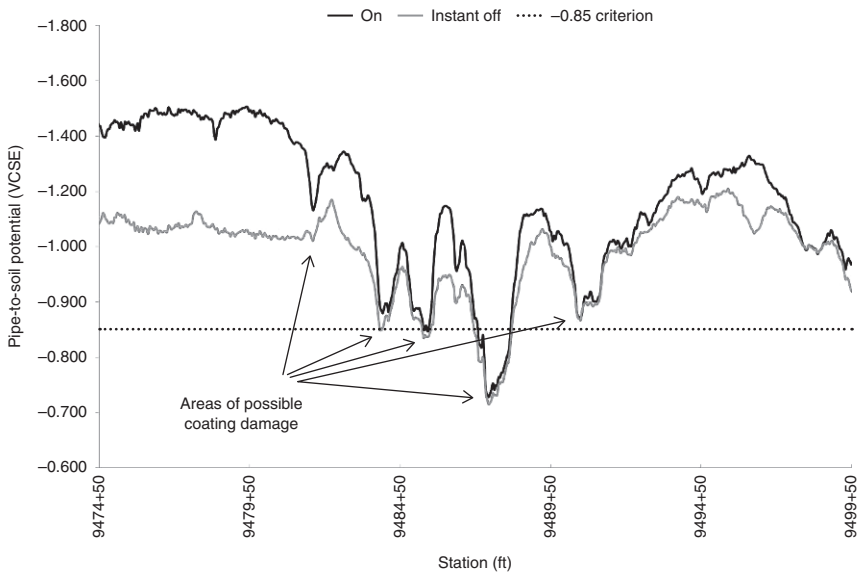

8.14 CIS plot indicating possible areas with coating damage.

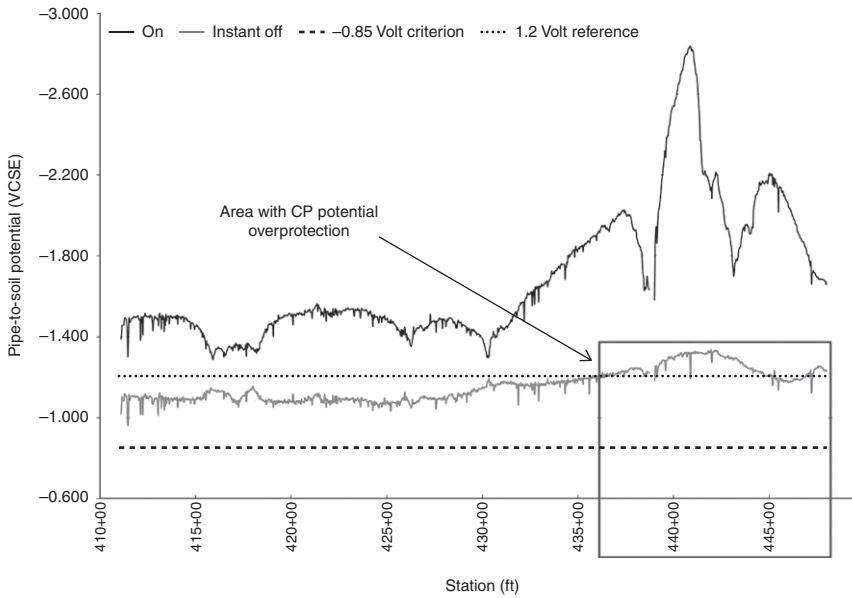

8.15 CIS plot indicating areas with CP overprotection.

CIS data may be aligned and integrated with data from other aboveground survey tools and used as part of a pipeline integrity assessment tool. NACE Standard SP0502[9] provides guidelines for implementing the external corrosion

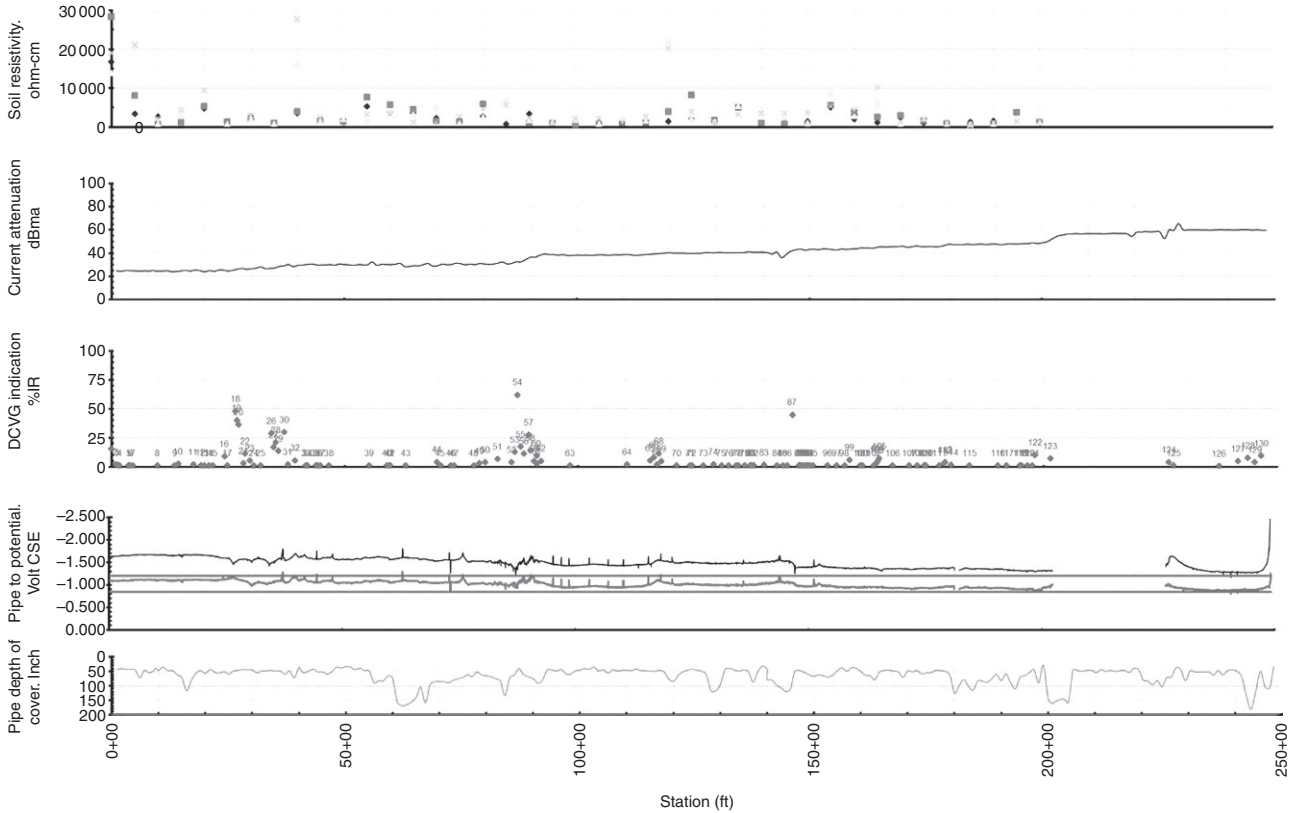

8.16 ECDA-aligned data plot including CIS data.

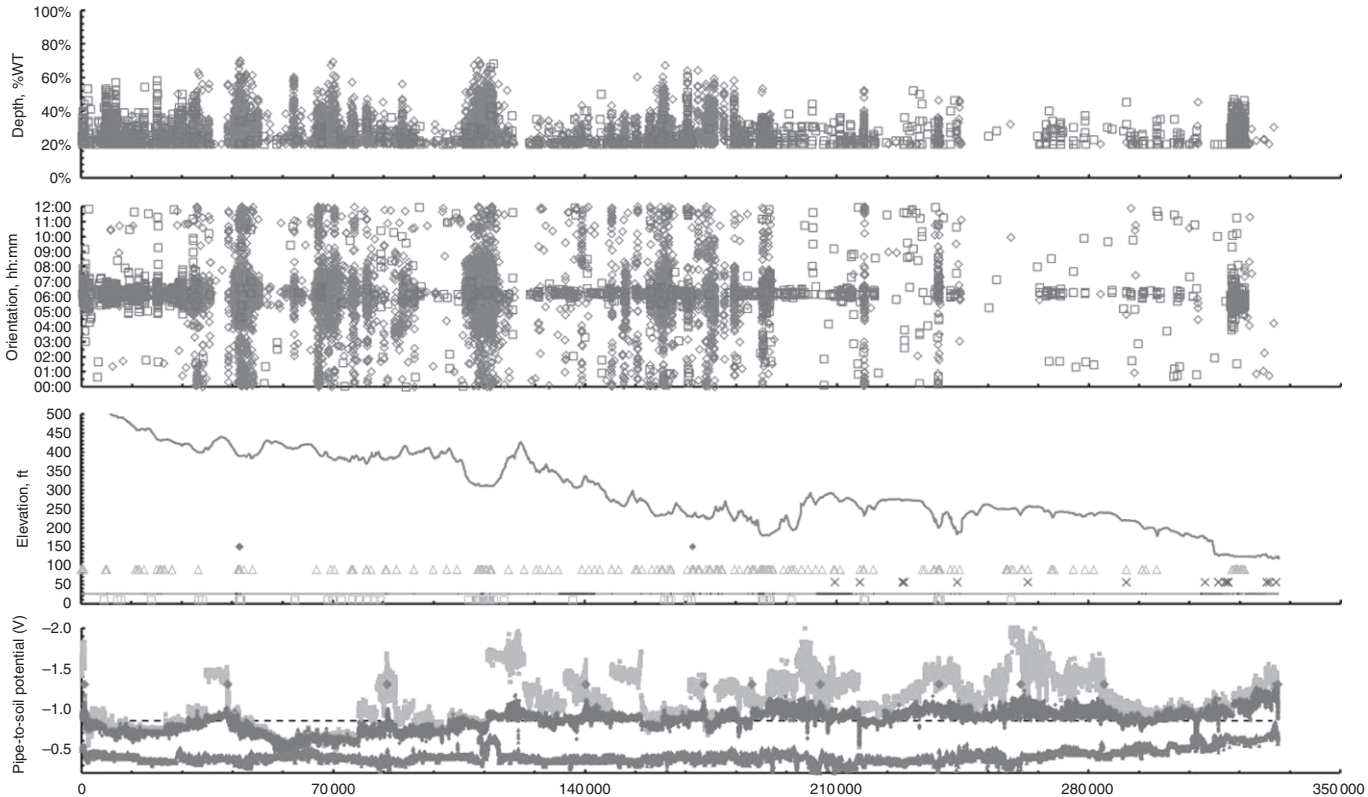

8.17 CIS and ILI data aligned.

direct assessment (ECDA) methodology which may be used to evaluate the impact of external corrosion on the mechanical integrity of buried pipelines. The use of CIS combined with other coating evaluation tools is part of the ECDA process, which allows the prioritization of coating anomalies (referenced as 'indications') based on the likelihood of current and past corrosion activity. Figure 8.16 shows an ECDA-aligned data plot that includes CIS data.

CIS data may also be aligned and integrated with data from other integrity assessment tools, such as ILI and pressure testing, to provide a more comprehensive mitigation plan. Aligning CIS and CP historical data with other above-ground survey data may identify the engineering root cause of external corrosion which, when coupled with ILI data, provides relevant information for developing short-, mid- and long-term plans to effectively mitigate external corrosion. Repair and rehabilitation will focus not only on areas where remaining wall thickness of the pipe poses a threat to the safe operation (short-term mitigation), but also on areas where additional CP may be needed (mid-term) and areas where coating repairs may be required (long term). Figure 8.17 shows CIS data aligned ILI data.

8.7 Summary of CIS benefits and disadvantages

CIS has many benefits, some of which are listed below:

- It identifies areas of inadequate CP or excessive polarization.
- It provides a continuous pipe-to-soil potential profile of the pipeline.
- It may locate anomalies in the coating, which are commonly validated by a secondary tool.
- It may locate areas of stray electrical current pickup or discharge.
- It may identify metallic structures such as casings directly connected (shorted) to the pipeline.
- It may detect unintended contact with other metallic structures.
- It tests the CP current demand and distribution along the pipeline.
- It may locate and prioritize areas more likely to experience metal loss due to external corrosion.

Some disadvantages of CIS are listed below:

- It is labor intensive; it requires the entire length of the survey segment to be walked.
- It requires that all land owners/occupants be notified prior to commencing the survey.
- It cannot be easily used over roads, paved areas, concrete, and rivers. Drilling holes may be required

- It does not indicate the severity of external metal loss.
- It is unlikely to indicate disbonded coating.
- Results may be affected by other metallic structures in close proximity of the target pipeline.

8.8 Future trends

CIS future trends will most likely be driven by innovation in technology. One present limitation being worked on is the need to have a direct connection to the pipeline and the reference electrode. Future surveys will most likely be conducted using wireless connection to the pipelines and the reference electrodes. Future data processing and data integration will also dictate future trends. Future field data-loggers will most likely transmit data in real-time, and smart software will integrate CIS and other survey tool data to identify areas where external corrosion may pose a threat to the safe operation of a pipeline.

8.9 References

1. ASM Handbook (2006), Volume 13 C, Corrosion: Environments and Industries.
2. NACE SP 0207 'Performing Close-Internal Potential Surveys and DC Surface Potential Gradient Surveys on Buried or Submerged Metallic Pipelines'.
3. Cathodic Protection Survey Procedures, W. Brian Holtsbaum, NACE.
4. Appalachian Underground Corrosion Short Course, Advanced Course, West Virginia University, Morgantown. W. Va.
5. Peabody's Control of Pipeline Corrosion (2001), Second Edition, A.W. Peabody, Edited by R.L. Bianchetti, NACE International.
6. SP0169-2007, 'Control of External Corrosion on Underground or Submerged Metallic Piping Systems'.
7. NACE SP0177 'Mitigation of Alternating Current and Lightning Effects on Metallic Structures and Corrosion Control Systems'.
8. NACE TM0497 'Measurements Techniques Related to Criteria for Cathodic Protection on Underground or Submerged Metallic Piping Systems'.
9. NACE SP 0502 'Pipeline External Corrosion Direct Assessment Methodology'.

9

The Pearson survey method for detecting corrosion in underground pipelines

D. EYRE, Penspen Limited, UK

DOI: 10.1533/9780857099266.2.247

Abstract: The Pearson survey is the oldest above-ground survey technique for finding coating holidays (or defects) on buried pipelines. The technique was first developed in the early 1940s. The chapter describes the technique, the equipment and recent developments in the equipment used for the survey. It discusses the advantages and disadvantages of this technique over similar above-ground pipeline coating and cathodic protection related survey techniques. Although other techniques have become more popular, it is still one of the easiest to carry out and, as such, is still in common use.

Key words: buried pipeline coating holidays, above-ground survey technique, AC audio frequency.

9.1 Introduction

The coating on a pipeline is the primary corrosion-protection barrier; the cathodic protection system, where applied, supplements and complements the coating, providing corrosion protection at coating holidays (or defects). It was recognised early on that a technique for assessing the condition of the pipeline coating was needed. This would enable ongoing corrosion to be detected, and coating repairs or rehabilitation to be carried out.

The Pearson survey is a technique for finding coating holidays on pipelines. It was named after JM Pearson, the engineer who developed it in 1941 (Pearson, 1941). As such, it is one of the oldest over-the-line survey techniques used by corrosion engineers to assess the condition of the pipeline corrosion-protection system.

9.2 Key principles of the Pearson survey technique

Although the equipment has evolved over the years, the principles of the technique remain the same. An AC signal in the audio frequency range is imposed on the pipeline. This is achieved using a transmitter and an earth

pin. The transmitter is connected to the pipeline at a convenient location, typically a cathodic protection test post. One terminal is connected by cable to the test point and the other is connected to the earth pin. The earth pin is pushed into the ground, typically up to 30 m from the pipeline. Alternatively, a secondary metallic structure not connected to the pipeline can be used as an earth, e.g. sheet piling.

The transmitter has a variable output voltage, which enables the surveyor to adjust the impedance of the circuit. Generally speaking, poorly coated pipelines require a low voltage; well-coated pipelines require a higher voltage. The transmitter is energised, adjusted, and the pipeline route is then traversed by two surveyors equipped with ground contacts and a receiver held by one of the surveyors. The receiver is adjusted until the base line signal is just audible. The gain on the receiver is gradually increased as the surveyors move away from the transmitter to compensate for signal attenuation. Whilst some AC will leak through the coating, substantial amounts will only leak through holidays, and the leaking current causes a change in the voltage gradient in the soil around the pipe. This change in voltage gradient is detected by the earth contacts and receiver.

The basic survey technique is illustrated in Fig. 9.1. The two surveyors walk approximately 7 m apart, as in Fig. 9.2. The earth contacts are usually metal

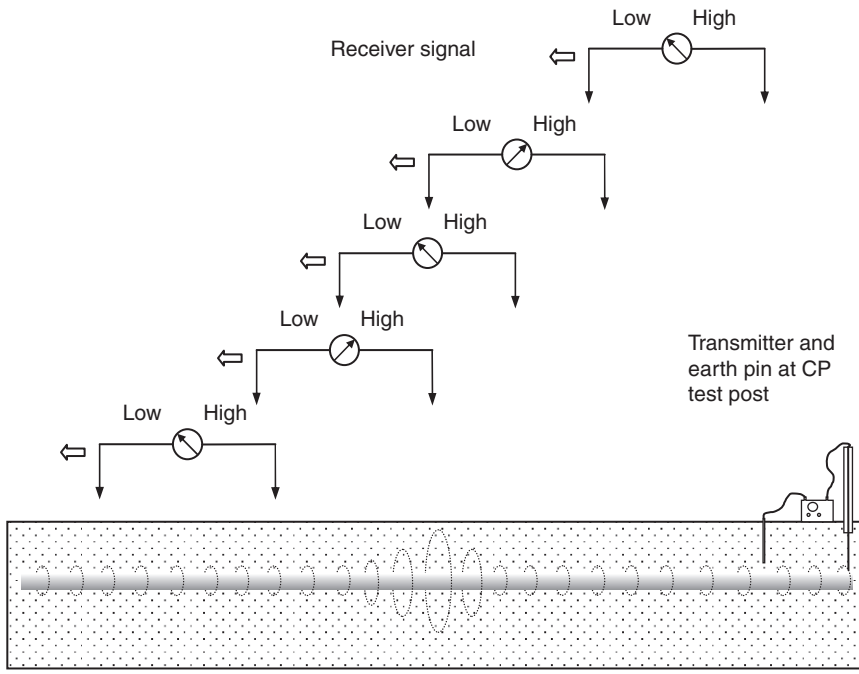

9.1 Diagram showing the basic principles of the Pearson survey technique.

9.2 The Pearson survey technique in practice. (Courtesy Tinker & Rasor.)

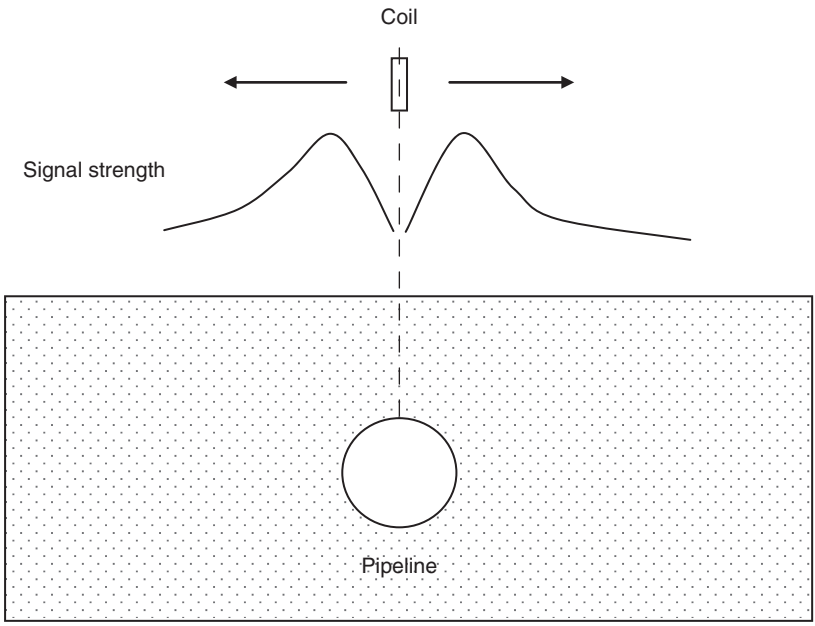

9.3 The null method of pipeline location using the coil in the Pearson equipment receiver.

cleats attached to each surveyor's boots. The cleats are connected by insulated cable to the receiver. One set of cleats acts as a reference to the other set. As the leading surveyor walks over a coating holiday, the receiver detects an increase in the signal, which is repeated as the second surveyor walks over the coating holiday. The location of the defect is then marked for later excavation.

The surveyors should walk more or less along the centre line of the pipeline. To enable the lead surveyor to locate the pipe, the receiver is equipped with a coil. This picks up the AC signal from the pipe by capacitive coupling, which enables the pipe to be located. By moving the receiver and coil over

the pipe at right angles, the signal picked up by the coil peaks either side of the pipeline with a null point on the centre line, as shown in Fig. 9.3.

If there is a series of coating holidays in close proximity the signals can be confusing, as each set of cleats will detect peaks as they pass over the holidays. Under these circumstances, the lead surveyor remains on the centreline of the pipeline but the second surveyor moves to a position at right angles to the pipe, some 7 m from the pipeline. The pair then traverse the section of pipeline, with the second surveyor walking in parallel to the lead surveyor. This enables the conflicting signals from the multiple coating holidays to be isolated from one another, and for each location to be marked for later excavation.

When surveying a pipeline with a good coating, several kilometres can be surveyed in either direction from the transmitter. When the signal is lost by the survey team the transmitter is relocated, enabling the next section to be surveyed. The distance which can be surveyed from a single transmitter location reduces with reduction in coating quality (low coating resistance). More frequent relocation of the transmitter is required under these conditions than on a pipeline with a high quality coating (high coating resistance).

The equipment can be used to detect shorts on the pipeline to other foreign services or other buried metallic structures. These are usually undesirable, because they will drain current from the cathodic protection system, thereby possibly compromising the level of protection afforded the pipeline by the cathodic protection system. The audio signal is impressed on the pipeline in the usual way, and the pipeline is traversed using the search coil.

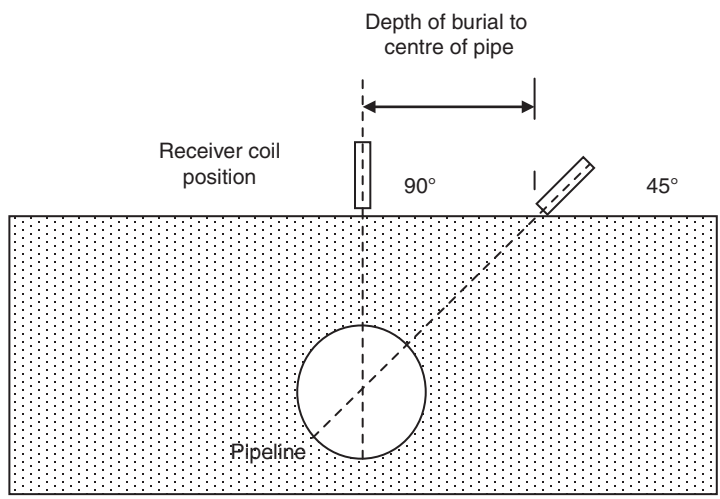

9.4 Depth measurement using receiver coil.

A short or contact with another structure is found where the average signal drops to a very low level.

The coil can also be used to establish the depth of burial of the pipeline. This may be built into the receiver, or sometimes an external coil is used, with the depth measured by triangulation as shown in Fig. 9.4. The centre line of the pipe is found first using the null method and its position marked; then, holding the receiver coil at 45° just above ground level, a second null is found orthogonal to the pipe, and this is also marked. The depth to the centre of the pipe is given by the separation between the two marks. Half the diameter of the pipe needs to be subtracted from this measurement to derive the depth of burial.

9.3 Advantages and disadvantages over other survey techniques

This survey technique is a coating survey only, and so can be used to find coating holidays. The survey itself gives no information on the effectiveness of the cathodic protection (CP) system, or whether there is any ongoing corrosion at any coating defects. The subsequent excavation and inspection of coating holidays allows the cathodic protection system performance and any ongoing corrosion to be assessed.

The entire pipeline section being surveyed is walked. For an operating pipeline this doubles as a right-of-way inspection. Progress depends on terrain and coating quality; if the coating quality is poor then the transmitted signal attenuates rapidly, requiring frequent repositioning of the transmitter. Also, with many coating defects the surveyors spend more time locating and marking each holiday. Progress can therefore vary from a ~5 km/day to ~10 km/day.

The equipment is easy to use and does not require a great deal of instruction in its correct use. However, the quality of the survey results does to some extent depend on the experience and interpretation of the lead surveyor. An experienced user can provide a subjective sizing of the coating holiday. It is subjective because the voltage gradient detected by the equipment will depend not only on the size of the coating holiday but also on the soil resistivity. The size of the signal will also depend on the receiver settings. In common with other pipeline coating survey techniques, it will not detect a disbonded coating unless a coating holiday is associated with the disbondment and there is metal-to-soil contact.

The equipment is very sensitive and may not distinguish between a coating defect and extraneous metal such as spent welding rods in the backfill surrounding the pipeline. The signal picked up by the equipment may also be adversely affected when in proximity to overhead power lines, although this does depend to some extent on the design of the equipment. In common with other survey techniques, it has reduced sensitivity in tarmac or

concreted areas, where capacitive coupling must be used instead of earth contact.

Obtaining a satisfactory earth contact can also be a problem in arid/desert areas. This is a problem not only for the transmitter but also the earth contacts for the receiver. The latter can be addressed by wetting the right of way using a water tanker ahead of the surveyors. This technique is commonly used for other types of survey such as direct current voltage gradient (DCVG) and close interval potential survey (CIPS), both of which suffer similar high resistance contact problems. The cathodic protection groundbed can be used as a good earth for the transmitter Alternatively, a 6 inch augered hole offset from each cathodic protection test post, 2 m deep and filled with bentonite installed during construction of the pipeline, provides an ideal method of achieving a reasonable earth for the transmitter.

The traditional survey technique requires two people and has in recent years become less popular than other survey techniques, such as DCVG, which can be carried out by a single surveyor and has the ability to more accurately size coating holidays than can a Pearson survey. The Pearson survey, however, remains popular with pipeline construction contractors as a means of checking the installed quality of the pipeline coating. On a new pipeline, the survey is relatively quick, does not require a high degree of skill, and enables the contractor to find and repair defects after backfilling but before full reinstatement, whilst equipment and personnel are fully mobilised rather than at a later date when the right of way has been fully reinstated. The pipeline owner may well require a DCVG survey and CIPS within 12 months of construction to ensure that the contractor fixes as many coating holidays as possible, but there is a clear benefit to the contractor if he carries out a Pearson survey shortly after backfilling before final commissioning of the pipeline, as excavation and coating repair are easier on the non-operating pipeline which has not been fully reinstated.

9.4 Basic equipment used for the Pearson survey

The basic equipment is shown in Fig. 9.5 (courtesy of http://www.tinkerrasor.com) and includes:

- transmitter
- receiver
- headphones
- shoe cleats
- connecting cables
- terminal boards.

9.5 Basic equipment used for the Pearson survey. (*Source*: courtesy of http://www.tinker-rasor.com.)

The whole is usually contained in a carrying case.

The modern transmitter contains a transistor circuit that converts low voltage DC to audio frequency AC. Early versions operated at around 1000 Hz; modern equipment often has two operating frequencies, a high frequency 750 or 925 Hz and a lower frequency 175 Hz, and some units even go as low as 4 Hz. The frequencies are chosen so that they are not harmonics of the electrical utility supply frequency 60 or 50 Hz. The lower frequency is used for thin film coatings such as fusion-bonded epoxy, because it has been found to attenuate less than the higher frequency on coatings of this type.

The transmitter may be equipped with internal batteries for low power surveys over small distances, but is usually powered from an external source such as a car battery if a major survey is carried out. With a car battery powering the transmitter, it will have an output around 25 W for a continuous output, somewhat lower for a pulsed output. A pulsed output makes the signal easier to identify when carrying out the survey. The unit usually has a variable voltage output between 2 and 100 V, which may be manually adjusted or automatically adjusted, and allows impedance matching with the pipeline to optimise the signal on the pipeline and to minimise attenuation.

The hand-held receiver is battery powered and contains a high gain amplifier which can be tuned to the frequency being used for the survey. It is equipped with filters to reduce interference from other sources such as overhead power lines. The receiver has an audible tone, which can be heard on a loudspeaker or via headphones plugged into a jack socket on the side of the receiver.

When in use the shoe cleats are strapped to the boots of the surveyors and are wired to a terminal on each surveyor's belt. A connecting cable runs between the surveyors' terminal and then from the lead surveyor's terminal to the receiver. Terminals that become loose cause signal noise and eventually loss of signal. An experienced team will carry a cable terminal repair kit with them, as the cleats are subject to significant physical impact.

9.5 Modern developments of the technique

The earth contact for the receiver does not have to be via cleats. One development uses ski poles; another uses an 'A frame' with pointed earth contacts one metre apart. The A frame allows short surveys in areas of interest to be carried out by a single surveyor. This can be a significant benefit where there is a relatively complex layout of buried pipe which would make it impossible to survey using the traditional method.

The Pearson recording was developed to address the requirement for a written record of the survey (http://www.solutechelectronics.co.uk). A prescriptive integrity management plan called for a Pearson survey every 5 years to monitor the degradation of the coating on a pipeline network. The recording survey was used to provide data to enable comparison between survey results. In its simplest form, the recording is achieved using a datalogger connected to the output of the receiver. A more complicated set-up would use a global positioning system (GPS) as well.

9.6 Conclusion

The Pearson survey is the oldest above-ground survey technique for finding coating holidays on pipelines. Despite being first introduced in 1941, to this day it remains one of a number of techniques that can be used. Although other techniques have become more popular, it is still one of the easiest to carry out and, as such, is still in common use.

9.7 References

Pearson JM, Electrical examination of coatings on buried pipe lines, The Petroleum Engineer, p82, Midyear 1941.

http://www.tinker-rasor.com. The website of Tinker & Rasor a well known manufacturer of Pearson survey equipment and other related equipment.

http://www.solutechelectronics.co.uk. The website of Solutech Electronics, manufacturers of Pearson survey equipment.

10

In-line inspection (ILI) methods for detecting corrosion in underground pipelines

S. BROCKHAUS, M. GINTEN, S. KLEIN, M. TECKERT, O. STAWICKI, D. OEVERMANN and S. MEYER, ROSEN Technology and Research Center GmbH, Germany, and D. STOREY, ROSEN Technology AG, Switzerland

DOI: 10.1533/9780857099266.2.255

Abstract: High pressure steel pipelines are an important part of our infrastructure. A wide range of flaws, such as corrosion or cracking, can affect these pipelines, degrading their integrity and leading to reduced lifetimes, severe ruptures or fatal errors. To ensure safe and economical operation, as well as to prevent failures, periodical assessments of the pipeline integrity are mandatory. In-line inspection (ILI) is accepted as the optimum approach, detecting and qualifying flaws as well as revealing growth rate information of active flaws. This chapter describes diverse measurement principles and associated non-destructive evaluation (NDE) systems for certain flaws to be inspected, while highlighting methods for the detection and characterization of pipeline corrosion. Operational information, data analysis and integrity aspects complete this overview of ILI capabilities.

Key words: pipeline flaws, corrosion, pipeline integrity, in-line inspection (ILI), non-destructive evaluation (NDE).

10.1 Introduction

ILI has been defined as follows:

ILI is the inspection for flaws of an operational pipeline by special equipment that is transported inside the pipeline by the normal flow of the gas or liquid product.

In this definition, a flaw is defined as an unintentional imperfection in the pipe wall; a defect is defined as a flaw that does not meet specified acceptance criteria (ASME B31G, 1991).

All pipelines are designed, built and operated according to a number of standards and codes that are intended to ensure safe and economical operations for long periods of time. Despite this, defects do occur, and to prevent failure some means of periodically assessing the pipeline condition must be used. Although hydrostatic pressure testing offers a possible solution to the revalidation of pipeline integrity, it is relatively expensive, inconvenient and technically deficient in several ways. In particular, the go/no-go nature of a hydrostatic test usually reveals nothing about any actively growing flaw which is of a size that only just survives failure on the day of the test, e.g. active internal or external galvanic corrosion. Such corrosion may grow sufficiently to cause an operational failure in a very short period of time after a hydrostatic pressure test. Consequently, after nearly 50 years of experience by pipeline operators worldwide, the optimum approach to pipeline condition assessment is now widely accepted to be ILI.

Based on NDE methods, ILI has the capability of detecting and quantifying relatively large, sub-critical flaws that exist close to the pipeline's failure limit but which would survive a hydrostatic pressure test. Not only this, ILI can report pipeline flaws, including corrosion, shortly after their initiation when they are still of little or no structural significance to normal pipeline operations. Successive ILI inspections over a number of years can reveal the growth rates of active flaws. Such early detection of flaws, together with calculations of their growth rates, allows the pipeline operator to take prompt corrective actions to reduce or eliminate the threat. The resulting cost savings of this preventative strategy can be enormous.

The last 20 years has witnessed the rapid growth of pipeline integrity management (PIM) as the preferred method of economically maintaining any operating pipeline in a safe and reliable condition. Indeed, in many cases PIM is a compulsory requirement for an operator since it has been set by the regulatory authorities and/or applicable pipeline codes and standards. In simple terms, a PIM system is a huge database of pipeline information that is used in a series of interacting analytical processes. All relevant pipeline data are entered into a single database to permit the collective analysis and interpretation of the entire data set. Typical PIM data relate to all phases of a pipeline's life, including pipeline design, manufacturing, construction, commissioning and operating phases. Satisfying the needs of PIM processes is today the main objective of virtually every ILI survey (API 1163 (2005)).

In operation an ILI tool – sometimes called a 'pig' because of the squealing noise it makes when moving in a pipe – behaves like a simple piston inside the pipeline. Special isolation traps located at each end of the pipeline are used to insert and extract the tool for an inspection operation. Encircled around each tool, sets of flexible polyurethane discs seal it in the pipeline so that the normal flow of gas or liquid product causes the tool to be driven piston-like along the line from one end to the other. As the tool travels, it

inspects the entire pipe wall for structural flaws using an excitation field of magnetic, ultrasonic or other suitable energy, together with special sensors that are constantly held in close contact with the pipe wall.

Because an ILI tool is driven by the normal flow of the pipeline product, there is no need to stop pipeline operations to inspect the line, so throughput can be maintained while an inspection run proceeds. The concept of ILI is familiar to most pipeline engineers, and the technology is applied routinely to detect and size flaws in pipelines throughout the world.

Choosing an appropriate NDE system for a particular pipeline is a critical step in the ILI process. Various inspection techniques can be mounted on an ILI tool, including magnetic flux leakage (MFL), ultrasonic testing (UT), eddy current (EC) and electromagnetic acoustic transducer (EMAT) methods. The NDE method finally chosen depends on the types of flaws to be inspected, with MFL being a common choice for internal and external corrosion and other kinds of metal-loss flaws, such as mechanical gouging.

Regardless of the applied NDE method, the main function of an ILI tool is to perform a defined, precise measurement at the inner surface of the pipe wall and to store this measurement. Since the inspection tool is an autonomous unit without any contact with the outside, it needs its own energy supply to power the on-board computer and other electronic systems.

The motive force for driving the tool forward is supplied by the flowing gas or liquid product, which means the inspection tool moves with the flow. To do this effectively, the tool must be equipped with components which guide and centralize the tool in the pipe. These components also possess sealing capabilities to allow a differential driving pressure to develop between the front and back of the tool. The components may even facilitate a controlled bypass if the product flow is too high for good quality measurements. A distance measurement is performed to pinpoint the location of any features of interest detected in the pipeline. Putting all these tool features together, the design of a typical inspection tool is summarized in Fig. 10.1.

Key components are:

(1) NDE system (MFL in this example).
(2) On-board computer unit and power supply.
(3) Odometer system to measure distance and speed.
(4) Driving element to guide and seal the tool while it is travelling through the line.
(5) Optional active flow control to keep the tool in a specified speed range.

The above components can be found on almost any inspection tool, regardless of the applied NDE method, tool size or the inspection vendor. A tool with a smaller diameter would either maintain its inspection performance by growing in length to distribute the components to more tool units, or it

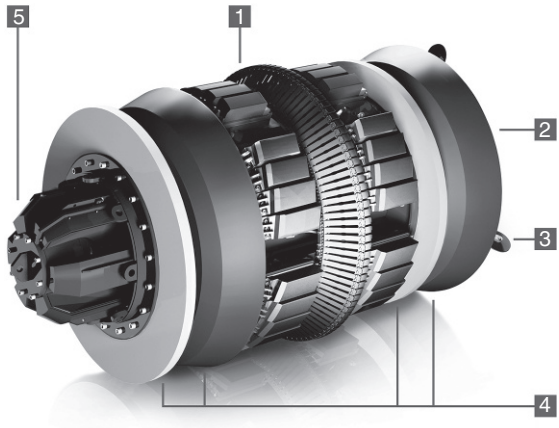

10.1 Key components of an ILI tool (56" axial MFL). See text for explanation of components.

would remain a single unit and deliver a degraded inspection performance, for example decreased maximum inspection distance or runtime.

Over the years, the mission of ILI has changed. The earliest goal, set in the 1970s, was to achieve an inspection specification that would find pipeline flaws to a standard at least equivalent to that yielded by a hydrostatic test. ILI tools of the twenty-first century are routinely set inspection goals that far exceed that early target. For example, they are built not only to find and size flaws that would fail a hydrostatic test, but also to measure them reliably and accurately at the very earliest stages of their initiation. At such an early stage, pipeline flaws are still far from having any adverse effect on the pipeline's structural integrity, but their early detection and characterization does allow appropriate preventative measures to be taken.

The ability to develop reliable, long-term PIM strategies based on dependable data is just one of the many benefits that accrue from the latest ILI inspection capabilities. Ultimately, the value gained by the pipeline operator is the reduced cost of integrity management over the life of the asset.

10.2 Pipeline flaws

High pressure steel pipelines experience a wide range of flaws that can degrade their integrity and lead to increased maintenance effort, reduced lifetimes, or even leaks and ruptures. The most important pipeline flaws can be considered in three groups (Walker, 2010):

- geometric deformation,
- metal loss,
- cracking.

The three groups contain a significant number of different flaws, each of which tends to originate from a unique cause (Argent, 2003). Risk assessment methods, especially threat analysis, can be used by a pipeline operator to determine which flaws pose the greatest probable threat to a particular pipeline. If a threat level exceeds a pre-defined value, or if there is an unacceptable uncertainty about the threat analysis, the operator may elect to inspect the pipeline with an appropriate ILI tool. The tool will collect precise, high definition information about the threat and its environmental circumstances to allow a much more accurate assessment to be made.

10.2.1 Geometric deformation

In a perfect world, all pipelines would be exactly circular in cross-section throughout their length. However, in the real world, pipelines are never exactly circular. Older pipelines may have particular problems with their geometries, due to the older manufacturing and construction technologies employed, but pipe joints made nowadays tend to meet very high standards of geometry. Consequently, operational upsets are of greater significance to geometric code violations in modern pipelines.

In simple language, an operational upset is anything that happens during pipeline operations that should not happen. Some examples of operational upsets are:

- unexpected pressure fluctuations
- extreme mechanical loading
- poor pipeline support
- excessive geological pressure
- poor compensation for temperature fluctuations
- poor workmanship
- third party damage (e.g. excavator strike onshore or anchor strike subsea)… even terrorism and vandalism.

All upsets, if they are serious enough, have the potential to lower the operational integrity of a pipeline to an unacceptable level. Each upset can lead to one or more pipeline flaws which change the geometry of the pipeline, sometimes to an unacceptable degree. Some examples of geometric flaws are:

- buckles
- dents (Fig. 10.2)
- ovalities
- wrinkles

10.2 Dent (probable cause: construction or agricultural equipment).

- roof topping
- other stress-induced geometric features.

The state-of-the-art solution for identifying, locating and sizing geometric flaws in operational gas and liquid pipelines is a high-resolution geometric inspection tool. Delivering high definition data about pipeline geometry, this tool is regularly used in many pipelines worldwide as an integral part of their pipeline integrity programmes.

Dents lead to mechanical strain. High definition data from a state-of-the-art geometric inspection tool can be used as input data to a suitable pipeline code which transforms geometric information from, for example, a dent, to deliver calculated strain values for the feature. Dent strain analysis describes the geometric distortion of the pipeline, by taking its undeformed shape as a reference.

Dent strain analysis is applicable not only to pipeline flaws such as dents; the same calculation can also be applied to the calculation of pipeline curvature and change in pipeline trajectory, which can themselves cause excessive bending strain depending on pipeline diameter (out of straightness analysis). Bending strain is related to the curvature of the pipeline at the location where it is subjected to a bending displacement. Such curvature can also be measured by other means, for example by using gyroscope technology to accurately monitor tool movements in all three dimensions within the pipeline (also called pipeline mapping or XYZ-mapping). Pipeline mapping functionality can be added to any geometry tool, or indeed to any other kind of ILI tool, as an add-on unit. The mapping function measures changes of pipeline direction vertically (inclination) and horizontally (azimuth).

10.2.2 Metal loss

Thinning of the pipe wall through metal loss can pose a serious risk to pipeline integrity, such as pipeline collapse or rupture. Causes of metal loss can be categorized as follows (Walker, 2010):

- corrosion
- erosion and abrasion
- gouging.

Individual causes can be as diverse as:

- classical rusting of ferrous metals in contact with air and water, or
- cavitation in the product, or
- galvanic corrosion by dissimilar metals in welded joints, or
- motion against the pipe wall of abrasive substances suspended in the product, or
- even microbes.

For each of these generic types a huge variety of metal-loss features exist. An example of pitting corrosion is shown in Fig. 10.3.

All metal-loss features can be classified according to their dimensions, and each anomaly class permits a large range of shapes as shown in the plot in Fig. 10.4, which is issued by the Pipeline Operators' Forum (POF):

ILI tools based on the MFL technique are generally the preferred choice for both gas and liquid pipeline operators to manage integrity for metal-loss features. This is due to MFL's inherent robustness and great versatility

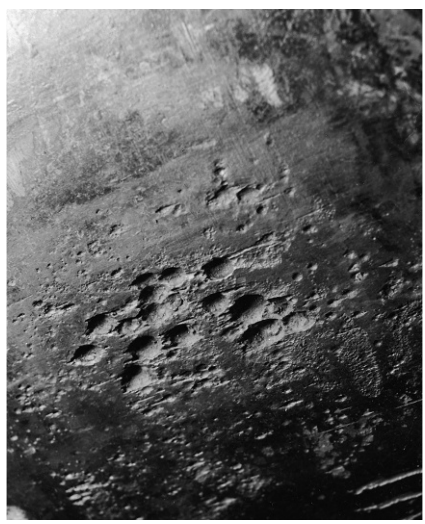

10.3 Pitting corrosion (external).

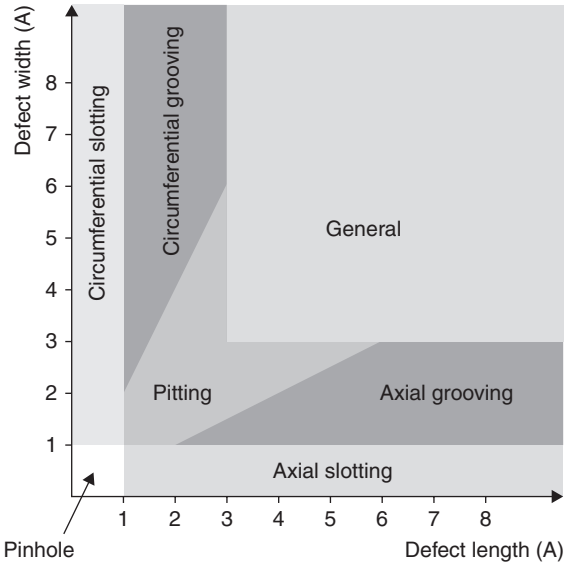

10.4 Graphical presentation of metal-loss anomalies (POF, 2009). *A* = wall thickness or 10 mm, whichever value is greater.

in application. The technique is highly tolerant of dirty pipeline conditions and geometric variations, and can be applied in different orientations to suit particular metal-loss morphology. It can also detect and locate extraneous ferrous debris that is buried close to or in contact with the pipeline. Such debris, for example discarded temporary steel rods used in construction, can puncture the external corrosion coating of the pipeline, damaging the corrosion protection system and initiating pipe wall corrosion. UT can also be used for corrosion inspection, although this method is mainly limited to liquid pipeline applications.

In certain situations, corrosion can develop as a shallow area of metal loss, perhaps at the top of the pipe due to condensation of water in a gas pipeline. Such shallow corrosion is a challenge for conventional MFL and UT tools, because the fraction of metal loss compared to the bulk of the wall is very small. For these features, a specialized inspection technology is used, the shallow internal corrosion (SIC) detection tool.

Inspection technologies can be combined on a single ILI tool, greatly increasing the versatility of the inspection operation and making an invaluable contribution to PIM. For example, with regard to active mechanisms resulting in corrosion growth, a combination of ILI technologies provides a highly effective tool for monitoring the degradation process.

10.2.3 Cracking

Cracking is one of the most serious threats to any pipeline's integrity, with particular risks involved for gas pipelines due to their generally higher potential for fatal consequences. Cracks can have a number of causes including:

Environment: environmentally assisted flaws such as stress corrosion cracking (SCC), which can be axially or circumferentially orientated, depending on stress directions

Thermal and load stresses: occasional loading (external loads, ground movement, etc.) and extreme thermal fluctuations, leading to axial pipeline stress and consequently to circumferential cracking.

Because the circumferential hoop stress is usually dominant in a pipeline, cracks that form tend to be axial in direction, e.g. SCC, axial fatigue cracks, and cracks in the longitudinal seam weld. Certain environmental conditions, as well as disbondment and puncturing of the corrosion coating, are essential for the start of threats such as SCC (Fig. 10.5).

Ultrasonic ILI technology represents the state-of-the-art solution for detecting and sizing cracks in operational pipelines. Conventional ultrasonic crack detection tools require a liquid medium to couple ultrasonic energy into the pipe wall, and so they are really suitable only for liquid pipelines. Gas pipelines are extremely difficult and expensive to inspect with conventional ultrasonic crack detection tools. EMAT technology, on the other hand, injects the energy electromagnetically to eliminate the need for a liquid couplant. EMAT-based tools are therefore suitable for both gas and liquid pipelines.

10.5 Stress corrosion cracking.

10.3 Inspection technologies and principles

Corrosion is a major risk for pipeline integrity. For instance, top-of-line corrosion (TLC) can occur in wet gas pipelines due to condensation. Growth rates have been recorded of up to several millimetres per year under certain conditions (Pugh *et al.*, 2009; Singer *et al.*, 2009). Other examples of deteriorative processes are microbially induced corrosion (MIC) and pitting. To monitor any kind of metal loss in a pipeline, various standard non-destructive examination methods are employed worldwide, ensuring that high value assets maintain their structural integrity.

10.3.1 Magnetic flux leakage

ILI tools equipped with MFL inspection technology represent a well-proven means of inspection for any kind of metal loss in a pipeline, either electrochemically-induced corrosion or in the form of erosion, mechanical gouging or grinding. Owing to their robust magnetic and sensor designs, MFL inspection devices ensure an excellent flaw detection performance, even under harsh operating conditions.

MFL is commonly used with other inspection techniques on the same tool to increase the versatility of the inspection. For example, Fig. 10.6 shows a two-segment 30" ILI tool carrying two different inspection technologies. The front segment is based on axial field MFL, and carries the magnetic yoke system with magnets and brushes. The magnetic sensor system is located between the two brushes of the yoke. The rear segment of the tool hosts an EC technology with contour following proximity sensors for the detection of SIC and geometric anomalies.

An ILI tool for circumferential MFL detection is shown in Fig. 10.7. The 48" single-body unit is equipped with saucer-shaped yoke systems orientated perpendicularly to the tool and thus to the pipe axis. Two sensor rings are used to achieve full coverage in the circumferential direction.

The principle of MFL involves the magnetic saturation of a ferromagnetic sample – here the pipe wall, with powerful permanent magnets. The magnets are mounted onto the ILI tool in a certain manner, which defines the direction of the resulting permanent magnetic field and hence whether the tool employs so-called axial or circumferential MFL.

Magnetic N and S pole pairs that are aligned longitudinally along the pipe axis (axial pole alignment) will create magnetic fields in the pipe wall of the same axial orientation. This is therefore called axial MFL, and it is best suited to the detection and sizing of flaws that are orientated or extend in a direction around the pipe circumference. Circumferential slotting and grooving are common examples of such flaws (Fig. 10.4). On the other hand, magnetic N and S pole pairs that are aligned circumferentially around the

10.6 ILI tool with combined axial MFL and EC technology (30″).

10.7 Single-body ILI tool with circumferential MFL technology (48″).

pipe wall (circumferential pole alignment) will create magnetic fields in the pipe wall of the same circumferential orientation. In this case it is called circumferential MFL, and it is best suited for the detection and sizing of flaws that are orientated or extend in a direction along the pipe axis. Axial slotting and grooving are common examples of such flaws (Fig. 10.4).

When in a pipe, a magnetic circuit between the tool's magnetic yoke system and the pipe is created (Fig. 10.8). The ferrous pipe wall material guides

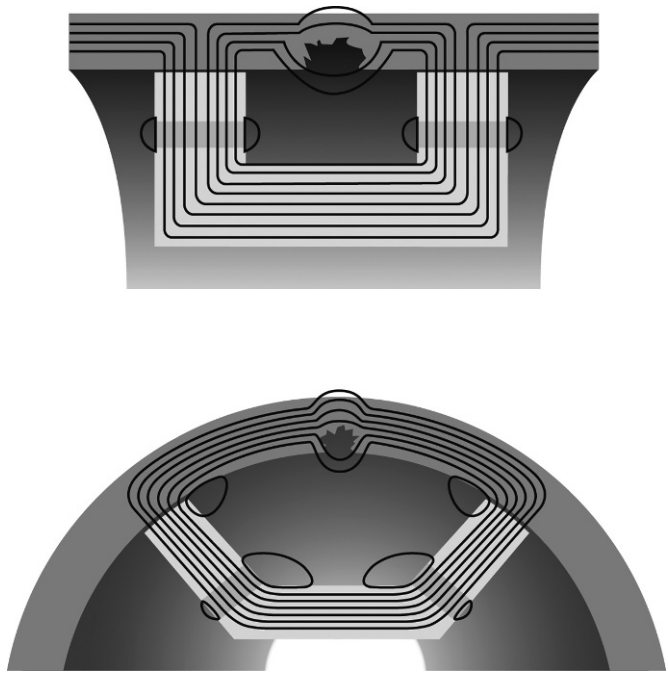

10.8 MFL basic principle (top for axial MFL, bottom for circumferential MFL). The yoke system and pipe wall constitute a magnetic circuit with defined magnetic flux line distribution inside the pipe material. Metal loss causes the magnetic field to leak out of the pipe material allowing it to be detected.

the magnetic flux lines either in the longitudinal direction of the pipe or along the pipe's circumference. Each approach has its pros and cons with respect to the detection of different flaw types and their dimensional characteristics. Sufficiently high magnetization (so-called magnetic saturation) of the pipe wall is essential for accurate flaw recognition and sizing. Magnetic saturation also helps to differentiate between metal-loss anomaly signals and other indications. The latter might originate from non-metallic inclusions in the pipe steel, or local metallurgical changes, both of which can lead to spurious signals.

In the absence of a flaw or other metal-loss anomaly, the magnetic field in the pipe wall maintains a smooth and linear profile throughout the cross-section of the pipe wall. The magnetic flux density is a function of the pipe wall's cross-sectional area. If an internal or external metal-loss feature is present in the body of the pipe, the cross-sectional area of the pipe wall is reduced, disturbing the flux density and forcing the magnetic

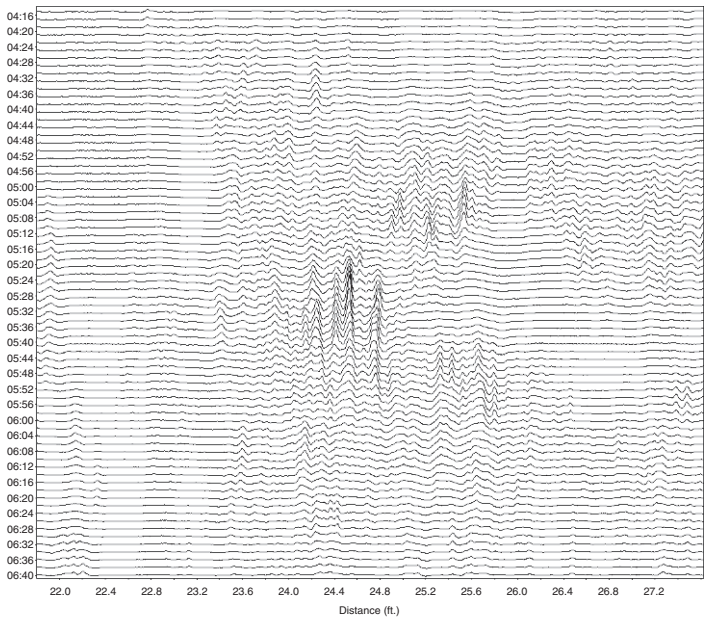

10.9 A typical example of raw sensor data generated by an MFL tool.

field to leak outside the pipe surface both internally and externally. A high density array of magnetic Hall-effect sensors, mounted circumferentially in a ring between the tool's magnetic poles, measure the leakage field precisely. The data recorded are minutely examined during the analysis phase where they are used to determine feature classification, geometry and severity.

Figure 10.9 shows a typical example of raw sensor data generated by an MFL tool. The smooth profile of undamaged pipe wall can be clearly seen, together with the distorted field regions caused by metal loss resulting from corrosion.

10.3.2 Eddy current

Another well-proven non-destructive examination method is based on the EC principle. ILI tools equipped with an EC detection system are considered in the industry as reliable inspection devices with high sensitivity and accuracy for the detection of internal corrosion, especially when combined with a geometry sensor for scanning the pipe surface for geometric anomalies such as dents (Stawicki *et al.*, 2009). Figure 10.10 shows a geometry tool with extended capabilities for measuring geometric anomalies. It uses two

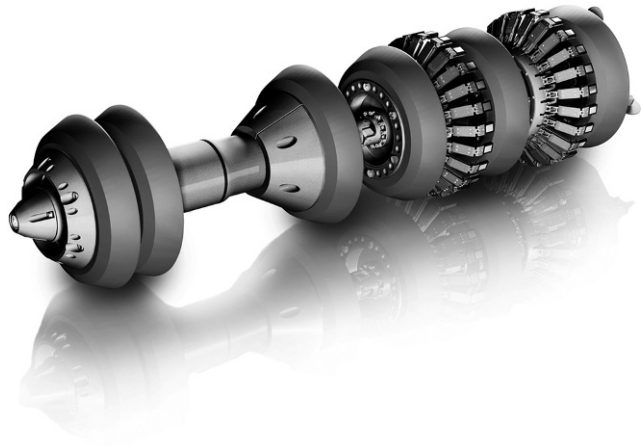

10.10 Extended geometry ILI tool (20″).

independent methods, one mechanical, the other EC-based, to derive precise information about the pipe's geometry.

The EC testing method is based on generating electrical currents in conductive materials, here the pipe wall. Figure 10.11 summarizes the principle. An alternating electric current with defined amplitude and frequency is applied to a coil system. The driving current generates an alternating primary magnetic field which causes ECs to flow in the surface of the nearby pipe wall by mutual inductance. The currents in the pipe wall produce a secondary magnetic field which is opposed to the primary field inducing it.

Flaw damage such as corrosion leads to a change of the EC's flow direction, which influences the mutual inductance. On the basis of this effect, material inhomogeneities can be detected and their properties determined by evaluating the amplitude and the phase shift between the input and output signals. Hence, by detecting ECs generated in the pipe wall via a coil system, a highly sensitive characterization of surface metal-loss flaws is possible.

Results obtained with EC can assist conventional MFL feature depth sizing algorithms for the relatively greater depths of metal loss where MFL is optimum. The two measurement approaches complement one another and show synergetic effects, and they can be used to improve the overall sizing performance for corrosion growth monitoring (Stawicki *et al.*, 2010). Figure 10.6 shows an MFL tool combined with a specialized unit for measuring SIC. The so-called MFL/SIC tool is able to detect and size both relatively deep metal loss and shallow metal loss down to 1 ± 0.5 mm.

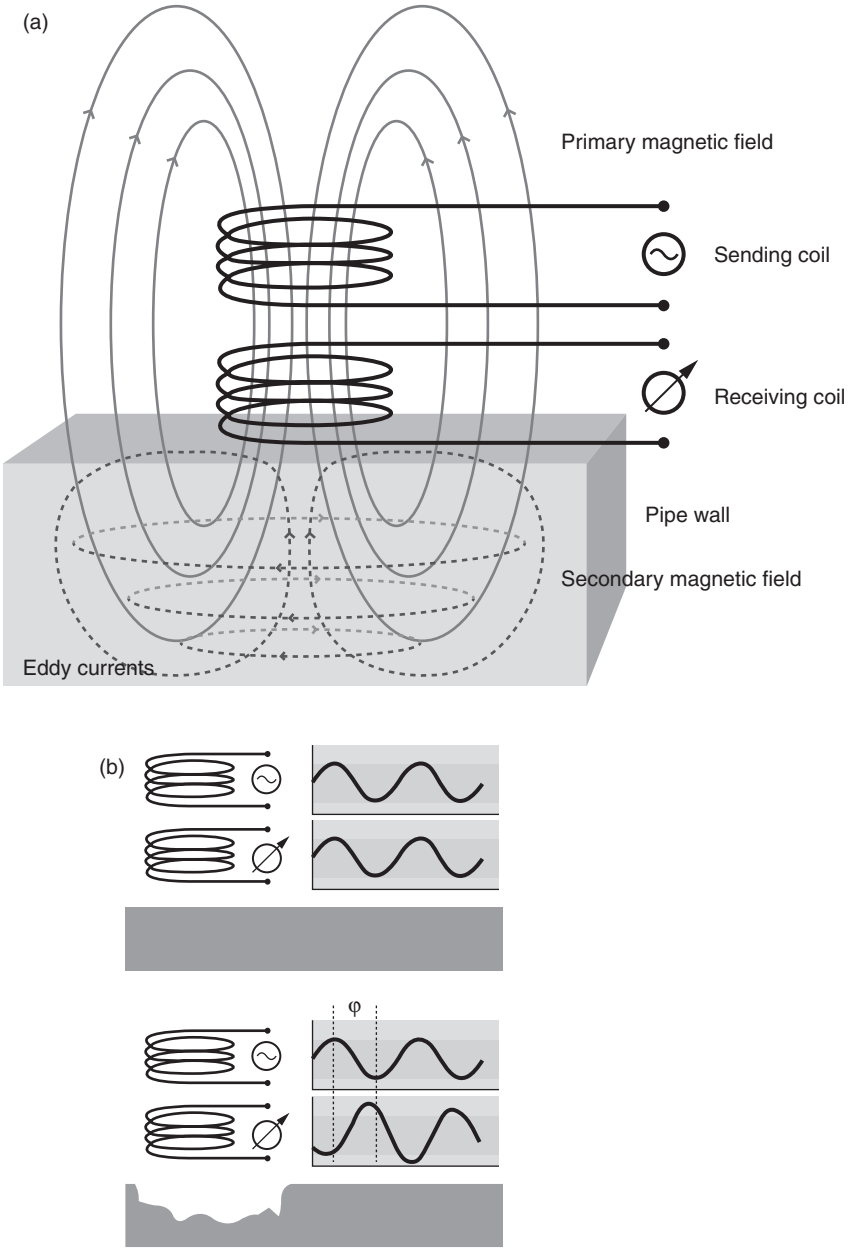

10.11 The EC principle. (a) An alternating current in a sending coil generates ECs in a steel sample. (b) Metal loss disturbs the EC distribution, resulting in a change in amplitude and phase of the received signal.

10.3.3 Ultrasonic testing for pipe wall thickness measurement

Ultrasonic pipeline inspection by ILI involves, in order:

- injection into the pipe wall of mechanical waves in the MHz region (effectively high frequency sound)
- transmission of the UT waves through the pipe wall
- reception and recording of UT echoes from features in the pipe wall
- analysis and interpretation of UT data.

The main objective of applying UT on an ILI tool is to detect wall thickness anomalies at the outer or inner pipe wall. In addition to anomalies associated with metal loss, such as general corrosion, inclusions or laminations within the pipe wall can be successfully detected. The minimum detectable lateral dimension of anomalies is determined by a number of parameters, including the tool's transducer-specific operating frequency and the number and size of transducers around the tool's circumference. The most basic and robust approach to wall thickness measurement by UT is based on measuring the time-of-flight (TOF) of a UT pulse between a transducer and a pipe wall feature.

When operating conventional piezoelectric UT transducers in the so-called pulse-echo mode, each ultrasonic transducer on an ILI tool acts as both emitter and receiver. After emitting a UT pulse, each transducer 'listens' for echoes originating from discontinuities in the pipe wall. Partial reflection of the ultrasound occurs at interfaces, for example the liquid couplant/pipe wall interface and the interface between the pipe wall and the pipe's outer environment (Fig. 10.12).

A typical so-called A-Scan representation of the UT echoes is recorded by a UT tool (Fig. 10.13). The A-Scan representation shows ultrasonic events

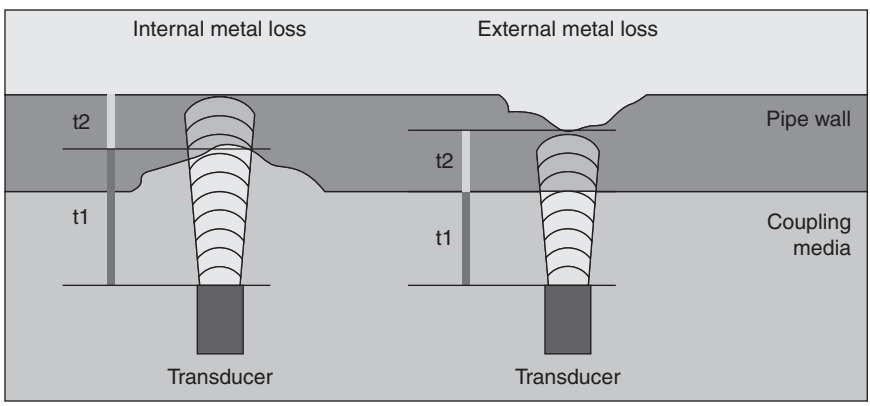

10.12 Principle of UT pipe wall thickness measurement.

10.13 UT ILI tool for wall thickness measurement (16″).

of a single transducer using a time-based single measurement. By capturing each individual A-Scan for each sensor over the whole pipeline distance, a high-resolution data image of the pipe wall thickness is recorded for post-ILI data analysis. With a knowledge of the speed of sound in the liquid couplant and in the pipe wall, it is relatively straightforward to determine the distances between the transducer and the inner and outer pipe walls and thereby determine the thickness of the pipe wall.

10.3.4 Ultrasonic testing for crack detection

Ultrasonic crack detection represents a reliable and accepted ILI technology for application in liquid pipelines. The ultrasonic module is based on the measurement of the TOF of ultrasonic signals reflected from internal/external surfaces of the pipe wall and flaws. A sufficient number of sensors ensure full circumferential coverage of the pipe wall inspected.

A typical ultrasonic crack detection inspection system consists of several transducers operated in an impulse-echo mode acting as emitter and receiver. The sensor carrier design must ensure that the incident ultrasound signals are refracted in a manner such that they will propagate under 45° inside the pipe (Fig. 10.14). Therefore, slanted probes are used. The ultrasonic probe generates high frequency ultrasonic energy, which is introduced and propagated through the materials in the form of shear waves. In the presence of a flaw, part of the energy will be reflected by the flaw surface. Reflected signals will be transformed into an electrical signal. Surface entry echo, external and internal crack echoes and their amplitudes can be assigned to associated TOFs. Information about location, size and orientation received from the signals can be determined.

Ultrasonic crack detection tools are designed for the detection of either circumferential or axial cracks (Fig. 10.15).

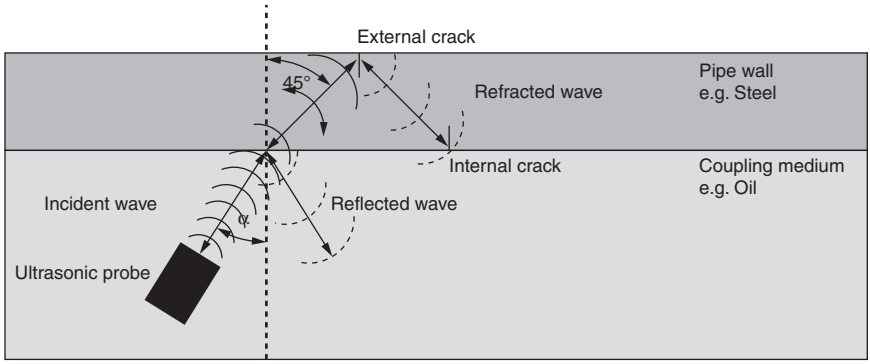

10.14 UT for crack detection.

10.15 UT ILI tool for crack detection (34″/36″).

10.3.5 Electromagnetic acoustic transducer for detecting stress corrosion cracking

The original, classical form of SCC was discovered in the mid 1960s in the USA. A form of intergranular cracking, classical SCC occurred in pipelines subject to relatively high stresses, elevated pH and temperatures, as well as depressed cathodic potentials. Nowadays, this form of SCC is referred to as intergranular, classical or high pH SCC. In the early 1980s a new type

of SCC different from the classical form in its mechanism and growth rate was discovered. In this new form of SCC, the cracking of the pipeline steel occurred in a transgranular fashion in a near-neutral pH environment and relatively low pipeline temperatures. This later form of SCC is nowadays referred to as transgranular or near-neutral pH SCC.

Transgranular SCC occurs on pipelines as a result of three conditions which must be present concurrently:

- susceptible pipe material,
- tensile stress, and
- conductive environmental conditions at the pipe surface.

Highly specialized ILI tools have been developed to detect and measure pipeline SCC. Based on an EMAT principle these tools can make accurate measurements of SCC features, in addition to pinpointing any areas of coating disbondment that may facilitate future SCC initiation. A typical EMAT tool is shown in Fig. 10.16.

The physical principle behind EMAT is the production of a guided ultrasonic wave through the combination of Lorentz force and magnetostriction (Fig. 10.17).

To generate this wave in a pipeline, a coil is placed on the pipe wall within an applied static magnetic field, and a short electrical current pulse is sent through the coil. As a result of this arrangement, mechanical (acoustic) forces are created within the pipe wall. If the pulses are short enough, an acoustic wave will develop from the associated mechanical forces within the boundary created by the pipe wall. The wave then propagates through

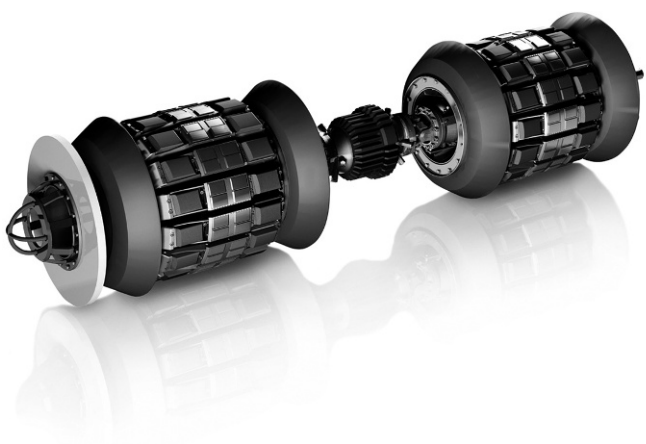

10.16 Crack detection and coating disbondment ILI tool (24″/26″).

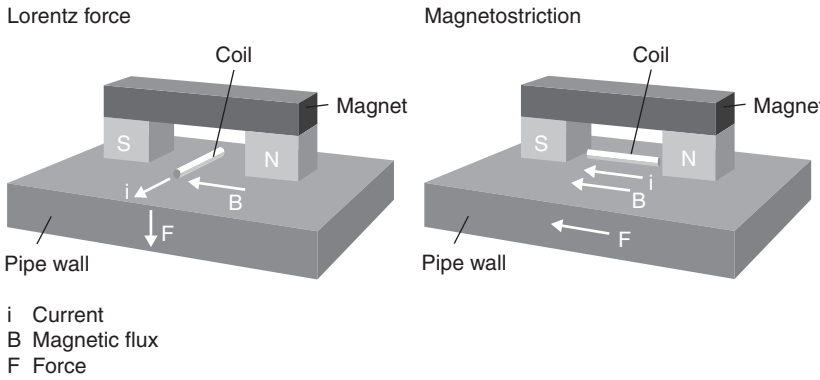

10.17 Principle of the electromagnetic acoustic transducer.

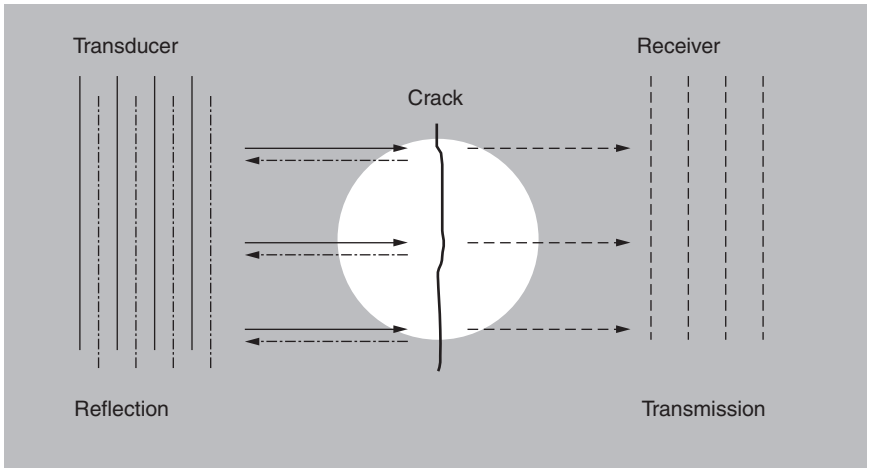

10.18 EMAT sensor arrangement. An ultrasonic shear wave is generated in the pipe wall travelling from transducer to receiver. An obstacle, e.g. crack situated in the sensitive area of the EMAT sensor results in reflection of the ultrasound.

the pipe wall and is returned as an echo from any flaws or other features that may be present. An EMAT receiver works in the reverse manner, whereby a returning acoustic wave will interact with the EMAT to produce a measurable current pulse that can be measured and recorded by an EMAT tool. Figure 10.18 shows a schematic representation of an EMAT arrangement.

A single EMAT probe inspects a small, well-defined area between transducer and receiver. Transmission and reflection signals are captured by two separate receiver sensors within the EMAT sensor arrangement.

On an inspection tool, sensors are arranged to allow for a high-resolution image of the pipeline. Due to the limited propagation distance of the waves between the measuring elements, this design ensures high signal-to-noise ratios as a basis for the accurate determination of the position and dimensions of pipeline anomalies.

Waves which propagate from transmitter to receiver through the pipe wall without hindrance are used to assess the external pipe coating. The ultrasound is attenuated by intact coatings resulting in a lower signal amplitude being captured by the receiver. However, where for example coating disbondment or a coating holiday (or defect) is present, the attenuation is reduced and a relatively higher signal amplitude is captured.

Pipe anomalies situated in the sensitive EMAT measurement area reflect part of the ultrasonic wave. Information on frequency, TOF and ultrasonic modes is used for discriminating cracks and volumetric features and for determining lengths and depths of features. The quality of EMAT signals obtained from crack and coating measurements is enhanced by quantifying possible lift-off effects and by making magnetization measurements.

10.4 Preparing for in-line inspection

Despite standardized procedures and highly evolved tool designs, many uncertainties can remain about a prospective ILI survey, and a huge amount of information may need detailed study. Where adverse circumstances or restrictive pipeline fittings are thought likely to cause problems prior to an actual inspection operation, special evaluation trials can be undertaken in short, pressurized test loops before the tools are mobilized to the field.

Operating with gas or liquid media, the test loops use simulated components to represent any potential hazards. Only after successfully passing a series of exhaustive tests under simulated conditions are the ILI tools shipped to a potentially challenging pipeline for inspections. Good preparation, coupled with a readiness to face unexpected and adverse situations, is a key ingredient for a successful inspection operation.

10.4.1 Preparation of the pipeline

A pipeline transports a gas or liquid product from its source to a number of possible end-users, as shown in the example of a gas pipeline system (Fig. 10.19).

Whatever products they transport, many pipelines are contaminated by debris of one sort or another. Eventually such debris can accumulate to cause a restriction that reduces the product flow, or even blocks the line in severe cases. Generally speaking, gaseous products tend to

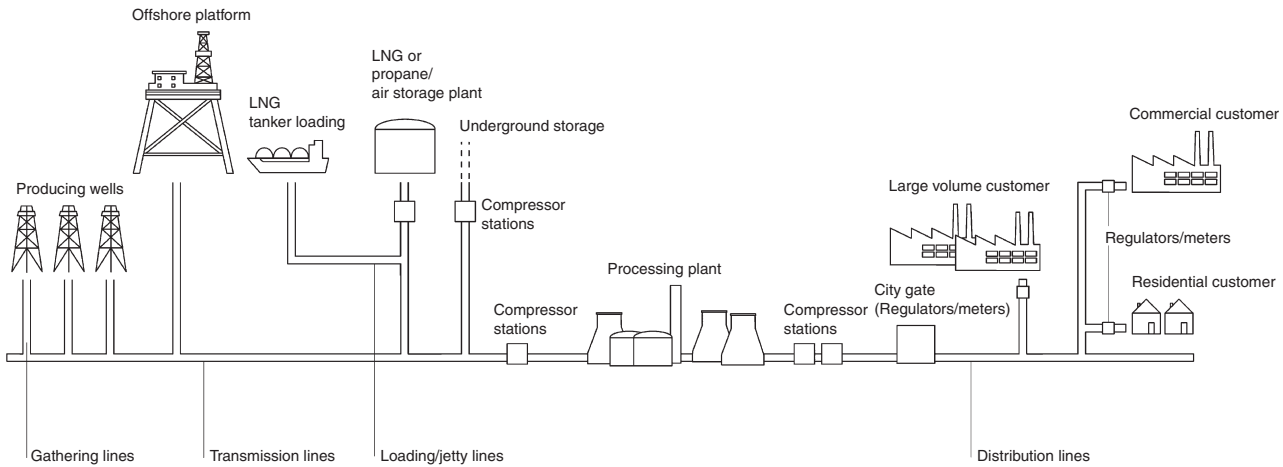

10.19 Typical natural gas pipeline system.

carry mainly dust, while oil products usually contain a certain amount of paraffin wax. Depending on environmental conditions, the wax can separate from the oil product and build up rapidly on the pipe wall. Pipelines carrying refined products and/or petrochemicals are relatively free of contaminants, but even they can be contaminated by sand, metal debris or other materials.

All kinds of contaminants are capable of adversely affecting an ILI survey or damaging a passing inspection tool. For this reason, a pre-inspection cleaning programme is normally an essential pre-requisite of an inspection survey.

10.4.2 Pre-inspection cleaning

Cleaning is one of the many elements in maintaining the integrity of a pipeline, and starts directly after pipeline construction is completed. Post-construction cleaning is performed to remove construction debris such as welding rods and metal scarf, or to dewater a pipeline after hydrostatic testing. Throughout the life of their pipelines, many operators themselves perform regular maintenance cleaning. This often uses low-cost options for the cleaning tools, such as foam cylinders, which can be sent through the line with the regular flow and product. Routine cleaning, even with low-cost tools, can reduce the likelihood of internal corrosion, by periodically removing water and other potentially corrosive materials from the pipeline.

A special cleaning task is usually performed by the ILI service vendor to make sure an inspection tool will not face unexpected problems in the pipeline when it is run. This task is called pre-inspection cleaning and is extremely important in maximizing the probability of inspection success.

10.4.3 Cleaning equipment

A typical cleaning tool basically consists of a steel cylinder with two flanges fitted at the front and rear. The flanges are used to fix key cleaning elements to the tool body, such as polyurethane discs, cups or steel bristles. In addition, the central part of the tool body might contain further scraping components, or strong magnets for extracting metal debris from the pipeline and its transported product. The first tool is usually equipped with a low frequency signal transmitter, offering the opportunity to track the pig during the run or locate it should it become stationary for some reason. Figure 10.20 shows a typical, standard disc cleaning tool equipped with spring-loaded brushes and magnets.

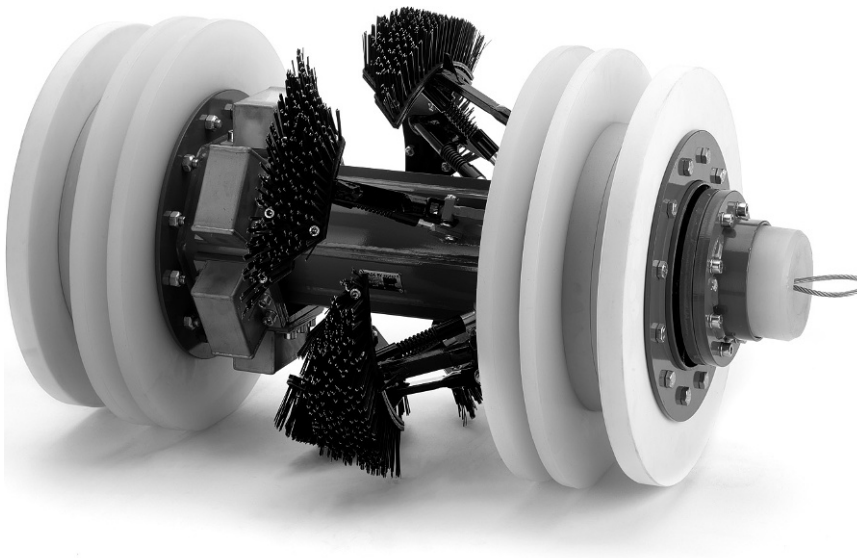

10.20 Cleaning tool equipped with brushes and magnets.

10.4.4 Internal geometry verification

The cross-sectional geometry of a pipeline should be nominally circular, making it a relatively simple task for an inspection tool to negotiate any bends or other construction features. However, irregular pipeline geometries can exist, such as dents, partially open valves, or bends that have abnormally sharp angles. These anomalies in the geometry of pipelines pose challenges to inspection tools, and can even cause them to be held up during the inspection survey. Inspection tools that get stuck in a pipeline cause enormous trouble to all involved parties, and the situation must be averted through special precautions.

To avert a stuck tool situation, the best industry practice is to run a special gauging tool before the actual inspection tool to detect any features that might impede or interfere with the inspection tool. Figure 10.21 shows a gauging tool with two alloy gauge plates that has just completed a run through a pipeline to verify its suitability for running an inspection tool.

Geometric flaws and pipeline features that could damage or impede an inspection tool can be located by a gauging tool and corrected before survey work begins. However, if additional data are required, the tool can be equipped with special sensors and a data-logger device to record information such as absolute temperature, product pressure, and the pressure difference between the front and back of the tool.

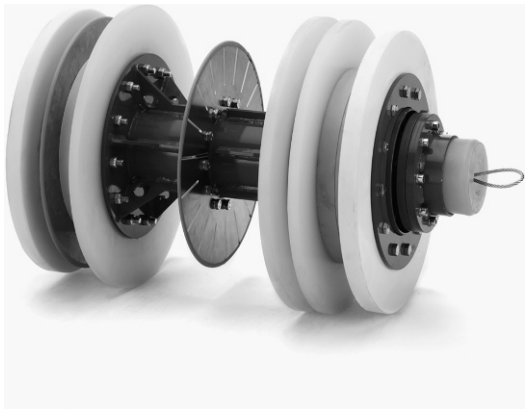

10.21 Bend gauge tool.

10.4.5 Preparation of the ILI equipment

As well as the pipeline, the intended inspection tool needs custom-preparation for a survey. Important pipeline details, such as operational conditions, pipeline length, wall thicknesses, and fittings, such as valves and launch/receive traps, differ from one pipeline to another. This means that any inspection tool must undergo an extensive preparation to meet the requirements of an upcoming survey.

Not all pipelines are suited to ILI operations, for instance, as a result of adverse operational conditions, aggressive products or unsuitable construction features. Consequently, only a fraction of global pipelines, both gas and liquid, are suitable for operating ILI equipment. These lines are said to be immediately 'piggable'. The remaining pipelines are not inspectable without major modifications to either the inspection equipment or the pipelines themselves. These lines are said to be 'unpiggable'.

10.5 Carrying out an ILI survey

A typical ILI survey involves launching the tool into the product flow, tracking it during its transit from one end of the pipeline to the other, and finally extracting it to recover the inspection data. These three components are commonly referred to as the launching, tracking and receiving operations.

10.5.1 Launching operations

In order to run through a pipeline, any tool must be first loaded into a special isolation trap as shown in Fig. 10.22.

The launching procedure is separated into three parts: the launcher preparation, loading of the inspection tool into the trap and the launching itself.

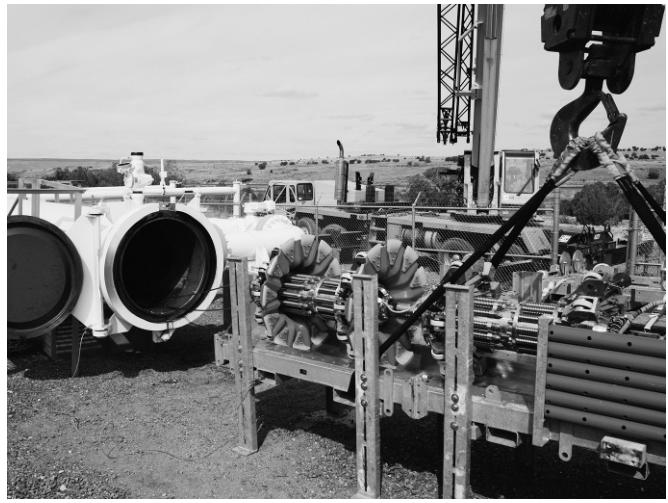

10.22 Standard launching of an ILI tool.

After the launcher is prepared, the tool is pushed into the trap so that a good seal is achieved. An effective seal is essential, otherwise pipeline product could bypass the tool, and it would not be possible to build up enough back pressure to drive the tool forward into the pipeline. Loading complete, the trap door is closed and the tool is launched into the main pipeline by a sequence of valve manipulations.

10.5.2 Tool tracking operations

Tool tracking is performed to ensure that a tool maintains accurate velocity and position by staying within pre-defined envelopes. In particular, later inspection data evaluation is made more accurate by the use of ample reference points to align with and confirm the distance information of the inspection tool.

Two methods of tracking are common. The first uses an alternating electromagnetic field, a low frequency radio pulse generated by an on-board transmitter. The second option tracks the static magnetic field of a tool and is therefore limited to inspection tools equipped with magnet-based technologies such as MFL. Both tracking methods are supported by an above ground marker (AGM).

10.5.3 Receiving operations

Receiving an inspection tool after a run is basically a reverse of the launching procedure. Once recovered from the pipeline, the tool is cleaned

to remove any debris and other contaminants picked up during the run. Careful assessments are made of the varying types and amounts of any debris brought out by the tool, principally to determine whether this could have affected the inspection data quality.

10.6 Analysis and interpretation of ILI data

The information provided by an ILI tool must be carefully analysed to provide a statement on the pipeline's integrity. Data processing and data alignment are followed by a detailed scrutiny of the inspection data for all reportable features in the line. These features are then classified and sized to provide a detailed description of the inspection findings. Finally, a possible approach to improving the pipeline's integrity is included in the inspection report to the pipeline operator.

During a tool run, a vast amount of data is collected. For example, the EMAT technique records the complete behaviour of 25 different parameters to produce up to 150 GB (30" EMAT tool, 50 km line length) of raw data. If this volume of data were to be printed out on A4 paper, it would result in a stack nearly half a kilometre (0.3 miles) high weighing around 20 t (44 000 lbs.). Hence in terms of resolution, finding a feature can be compared to identifying a single blade of grass on 20 football fields. To reduce this amount of data to manageable proportions, a first data reduction is carried out on-board the ILI tool during the inspection run. On completion of the survey, the reduced data set is downloaded to a computer for further data processing, analysis and interpretation.

For all types of ILI tool, data from different sensor units are merged so that all locations on the pipeline are shown in corresponding positions in the data, even though the data are collected from different sensor locations. To optimize the data quality, several filters are applied, including noise filters and special calibrations.

10.6.1 Feature assessment and reporting

After being correctly distance-aligned, the inspection data are scrutinized for relevant features. Searches look for significant amplitudes in the data using different approaches, depending on the type of corrosion sought and on the ILI technology involved. As an example, MFL technology algorithms search for areas of higher magnetization.

Indications of interest found in the data are automatically sized in depth, length and width and stored in a list system that is synchronized with a data viewer. For this visualization, the popular method is to 'flatten out' the

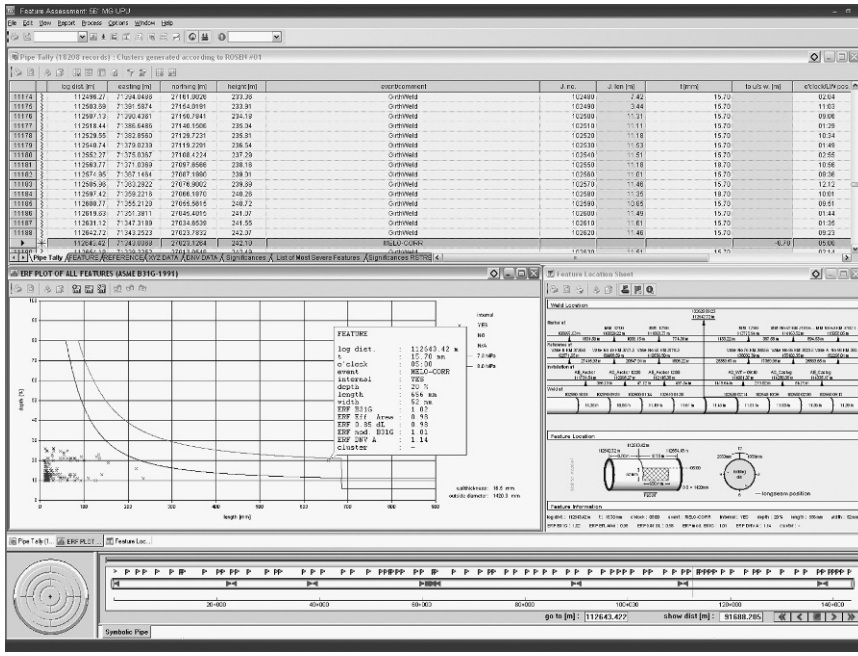

10.23 Detailed feature information allows excavation of important sites.

cylindrical pipe and depict it as a flat strip of metal on which the position and extent of features can be seen.

All indications are sorted into different categories, and the most serious in terms of the pipeline's immediate operational integrity are urgently reported to the operator.

The 'final report' delivered to the pipeline operator contains all indications found by the ILI tool, along with their dimensions and precise locations. All data are aligned to actual pipeline positions. Figure 10.23 shows a typical data sheet that is generated to enable the precise location in the field of reported features.

The different values of flaw size that are generated for different ILI indications are used to create a priority listing for remedial actions on the pipeline. It is therefore relatively easy to create an optimum remediation programme for the pipeline, phased to ensure continued safe operations while minimizing costs.

In most cases, dedicated ILI reporting software is provided to the pipeline operator by the ILI vendor to facilitate highly versatile data viewing. The operator obtains a comprehensive overview of the data and can even manipulate them to investigate a virtually unlimited number of possible situations on the pipeline.

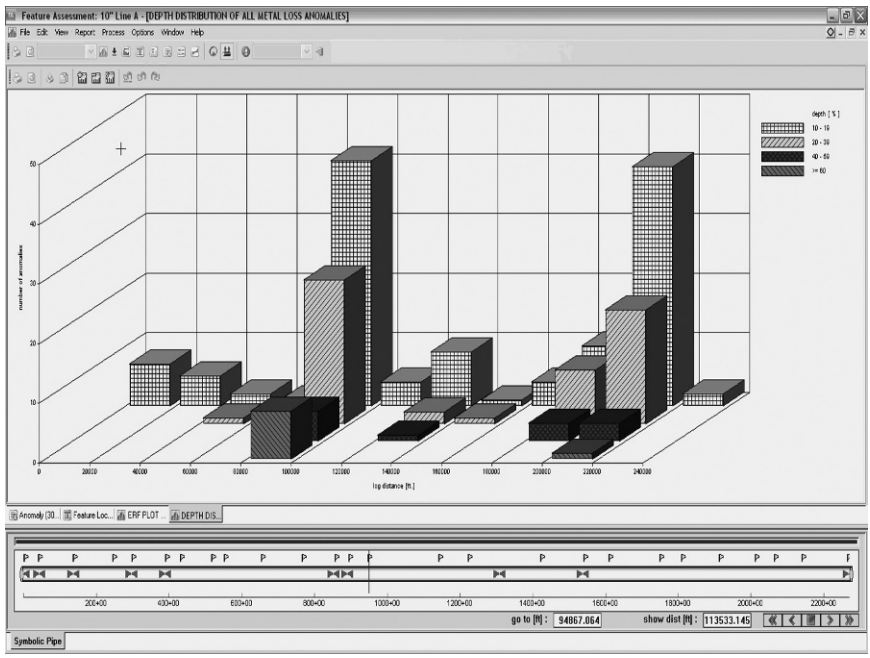

10.24 Statistics of different kinds of data which are used in an integrity management process.

10.6.2 Further investigations and benefits to pipeline integrity

Based on an ILI report, further pipeline integrity assessments can be performed. The exact details of such assessments depend on the requirements of the pipeline operator; however, many of them are extremely complex with vast data sets involved. Custom-designed, highly specialized software is therefore needed to perform the assessments efficiently. Such software is a collection of interoperable tools for helping to maintain pipelines in a reliable, safe and cost-effective condition. This is done by allowing operators to visualize, explore and analyse complex information, systems, and processes. Figure 10.24 shows a typical graphic of multiple data sets used in an integrity management process.

10.7 Future trends

For over 50 years, ILI technologies have progressively grown in capability and scope of application. They have done so by taking advantage of the lessons learned from operational experiences in ever-more challenging pipelines during a half century of applications, and by harnessing the great technological advances made in that time in materials, NDE methods,

sensor designs, electrical power systems and data acquisition, processing and storage systems.

Driven by the needs of ever-more sophisticated and data-hungry PIM programmes, ILI vendors have massively increased the utility of their ILI technologies to achieve exceptional performances in identifying, sizing and locating all types of pipeline flaws. Consequently, ILI is nowadays one of the most important sources of the precise, trusted data needed for the codified processes of PIM.

Even so, the world's pipelines continue to present new challenges to ILI technologies, including the need to inspect ever-deeper offshore pipelines and lines transporting aggressive products. In addition, there are pipelines operating at very high pressures, temperatures and/or product flow rates, and those containing components with difficult geometries, such as wye-piece connections, multi-diameter pipe bores and thick wall pipes. To address these new challenges, ILI vendors are continually extending ILI tool capabilities. The latest technologies and methods being developed and applied include robotics and adaptive engineering processes that allow an ILI tool to be comprehensively customized to suit a particular pipeline application. Such specialist customization is essential for the safe and efficient inspection of an increasing number of highly challenging pipelines.

Deep offshore pipelines are prime examples of challenging applications, since they pose an elevated risk relative to pipelines located in shallow waters and onshore. Deep water pipelines, sometimes installed several thousand metres below sea level, are exceptionally difficult and expensive to access should an ILI tool become stuck. Before actual deployment offshore, ILI systems that have been newly customized for highly challenging applications are therefore subjected to the most exhaustive evaluations under a wide range of live operational conditions in specialized pipeline test loops. The loops are built to contain all of the key constructional features that could adversely affect the safe passage of an intended ILI tool. Normally supplied by the pipeline operator, these key features can include non-standard valves, wye-pieces, pipe diameter changes, and thick wall sections.

ILI tools gather critical data for PIM systems; in particular, they supply accurate information about any relatively serious flaws that may pose a threat to pipeline safety in the short term. Once identified and classified, these larger flaws are remedied as a priority. Increasingly, however, PIM systems are demanding more and more information about relatively small flaws that do not immediately affect integrity but which may grow to do so, perhaps in a short time frame. ILI vendors are responding to this need to measure flaws at their earliest onset by evolving ever-more sensitive methods and equipment to provide precise details about the smallest features of interest.

The future of ILI technology will be one of continuing innovation and increasing capability as ILI vendors invest more resources in research and development of their technologies.

10.8 References

API 1163 (2005), In-Line Inspection System Qualification Standard, American Petroleum Institute (API), API Publishing Services, Standards Department, Washington D.C.

Argent, C. (2003), 'Macaw's pipeline defects, Yellow Pencil Marketing, ISBN 0-9544295-0-8.

ASME B31G (1991), 'Manual for Determining the Remaining Strength of Corroded Pipelines, A Supplement to ASME B31 Code for Pressure Piping, ASME B31G-1991 (Revision of ANSI/ASME B31G-1984)', The American Society of Mechanical Engineers, New York, USA, 1991.

POF (2009), Specifications and requirements for intelligent pig inspection of pipelines, Pipeline Operator Forum, Version 2009.

Pugh, D., Cai, J., Ibrahim, F., Venaik, S., Asher, S., Pacheco, J., Dhokte, A., Sisak, W., Wright, E. and Robson, D. (2009), 'Top-of-Line Corrosion Mechanism for Sour Wet Gas Pipelines', technical paper no. 09285, NACE 2009, Atlanta, Georgia.

Singer, M., Zhang, Z., Wang, H. V., Hinkson, D. and Nesic, S. (2009), 'CO2 top of the line corrosion in presence of acetic acid: A parametric study', technical paper no. 09292, NACE 2009, Atlanta, Georgia.

Stawicki, O., Ahlbrink, R. and Schroeer, K. (2009), 'Shallow Internal Corrosion sensor technology for heavy pipe wall inspection', Presented at the 2009 PPSA Seminar, Aberdeen, UK, Available from: http://www.ppsa-online.com/papers/09-Aberdeen/2009-05-Stawicki.pdf.

Stawicki, O., Beuker, T., Ahlbrink, R. and Brown, B. (2010), 'Monitoring of top of line corrosion with Eddy Current technology combined with Magnetic Flux Leakage Method', technical paper no. 10094, NACE 2010, San Antonio, Texas.

Walker, J. (2010), In-Line Inspection of Pipelines – Advanced technologies for economic and safe operation of oil and gas pipelines, Munich, Sueddeutscher Verlag onpact GmbH.

11

The use of probes for detecting corrosion in underground pipelines

C. SEAN BROSSIA, Det Norske Veritas (U.S.A.) Inc., USA

DOI: 10.1533/9780857099266.2.286

Abstract: Corrosion monitoring is a critical component in the overall corrosion management of structures and systems. Effective corrosion monitoring can be achieved through the selection of appropriate monitoring methods, the use of suitable reassessment intervals, and the use and application of the data generated. When done properly, corrosion monitoring can also serve as an early warning system before the onset of corrosion-related failures.

Key words: corrosion monitoring, cathodic protection, integrity assessment.

11.1 Introduction

Pipelines are the most effective and efficient means of delivering water, oil, natural gas, refined products, and other liquids and gases. As a result, there are millions of miles of pipelines installed worldwide. Most are installed underground, and are subjected to degradation and corrosion. The mechanisms of corrosion found on buried pipelines and other metallic structures are discussed elsewhere in this book (see Chapters 1–3). Similarly, the primary methods of preventing corrosion through the use of coatings and cathodic protection are covered in other sections (see Chapter 1). In this section, the discussion will focus on corrosion monitoring of pipelines.

Corrosion monitoring for pipelines, and really any structure or system, is typically done for reasons including: identifying when maintenance action should be taken; establishing inspection intervals; determining if active corrosion is taking place; and ensuring that effective cathodic protection is being applied. All of these help to provide confidence in the overall integrity of the pipeline and ensure operability.

For the most part, the construction materials tend to be carbon steel or other ferrous alloys. To mitigate corrosion and degradation, many of these systems use coatings and paints, as well as impressed current and sacrificial

anode cathodic protection systems. The corrosion-related failure modes encountered include general (thinning) corrosion, localized pitting and crevice corrosion, microbiologically influenced corrosion, and environmentally assisted cracking.

To monitor for these failure modes, as well as to better understand the condition and the protectiveness of the coating (as well as the effectiveness of the cathodic protection system), a wide range of technologies have been used to study external corrosion in underground pipelines. These include installing coupons where weight changes and/or potential measurements are taken; the use of linear polarization resistance (LPR) or other electrochemical methods such as impedance; electrical resistance probes; and optical and acoustic technologies. Each of these approaches is discussed below.

11.2 Electrochemical methods

Corrosion in soil and aqueous environments typically takes place via an electrochemical process. Four main elements are required for electrochemical corrosion to take place: an anode, a cathode, an electrically conductive path, and an ionic conductive path. In most corrosion situations, the anode will be the metal that is corroding and the cathode will usually be associated with the reduction of some environmental species such as oxygen or hydrogen (though there are many others that can be involved). The electrical conductive path is through the metal itself, while the ionic conductive path is the environment. In the case of soils, there is considerable variability in soil resistivity. This variability depends not only on geography and location, but also on seasons – some soils become more conductive through water table changes, farm runoff, and even permafrost and soil freezing.

During the corrosion process, metallic atoms are oxidized to cations at the anode, and then leave the metal surface and enter the environment. These metal cations then tend to form oxides, hydroxides, carbonates, and so forth as corrosion products or films. When the metallic cation leaves the metal, electrons are left behind, which are consumed by the cathodic reduction reaction. It is this transfer of electrons that forms the basis of electrochemical monitoring methods. The flow of electrons is current, measured in amperes. The ampere is not a base unit but instead is derived from the number of coulombs (C) passing per second, with each electron having the equivalent charge of approximately 1.602×10^{-19} C. In electrochemical methods, the anode and cathode are physically separated and the current flow between them is measured through the use of sensitive instrumentation. One of the outcomes of using such instrumentation is to enable electrochemical methods to respond to very slow corrosion.

Several electrochemical methods are used in corrosion monitoring of pipelines. Some methods, such as LPR, are established and very widely used, whereas others, such as electrochemical impedance spectroscopy (EIS), are less established as field-monitoring methods, although they are gaining acceptance. One advantage of electrochemical methods is that the fundamental basis for their operation is supported by almost two centuries of research and laboratory study, starting with the work of Davy (Davy, 1824) and Faraday (Faraday, 1849). Though electrochemical methods are sensitive and, in most cases, the reactions and what is being measured are fairly well understood, data interpretation can sometimes be complex, and proper use of the methods can be challenging.

11.3 Potential measurements

In many cases, simply monitoring the corrosion potential or the applied potential in the case of cathodically protected structures is all that is needed to understand the status of the system (Gartland and Bardal, 1983). The utility of measuring and knowing corrosion potentials is evident in the use of the galvanic series, which is used in determining the risks of galvanic corrosion (LaQue, 1941). Shifts and changes in the measured corrosion potential have also been associated with the formation of surface films (e.g., carbonate), changes from general to localized corrosion, and differences in environmental conditions, such as the effects arising from the metabolism of bacteria.

For buried pipelines, the most common use of potential measurements is to evaluate the effectiveness of cathodic protection. These potential measurements are often made directly on the pipeline itself, but are sometimes made using buried coupons. The use of coupons for estimating the level of cathodic protection on pipelines was first discussed by Peabody (1967). For example, Khan (2007) reviewed the basis for using coupons to monitor cathodic protection (CP) levels as a means of ensuring that adequate protection has been applied. In his discussion, Khan showed that the coupons have been used to monitor the polarized off-potential, and also for measuring depolarized potentials for pipelines. In a separate work, Lawson and Thompson (1998) compared coupon potential measurements with pipe potential measurements at different levels of cathodic protection and coating condition. They showed that the coupons tended to respond to changes in the applied cathodic protection similar to comparably sized coating holidays (or defects) on the pipe. They observed that coupons served as a useful means of determining the effectiveness of the cathodic protection system, and were especially useful in locations where interruption of all current sources to the pipeline was difficult (e.g., locations of stray currents).

The successful use of coupons to monitor CP levels was also demonstrated on the TransAlaska Pipeline. In their laboratory research and extensive field testing at over 400 locations, Stears *et al.* (Stears *et al.*, 1997, 1998; Moghissi *et al.*, 1997) were able to demonstrate that coupons installed in the vicinity of the pipeline effectively measured the level of CP on the pipeline. That is, coupon monitoring was shown to be effective in establishing that either the –850 mV vs copper sulfate electrode (CSE) polarized on-potential or the 100 mV polarized off-potential criteria had been met. They were also able to show that the coupons could also be used to capture the influence of telluric currents on the pipeline.

Robinson (1993) similarly described a program of using coupons to monitor the effectiveness of cathodic protection applied to pipelines and underground storage tanks. In this work, the author demonstrated that buried coupons could be used to establish the effects of stray currents due to nearby rail lines on both the corrosion rate and the effectiveness of cathodic protection. The coupons were used to help determine the on- and off-potentials for the structure, as well as the magnitude of the IR drop involved. Further, the corrosion rate was also estimated using retrievable weight loss coupons.

The success of using coupons to monitor CP levels is evident in this approach being incorporated into both a NACE Standard Practice (NACE, 2010), and as part of a NACE International Test Method Standard (NACE, 2012). In NACE SP0104, it is mentioned that one of the advantages of using coupons is to be able to better establish instant-off-potential measurements using coupons, because they can more easily be disconnected from the cathodic protection system (and other current sources), and placement of reference electrodes in close proximity to the coupon reduces IR drop effects. The standard does state that the potentials measured using the coupons are not identical to those of the actual structure and can cause the off-potential of the structure to be markedly different from the coupon. Some of the differences can be countered using good coupon design and placement. A schematic illustration of a coupon installation is shown in Figs 11.1 and 11.2. The differences in measured potentials for the coupon and the actual pipeline can be minimized by installing the coupon near the pipe so that the soil environment and the CP current for the coupon and the pipe are similar.

11.4 Linear polarization resistance

In addition to conducting potential measurements, LPR is also commonly used. Unlike potential measurements, which do not provide any information on the corrosion rate, the LPR method does provide corrosion rate information. It is based on the Stearn-Geary (1956) relationship between potential and current given by:

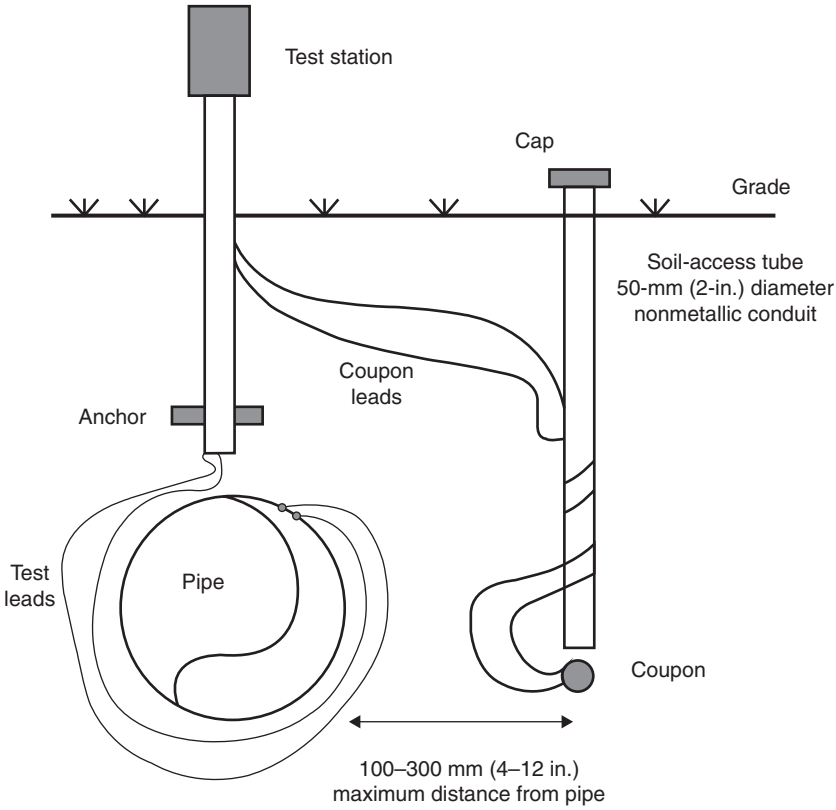

11.1 Schematic (end view) of coupon station for monitoring CP (NACE 2010).

$$R_p = \frac{\Delta E}{\Delta I}$$

where E is the potential, I the current, and R_p the polarization resistance.

The polarization resistance is inversely proportional to the corrosion current, and thus to the corrosion rate. The corrosion current can be calculated using:

$$I_{\text{corr}} = \frac{1}{R_p}\left(\frac{\beta_a \beta_c}{2.303(\beta_a + \beta_c)}\right)$$

where β_a and β_c are the anodic and cathodic Tafel constants, respectively.

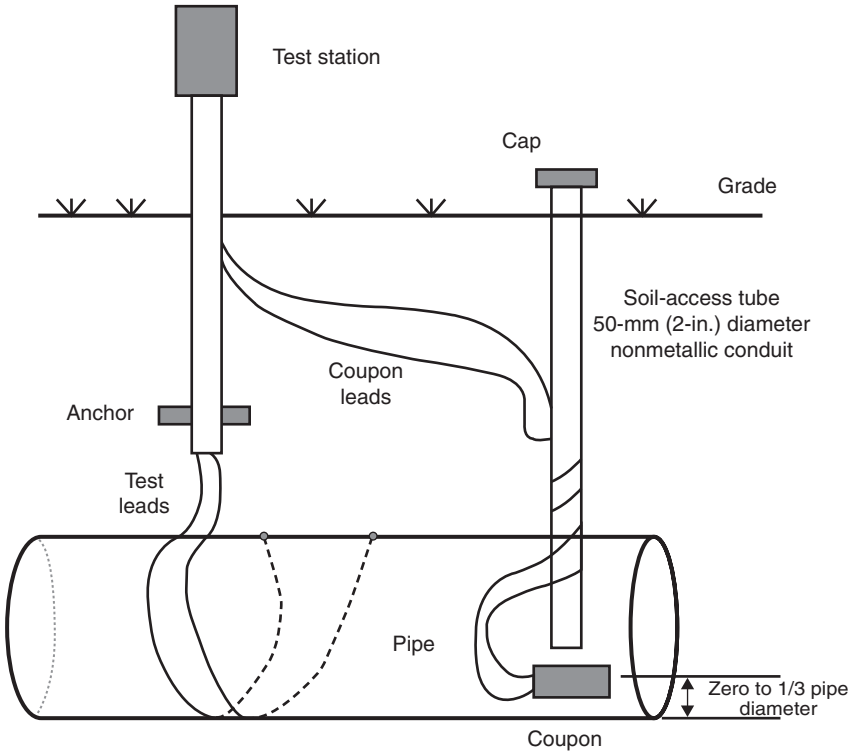

11.2 Schematic (side view) of coupon test station for CP monitoring (NACE 2010).

The corrosion current and the corrosion rate are directly proportional. The corrosion rate can be calculated from the corrosion current by first determining the corrosion current density. This is simply the corrosion current divided by the area of the exposed metal. Then, the corrosion rate can be found using:

$$\mathrm{CR} = K_1 \frac{i_{\mathrm{corr}}}{\rho} \mathrm{EW}$$

where K_1 is a unit conversion constant, i_{corr} is the corrosion current density (I_{corr} divided by the area of the material), ρ is the density of the material, and EW is the equivalent weight. In order to have high fidelity corrosion rate measurements, the anodic and cathodic Tafel slopes need to be known. In many cases, these data may not be known, so assumed values are required, which can lead to conservative and non-conservative corrosion rate estimates. It is also important to realize that the corrosion rate measured using

LPR represents the instantaneous corrosion rate at the time the measurement is taken. It does not provide any information regarding any corrosion rates experienced in the past, nor what corrosion rates might be observed in the future. Because these measurements provide snapshot estimates of the present corrosion rate, LPR measurements are often carried out on a periodic basis over an extended period of time. The inclusion of LPR for corrosion rate determination for buried structures and pipelines in standard methods and practices speaks for its ubiquitous nature and overall acceptance.

In analyzing the data, it is generally assumed that the corrosion process is uniform across the entire metal surface. As a result, LPR is generally not well suited for detecting localized forms of corrosion, such as pitting or crevice corrosion. If, however, the rates of pitting and crevice corrosion are sufficiently high, LPR measurements can be used to detect deviations from steady-state conditions in which little or no corrosion is occurring to cases where rapid corrosion is taking place. The corrosion rates measured using LPR when localized corrosion is taking place are generally not accurate. In these situations, LPR can be used as a diagnostic indicating tool. LPR measurements can also be adversely influenced by electrochemically active species. That is, if there are any other oxidation or reduction reactions that take place at sufficiently high rates, then artificially high or low corrosion rates will be indicated from the LPR measurement.

The use of LPR probes for monitoring underground pipelines is reviewed in NACE Report 05107 (NACE, 2007). This report clearly describes the advantages and disadvantages of using the LPR approach for estimating the corrosion rates of buried pipelines. The primary advantages are that the methodology is relatively easy to conduct with commercially available instrumentation. In addition, corrosion rate changes that result from environmental changes (e.g., seasonal runoff, changes in water table depth) can be readily and rapidly determined. The primary limitations of the LPR approach are that it cannot be used to determine the corrosion rate under applied cathodic protection and the soil environment must be sufficiently conductive to make reliable electrochemical measurements. If the soil resistance is not corrected in the determination of corrosion rate from the polarization resistance measured using LPR, non-conservative low corrosion rates will be indicated. Remember that the corrosion rate is inversely proportional to the polarization resistance, and the estimated polarization resistance can be artificially inflated due to high soil resistance. In some cases, this resistance can be compensated for in order to obtain more reliable polarization resistance values. Shown in Fig. 11.3 are guidelines for the range of soil resistivity and steel corrosion rates where LPR measurements can be considered viable.

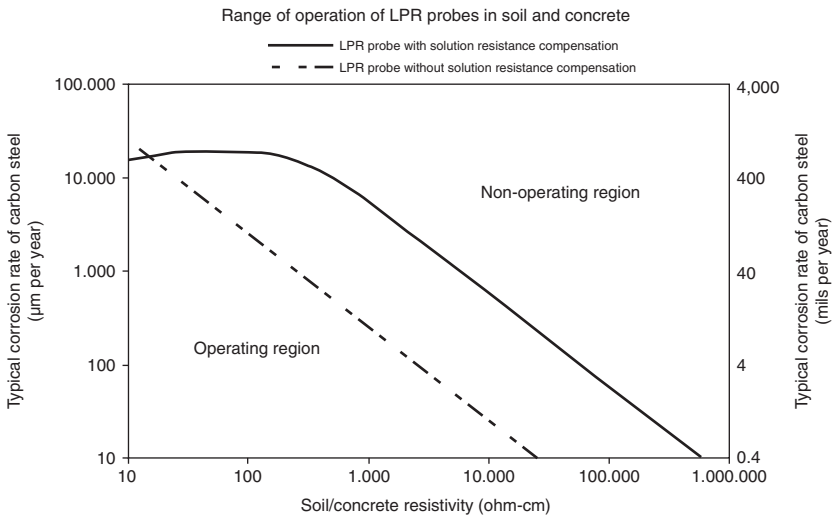

11.3 Soil resistivity and steel corrosion rate guidelines showing the range of conditions where reliable LPR measurements are possible (NACE, 2007).

11.5 Electrochemical impedance spectroscopy

In addition to determining the polarization resistance using LPR, it can also be determined using EIS. In EIS, a small amplitude alternating potential is imposed, usually over a range of frequencies, and the current response is measured. The alternating current (AC) impedance is then given by dividing the current into the voltage, as is done to determine the polarization resistance in LPR, except that this is done at every frequency tested. One of the main advantages of using EIS is that a determination of the polarization resistance is not compromised by ohmic, or IR, drop issues that may arise in high resistivity environments. In addition, EIS can also be conducted on coated materials and used to evaluate the integrity of coatings.

To determine corrosion characteristics from EIS data, several approaches have been attempted. In ideal instances, the impedance response as a function of frequency is modeled and fitted using equivalent electric circuits composed of resistors, capacitors, inductors, constant phase elements, and the like. If sufficient information is known, the processes and reactions occurring can be modeled and studied. These electrical circuits are constructed so that they have identical or very similar impedance vs frequency response to the actual system being studied. Because elements can be created and put together, resulting in a near infinite number of equivalent circuits, there is no unique single circuit model that is used. A simple Randle's

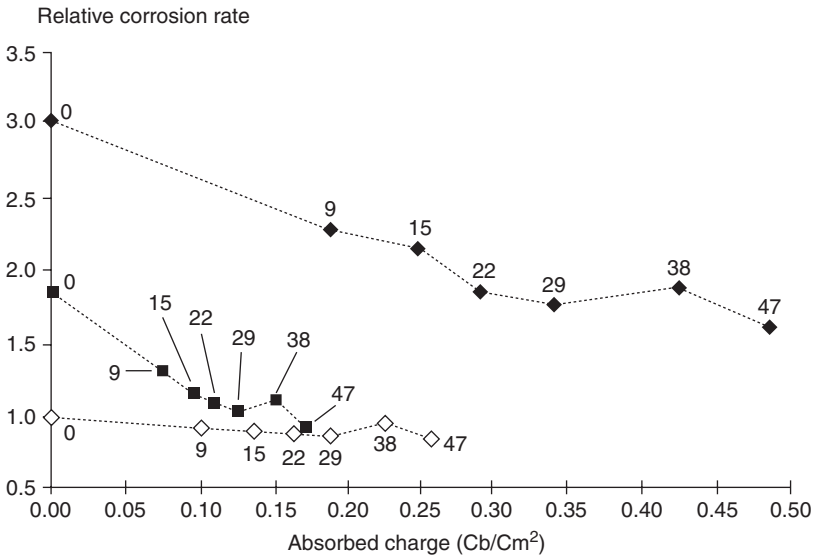

11.4 Relative corrosion rates determined using EIS while continuous CP was applied. Numbers indicate the number of days of applied CP (Pruckner *et al.*, 1996).

circuit composed of a capacitor–resistor parallel circuit that is in series with another resistor is an exception wherein corrosion reactions for uncoated metals in simple environments can be conducted. Pruckner *et al.* (1996) was able to use this model circuit to study rebar corrosion in concrete, including the effect of CP on the corrosion rate (Fig. 11.4). In addition, Hack and Scully (1991) used EIS to estimate defect areas on coated metallic samples. They were able to show that the impedance responses of intact and defective coatings were sufficiently different and so complicated analysis of the data was unnecessary. Though not specifically a buried pipeline example, the utility of this approach can be seen.

In a modified version of the traditional EIS methodology, the magnetic field created due to current flow at discrete corrosion sites in a buried structure was measured using a magnetometer (Murphy *et al.*, 1988; Srinivasan *et al.*, 1991), giving rise to the magnetic electrochemical impedance spectroscopy (MEIS). In this work, the authors induced an AC voltage signal of varied frequency to the pipe and then used a non-contact magnetometer to monitor the current response instead of measuring the current directly from the pipe. The primary advantage the authors cited, compared to traditional EIS, was that MEIS could provide quantitative information on localized corrosion rates. That is, this approach was able to determine discrete corrosion rates along the length of a pipeline that exhibited spatially varied rates along its length.

One of the challenges in conducting EIS measurements is in interpreting the results. This is often accomplished by creating equivalent electrical circuits to model the physical processes involved. Because of the complexities and challenges associated with developing robust and realistic equivalent electrical circuit models, a more simplistic approach is sometimes used. For example, if a key characteristic in the impedance response that is directly related to the polarization resistance or to the corrosion reaction itself can be identified, it can sometimes be utilized to determine the corrosion rate or, at a minimum, be used as a diagnostic to determine if conditions have changed and the corrosion rate has increased or decreased. Though the impedance measured at any given frequency is complicated, because it is an amalgam of all impedances in the system, including the corrosion reaction, coating changes, and other processes, the approach has found utility because of its relative simplicity. For example, Scully (Scully, 1989) was able to show that high values for the low frequency (~<10 mHz) impedance corresponded to an intact coating, whereas a low impedance value signified coating failure and stable corrosion rates. Even with these simplified approaches to data interpretation, because of the complexity of the data analysis and the need for prior knowledge of the Tafel slopes and other parameters to obtain reliable corrosion rates, commercially available EIS-based monitoring systems are uncommon.

11.6 Galvanic sensors

In a three-part study, Choi *et al.* (Choi and Kim, 2005; Choi *et al.*, 2006, 2007) presented their research, developing and testing a galvanic-coupling-based sensor for monitoring pipeline corrosion. In their study, the authors investigated carbon steel–304 stainless steel and carbon steel–copper couples. They were able to demonstrate that the current flow between the two metals of the sensor (measured using a zero resistance ammeter) was proportional to the corrosiveness of the environment and correlated reasonably well with weight loss coupons, LPR, and electrochemical impedance measurements. In their tests, they showed that the carbon steel–copper system tended to show better agreement with the corrosion rates measured with weight loss coupons and LPR measurements. Example results from their study evaluating the effect of applied cathodic protection are shown in Fig. 11.5. As can be seen, before cathodic protection is applied, the pipeline potential was on the order of –0.8 V_{SCE} and the sensor current was positive or near zero. Positive sensor currents indicated that the carbon steel element was the anode and the copper element the cathode. When cathodic protection was applied, the measured sensor current changed sign, indicating that the copper element was the anode and the steel element was the cathode. This behavior was observed when the sensor was uncoupled and coupled to

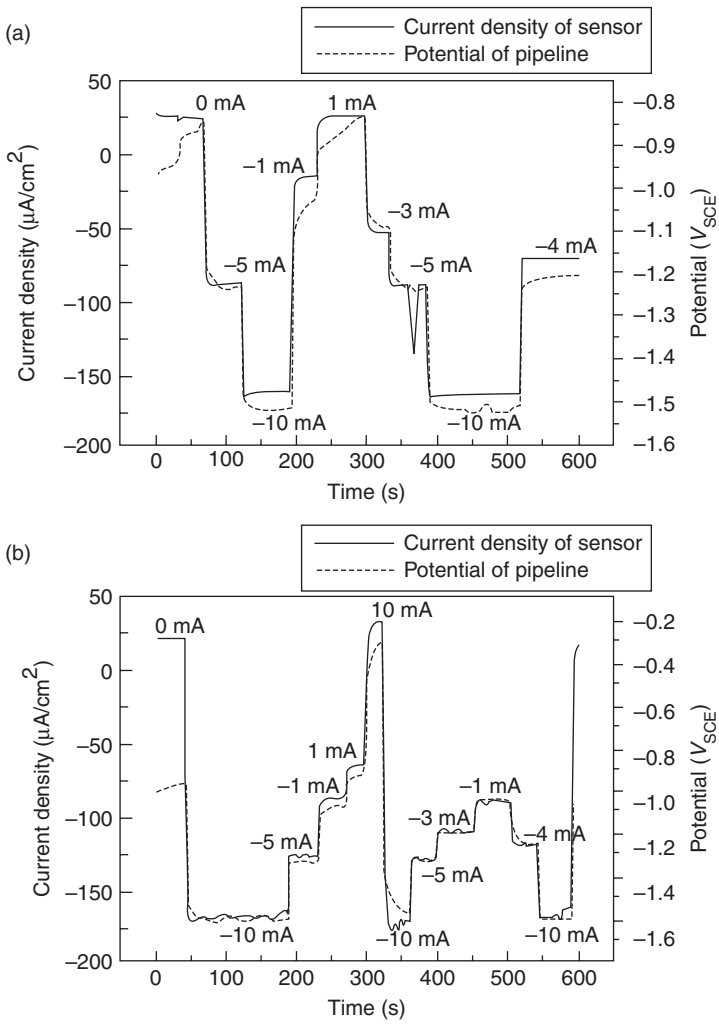

11.5 Galvanic sensor response (current) at different applied cathodic protection potentials with the sensor (a) disconnected and (b) connected to the pipe (Choi *et al.,* 2007).

the pipe, though the pipe-coupled sensor tended to respond more rapidly to applied potential changes. When the pipe potential was increased to less negative values, the sensor response clearly indicated a change where the steel became the anode. It is unclear if this system has been commercialized, but the approach seems to provide a viable methodology of determining if cathodic protection is effectively applied.

A variation of this theme has been investigated by Gao *et al.* (2008). Though it was not strictly a galvanic couple comprising dissimilar metals,

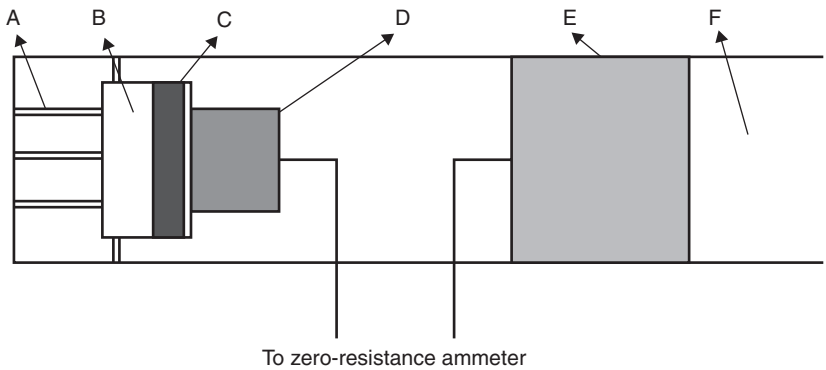

11.6 Schematic of localized corrosion sensor developed by Gao showing: (A) holes to allow ingress of the environment; (B) the artificial crevice/occluded region; (C) a polymer membrane; (D) the anode; (E) the cathode (boldly exposed element); (F) nylon base (Gao *et al.*, 2008).

the authors utilized a zero resistance ammeter to monitor the current flow between a boldly exposed element and an element that was embedded in plastic in such a way as to create a crevice. That is, the authors created a crevice/localized corrosion sensor by galvanically coupling an artificial creviced sample to a boldly exposed sample. This is shown schematically in Fig. 11.6. The authors evaluated the performance of this sensor system in both laboratory and field tests. These tests were aimed at investigating the possibility of internal corrosion of a water injection system. They were able to show that the measured sensor response and corrosion rates corresponded well with long-term installed coupons. Though not developed for the purpose of monitoring underground corrosion, it seems that this design could be modified to study possible corrosion under coating disbondments that were due to microbial colonies, and other situations of interest in external pipeline corrosion monitoring.

11.7 Non-electrochemical methods: coupons

The most widely used corrosion monitoring method is coupons. Coupons tend to be simple and inexpensive, and can come in a variety of configurations to examine general corrosion, localized corrosion (e.g., creviced coupons), and stress corrosion cracking (i.e., stress coupons). After being exposed at the location of interest, the coupons are then removed and assessed. The assessment tends to vary depending on the intent of the monitoring, but usually would include weight loss, evidence of localized corrosion or cracks, the presence of scales and films, and the overall visual appearance of the

coupon. After coupons, the next most commonly used non-electrochemical methods to monitor for corrosion are those based on the electrical resistance probe and optically based methods.

11.8 Optical-based methods

Optical methods, including fiber optic strain sensors, have been used to monitor pipeline corrosion. Zou *et al.* (2008) described an optical fiber-based sensor system designed to measure the hoop and axial strains along with temperature as a means to detect locations of decreased wall thickness due to corrosion. These sensors measure the strain on a structure that can change with use and time by changing the level of stress and deformation on the optical fiber. These changes in stress and deformation on the fiber in turn change its optical refraction properties. Zou *et al.* (2008) were able to show that defects in the order of 50–60% of wall thickness could be detected as a deviation in the strain/pressure relationship. These defects were detectible with pressure changes as small as 300–500 psi. In a different study using a similar approach, Yan and Chyan (2010) demonstrated that by using optimized detection methods and data algorithms, changes in the strain on the pipe could be detected over distances beyond 100 km. Even though this type of methodology appears to be able to provide a viable approach to monitoring corrosion of pipelines, it is unclear what the minimum detectable wall loss might be. Thus, further research, testing, and development will be needed before it can be deployed.

In a different approach using optical fibers, Wade *et al.* (2008) deposited a thin metallic film on the optical fiber. As corrosion of the thin film occurs, the stress on the fiber changes, which in turn causes changes in the optical transmission properties of the fiber. In other cases, corrosion of the thin film resulted in complete breakage of the fiber. Though developed to monitor for seawater corrosion of aluminum, this concept could be adapted for in-soil pipeline monitoring.

11.9 Electrical resistance probes

Electrical resistance methods to monitor corrosion have been in use since the 1950s (Dravnieks and Cataldi, 1954; Freedman *et al.*, 1958). In electrical resistance measurements, a metal sensing element of the material of interest is exposed to the environment and, as corrosion takes place and the cross-sectional area of the element decreases, its resistance increases via:

$$R = \frac{\rho l}{A}$$

where R is the resistance, ρ is the resistivity of the metal, l is the length of the element, and A is the cross-sectional area. The sensitivity to low corrosion rates and longevity of the probe in service depends on its size. Sensing elements with larger cross-sectional areas will last longer than smaller elements but also lose some sensitivity as the same amount of corrosion loss represents a smaller fraction of the cross-section. Electrical resistance (ER) probes can also give false negative results when conductive scales and deposits are formed such that small or no changes in resistance are detected even if corrosion occurs.

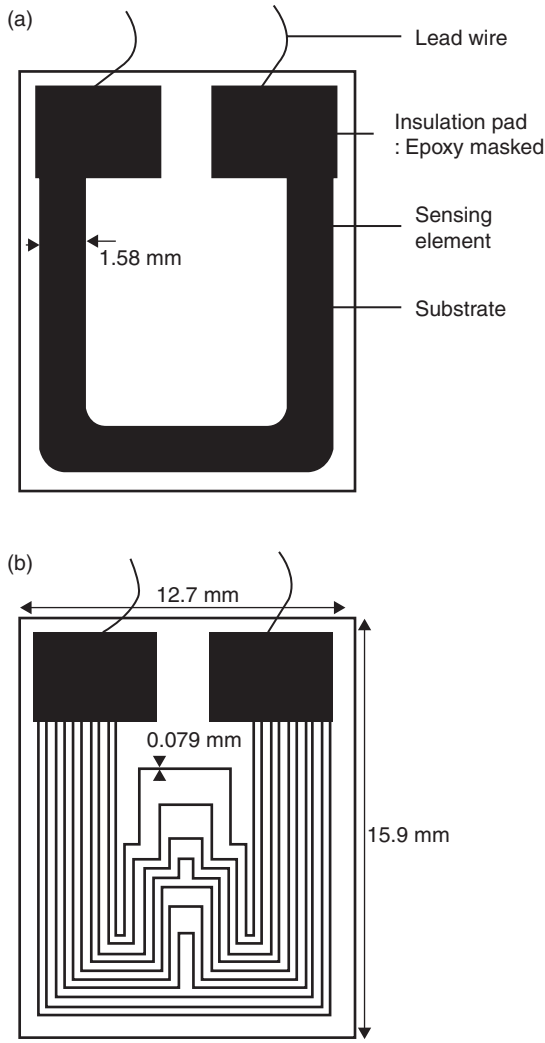

11.7 (a, b) Thin film ER sensors developed by Li *et al.* (2007a,b).

As discussed in NACE Report 05107 (NACE, 2007), ER probes have several advantages. These include the ability to measure corrosion rates even when cathodic protection is applied. ER probes can also be used in cases where the environment is highly resistive, where IR problems make LPR and other methods unsuitable. The primary assumption, however, in using ER probes is that corrosion is assumed to be relatively uniform on the probe, thus making localized corrosion difficult to detect.

To improve the sensitivity of the ER methodology, Li *et al.* (2007a,b) developed and tested a system where the sensing element was a metallic thin film in two configurations: a continuous film, and a discretized multi-line thin film (Fig. 11.7). For their system, the authors sputter deposited steel onto an inert substrate to a thickness of 6 μm. They then compared the response of their thin-film design with bulk weight loss coupons and observed good agreement in the measured corrosion rates. On the basis of laboratory testing, they estimated that corrosion rate measurements down to 0.01 mm/y were possible. They then tested the different sensor designs and compared the corrosion rates measured that were observed using coupons under stray current, cathodic protection, and microbially influenced corrosion situations. When microbially influenced corrosion occurred they noted abrupt changes in the resistance of the multi-line element as

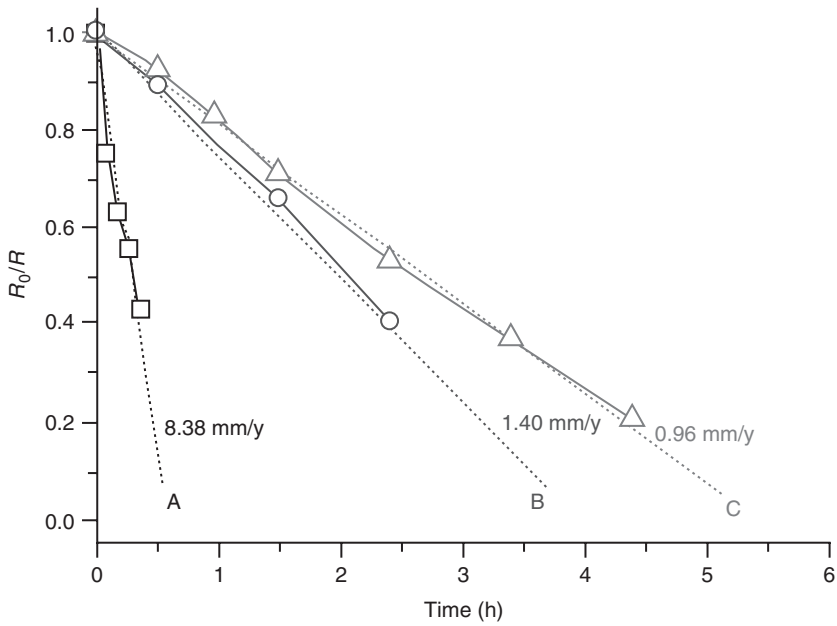

11.8 Response of thin film ER probes at three distances from a stray current source (Li *et al.*, 2007b).

individual lines were perforated. When the sensor elements were connected to the cathodic protection system, the appropriate reduction in corrosion rate was observed. When the authors investigated the effects of stray currents, they observed corrosion rates of 8.4 mm/y in close proximity to the current source and of less than 1 mm/y at locations away from the source (Fig. 11.8).

11.10 Challenges and limitations in using probes

Regardless of which monitoring method (or a combination of methods) is used, one of the primary issues is deciding the location for installing the probe. This issue is further complicated because corrosion probes offer a spot location measurement, whereas corrosion rates can be spatially distributed and may not occur at the location where the probe is installed. The precise location where corrosion will take place is not always known *a priori* and, as a result, installation of monitoring systems at incorrect locations is a much more common occurrence than is desirable. For example, there have been cases where corrosion failures and leaks have occurred within a very short distance, on the order of centimeters, of where monitoring probes were located but corrosion was not detected. As a result, consideration of the possible locations of interest along the length of the pipeline, as well as the o'clock position, need to be considered. Other factors, such as high consequence areas, high stress locations, river crossings, casings, and other possible areas of concern, need to be considered.

A second major challenge with corrosion monitoring is that in most cases the corrosion being measured is on the probe and not on the actual structure. This poses a challenge, because corrosion of the probe is assumed to be nearly identical to the corrosion that is occurring on the structure. This assumption that the probe accurately mimics the structure is usually, but not always, valid.

Assuming that valuable data are obtained and the probes are installed at good locations, a remaining challenge is to consider how the data will be used. Monitoring data have been used to validate and modify inspection intervals and life prediction models that aid in asset management.

11.11 Conclusion

In choosing corrosion monitoring, there are a range of viable options depending on what is of interest. All commercially available monitoring systems will work and provide good information under some circumstances. All of the different methodologies have advantages, and usually some limitations as well. They also vary widely in complexity. From the simplest method of deploying weight loss coupons that are removed over

time to determine the corrosion rate, to more complex systems using electrical, optical, and electrochemical methods, which can sometimes provide real-time indications of the onset of corrosion, selecting an appropriate monitoring method can be a non-trivial exercise.

Beyond the complexities in selecting from the range of possible monitoring methods, the objective of monitoring also needs to be considered. For example, determining the effectiveness of cathodic protection and confirming reassessment intervals may require different types and ways of corrosion monitoring. The type of data needed and the monitoring methods to obtain that data will be different depending on the situation. In more challenging situations with the need for higher reliance on the data to make decisions, the robustness of the monitoring method will increase and the data that are generated need to be clearly understood. Once a method is selected, the challenge of where to install the monitoring system must be addressed. This could mean installing multiple systems to effectively capture the spatial variability in corrosion. Selecting locations where the consequence of a corrosion failure is high can provide some basic guidance on where to monitor.

In summary, there are a wide range of engineering and operational considerations that need to be evaluated before selecting and installing a corrosion monitoring system. In many cases, the optimal solution for monitoring is a combination of methods that provide complementary information on the present status of the pipeline as well as trending information so as to make predictions as to when preventive maintenance and corrosion mitigation methods should be performed.

11.12 References

Choi, Y. S. and J. G. Kim (2005). 'A galvanic sensor for monitoring the corrosion damage of buried pipelines: Part 1 – electrochemical tests to determine the correlation of probe current to actual corrosion damage in synthetic groundwater'. *Corrosion* **61**(3): 293.

Choi, Y. S., J. G. Kim and J. Y. Koo (2007). 'A galvanic sensor for monitoring the corrosion damage of buried pipelines: Part 3 – correlation of probe current to cathodic protection and stray current'. *Corrosion* **63**(10): 951.

Choi, Y. S., J. G. Kim and S. J. Yang (2006). 'A galvanic sensor for monitoring the corrosion damage of buried pipelines: Part 2 – correlation of sensor output to actual corrosion damage of pipeline in soil and tap water environments'. *Corrosion* **62**(6): 522.

Davy, H. (1824). Phil. Trans. Royal Soc. London **114**: 151.

Dravnieks, A. and H. A. Cataldi (1954). *Corrosion* **10**: 224.

Faraday, M. (1849). *Experimental Researches in Electricity* **1**.

Freedman, A. J., E. S. Troscinski and A. Dravnieks (1958). *Corrosion* **14**: 175.

Gao, L., H. Peng, L. Lei, Y. Yan and Y. Du (2008). 'Technical Note: research and development of localized corrosion rate monitoring instrument for nonpassivable metal in corrosive media'. *Corrosion* **64**(8): 641.

Gartland, P. O., R. S. and E. Bardal (1983). *Mater Perform* **22**: 40.
Hack, H. P. and J. R. Scully (1991). *J. Electrochemical Soc*. **138**(1): 33.
Khan N. (2007). 'Using coupons and ER soil corrosion probes in applying pipeline CP criteria'. *Mater Perform* (April): 26.
LaQue, F. L. (1941). *J. American Soc. of Naval Engineering* **53**: 29.
Lawson, K. M. and N. G. Thompson (1998). *Corrosion 98*. Paper No. **672.**
Li, S. Y., S. Jung, K. W. Park, S. M. Lee and Y. G. Kim (2007a). 'Kinetic study on corrosion of steel in soil environments using electrical resistance sensor technique'. *Materials Chemistry and Physics* **103**: 9.
Li, S. Y., Y. G. Kim., S. Jung, H. S. Song and S. M. Lee (2007b). 'Application of steel thin film electrical resistance sensor for in situ corrosion monitoring'. *Sensors and Actuators B* **120**: 368
Moghissi, O. C., P. F. Lara, L. Bone III, C. D. Stears and R. M. Degerstedt (1997). Corrosion 97, NACE International. Paper No **563**.
Murphy, J. C., G. Hartong., R.F. Cohn, P. J. Moran, K. Bundy and J. R. Scully (1988). *J. Electrochemical Soc*. **135**(2): 310.
NACE (2007). Report on Corrosion Probes in Soil or Concrete. Houston, TX, NACE International.
NACE (2010). *The Use of Coupons for Cathodic Protection Monitoring Applications*. Houston, TX, NACE International. **SP0104**.
NACE (2012). *Measurement Techniques Related to Criteria for Cathodic Protection on Underground or Submerged Metallic Piping Systems.* Houston, TX, NACE International. **TM0497**.
Peabody, A. W. (1967). *Control of Pipeline Corrosion*. Houston, TX, NACE International.
Pruckner, F., J. Theiner, J. Eri and G. E. Nauer (1996). *Electrochimica Acta* **41**: 1233.
Robinson, R. C. (1993). *Mater Perform* (February): 30.
Scully, J. R. (1989). *J. Electrochemical Soc*. **136**: 979.
Srinivasan, R., J. C. Murphy, C. B. Schroebel and R. S. Lillard (1991). *Mater Perform* (March): 14.
Stears, C. D., O. C. Moghissi and L. Bone III (1998). *Mater Perform* (February): 23.
Stears, C. D., R. M. Degerstedt, O. C. Moghissi and L. Bone III (1997). *Corrosion 97*, NACE International. Paper No **564**.
Stern, M. and A. L. Geary (1956). *J. Electrochemical Soc*. **104**: 56.
Wade, S. A., C. D. Wallbrink, G. McAdam, S. Galea, B. R. W. Hinton and R. Jones (2008). *Sensors and Actuators B* **131**: 602.
Yan, S. Z. and L. S. Chyan (2010). 'Performance enhancement of BOTDR fiber optic sensor for oil and gas pipeline monitoring'. *Optical Fiber Technology* **16**: 100.
Zou, L., O. Sezerman and W. Revie (2008). Corrosion 2008, NACE International. Paper No **08146**.

This page intentionally left blank

Index

This page intentionally left blank

This page intentionally left blank